Rare Earth Metals Effects on Machinability of Aluminium Based Hybrid Composites Using Magnetic Abrasive Flow Machining Process

A thesis submitted in fulfilment of the requirement for the award of the degree of

DOCTOR OF PHILOSOPHY

IN

MECHANICAL ENGINEERING

Submitted by

VIPIN KUMAR SHARMA

Roll No. 951608004

Under the supervision of

Dr. VINOD KUMAR
Associate Professor, MED

Dr. RAVINDER SINGH JOSHI
Assistant Professor, MED

Department of Mechanical Engineering,

Thapar Institute of Engineering and Technology, Patiala-147004, India

(Deemed to be University)

December, 2020

CANDIDATE'S DECLARATION

I, Vipin Kumar Sharma, Roll No. 951608004, hereby declared that the thesis entitled **"Rare Earth Metals Effects on Machinability of Aluminium Based Hybrid Composites Using Magnetic Abrasive Flow Machining Process"** submitted to the Department of Mechanical Engineering at Thapar Institute of Engineering and Technology, Patiala, Punjab (India) is an authenticated record of my own research work for the award of the degree **"Doctor of Philosophy"** under the supervision of **Dr. Vinod Kumar and Dr. Ravinder Singh Joshi**. This report has not been submitted to any other institute for the award of any other degree.

Place: Patiala

Vipin Kumar Sharma

Dated: 01-12-2020

Roll No. 951608004

This is to certify that above declaration made by the student is correct to the best of my knowledge.

Dr. Vinod Kumar

Associate Professor
Department of Mechanical Engineering
Thapar Institute of Engineering
and Technology, Patiala-147004 (Punjab) India
(Supervisor)

Dr. Ravinder Singh Joshi

Assistant Professor
Department of Mechanical Engineering
Thapar Institute of Engineering
and Technology, Patiala-147004 (Punjab) India
(Supervisor)

ACKNOWLEDGEMENT

"Every search begins with beginners luck and ends with the victors being severely tested"

-The Alchemist, Paulo Coelho

Fortunately the path is shown by a guiding beacon and support is derived from many fellow pilgrims, helping one to reach his destination. With great gratitude I would like to express my deepest regard for my supervisors **Dr. Vinod Kumar**, Associate Professor, Department of Mechanical Engineering, Thapar Institute of Engineering & Technology, Patiala and **Dr. Ravinder Singh Joshi**, Assistant Professor, Thapar Institute of Engineering & Technology, Patiala; for providing me with the opportunity to excel under their guidance. Without their inspiration, continuous support, constant review, constructive inputs and critical evaluation of my research work; it would not have been possible to conclude this thesis.

Heartfelt thanks are due to Prof. Prakash Gopalan (Director, Thapar Institute of Engineering & Technology, Patiala) and Dr. Rafat Siddique (Dean, Research and Sponsored Projects, Thapar Institute of Engineering & Technology, Patiala), Dr. Ajay Batish (Deputy Director, Dean of Partnerships & Accreditation and Professor in Mechanical Engineering Department, Thapar Institute of Engineering & Technology, Patiala), Dr. Tejinder Paul Singh (Prof. & Head, Department of Mechanical Engineering, Thapar Institute of Engineering & Technology, Patiala), Dr. Kulvir Singh (Prof. & Associate Dean Strategy, School of Physics & Materials Science), Dr. Tarun Nanda (PhD coordinator) and Dr. Gagandeep Bhardwaj (PhD coordinator) for their encouragement and support during this research work.

I am thankful to Prof. N M Suri and Mr. Gopi (Lab Superintendent) at Production and Industrial Engineering Department, Punjab University, Chandigarh for providing laboratory facilities (Bottom Pouring Stir Casting Machine).

I would like to wholeheartedly thank to Prof. Indradev S. Samajdar, Department of Metallurgical Engineering and Materials Science, IIT Bombay for permitting the use of Electron Back Scattered Diffraction Apparatus for image microscopy of the samples.

The author is also thankful to Head of the Department, Department of Mechanical Engineering, IIT, Ropar for permitting the use of Corrosion Testing Apparatus.

I would like to wholeheartedly thank to Dr. Leena Nebhani, Assistant Professor, Department of Material Science and Engineering, IIT Delhi for permitting the use of Drop Shape Analyzer for hydrophobicity analysis of composites.

I would like to wholeheartedly thank to Prof. M. Parida, Head Institute Instrumentation Centre, IIT Roorkee for permitting the use of scanning probe microscope for the AFM (Atomic Force Microscopy) analysis.

I wish to thank my seniors, colleagues and dear friends- Dr. Rajeev Kumar Agarwal, Dr. Siddhartha Jain, Dr. Dinesh Kumar, Dr. BN Tripathi, Dr. Pardeep Kumar, Dr. Ansar Ali SK, Dr. Tushar Jain, Dr. Piyush Gupta, Mr. Sandeep Kumar, Mr. Santosh Rai, Mr. Dinesh Kumar Patel, Mr. Sagar Goswami, Mr. Mayank Bhardwaj, Mr. Pawan Kumar, Mr. Omkar, and Mr. Omveer and many others for their constant moral support and camaraderie.

I would like to express respect and great admiration for my father Mr. Ved Prakash Sharma, my mother Smt. Kamlesh Sharma, my wife Dr. Nitasha Bhardwaj, loving son Vedant and loving daughter Tushti for being the guiding light and encouraging force behind this endeavor. I would like to humbly dedicate this thesis to my parents, Nitasha, Vedant and Tushti.

I thank all the souls who helped me in this herculean task. Finally, I bow my head to the **ALMIGHTY** for all the blessings he has showered on me.

(VIPIN KUMAR SHARMA)

ABSTRACT

In the era of globalization, the demand of composite materials with some unique combination of properties as well as with improved surface finish rises continuously. The aluminium alloy metal matrix composite have tailored properties to fulfill the application-specific properties (like high stiffness, high strength, and low density) related to automobile and aerospace applications, etc. However, the inferior surface properties of the aluminium alloy based composites; such as poor corrosion resistance, poor hydrophobicity behaviour and low wear resistance have restricted the use of these aluminium alloys based composites in aerospace applications under hazardous environmental conditions. Moreover, the imperfections such as shrinkage and porosities observed in the as-cast alloys effect their properties and make them unacceptable for these application areas. Introduction of secondary phase in the form of reinforcement helps in improving the performance of the matrix material through changing its surface morphology, mechanical properties and microstructure. Rare Earth Oxides (REOs) as secondary phase reinforced hybrid composites are increasingly being used in aviation and automobile applications because of their tailored properties combinations of high temperature stability, satisfactorily level of wear resistance, online monitoring control ability, excellent corrosion resistance, good hydrophobicity behaviour, good sintering temperature and high specific strength. The aim of the present work is to develop aluminium stir cast hybrid composites reinforced with alumina and silicon carbide after incorporation of traces amount of REOs. Finally, magnetic abrasive flow machining process has been used for the internal finishing of hybrid composite that can be used in aircraft industry mainly for esthetic and architectural components.

Earlier various types of ceramic particulate based composites like Al-SiC, Al-Al_2O_3, Al-B_4C and Al-TiB_2have been fabricated for mechanical and metallurgical characterization. Various researchers have been characterized various composite systems on the basis of mechanical and metallurgical testing based on TiC, MgO, TiO_2,TiB_2, CNTs and ZrO_2 etc. However still there is need of exploration that has to be done on Al-6061 reinforced with mixture of (Al_2O_3+ SiC) and rare earth element CeO_2(cerium oxide) as additive. The most commonly used particulate reinforcements of micro level are silicon carbide (SiC) and aluminium oxide (Al_2O_3). SiC reinforcement not only increases the tensile strength, hardness and density but also improves the wear resistance of aluminium alloy composites. The other micro level

particulate reinforcements Al_2O_3 have good compressive strength and wear resistance capability. Among all the available alloys of aluminium, Al-6061 was generally preferred for preparing MMCs for aircraft and tribological applications due better wear resistance characteristics, good corrosion resistance, low stiffness and high impact strength. Among all rare earth oxides, the cerium oxide possesses high temperature stability, excellent corrosion resistance capability, excellent water repellent properties and high specific strength. Hence, cerium oxide is selected as a potential candidate to be used in aluminium hybrid composites as reinforcement element. Keeping in mind the above facts, novel hybrid composites with traces amount of REOs have been synthesized via bottom pouring stir casting process. The weight percentage of CeO_2 as REOs varied from 0.5 wt% to 2.5 wt% and SiC /Al_2O_3varied from 2.5 wt% to 7.5 wt%. Finally, the prepared hybrid composites are tested under mechanical, metallurgical and tribological testing. The finishing of the hybrid composites was done with the help of MAFM process in this thesis work. Mechanical testing like ultimate tensile strength (UTS), percentage elongation, hardness (VHN), impact strength and flexural strength of hybrid composite samples with standards ASTM (American Society for Testing and Materials) and IS (Indian Standards) are carried out to see the effect of cerium oxide. The ultimate tensile strength rises from 30 MPa to 123 MPa after incorporation of optimum amount of 2.5wt% of cerium oxide. Percentage elongation was increased from 2.0% to 11.5% with the increase in amount of cerium oxide.

Hardness results shown that with the addition of cerium oxide from 0.5 wt% to 2.5 wt%, micro hardness of Al-6061 hybrid composites increased significantly. In Al-6061 hybrid composites with 7.5wt% of (SiC+Al_2O_3), the hardness is increased from 77 HV to 94 HV after addition of 2.5 wt% of cerium oxide. The Rockwell hardness of the base alloy Al-6061 increased from 61.73 HRB to 82.6 HRB with a percentage increase of 33.80% with the addition of 2.5wt% of cerium oxide. Whereas in case of 7.5 wt% of (SiC+Al_2O_3), the hardness value increased from 61.73 HRB to 71.8 HRB with a percentage increase of 16.32%. The impact strength of the hybrid composite increases 50 J to 56 J after addition of 0.5 wt% and 1.5 wt% of cerium oxide. But the trend of impact strength decreases after addition of 2.5 wt% of cerium oxide and the value of impact strength is observed as 46 J due to material properties tends to change from ductile to brittle which cause reduction in hardness and because of which ability of a material to absorb shock decreases and it break with less force as compared to other prepared composites. The flexural strength of the Al-6061 base alloy increased from 340 MPa to 450 MPa with the addition of 7.5 wt% of

($SiC+Al_2O_3$) reinforcement. The flexural strength of Al-6061 base alloy increases up to 615.6 MPa with the addition 2.5 wt% of cerium oxide.

Wear tests were performed on hybrid composites with highest value of hardness and the base alloy. Optimal value of hardness was found in hybrid composite reinforced with 7.5 wt% of both Al_2O_3/SiC and 2.5 wt% CeO_2. The results of wear test performed at sliding velocity of 0.5m/s and load value of 10N showed a significant improvement in wear rate of hybrid composites using cerium oxide particulates as reinforcement. The rate of wear in sample containing 7.5 wt% of both Al_2O_3 and SiC showed an improvement of around 38% in comparison to the base metal sample. Whereas, addition of 2.5 wt% of cerium oxides particulate in sample containing 7.5 wt% of Al_2O_3 and SiC led to 87.28% improvement in wear rate. Different wear mechanisms like oxidation, abrasion and delamination in samples were determined using SEM and EDS analysis of worn surfaces and wear debris for aerospace application.

The microstructure analysis was done using SEM, XRD and EDS techniques. The SEM microstructure analysis shows a very significant refinement of the composites after addition of REOs. XRD and EDS analysis shows very good results in terms of fabrication of hybrid composite particles. The XRD study of CeO_2 modified aluminium alloy showed that presence of α-Al ,SiO_2, Mg_5Si_6, MgO, Al_4Ce, Al_3Ce and $Al_{11}Ce_3$ phases. The presence of rare earth particulate helps in grain refinement of the matrix with well defined grain boundaries is seen via Electron Backscatter Diffraction (EBSD) analysis.

Wettability behaviour analysis between the aluminium liquid matrix and Al_2O_3/SiC reinforcement can be improved by the addition of REOs as measured by sessile drop method. The contact angle of composites with Al_2O_3/SiC reinforcement lies in the range of 87.94^0 to 98.52^0. But after incorporation of 2.5 wt % REO, the contact angle raised above 100.78^0. This result of increase in contact angle with addition of REOs helps to convert composites from hydrophilic to hydrophobic nature. Because of the hydrophobicity, the hybrid composites with REOs show better corrosion resistant properties. Magnetic abrasive flow machining process is generally used for finished intricate shapes of various parts used in aerospace applications. Current theses analyze the effect of a various process variable of MAFM process on the output response surface roughness. Response surface methodology has been applied to find out the effect of input parameters like magnetic flux density, number of cycles and extrusion pressure, size of abrasive particles and working gap on response parameter

surface roughness. The experimental plan is based on Box-Behnken design. Response parameters have been optimized using the desirability approach in response surface methodology. The significance of different parameters is identified using analysis of variance. An optimum combination of parameters is designed for the process. Experimental results shows that magnetic flux density and extrusion pressure has a predominant effect on surface roughness while internal finishing of the aluminium hybrid composites as compared to the number of cycles. Furthermore, specimens were examined and analyzed using atomic force microscopy for seeing the topography of finished samples.

TABLE OF CONTENTS

LIST OF FIGURES

LIST OF TABLES

LIST OF RESEARCH PUBLICATIONS

The following is the list of research papers published in Journals/Conferences as a part of present research work is given below:

PAPERS PUBLISHED IN INTERNATIONAL JOURNALS (SCI-Indexed)

1. V.K. Sharma, V. Kumar, R.S Joshi. Effect of addition on wear behaviour of an Al-6061 based hybrid composite. **Wear**, 2019, 426-427, 961-974. **(SCI; IF- 4.108)**.
2. V.K. Sharma, V. Kumar, R.S Joshi. Investigation of rare earth particulate on tribological and mechanical properties of Al-6061alloy composites for aerospace application. **Journal of Material Research & Technology**, 2019, 8(4), 3504-3516. **(SCI; IF- 5.289)**.
3. V.K. Sharma, V. Kumar, R.S Joshi. Experimental investigation on effect of RE oxides addition on tribological and mechanical properties of Al-6063 based hybrid composites, **Material Research Express**, 2019, 6(8), 1-38. **(SCI; IF -1.929)**.
4. V.K. Sharma, V. Kumar, R.S Joshi, D. Sharma. Experimental analysis and characterization of SiC and RE oxides reinforced Al-6063 alloy based hybrid composites, **The International Journal of Advanced Manufacturing Technology**, 2020,108, 1173-1187. **(SCI; IF -2.633)**.
5. V.K. Sharma, V. Kumar, R.S Joshi. Parametric study of Aluminum-Rare Earth based composites with improved hydrophobicity using Response Surface Method, **Journal of Material Research & Technology**, 2020, 9(3), 4919-4932. **(SCI; IF -5.289)**.
6. V.K. Sharma, V. Kumar, R.S Joshi. Investigation on Surface Roughness during Finishing of Al-6061 Hybrid Composites tube With Traces of Rare Earth Metals Using Magnetic Abrasive Flow Machining, 2019, **Advances in Unconventional Machining and Composites,** ISBN 978-981-329-471-4. **(Springer Procedia Non SCI)**.

PAPER PRESENTED IN INTERNATIONAL CONFERENCES

1. V.K. Sharma, V. Kumar, R.S Joshi, D. Sharma. Experimental analysis and characterization of SiC and RE oxides reinforced Al-6063 alloy based hybrid composites, 2020, 108, 1173-1187. 40th International **MATADOR** Conference on Advanced Manufacturing Hangzhou, China on 8-10 July 2019. **(SCI; IF -2.633)**.

2. V.K. Sharma, V. Kumar, R.S Joshi. Effect of addition on wear behaviour of an Al-6061 based hybrid composite. Wear (22nd International Conference on **Wear of Materials**, Miami Florida USA, 14-18 April, 2019), 2019, 426-427/961-974. **(SCI; IF- 4.108)**.

ABBREVIATIONS

MMC	Metal Matrix Composites
AMC	Aluminium Matrix Composites
DRAMC	Discontinuous Reinforced Aluminium Matrix Composites
REE	Rare Earths Elements
CeO_2	Cerium Oxide
UAV	Unmanned Aerial Vehicle
MAFP	Magnetic Abrasive Finishing Process
SEM	Scanning Electron Microscope
XRD	X-Ray Diffraction
EBSD	Electron Back Scattered Diffraction
EDS	Energy Dispersive Spectroscopy
RSM	Response Surface Methodology
AFM	Atomic Force Microscopy
CNC	Computer Numerical Control
REOs	Rare Earth Oxides
Nd	Neodymium
La	Lanthanum
Pr	Praseodymium
UTS	Ultimate Tensile Strength
CTE	Coefficient of Thermal Expansion
HV	Vickers Microhardness
wt%	Weight Fraction in %
$\Delta(R_a)$	Average value of Change in Surface Roughness
R_a	Average value of Surface Roughness
CIPs	Carbonyl Iron Particles
Er	Erbium
Zr	Zirconium

CHAPTER 1

INTRODUCTION

1.1 MOTIVATION FOR THE PRESENT WORK

A rapid development in engineering and technology demands a high accuracy as well as high precision in the development of the fragile components. Surface quality of the finished products is a very vital factor in the industries related to the field of automobile applications, aerospace applications and biomedical applications etc. A small burr or scratch may cause big loss to the industries such as energy loss in engine parts, fatigue failure of aerospace devices and malfunctioning of the components etc. In order to make the components free from any burr or scratch, industries are willing to spend more and more money. From the past four decades industries are using the traditional types of finishing processes like lapping, honing etc to get the required surface finish on the machine components. However due to their limitations to up to particular geometries and materials, these methods cannot be used for the finishing of complex and intricate shapes to get the required degree of surface finish. In order to nullify the effect of traditional methods, advanced finishing processes like magnetic abrasive finishing processes have been developed, which are used to machine difficult parts internally as well as externally in all types of materials including oxides and non-oxides based ceramics, MMCs, polymers and refractory materials etc.

1.2 INTRODUCTION TO COMPOSITE MATERIALS

Composite materials are composed of mainly two materials namely matrix and powder reinforcement. The purpose of matrix is to offer a satisfactorily level of performance to the composite structure by holding the fibres jointly and transmit the load to the fibres which finally stop the cracks formation. Reinforcement helps in the load carrying property of the composites. Almost every mechanical property from stiffness to strength and strength to thermal stability results of reinforcement type used in the composite materials. Advanced materials which are stronger, lighter and less expensive are specially required for the applications of the current engineering scenario. An example of this type of material which has good strength to density ratio and stiffness to density ratio appropriate for aerospace applications. Metal matrix composites (MMCs) have been emphasis mainly above properties used in engineering applications [Tjong, 2014; Rino et al., 2012]. Some of these property combinations are higher sintering temperature, high stiffness to density ratio, low coefficient thermal expansion, superior wear resistance, high strength to density ratio and adequate level of corrosion resistance [Alaneme and Bodunrin, 2011].

MMCs are very good substitutes of other metals and alloys because of very wide range of applications from aerospace to defence sectors, naval submarines and in sport items include golf sticks [Das et al., 2014]. MMCs are fundamentally any metal based alloys reinforced with the synthetic particulates of various ceramics. The very familiar metal based alloys include various light metals (Al, Mg and Ti). However, other metal based alloys mainly zinc (Zn), copper (Cu) and stainless steel can be used as better choice for producing composite materials. Generally, aluminium can be used as a better choice for matrix material in the growth of MMCs [Das et al., 2014]. Apart from above properties few issues have been reported by using the MMCs in the aviation application like low ductility and low toughness.

1.2.1 Challenges Related to Aluminium Matrix Composites (AMCs)

Metal Matrix Composites based on aluminium have some vital issues during their manufacturing. Generally the composites based on the discontinuous reinforced aluminium matrix (DRAM) connected mainly with the three issues. These are given below:

1) The cost of conventional ceramic particles reinforcing materials is very high and very inadequate supply of ceramic particles especially in rising countries like India has a foremost trouble connected with producing aluminium matrix composites having reinforcement of discontinuous nature [Oghenevweta, 2014].

2) Very poor ductility and little rupture toughness is a different setback linked among the AMCs [Oghenevweta, 2014].

3) Other problems allied with the AMCs relates to its incapability to calculate the corrosion behaviour [Oghenevweta, 2014].To rectify this problem, AMCs required embedded sensors and which is a costly affair.

1.2.2 How to Resolve these Problems Related with the AMCs?

By exhaustive study of literature survey, it is revealed that proper selection of particulate reinforcement and its weight percent play an incredibly role for the manufacturing of composites. This is a signal that particulate reinforcement plays a considerable function for the performance enhancement of the composites. Considering various available articles surveyed, it was analyzed that too many approaches have been adopted to improve the performance of AMCs.

The third approach as shown in figure 1.1 gives opportunity for producing AMCs having less cost with better performance characteristics optimization. Few researchers have reported comparable or superior performance characteristics of hybrid AMCs over single reinforced particulate AMCs even the price of processing was less [Shivaraja and Kumar, 2014].

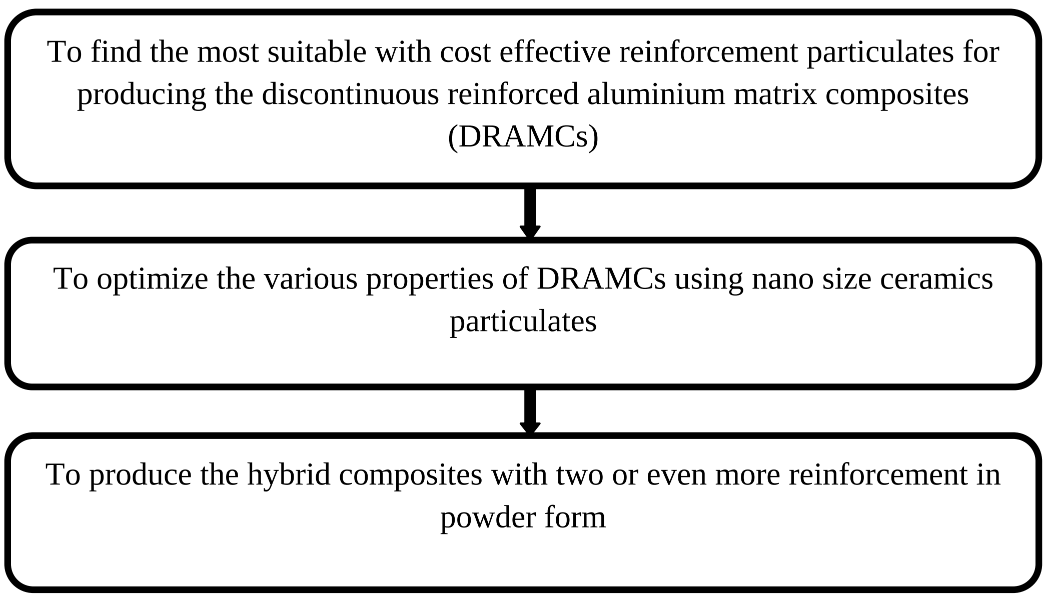

Figure 1.1 Approaches used for Performance Optimization [Shivaraja and Kumar, 2014]

The above mentioned approach of producing hybrid reinforced AMCs anticipate the enormous guarantee of emergent performance as well as low cost MMCs through this path. Thus researchers are trying to use diversified grouping of powder reinforcement synthetic materials for synthesize the hybrid AMCs and its effects on performance of developed AMCs.

1.2.3 Reinforcement Particulates used in AMCs

Ceramic particulates made by synthetic methods, large amount of waste produced by industries and various waste of agricultural crops etc generally used as particulate reinforcement in the development of AMCs. Reinforcement particulates properties plays a very significant role along with the matrix alloy for producing the suitable hybrid composites targeted for a specific applications [Alaneme and Aluko, 2012]. Design analysis of AMCs mainly depends upon the parameters which are mostly affected by the type of particulate reinforcement to be used composites. These parameters include particulate reinforcement type, particulate dimension, its profile, hardness and allocation in matrix etc.

Based on the research articles, it was found that hybrid AMCs is divided into three groups based on the different combination of reinforcement as shown in figure 1.2.

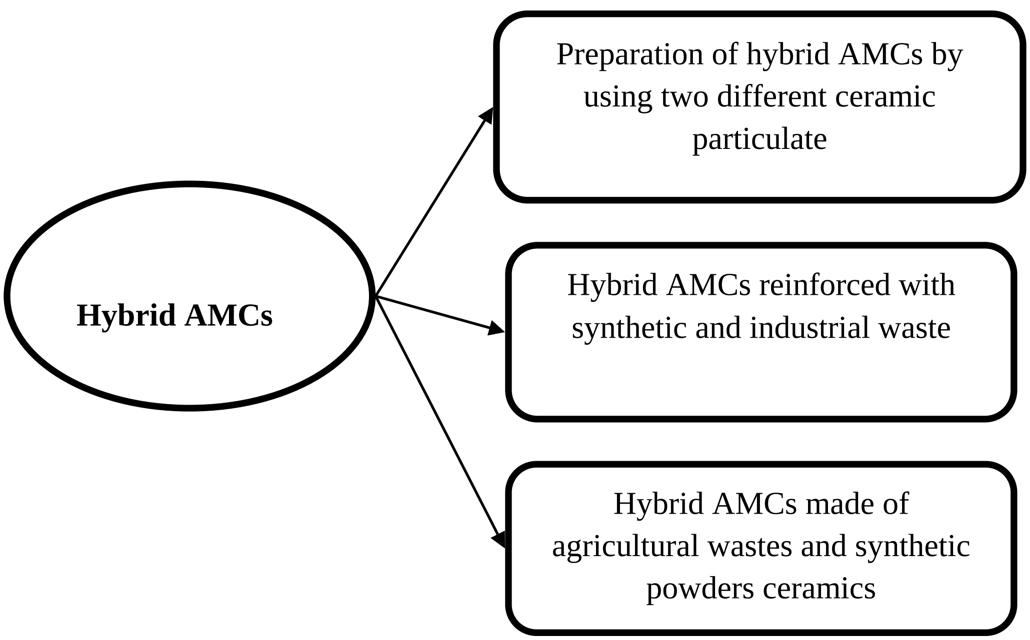

Figure 1.2 Hybrid AMCs Based on Different Combinations of Reinforcement [Alaneme and Aluko, 2012]

Hybrid composites reinforced with ceramic materials have been consistently used in aerospace applications because of performance optimization and less consideration on cost. Out of various synthetic particulates, silicon carbide and alumina are mostly utilized.

1.2.4 Rare Earth Elements-Lanthanides

Rare earths elements (REEs) (called “lanthanide series elements”) are a series of chemical elements (refer figure1.3) found in the third subgroup in the periodic table. This subgroup consists of 15 elements having atomic number varies from 57 to 71. Rare earths (REs) elements have been increasingly used in every sector of engineering field due to their high strength at room temperature, good thermal conductivity, excellent magnetic properties, usability in miniaturization products, thermal stability and mechanical properties.

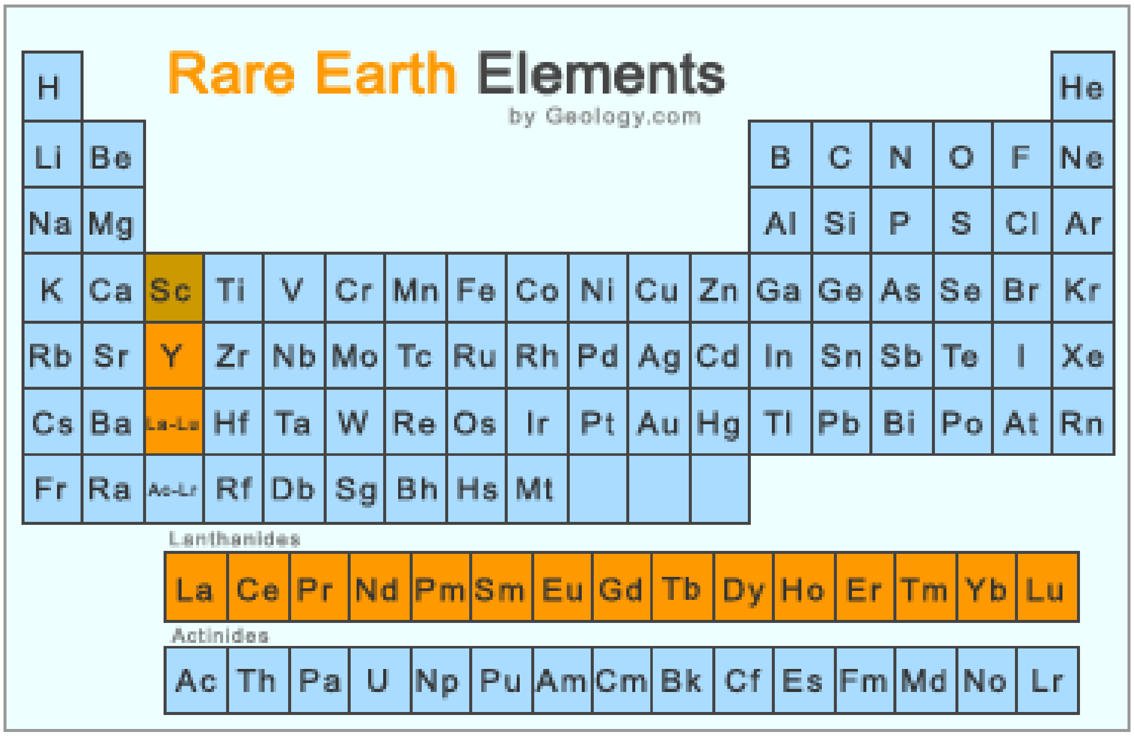

Figure 1.3 Rare Earth Elements Location in Periodic Table (Courtesy: Geology.com)

The rare earth particulates may be a good choice in order to improve the properties of hybrid composites due to their unique properties as shown in figure 1.4. It was found that by adding the rare earth particulates leads to ductility and strength improvement in various composites that are used in aerospace applications [Li et al.,2002; Guo et al.,2012; Wang et al.,2011; Xihua et al.,2008; Torre et al.,2013; Chai et al.,2009]. Recently rare earth particulates are widely used in the aerospace industries which are making new generation predator drones, unmanned aerial vehicle (UAV) and other defence purposes unmanned vehicles.

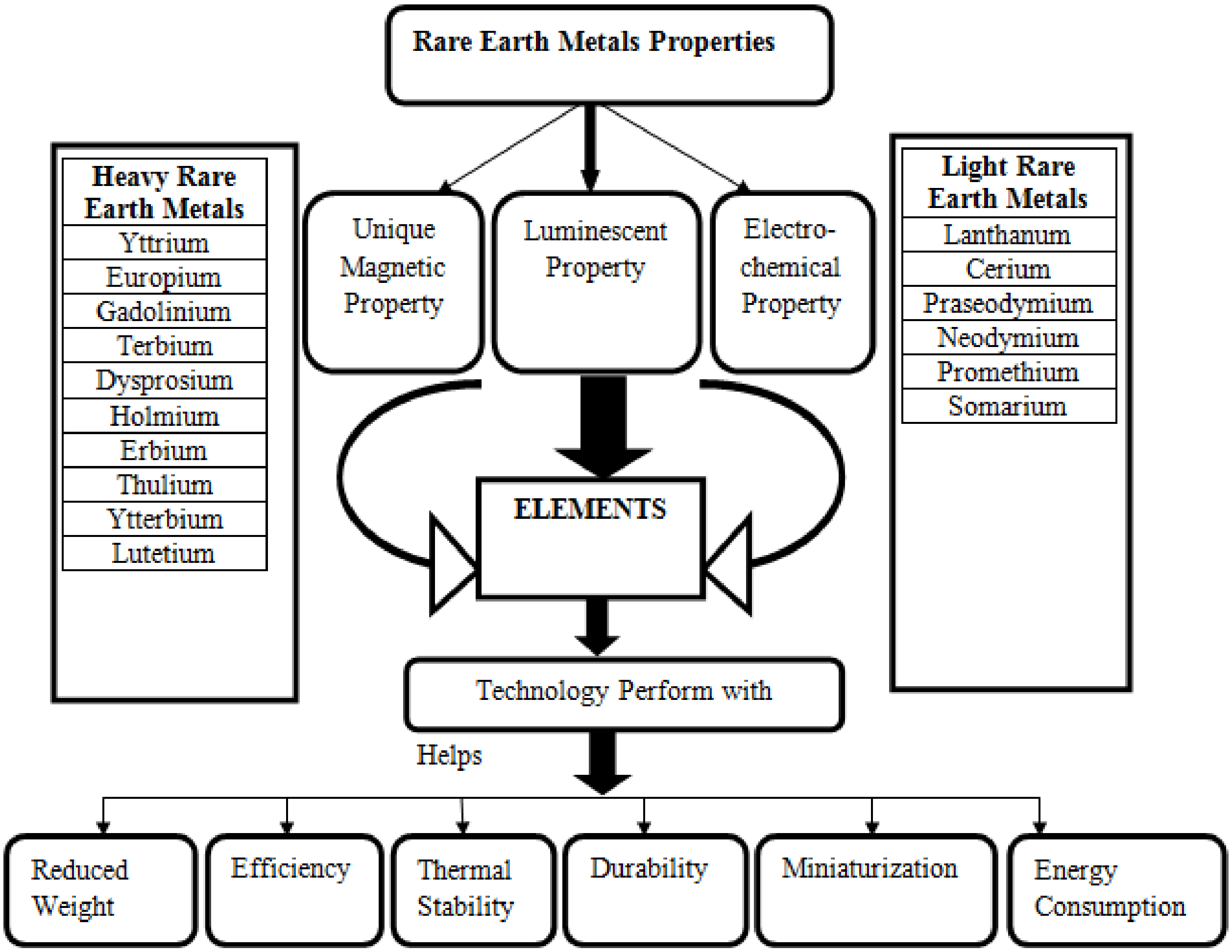

Figure 1.4 Rare Earth Metals Types and Their Properties [Li et al., 2002; Guo et al., 2012]

1.3 INTRODUCTION TO MAGNETIC ABRASIVE FINISHING PROCESSES

The life of product is very much affected by their surface textures that include its lay, roughness and waviness [Kenton, 2009]. The thrust on various finishing processes increased continuously due to the rise in demand of miniaturize products with micro to nano level finish. In addition, the expansion of new kind of materials also leads to demand of advanced finishing processes. Out of the existing finishing processes, magnetic abrasive flow machining processes are gaining much importance due to the better surface finish capability with least damage to the surface. Another reason is getting attention by researchers towards magnetic abrasive based finishing processes due to its ability of controlling the finishing forces during process of finishing [Jain, 2009].

1.3.1 Working Principle of Magnetic Abrasive Finishing Process (MAFP)

The principle of working of magnetic abrasive flow machining process is totally different as compared to conventional abrasive flow machining process. The abrasive particles (Diamond, Aluminum Oxide (Al_2O_3) and Silicon Carbide (SiC) etc.) with sharp edges are mixed with the slurry of ferromagnetic particles to form a uniform mixture. During the finishing process, uniform mixture of slurry along the magnetic field direction forming a flexible magnetic abrasive brush. The flexibility of the brush can be altered by adjusting the magnetic field generated by a permanent or alternating magnet system. The brush used as a multi-point cutting tool for finishing process because it has the ability to modify itself according to surface contours. The friction between the abrasive and the finish surface are overcome by the use of strong magnetic field and surface finish occurs due to the motion of abrasive brush. In this process, ferromagnetic particles sintered with above mentioned non-metallic abrasives (diamond, Al_2O_3, SiC, or CBN) and such particles are called magnetic abrasive.

The finishing mechanism of magnetic abrasive finishing process is depends upon the amount of force generated by the magnetic field. Figure 1.5(a) and figure 1.5(b) show the two dimensional distribution of magnetic field and its amount on the ferromagnetic particles. It is clear from the figure 1.5(a) that the force ‘F’ is the value of magnetic force intensity on the ferromagnetic particles (A) due to magnetic field. The value of magnetic force intensity can be further resolved into two parts say Fx and Fy.

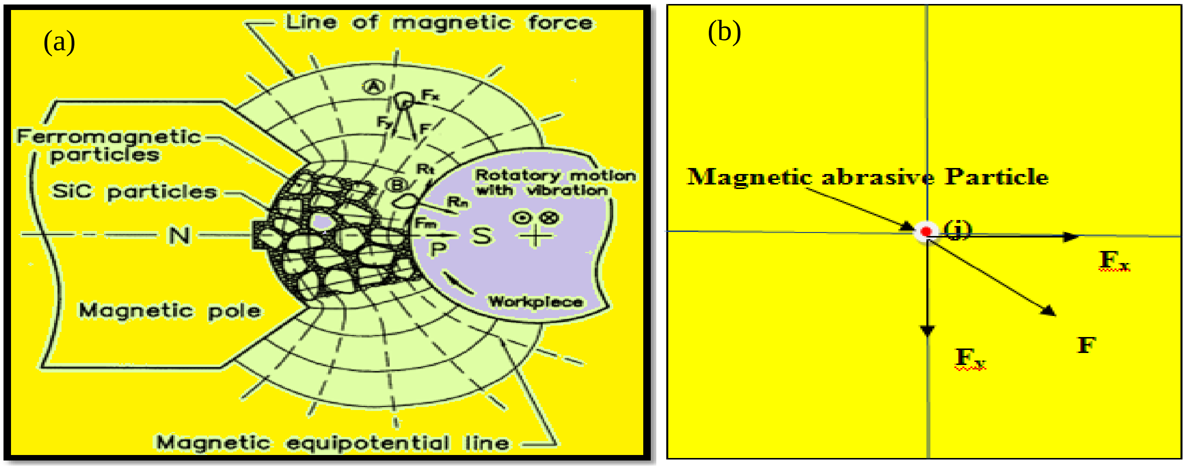

Fig 1.5 Mechanism of MAFM Process (a) Distribution of Magnetic Field (b) Magnetic Force Acting on Ferromagnetic Particle [Yamaguchi et al., 2007]

The intensity of magnetic force (F) which acts on the single volume of magnetic abrasive particle at the position " j" which is generally situated at the outside of the working zone can be written as:

$$\boldsymbol{F = V_0\, B\nabla B/\mu} \quad \text{...} \quad \textbf{Eq. (1.1)}$$

B is the magnetic induction and ∇B is the Gradient of magnetic induction at the 'j' position of the abrasive particles. It was found that the magnetic permeability of the magnetic particles used in the MAF process have larger value as compared to the permeability of free space i.e. ($\mu>\mu_o$). Hence the value of magnetic force in equation (1.1) can be resolved into two dimensional magnetic field distribution equations as written below:

$$\boldsymbol{F_x = V_0 \quad X_m\, \mu_o \mathrm{H}\frac{\partial H}{\partial x}} \text{...} \textbf{Eq. (1.2)}$$

$$\boldsymbol{F_y = V_0 \quad X_m\, \mu_o \mathrm{H}\frac{\partial H}{\partial y}} \text{...} \textbf{Eq. (1.3)}$$

Component of magnetic force in x-direction is F_x and in y-direction is F_y. Volume of the magnetic particle is denoted by V_0. X_m is the magnetic susceptibility of the magnetic particles and permeability of free space is μ_o. Magnetic field strength at point 'j' is given by H. The values of magnetic gradient in x and y directions indicated by $\frac{\partial H}{\partial x}$ and $\frac{\partial H}{\partial y}$.

It is observed from the equations 1.2 and 1.3 that the magnetic force in x and y directions is proportional to the volume of the abrasive particles, magnetic susceptibility, strength of magnetic field and magnetic gradients in x and y direction. The values of magnetic force in x and y direction helps to prevent the splashing of magnetic particles in the finishing process of the parts which are generally caused by the value of high speed of rotation of magnetic poles.

In the finishing process of MAF technique, large number of magnetic abrasive particles in the direction of magnetic lines of force forming a flexible magnetic abrasive brush inside the working region, which ultimately causes the pressure 'P' on the free form surface and this pressure will act on the work surface to remove the burr or scratch on it. The value of pressure 'P' is given by

$$\boldsymbol{P = \left[\mu_o \; H^2 \left(1 - \frac{1}{\mu_m}\right)\right] / 2} \qquad \textbf{Eq. (1.4)}$$

In equation (1.4), μ_m represents the relative magnetic permeability of the magnetic abrasive particles.

1.4 OBJECTIVE OF THE STUDY

The objectives of the present work are given below:

1. Preparation of hybrid composites with traces of rare earth metals using stir casting process and mechanical and metallurgical characterization of samples prepared for the experimentation work.
2. To investigate and optimize the effect of various process parameters on performance characteristics of Magnetic Abrasive Flow Machining process.
3. To study the surface morphology of finished hybrid composites using Magnetic Abrasive Flow Machining process.

1.5 SCOPE OF WORK

The work has been limited to Magnetic Abrasive Flow Machining of hybrid composites as work material under the different experimental conditions by varying the process parameters (magnetic flux density, no of cycles, extrusion pressure, size of abrasive particles and working gap) using suitable optimization technique. The results obtained have been modelled for their application in aerospace industry because of their great potential for the production of light weight and structurally efficient aerospace components.

1.6 PHASES OF RESEARCH

- Literature review
- Preparation of hybrid composites using Bottom Pouring Stir Casting technique
- Mechanical, Surface, Metallurgical, Structural and Chemical characterization of Prepared hybrid composite samples
- Surface finishing of hybrid composites using Magnetic Abrasive Flow Machining process
- Design of Experiment
- Experimentation Work
- Optimizing the results

1.6.1 Preparation of Hybrid Composites Using Bottom Pouring Stir Casting Technique

Al-6061 based hybrid composites were prepared by stir casting method with different weight percent composition of SiC and Al_2O_3 as reinforcements and traces of CeO_2 as rare earth particulate. The total weight of each Al-6061 alloy/Al_2O_3 /SiC/CeO_2 composite was maintained at 900 gm.

1.6.2 Mechanical, Surface, Metallurgical, Structural and Chemical characterization of Prepared Hybrid Composite Samples

The mechanical properties of the hybrid composite samples were characterized by conducting hardness, tensile and percent-age elongation tests, wear test and impact test. The metallographic characterization was done using scanning electron microscopy (SEM) and Electron back scattered diffraction (EBSD). The chemical characterization or elemental analysis was generally done using as analytical technique called Energy dispersive spectroscopy (EDS). For structural characterization of the hybrid composite samples, X-ray diffraction (XRD) technique has been used.

1.6.3 Surface Finishing of Hybrid Composites Using Magnetic Abrasive Flow Machining Process

During the magnetic abrasive flow machining process, the mixture of abrasive particles and ferrous particles is pushed against the inner surface of hybrid composites under the influence of magnetic field. Due to the relative motion between the abrasive and work surface of composites resulted in increase of material removal rate. The increased MRR ultimately leads to good surface finish of the composites.

1.6.4 Design of Experiments

For designing and planning of the experiments, response surface methodology has been implemented. To explore the influence of various process parameters viz. magnetic flux density, no of cycles, extrusion pressure, size of abrasive particles and working gap on the response surface roughness, pilot experiment was carried out before designing the final experimentation. Outcome of pilot experiments were used as a basis for selection of process parameters with various levels for the plan of main experiments in MAFM process. One-factor-at-a-time approach was used to conduct pilot experiments.

1.6.5 Experimentation Work

The experimentation has been done on magnetic abrasive flow machining set-up on hybrid composite (Al-6061 matrix reinforced with $SiC/Al_2O_3/CeO_2$) as work material, so as to find out the impact of following machining parameters on surface quality.

1. Magnetic flux density
2. Number of cycles
3. Extrusion pressure
4. Size of abrasive particles
5. Working gap

1.6.6 Optimization of Results

The results obtained have been optimized using desirability approach.

1.7 ORGANIZATION OF THESIS

The thesis is presented in six chapters. The brief explanation of the all the chapter's contents has been given below:

Chapter 1 contains an **"Introduction",** about the motivation for the current research work related to fabrication of Al-6061 matrix hybrid composites with rare earth oxides. The salient features of composite materials with various combinations of reinforcement materials, various challenges associated with the aluminium matrix composites and remedies to rectify these challenges have been discussed. A brief introduction of rare earth elements has also been discussed with various applications. Various aspects of MAFM process, including its working principles have also been included. Objectives, scope and overall methodology of the work have also been described.

Chapter 2 describes the **"Literature review"** to present the contributions of different researchers while fabrication of ceramic reinforced aluminium hybrid composites via liquid processing technique. It also contains detailed literature review on the research work reported in the past by various researchers in the field of MAFM process. This chapter also includes the surface integrity aspects of MAFM surface which depend upon surface topography and surface metallurgy. Gaps in the literature have also been identified. Literature review also presents a discussion on various optimization techniques used by many researchers.

Chapter 3 presents **"Formulation of Problem"** of the present research work. The present research work is carried out on the rare earth based hybrid composites with SiC and Al_2O_3 reinforcement targeted for aerospace applications. It was reported that aluminium alloys have lack of tailored properties like poor wear resistance, low hardness, low corrosion resistance and poor hydrophobicity while used in the aircraft parts where fluid is flowing under pressure. Actuators, control surfaces, O-rings and landing gears are the components of aircraft where the surface required with good finish, so that the self cleaning actions occur automatically due to good hydrophobicity. Therefore the introduction of secondary phase into the aluminium alloy is required. REOs, SiC and Al_2O_3 were found to be used as secondary phase for enhancing the properties of aluminium alloy. Finally, aluminium hybrid composites were fabricated after addition of REOs, SiC and Al_2O_3. The wear resistance and hardness of the aluminium alloy is improved with the addition of SiC and Al_2O_3 reinforcement. Generally, it has been reported by many researchers that REOs have excellent hydrophobicity due to its intrinsic hydrophobic behaviour.

Chapter 4 deals with **“Experimental Procedure”** presenting the experimental details of fabrication of hybrid composites via bottom pouring stir casting route. The hybrid composites are fabricated with different wt% of Al_2O_3, SiC and CeO_2. Microstructural studies are carried out to reveal the effect of alumina, silicon carbide and cerium oxide on the hybrid composite. Polished and etched hybrid composite specimens are observed using scanning electron microscopy (SEM) and electron back scattered diffraction (EBSD). The grain size and distribution is observed by the morphology test. Structural characterization using X-ray diffraction (XRD) revealed the presence of cerium, aluminium and silicon in the hybrid composites. The elemental analysis is carried out by energy dispersive spectroscopy (EDS) that revealed successful addition of various reinforcement elements in the composites. The mechanical characterization involves the microhardness testing, tensile testing, flexural strength and impact strength analysis. Physical characterization involves density and porosity determination. Wear testing using pin-on-disc configuration was performed on hybrid composites at room temperature. The dominant wear mechanism was studied using SEM and EDS analysis of worn surfaces and wear debris. Wettability behaviour analysis of aluminium hybrid composite samples surface was studied using sessile drop shape analyzer. Surface quality of the hybrid composites samples finished using MAFM process with the following process parameters; like magnetic flux density, number of cycles, extrusion pressure, size of abrasive particles and working gap has been analysed. The relationships between different machining parameters (magnetic flux density, no of cycles, extrusion pressure, size of abrasive particles and working gap) and machining characteristics (Surface quality) have been established using Box-Behnken design. The theoretical aspects of model adequacy building and checking using regression analysis are also discussed. The parametric influence on response measures was determined using surface plots. Optimization of process parameters using desirability approach is then presented. Thereafter, results of confirmatory experiments are presented. The surface integrity of machined surfaces was also analyzed through atomic force microscopy. AFM analysis was used for quantitatively measuring the surface roughness of hybrid composites.

Chapter 5 reports **"Results and discussions",** from the various formulated experiments. The microstructural analysis reveals uniform distribution of aluminium oxide, silicon carbide and cerium oxide in the matrix of Al-6061 alloy. The unwanted products formation due to interfacial reaction are not seen signifying strong bonding of reinforcement particles with the matrix alloy after addition of REOs. Finer morphology of the matrix is observed after incorporation of cerium oxide within range of 0.5 wt% to 2.5 wt%.

The UTS value has increased from 28 MPa to 123 MPa after addition of 2.5wt% of cerium oxide and 7.5 wt% of ($SiC+Al_2O_3$). The highest percentage elongation was observed at 2.5 wt% of cerium oxide. Vickers microhardness has increased with the increase of cerium oxide percentage from 0.5 wt% to 2.5 wt%. Impact strength has increased with the increase of cerium oxide percentage from 0.5 wt% to 1.5 wt% and thereafter decreased with further increase to 2.5 wt%. Flexural strength value has increased from 340 MPa to 615.6 MPa after addition of 2.5 wt% of cerium oxide and 7.5 wt% of ($SiC+Al_2O_3$).

Wear behaviour of the hybrid composites samples with hemispherical pin shaped has been determined in terms of wear volume losses. The better wear resistance was observed at 2.5 wt% of cerium oxide corresponding to normal load of 10N and sliding velocity 0.5m/s. Wear tracks and wear debris were analyzed under SEM and EDS. The hydrophobicity behaviour of the hybrid composites has been improved after addition of cerium oxide. Improvement in hydrophobicity was observed due to large contact angle. At last the finishing of the hybrid composites has been done with MAFM process. The Box-Behnken design approach has been used to optimize the process parameters for response surface roughness. The optimum value of change in surface roughness of Al-6061 hybrid composites was observed to be 1.03 μm with percentage improvement in surface finish of 68.2 %. This percentage improvement was observed at magnetic flux density of 0.75 Tesla, numbers of cycles 172 and extrusion pressure 4.13 MPa. The surface integrity of machined surfaces has been analyzed through atomic force microscopy.

Chapter 6 contains the major **"Conclusions"** from this present research work and provides suggestions for future work in the chosen subject.

CHAPTER 2

LITERATURE REVIEW

2.1 INTRODUCTION

The literature review is carried out as a part of the thesis work to provide an overview on the fabrication of Aluminium hybrid matrix composites (AHMC's). This section also deals with the metallographic, structural, elemental and mechanical characterization on various aluminium hybrid composites carried out in the past. Some discussion about constituent morphology, tribological behavior analysis, hydrophobicity analysis and corrosion analysis done by various researchers is also summarized. Finally, finishing of hybrid composites via magnetic abrasive flow machining process (MAFM) and optimization of process parameters using various response surface methodologies are discussed in detail. Various aspects associated with fabrication of AHMC's using stir casting technique and advantages offered by stir casting fabrication routes against solid metallurgical processing routes have been presented. Morphology including shape and size of aluminium oxide powder, silicon carbide powder and rare earth oxides (REOs) has been discussed. The morphology of base alloy and prepared composites, its composition, structural details, characterization and application areas also has been discussed. Development of hybrid aluminium composites reinforced with silicon carbide, aluminium oxide and rare earth oxides (REOs) has been reviewed chronologically to offer a comprehensive understanding of fabrication methods and properties assessment of the metal-matrix composite interface. Finishing of hybrid composites via MAFM process and optimization of process parameters has been reviewed to see the effect of various parameters such as magnetic flux density, extrusion pressure, number of cycles, working gap, weight percent of abrasive particles, rotational speed and process time on response surface roughness.

The literature review of the thesis work is divided into three sections. The first section deals with fabrication of aluminium hybrid matrix composites using various powder particulates via stir casting technique. Second section highlights mechanical characterization, metallographic characterization, tribological characteristics and hydrophobicity analysis along with the corrosion testing. Third section deals with finishing of aluminium alloy and aluminium hybrid matrix composites via MAFM process in the past. All aspects related to MAFM optimization of process parameters on response surface roughness have been discussed in details using various optimization techniques by various researchers. Finally objectives of the present work have been formulated after identifying gaps existing in the literature. The detailed literature review is presented here:

2.1.1 Fabrication of Hybrid Composites via Stir Casting Technique using Different Particulate Reinforcement

In this method of composite fabrication, reinforcements (ceramic particles and short fibers) are mixed with a molten matrix metal by means of mechanical stirring. This section presents the contribution of various researchers in the area of fabrication of aluminium alloy based composites with different combination of reinforcements via stir casting route. Since in the present work, the route followed to manufacture the composite was stir casting, only that method is explained here.

2.1.1.1 Stir Casting

In stir casting technique, the ceramic particulates put into the aluminium melt and allowed to solidify it. Proper wetting between the aluminium melt and particulate reinforcement is the crucial thing taken care. The stir casting technique is also known as vortex technique because it involves the introduction of pre-heated powder particulates into the vortex of the molten alloy by means of rotating impeller. Lloyde reported that vortex mixing techniques for the fabrication of aluminium matrix composites reinforced with ceramic particle was originally developed by Surappa & Rohatgi (1981) at the Indian Institute of Science. Afterward numerous aluminum companies further refined and modified the processes which are at present employed to manufacture a variety of AMCs on commercial scale.

The different sizes of particulate reinforcement used in AMCs have different role in the matrix. The purpose of nano-particles dispersed over matrix is to offer a satisfactorily level of performance to the composite structure by holding the fibers jointly and transmit the load to the fibers which finally stop the cracks formation. Nanoparticles not only help in the load carrying property of the composites but also maintain the ductility of the matrix alloy [Mao et al., 2015] The particulate reinforcement having micro level improved the hardness, stiffness and wear characteristics of composites by sustaining the matrix skeleton. The overall performance improvement of the composite depends upon the integrated utilization of nano and micro sizes particulates with better synergy. It was further stated that if the particulate reinforcement of micro level increased by weight percent above 30% in AMCs during fabrication or in service condition leads to the creation of little voids and cracks. These defects cause brittle fracture under low tensile loads. Ultimately leads to loss in strength, low ductility and low toughness properties of ceramics particulates used in various structures. This problem can be further reduced by making the composites with higher content of nano particulates reinforcement as compared to micro size particulates [Yang et al., 2004]. To achieve the better properties of composites, it is essential to properly mix the nano particulates in the matrix material so that perfect bonding formed between them.

2.1.1.2 Advantages of Liquid State Processing

The main advantages associated with liquid state processing techniques include large scale of process capability, less requirement of infrastructure in foundry and very low cost of production [Kandpal et al., 2018]. Apart from these advantages, few limitations are also associated with the fabrication of composites via stir casting route. The major limitations included insufficient wetting of the reinforced particles into the melt and lack of homogenous dispersion of the ceramic particles. Some of the researchers also observed various structural defects in the prepared composites like large porosity, clustering of particles , various inclusions in the form of oxides and reactions occur between interface of reinforcement and matrix results due to inadequate casting machinery [Lloyd ,1994; Samuel et al., 1993].

In spite of above mentioned limitations, among the various techniques available for fabrication of hybrid composites as indicated by figure 2.1, liquid metallurgical processes have been leading consistently due to their simplicity, economy and scalability for large volume production. Table 2.1 clearly indicates the Liquid Metallurgy is the best method of fabrication of powder reinforced composites while comparative analysis of different methods of fabrication.

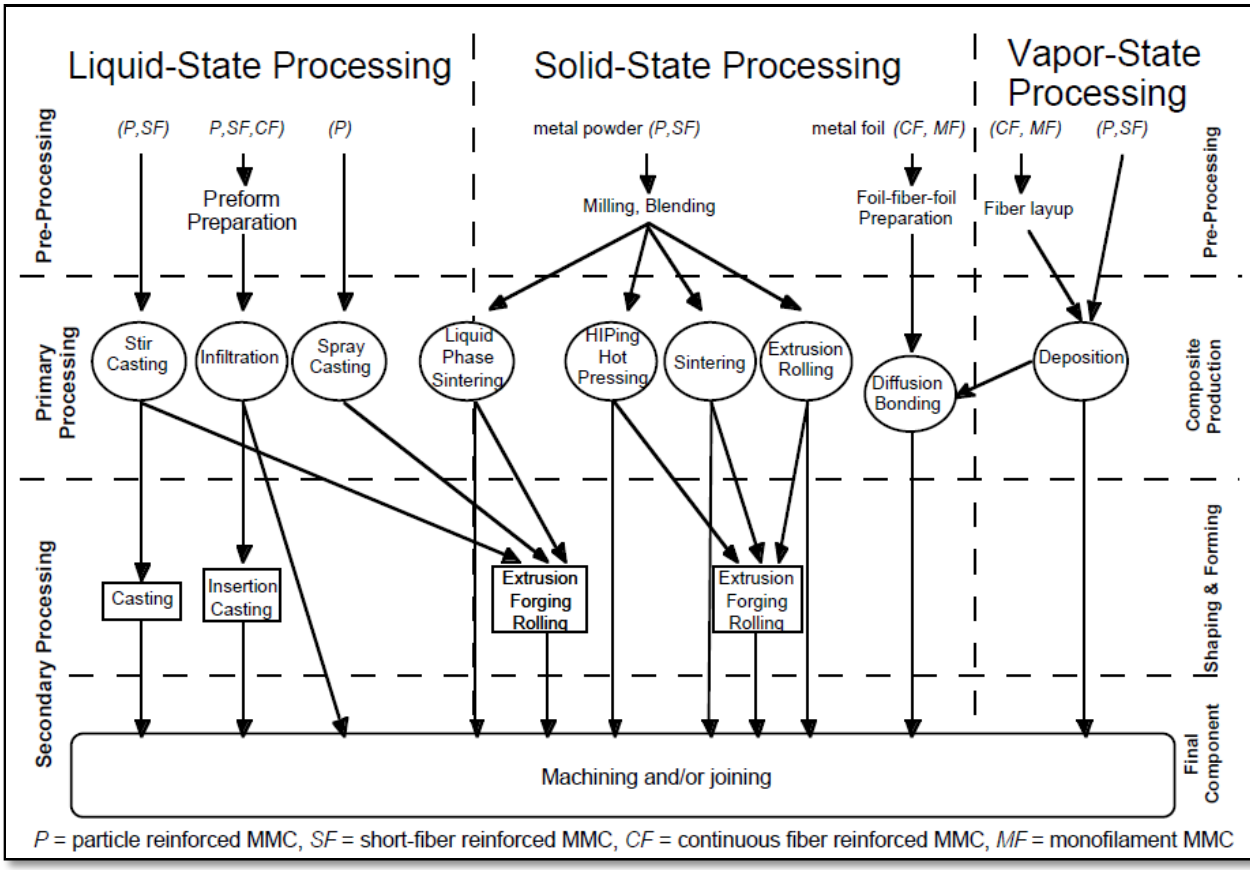

Figure 2.1 Various Processing Routes for Fabrications of MMCs [Clyne, 2001]

Table 2.1 Comparative analysis of various methods of fabrication of composites [Clyne, 2001]

Method	Range of Shapes and Sizes	Metal Yield	Range of Vol. Fraction	Damage to Reinforcement	Cost
Liquid Metallurgy	Wide range of shapes, large sizes up to 500 Kgs	Very High greater than 90%	Up to 0.3	No damage	Least Expensive
Squeeze Casting	Limited by perform shapes, up to 20 cm height	Low	Up to 0.45	Severe damage	Moderate Expensive
Powder Metallurgy Processing	Wide range, Restricted size.	High	Up to 0.4	Reinforcement fracture	Expensive
Spray Casting	Limited shapes, large size.	Medium	-	-	Expensive

2.1.2 Characterization of Prepared Aluminium Composites via Stir Casting

2.1.2.1 Characterization of Hybrid AMCS with two Different Synthetic Ceramic Particulate

From the experimental study, it has been seen that for design of aluminium matrix composites with good characterization behaviour a careful selection of secondary (or reinforcement) phase is required. Generally, the aluminium metal matrix composites with low value of coefficient of thermal expansion (< $13x10^{-6}$ K^{-1}), high dimensional stability (limit of relaxation>30MPa) and high wear resistance requires a secondary phase with low value of coefficient of thermal expansion. Mostly ceramics like SiC, Al_2O_3, B_4C, TiC, TiB_2, MgO and TiO_2 as secondary phases must be added in optimum quantity to reduce the value of coefficient of thermal expansion of composites. As the amount of secondary phase exceeds from the optimum quantity, it results in lowering the relaxation ability (ability to resist micro-plastic deformation) and ultimately leads to lowers the dimensional stability of composites. Proper balancing between these two factors is to be taken care while fabricate the composite with above tailored combination of properties (ASTM Handbook on composites Vol 21, P 845). Many researchers have carried out efforts to study the various characterizations of prepared composites on the basis of mechanical characterization, metallographic characterization and surface characterization. The related contribution is discussed below:

[Alaneme et al., 2019] fabricated Al-Mg-Si alloy composites reinforced with steel, graphite and silicon carbide particles having mean particle size of 100 μm, 30 μm and 30 μm by stir casting process. The hardness increased by 11% after addition of 4 to 8 wt% of steel particles. The hardness value of composites decreased by 3.2 % after addition of 8 wt% of SiC particles. Wear rate of the composite decreased with the use of steel and graphite reinforcement. The wear rate improved significantly after the addition of SiC particles. Abrasive wear was observed as most prevailing mechanism in the composites.

[Rana et al., 2014] optimized the wear performance of Al-5083 alloy matrix composites reinforced with 10 wt% SiC using Taguchi method. The wear behavior of the composites prepared has investigated under dry sliding wear condition. Taguchi method of optimization confirmed that applied load has the highest influence on wear rate followed by sliding distance and sliding speed.

[Kumar et al., 2014] fabricated aluminium MMCs using Al-2219 as base alloy reinforced with B_4C/MOS_2 and observed the effect of reinforcement on mechanical properties of the alloy. The density and hardness of MMCs increased after incorporation of B_4C and MOS_2. The UTS and yield stress decreased after addition of MOS_2 in increased amount. The decreased in the UTS of the composites primarily due to the formation of voids as well as nucleation sites formed in the matrix around the reinforced particles. The SEM images (figure 2.2) of Al-2219 fractured surfaces showed dimple patterns & the fractured surfaces of hybrid composites consist of both dimple patterns and tear ridges; this again showed the ductility and brittle fracture of mixed mode.

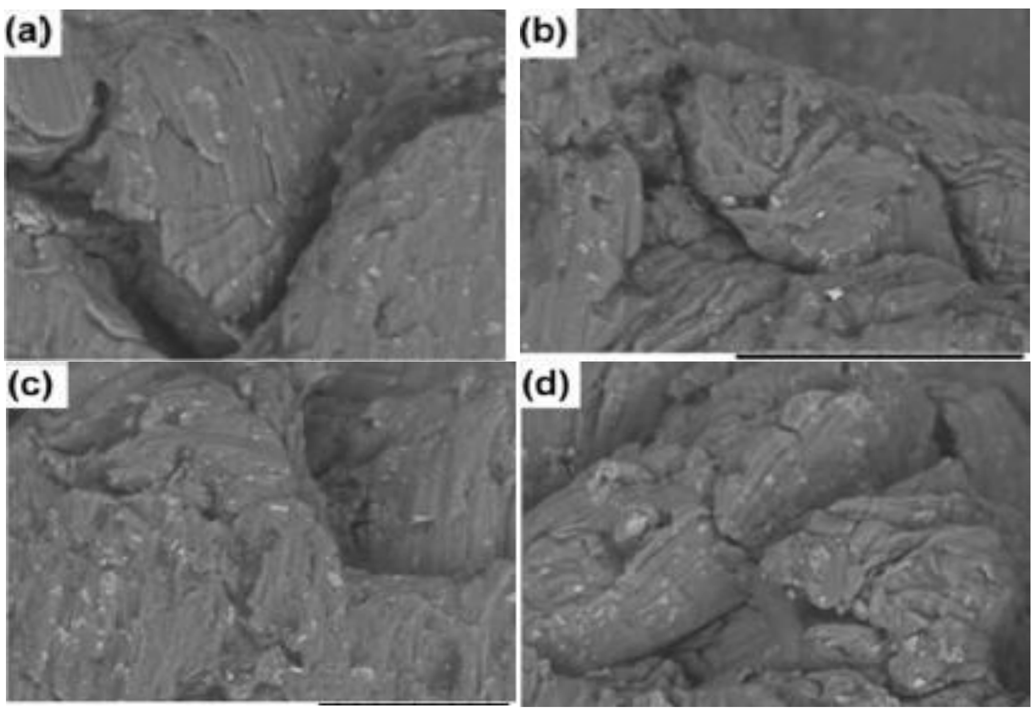

Figure 2.2 SEM Micrographs of fractured surface of (a) Al alloy (b) Al+3% B_4C +3% MOS_2 (c) Al+3% B_4C +4% MOS_2 (d) Al+3% B_4C +5% MOS_2 [Kumar et al., 2014]

[James et al., 2014] prepared a composites reinforced with titanium di-boride (TiB_2) and silicon carbide (SiC). Results showed that hardness and tensile strength increased with addition of 10 percent of SiC by weight and changing the composition of TiB_2 from 0 to 2.5 wt%. It was reported a decrease in hardness and tensile strength with further addition of TiB_2 up to 5 wt%. The decreased in hardness and tensile strength as reported primarily due to the increased in porosity as suggested by SEM.

[Singh and Goyal, 2017] fabricated AA6082/SiC/B_4C particle reinforced composites with mean particle size 35 μm by conventional stir casting process. The hardness of the composite increased with the addition of 5, 10 and 15 wt% of (SiC+ B_4C) as reinforcement. The increased in hardness was observed due to the intrinsic hard nature of the reinforcement particles. It was reported a decrease in hardness with addition of 20 percent of (SiC+ B_4C) by weight due to the formation of clustering into the matrix. The impact strength of the composite decreased with the increased in wt% of the reinforcement. The ultimate tensile strength increased from 318 to 385 MPa with 15 wt% of (SiC+ B_4C) particles. The increased in tensile strength have reported primarily due to the uniform dispersion of the reinforcement particles in the matrix.

[Selvam et al., 2013] used fly ash with 7.5 wt% along with SiC with weight percent varied from 7.5 to 10 % as reinforcement and Al-6061 alloy as base material to form AMC. The micro-hardness, macro-hardness and tensile strength improved significantly with the addition of mixed amount of fly ash and silicon carbide particles. SEM images of composites have depicted the homogenous dispersion of fly ash and silicon carbide into the aluminium melt resulted in a better microstructure evolution.

[Madheswaram et al., 2015] aimed to develop light-weight aluminum-boron carbide composite with Al-6063 as matrix alloy and evaluated the mechanical properties with the effect of addition of calcium carbide as additive. Tensile strength, shear strength and toughness of the fabricated composites improved significantly with the addition of boron carbide and calcium carbide. The addition of calcium carbide resulted in the formation of light weight composites which again used as a good candidate material for aerospace and automobile applications

[Parabhakar et al., 2014] measured the wear rate of aluminium composite reinforced with boron carbide under dry sliding condition. Results delineated that both coefficient of friction and wear reduced with sliding distance and velocity and increased with load. Afterwards worn out surfaces were analyzed using scanning electron microscope and observed that severe delamination occurred as applied load increases from 10N to 30N.

[Pal et al., 2015] prepared aluminium matrix composites reinforced with nickel via stir casting route. Initially the composite specimens with Ni compositions of 10, 20, 30 and 40 weight percentage were fabricated and then tested. The BHN value of the composite increased by 14.80%, Rockwell hardness increased by 2.43%, ultimate tensile strength increased by 1.003% and thermal conductivity decreased by 24.98% as compared to aluminum alloy at optimum value of 20 wt% nickel.

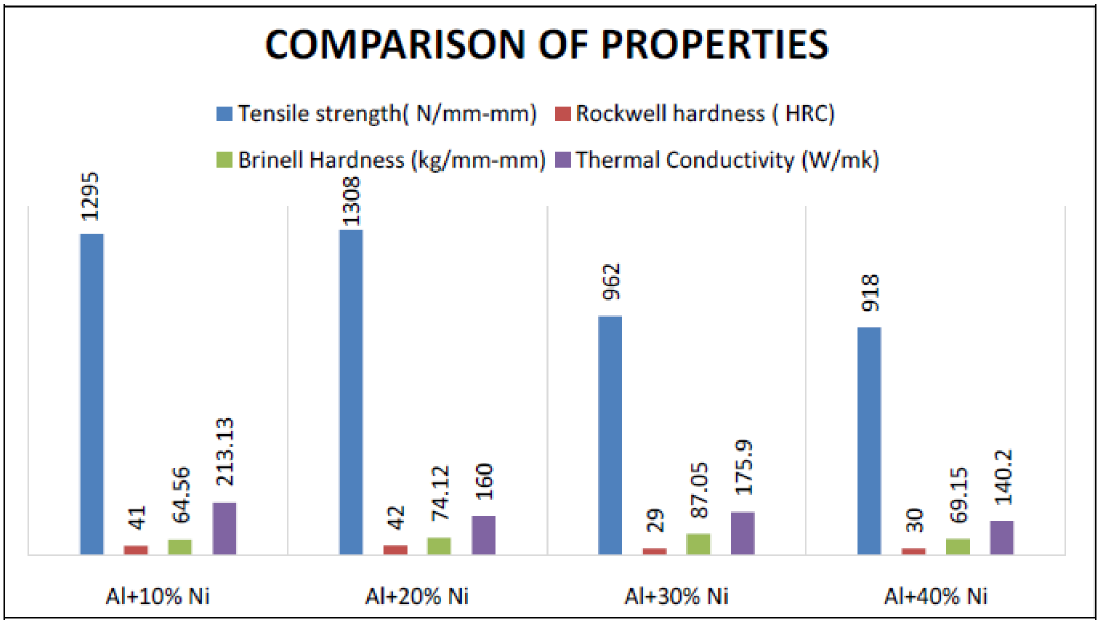

Figure 2.3 Graph showing the properties of composites in a nutshell [Pal et al., 2015]

[Prakash et al., 2016] investigated wear as well as mechanical behavior of Mg/SiC/Gr hybrid composites. The micro-hardness increased up to 80 HV after addition of 10 wt% SiC. Hardness of the composites was found to be decreases with the addition of Gr content due to brittle fracture occurred in the structure which was observed from SEM images. The composite showed better wear characteristics reinforced with SiC content as compared to the Gr reinforced composites.

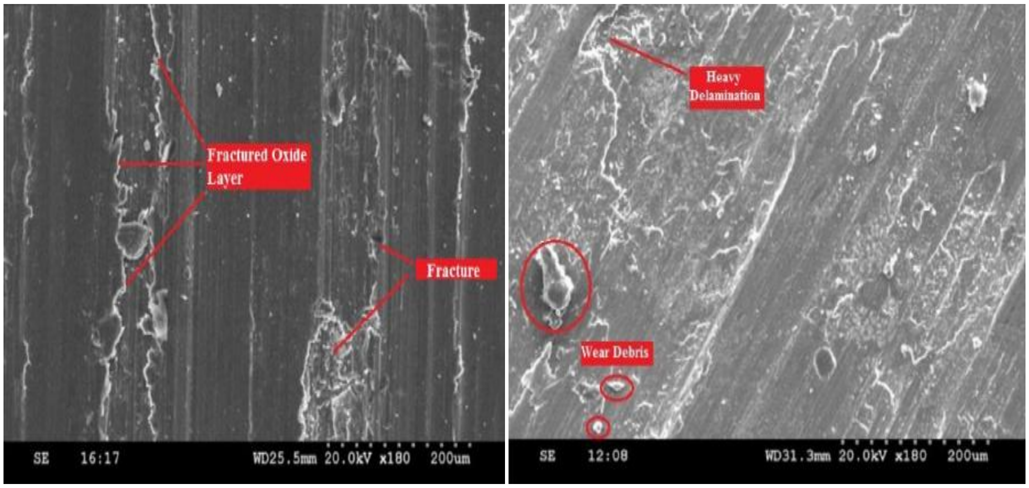

(a) **(b)**

Figure 2.4 Worn Surface SEM Images of (a) Mg-5SiC-5Gr (b) Mg-10SiC-10Gr [Prakash et al., 2016]

[Kaushik et al., 2016] prepared the Al-6082-SiC-Gr hybrid composites using stir casting and studied the abrasive wear behaviour of hybrid composites by comparing it with Al-6082-SiC composite and Al-6082 alloy. The result showed that the wear resistance of Al-6082-SiC-Gr hybrid composite was better as compared to Al6082-SiC composites and Al6082 alloy.

[Xihua et al., 2008] successfully fabricated Al-TiC/Al_2O_3/RE hybrid composites after incorporation of mixed amount of rare earth elements neodymium (Nd), (cerium) Ce, (lanthanum) La and (praseodymium) Pr. The bending strength increased from 130 MPa to 326.7 MPa after incorporation of 3 wt% of mixture of rare earth elements. The hardness increased from 17.84 GPa to 18.41 GPA. The fracture toughness was observed as 3.69 $MPa^{1/2}$ with incorporation of rare earth as compared to 3.13 $MPa^{1/2}$ observed in base alloy.

[Torre et al., 2013] investigated the mechanical behavior of A-356 alloy after incorporation of cerium and lanthanum. The tensile strength and hardness of A356 alloy increased up to 15 % and 11 % after incorporation of 0.2 wt % of cerium and lanthanum mixture. The homogenous dispersion of the rare earth elements into the aluminium melt leads to an improvement of mechanical properties. Some intermetallic like $AlLa_4$, $CeAlO_3$ and $Al_{11}Ce_3$ have been formed during the incorporation of rare earth element into the aluminium melt, which resulted in improvement of mechanical properties.

[Liu et al., 2004] studied the effect of 0.5 wt% cerium oxide addition with mean particle size of 74 μm on TiC/Al-Si hybrid composite. Mechanical properties were found to be improved after incorporation of 0.5 wt% of cerium oxide in TiC/Al-Si composite. The hardness increased from 47.2 to 81.4 HB, tensile elongation rose from 2.4 to 5.4 % and tensile strength increased from 110 to 163 MPa after incorporation of 0.5 wt% cerium oxide. The improvement in mechanical properties reported due to formation of intermetallic compounds like Al_4Ce, Al_2Ce and SiCe as observed by XRD pattern.

[Mao et al., 2015] developed A356 matrix composite reinforced with 0.02 to 0.1 wt% of europium as rare earth element. They reported an increase in tensile strength (UTS) up to 265 MPA and percent elongation (EI) up to 14.7 % after incorporation of 0.1 wt% of europium. The improved mechanical properties have reported primarily due to uniform distribution of the europium into the matrix alloy.

[Singh et al., 2015] prepared aluminum composite after incorporation of SiC as reinforcement with mesh size of 220. The tensile strength of the aluminium alloy increased from 32 MPa to 88.46 MPa after addition of 25 wt% SiC particles. Tensile strength increased up to 104 MPa after addition of one percent magnesium by weight. The increased in tensile strength was observed due to increased in wettability of aluminium composites.

[Poovazhagan et al., 2015] developed Al-6061 composites after addition of 0 to 20 wt% of SiC reinforcement. It was reported that tensile strength raised up to 46 % after incorporation of 15 wt % of SiC. The hardness increased up to 65 % after addition of 20 wt% SiC. Wettabilty of the aluminium composites improved significantly after addition of 1 wt% Mg as wetting agent.

[Kozhukharov et al., 2012] enhanced the corrosion resistance of the AA-2024 composites after addition cerium sulphate. The atomic force microscopy results reported that the aluminium composite surface with improved surface roughness have less tendency of corrosion layer formation. The hydrophobicity of aluminium composite improved after addition of cerium sulphate which ultimately leads to better corrosion resistance.

Ceramic particulate reinforcement used in the composite material utilized for the aerospace applications because the hybrid composite based on synthetic ceramic particulate reinforcement developed for performance optimization with very less consideration on the cost prediction. Out of various synthetic particulates, silicon carbide and alumina are mostly utilized. Some of the key findings of various researchers are discussed in Table 2.2 by utilizing the two different combinations of synthetic ceramic reinforcement materials on AMCs:

Table 2.2. Key findings using two different ceramic particulates as reinforcement materials

Author Name	Aluminium Alloy	Types of Particulate reinforcement	Key findings
[Devaraju et al.,2013]	Al-6061-T6	SiC/Gr and SiC/ Al_2O_3	Composites reinforced with SiC and Al_2O_3 showed higher strength as compared to composites containing SiC and Gr while the composites showed inferior wear resistance reinforced with Al_2O_3.
[Kumaran et al., 2015]	Al-6351	SiC/B_4C	Composites reinforced with B_4C showed an improved machinability but surface roughness found to be poor as the weight percentage of B_4C increased upto certain extent.
[Ravindran et al., 2013]	Al-6061	SiC/Gr	Hybrid composites reinforced with Gr and SiC showed an improvement in strength and wear resistance as compared to single reinforcement SiC.
[Radhika and Subramanian, 2013]	Al-Si10Mg	Al_2O_3/Gr	Hybrid composites reinforced with alumina showed an improvement in hardness, tensile strength and shear strength. Results revealed that the aluminium alloy reinforced with alumina and graphite particles showed highest wear resistance compared to unreinforced alloy.
[Tan et al.,2017]	Atomised	SiC/TiB_2	Hybrid composites reinforced with

	Al-7 Wt-%Si alloy powder		SiC & TiB_2 showed an improvement in ultimate tensile strength and yield strength.
[Rejeshwari et al., 2015]	Al-7075	SiC/ Al_2O_3	Hybrid composites showed an improvement in tensile strength after addition of alumina and silica powder with increased amount.
[Kumar and Xavior, 2016]	Al-6061	SiC-Graphene	Hybrid composites showed a significant improvement in hardness, flexural strength and wear resistance with the addition of graphene and silica particulate as compared to monothilic alloy.

2.1.2.2 Rare Earth Particulates as a Better Choice for Enhancing Performance of Hybrid Composites used in Aerospace Industries

The rare earth particulates may be a good choice in order to improve the properties of hybrid composites as per the properties discussed in figure 2.5. Some of the researchers have found that by adding the rare earth particulates leads to ductility and strength improvement in various composites that are used in aerospace applications. Recently rare earth particulates are widely used in the aerospace industries which are making new generation predator drones, UAV [Jackson, 2020] and other defense purposes unmanned vehicles. The various applications of the rare earth particulates in defense field is shown in figure 2.6 and figure 2.7. Several researchers had discussed that powder form rare earth in various composites used as a corrosion resistance material. So in future it will be a better choice to make hybrid composites with the traces of rare earth particulates targeted for aerospace applications. The work of various researchers on hybrid composites and alloys using rare earth particulates is shown in Table 2.3.

From research finding as discussed in Table 2.3, it is very much clear that rare earth metals in particulate form should be better choice as a reinforcement element for the performance enhancement of hybrid composites. Not only the ductility but other important properties of hybrid composites improved significantly which are used in the structural parts of the aircraft. Generally, it was found that bending strength, hardness and toughness increases with the ductility after using the rare earth particulates as reinforcement in the composites. Hence rare earth particles can be better choice of reinforcement in the ceramic based hybrid composites which are used now days in the aerospace application for performance enhancement.

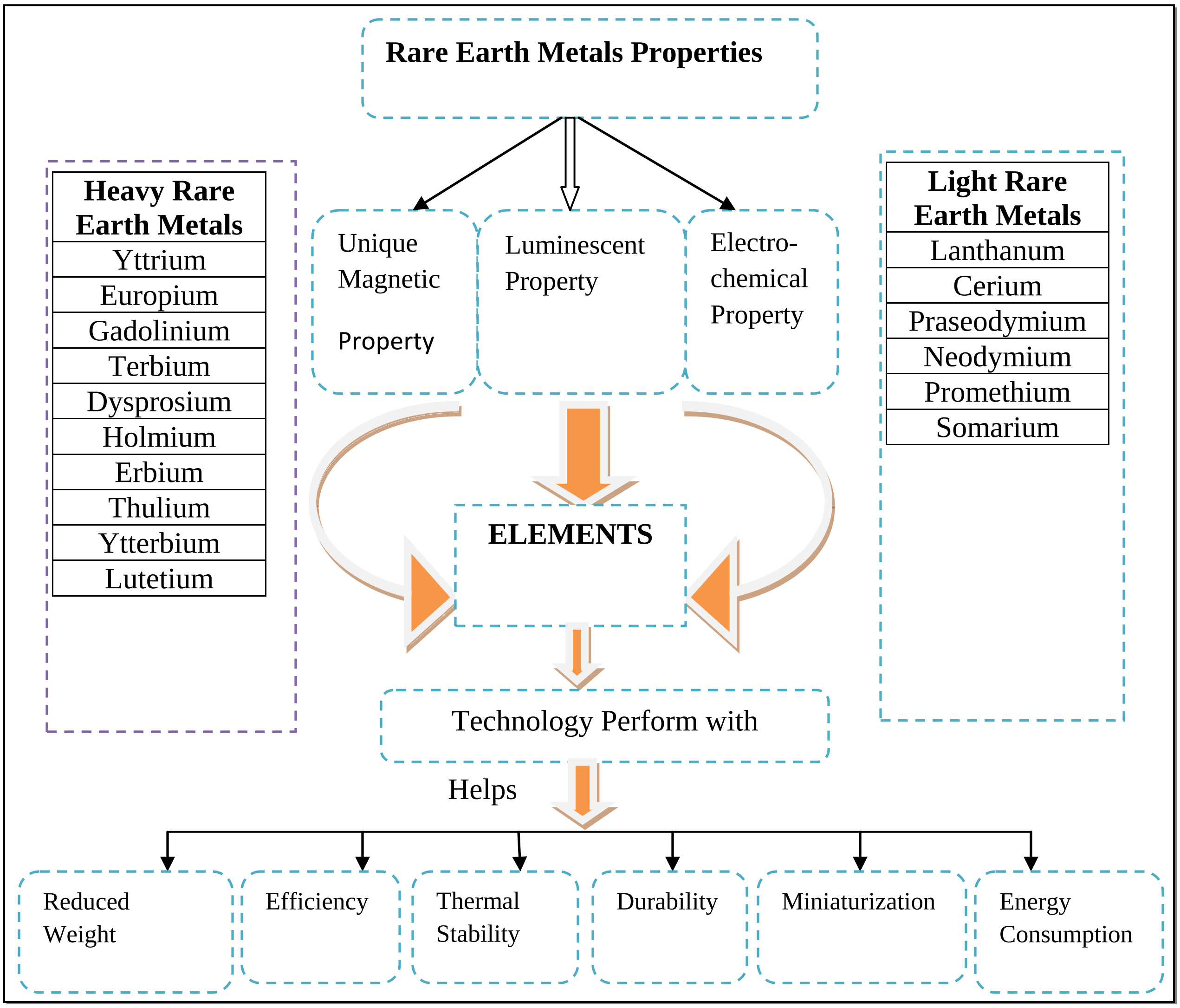

Figure 2.5 Rare Earth Metals Types and Their Properties [Guanming et al., 2007]

Advance Weapons	(a) Predator Drones	(b) F-22 Fighter Jet	(c)Tomahawk Cruise Missile
Rare Earth Elements	Neodymium, Somarium	Europium, Yttrium Terbium, Erbium	Neodymium, Somarium
To be used in parts	Electric Motors and Guidance	Optical Systems, Visuals and fiber Optics	Electric Motors and Guidance

Figure 2.6 Applications of Rare Earth Metals in Advance Weapons Related to Defence Industries (Courtesy: By American Elements; the Advanced Materials Manufacturer)

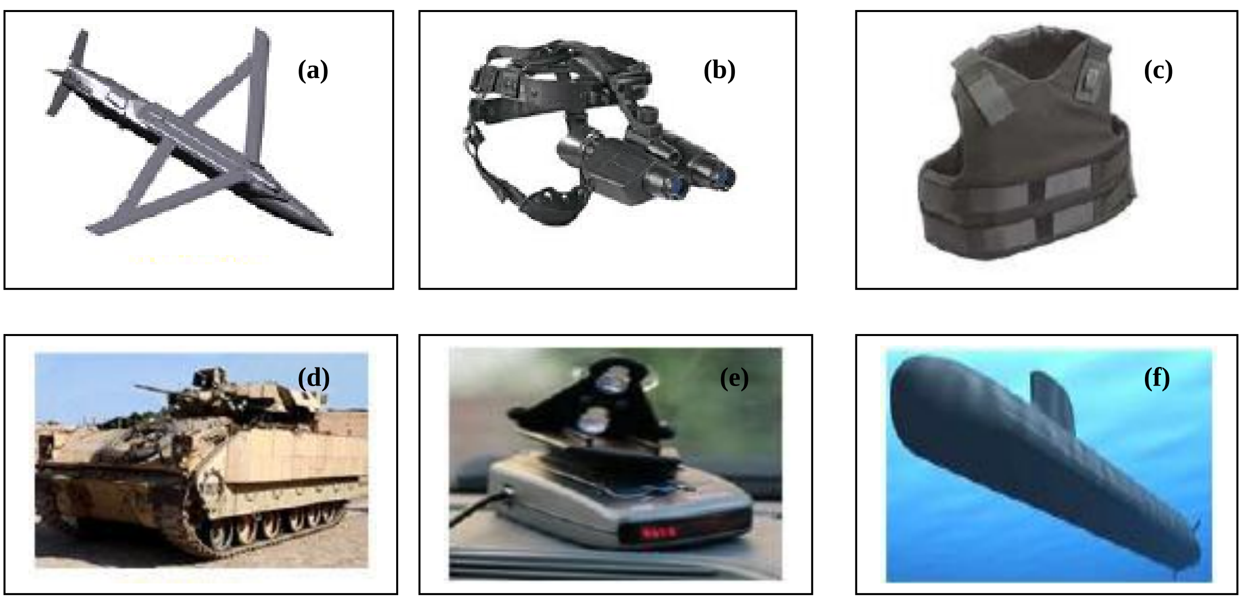

Military Accessories	Rare earth Elements	Where Rare earth is used?
(a) Smart Bomb	Neodymium, Somarium	Electric Motors and Guidance
(b) Night Vision Goggles	Terbium,Erbium,Gadolinium	Optical Lenses
(c) Bullet Proof Vest	Yttrium	Hardened Ceramics
(d)Bradley Tank	Yttrium	Hardened Ceramics
(e)Radar Detection	Europium, Lutetium	Signal Amplification
(f) Nuclear Submarine	Europium, Lutetium	Sonar Detection

Figure 2.7 Applications of Rare Earth Metals in Other Military Weapons (Courtesy: By American Elements; the Advanced Materials Manufacturer)

Table 2.3. Key Findings of Researchers using Rare Earth Particulates

Author Name	Rare Earth Particulates	Matrix/alloy	Types of reinforcement	Key findings
[Li et al., 2002]	Europium	Silica Matrix	-	Mechanical properties of the rare earth complexes were improved by matrix.
[Kozhukharov et al.,2012]	Cerium sulphate Inhibitor {$Ce_2(SO_4)$}	AA-2024	Al_2O_3	Protective coating was obtained by introducing the Ce-salt particulate in the hybrid composites. Protective ability of coating was evaluated by means of AFM, SEM and EIS.
[Guo et al.,2012]	La_2O_3 rare earth oxide	Titanium matrix	TiB/La_2O_3	Rare earth particulates showed an improvement in strength and ductility of titanium alloy. Rare earth metals also act as a driving force for increasing the yield strength.
[Wang et al., 2011]	Neodymium (Nd)	Al-17Mg	M40 graphite	Hardness of the composites improved significantly with neodymium addition. Bending strength decreased significantly from 1463MPa to 791MPa with the addition of neodymium.
[Xihua et al., 2008]	Mixed Rare Earth Metals (Nd,Ce,La, Pr)	AlTiC (Al8%Ti-2%C) Aluminium matrix	Al_2O_3	With addition of 0.5% of rare earth particulate results in improving bending strength and fracture toughness. With further addition of rare earth powders, hardness and toughness value changes slightly.

[Tsai et al., 2011]	Ce	A-356	-	After addition of Ce, cracks no longer easily grow along the interface of eutectic silicon and aluminium matrix which results in a great increase in ductility. Optimum concentration of rare earth metal was found to be 0.6 wt %. Percentage elongation was found to be increased with the addition of 0.6 percent of cerium by weight.
[Li et al.,2013]	Er and Zr	Pure aluminum	-	Recrystallization temperature of aluminium increased from 350^{o}C to 450^{o}C after addition of erbium and zirconium.
[Torre et al.,2013]	La and Ce	A-356		Uniform distribution of La/Ce particulate in A-356 alloy leads to improvement in mechanical properties.
[Bai et al.,2016]	La	Al	Mg_2Si	Better mechanical properties of the aluminium composites have been achieved at 0.4 wt% La.
[Chai et al.,2009]	La/Ce/Nd	Mg alloy	-	Yield strength increases and percentage elongation decreases with the addition of rare earth metals.
[Liu et al., 2004]	CeO_2	Al	TiC/Al-Si	CeO_2 rare earth oxides help in the mechanical properties like hardness, tensile strength, and percentage elongation.

2.1.2.3 Applications of Rare Earth Particulates in Ceramic Materials

The demand of the rare earth elements in powder form increased continuously in ceramic based industry as the satisfactorily progress made by these industries [Qian and Yubing, 2004]. The various reports suggested that most of the rare earths produced were consumed by the ceramic industries [Baldacim et al., 2004]. Report also suggested that china is the largest producer of the rare earth metals and have sufficient amount of rare earth elements for their ceramic industries [Inoue et al., 1995]. The global rare earth metals sales and production by various countries are shown in figure 2.8. It was reported that only 6 % of rare earth elements out of total rare earth output have been used by the China constantly. In future, it is very essential to explore and promote the application of rare earth metals in ceramics particulate form [Terao et al., 2002; Xu and Ai, 2001]. The various researchers have reported that strength, toughness and ductility of some structural ceramics enhanced after incorporation of rare earth elements in oxide powder form. This is primarily due to the special ability of rare earth elements to act as a stabilizer, sintering aids to reduce sintering temperature and low production costs [Chonghai and Xing, 2001].

Above discussions has revealed that rare earth powder oxides can be used in oxide ceramics, non oxides ceramics and in functional ceramics. The other applications are discussed in figure 2.9.

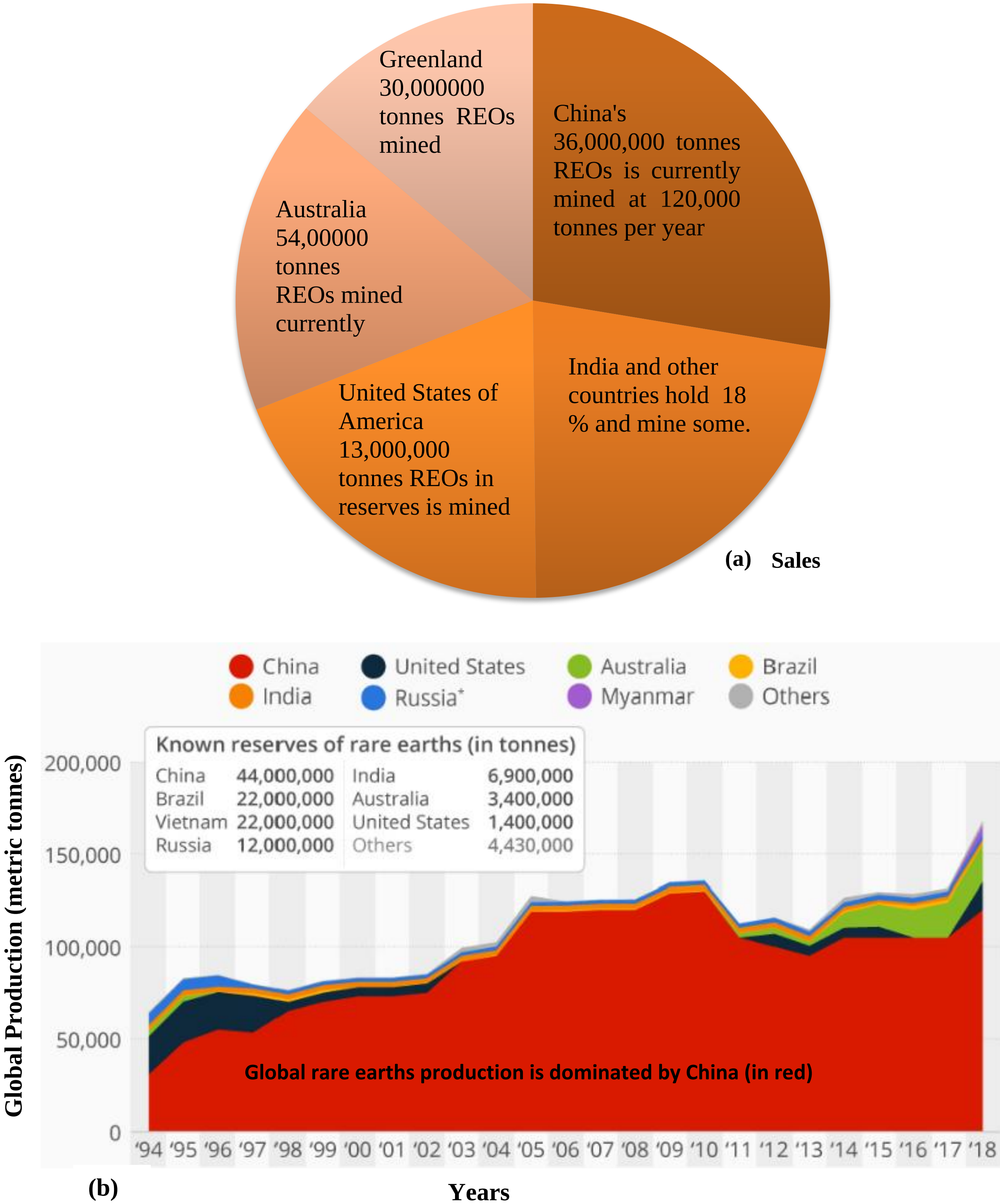

Figure 2.8 (a) Sales (b) Production of Rare Earth Oxides (Courtesy: US Geological Survey)

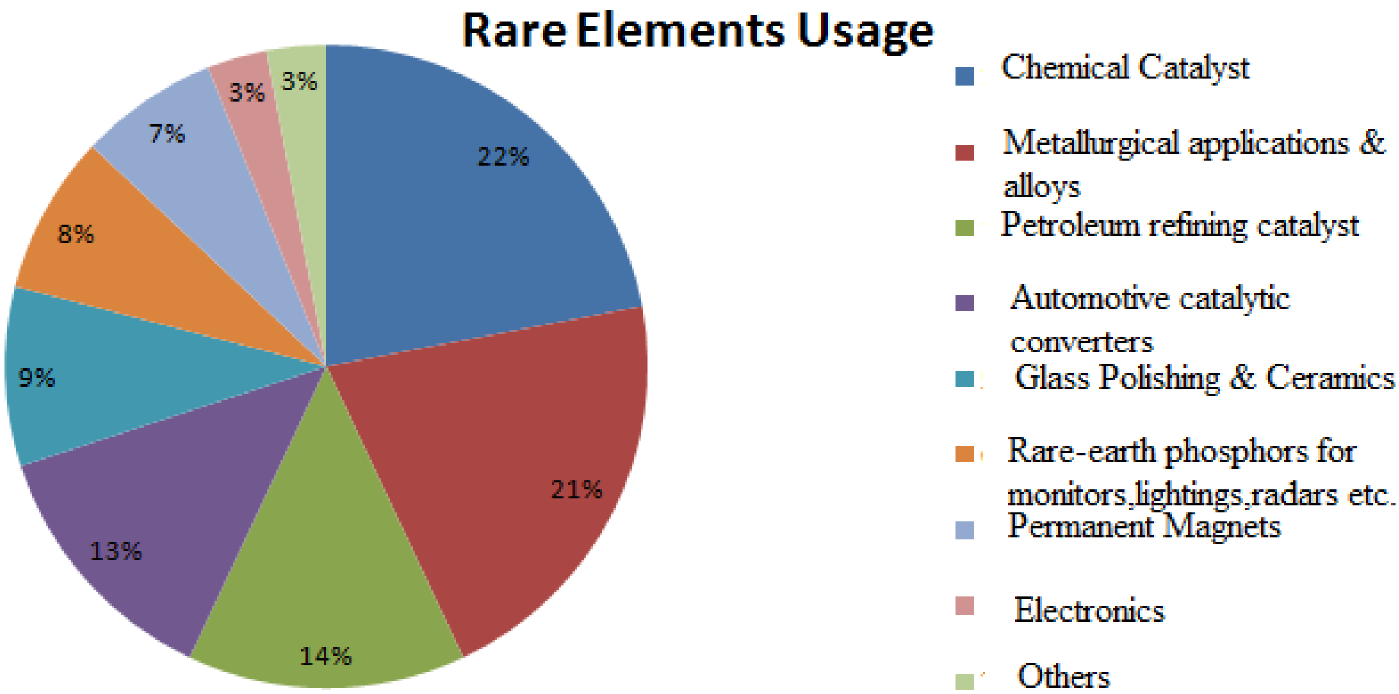

Figure 2.9 Rare Earth Elements Applications Area (Courtesy: US Geological Survey Mineral Commodity, 2017)

2.1.2.4 Applications of Rare Earth Powder Oxides in Al_2O_3 Oxides Ceramics

As now a day's composite materials widely used Al_2O_3 oxides in particulate form as reinforcement material because of its characteristics like high mechanical strength, big insulation resistance, high hardness, abrasion resistance, corrosion and high temperature resistance etc [Chonghai et al., 1999]. The above said properties are generally useful for making light weight composite material targeted for aerospace applications. Apart from aerospace applications, Al_2O_3 oxide ceramic are widely used in textile, coal, petroleum, power and construction industries [Chonghai et al., 1999].

Addition of La_2O_3 rare earth oxides to the alumina ceramic oxides as additive as shown in figure 2.10 can play a significant role by forming a rare earth aluminate, thereby enhance the thermal stability and reduce sintering temperature [Kenyon, 2002]. The further improvement in materials properties of alumina ceramic oxides have been observed after incorporation of Y_2O_3 or Nd_2O_3 .

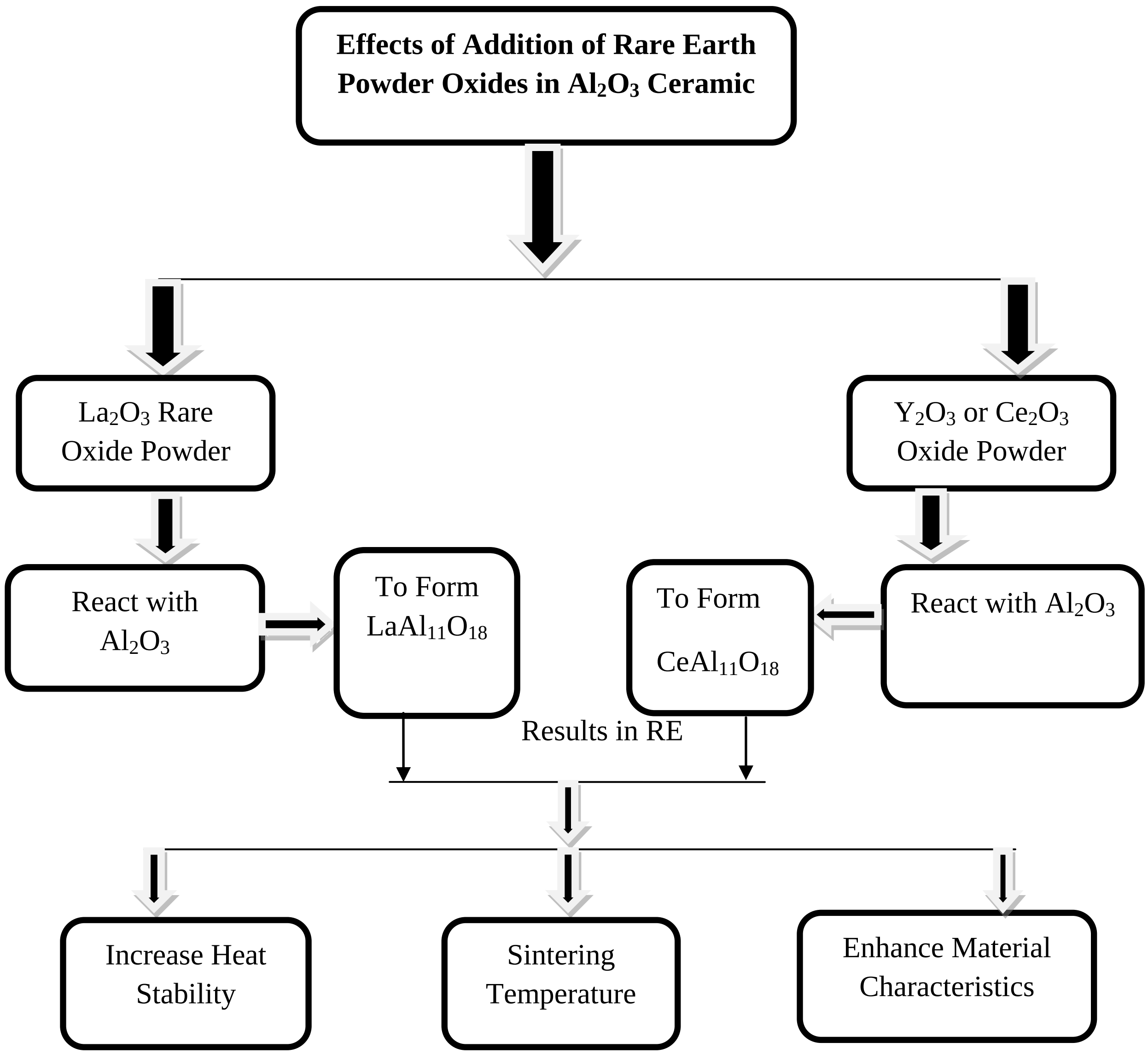

Figure 2.10 Effects of Rare Earth Powder Oxide on Al_2O_3 [Guanming et al., 2007]

2.1.2.5 Applications of Rare Earth Powder Oxides in SiC Non- Oxides Ceramics

The widely used powder oxide form of rare earth metals includes Y_2O_3, CeO_2 , La_2O_3 and Nd_2O_3 in industrial applications [Young et al. 2007]. The very important application of powder oxide rare earth metals as an additive in the SiC ceramic for the performance enhancement of hybrid composites. Accumulation of rare earth powder oxides is shown in figure 2.11. SiC reinforcement adds properties to the composites like high hardness, capability to hold up at higher temperature, ability to conduct heat, to defy the radiation effect and higher mechanical strength etc.

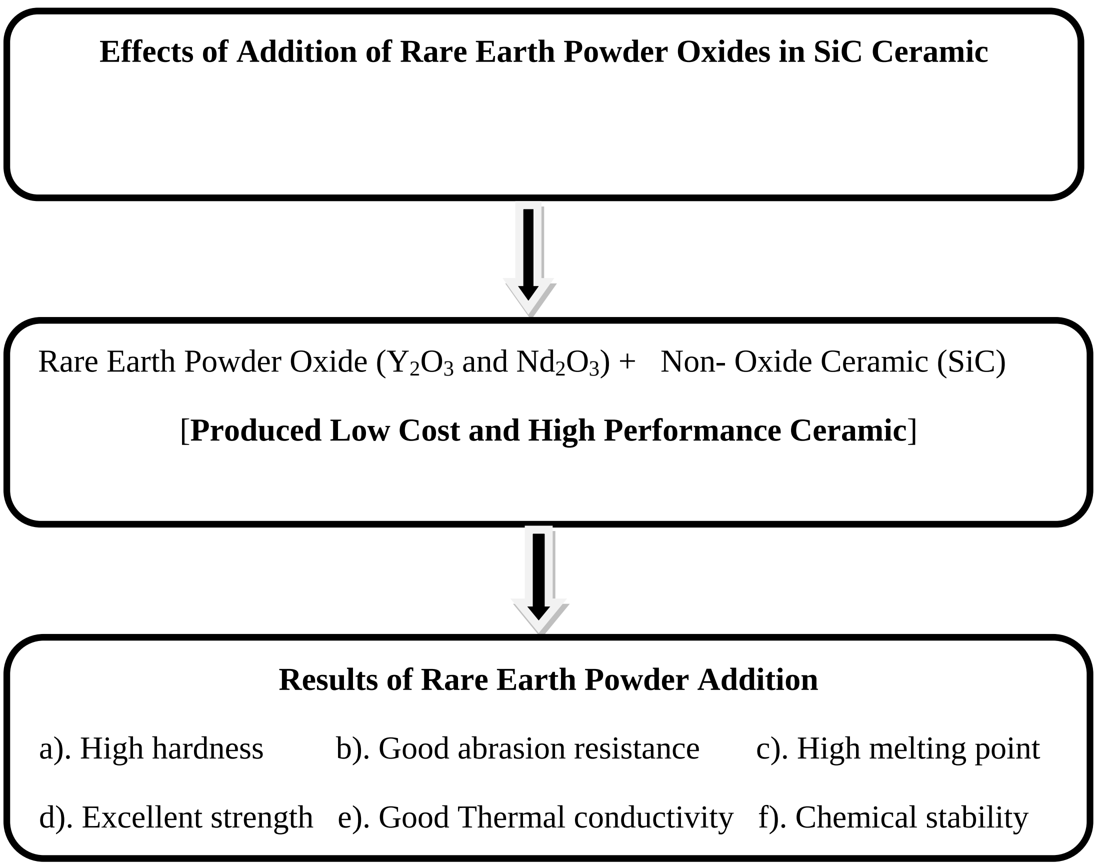

Figure 2.11 Effects of Rare Earth Powder Oxide on SiC [Guanming et al., 2007]

These above properties are very much desirable in the hybrid composites to be used as good candidate for structural components of aircrafts. Accumulation of rare earth powder oxides to the SiC non-oxides ceramic as additive can play a major role in the preparation of low cost and high performance [Young et al., 2007] SiC ceramics which plays considerable role in the aviation sector.

2.1.3 Finishing of Aluminium Based Composites Using Magnetic Abrasive Flow Machining Process (MAFM)

Some of the researchers have found that the required surface finish achieved in the machining various intricate shapes by abrasive flow machining process takes lot of time and also leads to low material removal rate. To improve the performance of abrasive flow machining technique several researchers developed the hybrid machining process to accomplish improved surface finish as well as high material removal rate in shorter period of time. As the name indicates "HYBRID", it means it is the combination of various machining processes. In Hybrid Machining processes various machining processes combines with the AFM process to produce the better results. The difference between the abrasive flow machining process and hybrid process can be easily understood by figure 2.12. Few researchers have used the hybrid approach which finally helps in the process improvement in the conventional AFM.

[Jain et al., 2008] explored a very new concept to energize the electromagnet using pulsating direct current irrespective of direct current as used by previous researchers. The percentage improvement in the surface finish of magnetic material has been achieved with the use of pulsating direct current. Better surface finish was achieved under the action of pulsating current in magnetic abrasive finishing process as compared to direct current.

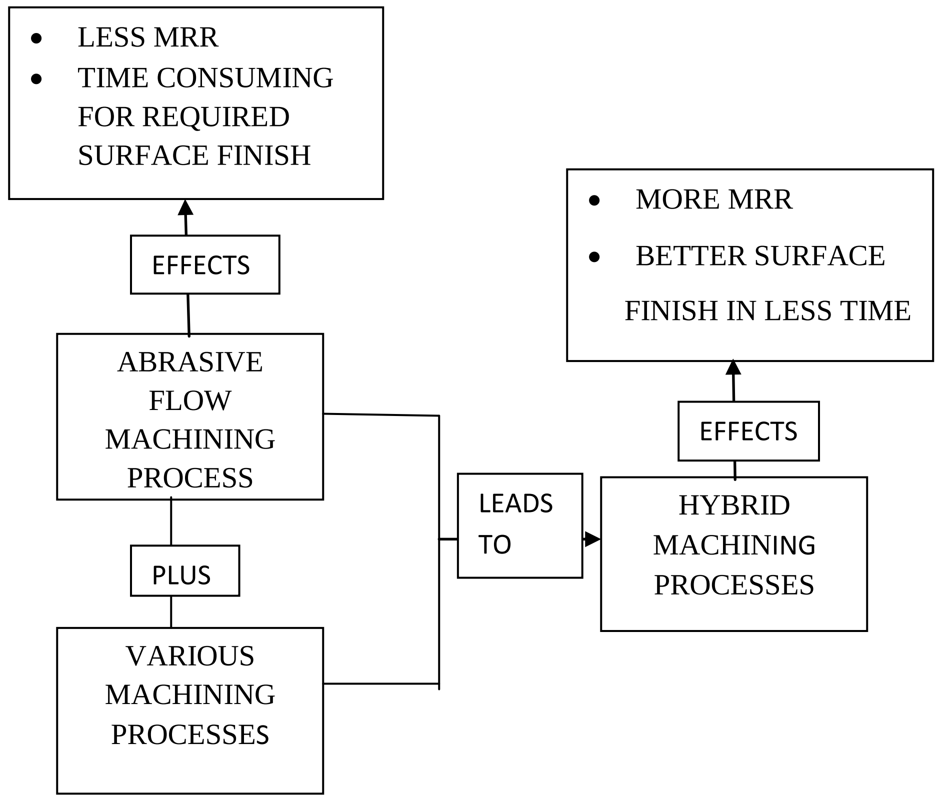

Figure 2.12 Need of Hybrid Machining Process [Jain et al., 2008]

[Yin and Shinmura, 2004] observed a mirror like smooth surface while finishing of stainless steel SUS 304 sample under the application of three modes of vibrations. The smooth surface was achieved with the use of vibration along the direction of feed while good polishing effectiveness observed with use of vibrations at perpendicular direction of feed. Both type of vibrations resulted in the improvement of surface finish.

[Mulik and Pandey, 2011] determined the surface roughness of bearing steel AISI 52100 with the help of ultrasonic vibrations assisted magnetic abrasive finishing process. Ultrasonic vibrations improved the polishing effectiveness of work sample. The surface roughness of AISI 52100 steel specimens improved from 100 nm to 22 nm due to ultrasonic vibration assisted MAF process.

[Mulik and Pandey, 2012] analyze the comparative study of machining forces during finishing of work sample via MAF and UAMAF processes. The tangential force increased significantly by the application of ultrasonic vibrations that ultimately leads to better finishing characteristics.
[Singh and Shan,2002] developed Magneto Abrasive Flow Machining (MAFM) process in order to improve surface finish as well as MRR by application of a magnetic field around the work piece. The magnetic flux density, volume flow rate, number of cycles, medium flow volume, abrasive grit size, abrasive concentration and reduction ratios were used as process parameters. ANOVA technique was used to identify the most significant parameters affecting surface roughness. Better surface finish with increased MRR was observed in MAFM over AFM.

[Kala et al., 2015] explored double disc magnetic finishing (DDMAF) process for finishing of the two paramagnetic materials and finally compared their finishing components. The experiments were carried out under the influence of different process parameters like working gap, rotational speed, percentage weight of abrasive, abrasive mesh size and feed rate. It was reported that working gap affected mostly on surface roughness of hard material like stainless steel while rotational speed affected mostly while finishing of soft materials like copper.

[Ko et al., 2007] proposed Magnetic abrasive finishing method (MAF) used for the burrs removal on the surface of small parts made from ferromagnetic or non-magnetic materials. Three kinds of movements were involved in this process like feed of the sample (work piece), inductor rotation and oscillation of the top plate with a sample in the direction normal to the feed direction. The better surface roughness was achieved at the continuous flow of coolant.

[Zou et al., 2010] explored a concept of magnetic abrasive flow finishing for finishing the seal ring groove which was used in conjunction with rubber seal. The results revealed that the MAF was an efficient way for obtaining high quality surface on seal ring groove.

[Kim et al., 2010] introduced a concept of magnetic abrasive polishing for the deburring of magnesium alloy plate so that the plate was used in the automotive field, manufacturing of mobile phones, laptop, computers, cameras and other electronic components.

[Yamaguchi et al., 2007] used magnetic abrasive finishing process for the finishing of Austenitic Stainless Steel capillary Tubes. Capillary tubes are generally used in nano-scale technologies, surgical instruments and chemical equipment where good surface finish was generally required.

The better surface roughness was achieved after using the combination of permanent magnet and pole tips.

[Yamaguchi and Shinmura, 2004] introduced a concept of magnetic field assisted finishing process for internal finishing of the alumina based ceramic components. The experiments were performed under the parametric analysis of volume of lubricant, ferrous particle size, and abrasive grain size on the response surface roughness. The aluminium components surface roughness was observed as 0.02 μm on altering the various parameters.

[Givi et al., 2012] explored a concept of magnetic abrasive finishing method for polishing of the aluminum sheets so that it can widely used in high-tech industries such as aerospace, die polishing, and medical instruments. The various experiments were performed under the parametric analysis of rotational speed of magnetic pole, working gap, number of cycles and weight of the abrasives particles while finishing the aluminium surface. It was observed from ANOVA results that the percent contribution of number of cycles and working gap suggested the most influencing factor on change in surface roughness. It gives the surface to aluminium like mirror shape finishing.

2.1.3.1 Modeling and Optimization Techniques for Process Parameter Optimization

Attempt has been made to develop a mathematical model or simulation to find the effect of various process parameters on the output responses namely surface finish and material removal rate (MRR). Models give the insight picture of the event occurring in real life situation. In the present section, the main task to discuss about the various research findings on modeling and optimization of process parameters. An approach in all the simulation based optimization is discussed in the figure 2.13.

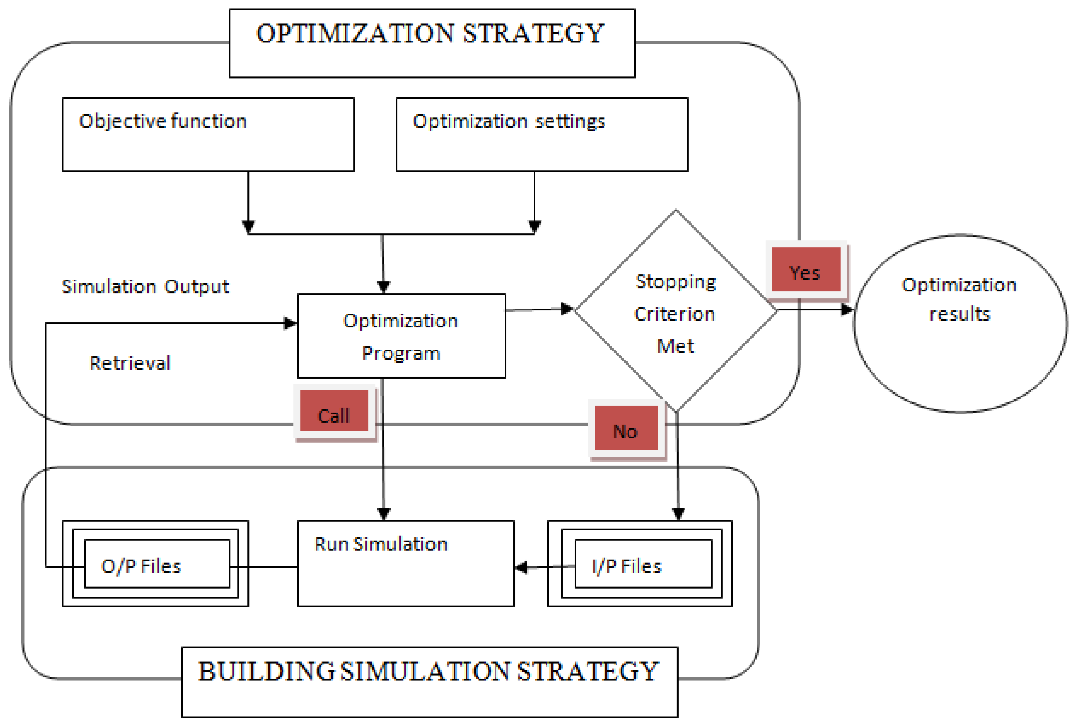

Figure 2.13 Optimization Strategies of Research Problems [Nguyen et al., 2014]

[Lin et al., 2007] attempted the optimization of process parameters of MAF process using Taguchi method while finishing of SUS304 stainless steel. The magnetic field, spindle revolution, feed rate, working gap, abrasive, and lubricant were selected as input parameters while the surface roughness as output response. Results showed that the working gap has the largest effect on the surface roughness by reducing surface imprints. From Taguchi experimental analysis, it was observed that working gap of 2.5 mm, feed rate of 10 mm/rev, and abrasive of 2 gm were found to be significant parameters affected surface roughness mostly. Finally, it was revealed that MAF process improved surface quality of stainless steel upto 0.102 µm.

[Singh et al., 2004] used a Taguchi design of experiments in order to determine the important parameters of MAF process which influenced the surface quality of advanced engineering materials like silicon nitride, silicon carbide and aluminium oxide. Voltage, working gap, rotational speed of the magnet, and abrasive size were found to be most significant parameters that affected surface roughness. The variation in surface roughness and process parameters was mathematically modeled by regression analysis.

[Givi et al., 2012] explored a concept of optimization of process parameters of magnetic abrasive finishing method while finishing of the aluminium sheets using three-level full factorial method. The rotational speed of magnetic pole, working gap, number of cycles and weight of the abrasive particles were selected as input parameters while the surface roughness as output response. A total of 54 experiments were carried out on aluminium sheets. ANOVA results showed that number of cycles and working gap were found to be most significant parameters that affected surface roughness followed by rotational speed and weight of powder. Finally, the mirror like finished surface of aluminium sheet was achieved that can be used in industries such as aerospace, die polishing, and medical instruments.

[Barman and Das, 2017] developed a finite element based model called Ansys. Maxwell is used for the simulation reading to find out the optimum design pattern and measurement of the tool for achieving superior finishing uniqueness in Magnetic Field Assisted Finishing (MFAF).The process parameters are characterized in three categories: rotational speed of tool, working gap and finishing time. Experiments are carried out on the flat titanium work piece in order to validate the Maxwell simulation results that shown good agreement between them.

[Kwak, 2012] derived the mathematical model for the improvement of surface roughness in non ferrous AISI316 stainless steel using magnetic assisted abrasive polishing. Rotational speed, magnetic flux density, applied current and working gap were selected the polishing factors while analyzed the surface roughness of stainless steel. Designs of experiments were planned according to the L_9 orthogonal array. ANOVA analysis revealed that rotational speed of 1500 rpm, magnetic flux density of 82 mT, applied current of 1.5 mA and the working gap of 1.5 mm were found to be most important parameters that affected the surface roughness mostly. Finally, the developed was confirmed and validated by the experimental results.

2.2 GAPS IDENTIFIED IN THE LITERATURE REVIEW

The purpose of the above concluded literature review was developing a state of art of fabrication of hybrid composites, their characterization and finishing using MAFM process has been reported. However, applicability of MAFM for rare earth based hybrid composites fabricated by stir casting is not fully explored. The present review reported the gaps which are identified as below:

1. It was found that Al_2O_3, SiC, B_4C, Gr and TiB_2 were used as reinforcement elements for the making of composites based on aluminium alloy.
2. Very less work is reported on use of Rare Earth Metals for enhancement of mechanical properties of aluminium alloys based on hybrid composites.
3. During machining of various metal and alloys by conventional methods like turning, milling, drilling etc, higher rate of tool wear was observed due to abrasive nature of SiC reinforcement. To overcome the problem of high tool wear, various hybrid abrasive flow machining process were used for finishing of different metals and alloys.
4. Poor surface finish is the major problem in case of machining the complex shapes in composites using conventional machining methods. To improve surface finish of these composites, researchers have tried out different Hybrid AFM processes.
5. It was found from the literature review that many researches had used various modeling and optimization techniques for validation of experimental results. Commonly used techniques for these were computational fluid dynamics, ANOVA, Response Surface Methodology, Finite Element Analysis etc.

It is concluded from literature survey that most of the researcher have used ceramic based reinforcement for making hybrid composites. There is need of work to be done on addition of Rare Earth Metals as reinforcement elements for performance improvements of composites while used in aerospace application. Moreover, finishing of Hybrid Composites using Hybrid Abrasive Flow Machining (AFM) processes will also be carried out.

CHAPTER 3

PROBLEM FORMULATION

3.1 INTRODUCTION

In the era of globalization, the demand of composite materials with tailored combination of properties rises continuously. Stronger, lighter, and less expensive materials with better surface finish are current requirement of engineering applications. This requirement leads to the development and emergence of the very new kind materials known as metal matrix composites (MMCs). MMCs are highly recommended materials to meet the ever increasing demand of modern technology, due to their excellent properties such as light weight, excellent wear resistance, good corrosion resistance, low stiffness and elastic modulus.

However, it has been reported that the poor tensile ductility, inadequate wear resistance, poor toughness and inferior fracture-related properties have been a severe limitations associated with these composites while used in aerospace applications. The low ductility and toughness can arise from brittle nature of ceramic reinforced particles. The other factor responsible for poor ductility related to poor wettability between ceramics and metallic melt interface. Over the past decades, a lot of evolution has been happened in the field of aluminium composites to rectify and upgrade above mentioned problems. Some common approaches involve modification of the processing technique, pre-heat treatment of reinforced particles and coating of reinforced particles with wetting agents. But the hybrid composite reinforced with nano and sub-micron level particles via stir casting techniques are mostly used.

Aluminium matrix composites (AMCs) have been successfully exploited in many technological sectors including, automobile, aerospace applications, marine and arms industry for the manufacturing of wide range of components and devices. These composites are also known as DRMMCs. The use of discontinuous reinforcement phase approach of producing hybrid reinforced AMCs anticipate the enormous guarantee of emergent performance as well as low cost MMCs through this path. So by the use of discontinuous phase in composites, engineers are trying to improve its structural efficiency, specific stiffness, high strength and satisfactorily level of wear resistance. The other properties including corrosion resistance, specific stiffness, high temperature stability, fatigue resistance, online monitoring control ability and rupture properties are also improved.

Above mentioned properties improvements would also guarantee to achieve the desired physical properties called coefficient of thermal expansion (CTE) for reinforcing a metal matrix by the selection of appropriate discontinuous phase. Generally, the properties enhancements are very much depend upon on the mutually interactive influences of: (a) intrinsic properties of the composite constituents; and (b) size, shape, orientation, volume fraction, and distribution of the secondary reinforcing phase in the metal matrix.

Proper selection of reinforcement with its type and shape is the backbone of every composite material for enhancing performance optimization with very less consideration on the cost prediction. The different sizes of discontinuous particulate reinforcement used in hybrid aluminium matrix composites (HAMCs) have different role in the matrix. The purpose of discontinuous particulate dispersed over matrix is to offer a satisfactorily level of performance to the composite structure by holding the fibers jointly and transmit the load to the fibers which finally stop the cracks formation. Discontinuous particulate not only help in the load carrying property of the composites but also maintain the ductility of the matrix alloy. The discontinuous particulate having micro level improved the hardness, stiffness and wear characteristics of composites by sustaining the matrix skeleton. So overall performance improvement of the composite depends upon the integrated utilization of nano and micro sizes discontinuous particulate with better synergy. It was further stated that if the particulate reinforcement of micro level increased by weight percent above 30 % in AMCs during fabrication or in service condition leads to the creation of little voids and cracks [Bharath et al., 2014]. These defects cause brittle fracture under low tensile loads. Ultimately leads to loss in strength, low ductility and low toughness properties of ceramics particulates used in various structures. This problem can be can be further reduced by making the composites with higher content of nano discontinuous particulate reinforcement as compared to micro size particulates. To achieve the better properties of composites up to maximum level it is essential to properly mix the nano particulates in the matrix material so that perfect bonding takes place between them. Additionally, the metal matrix reinforced with discontinuous phase maintains their amenability to conventional metallurgical processing techniques, fabrication and characterization methods and finishing techniques currently utilized for the unreinforced counterparts.

3.2 SCOPE OF THE PROPOSED RESEARCH WORK AND WORK PLAN

Keeping in mind with all the above said advantages it made interesting to develop and test hybrid composites based on Al-6061 alloy matrix reinforced with Al_2O_3/SiC/CeO_2 via stir casting route. Silicon carbide was generally used because of its excellent workability, good machinability, low cost, high hardness, capability to hold up at higher temperature, ability to conduct heat, to resist the radiation effect, higher mechanical strength etc. The purpose of adding Al_2O_3 was to further enhance the properties of Al-6061 based hybrid composite such as high mechanical strength, insulation resistance, high hardness, abrasion resistance, corrosion and high temperature resistance etc. CeO_2 as REOs was selected because of its high specific stiffness, superior high temperature mechanical properties, excellent oxidation resistance and easy availability.The strength, toughness and ductility of some structural ceramics can be improved by addition of rare earth particulate because of their ability to act as a stabilizer, sintering aids to reduce sintering temperature and production costs. After exhaustive literature review, it has been seen that no work has been done on the hybrid composites based on Al-6061 matrix reinforced with Al_2O_3/SiC/CeO_2 with improved mechanical, metallurgical and surface characterization along with better wear properties targeted for aerospace applications.

The present work concentrated on preparing the hybrid composites via bottom pouring stir casting route with different weight percent composition of SiC and Al_2O_3 as reinforcements and traces of CeO_2 as rare earth particulate. Aluminium alloy was placed inside the graphite crucible and heated to a maximum temperature of 850^oC to convert it into the molten form. The particulates of SiC and Al_2O_3 were mixed thoroughly for uniform distribution of particles and the packets of 5, 10, 15 wt% of mixture were prepared which were then preheated in an oven for 1-2 hour to get their surface oxidized. The other hybrid composites were prepared with a mixture of (Al_2O_3+SiC+CeO_2) after incorporation of 0.5, 1.5 and 2.5 wt% CeO_2. The preheated powder was then fed at uniform rate into the molten metal with the help of a conical hopper. Then mixture was stirred for about 8-10 min at a speed of 350 rpm with the help of a graphite stirrer to get a homogeneous mixture. From the literature, it has been found that various researches has been carried out by utilizing the different types of reinforcement particles SiC, TiC, Al_2O_3, Gr, B_4C and CaC_2 alone or combining with different aluminium alloys to estimate mechanical properties and mechanical characterization of composite but among all of us only aluminium based composites with nano particulates has shown outstanding mechanical, microstructure and wear properties

Bottom pouring stir casting technique has been chosen in this research which remains an attractive choice among all the solidification processing routes. The major advantages of stir casting process like very large scale of process capability, very less requirement of infrastructure in foundry and very low cost of production over conventional casting. Accordingly, the aim of the present investigation is to synthesize Al alloy based composite reinforced with Al_2O_3/SiC/CeO_2 particles using stir casting technique. The composites thus obtained were characterized for their microstructure, mechanical properties especially the tensile, micro hardness and wear behavior, surface properties including corrosion and hydrophobicity analysis. Particular emphasis is placed to study the effect of presence of nano particulates and its increasing amount on the microstructure and mechanical properties of standard Al-6061 alloy which is exclusively used for aerospace applications.

In the present investigation, Al-6061 aluminum alloy is reinforced withAl_2O_3/SiC/CeO_2particles as the reinforcement is henceforth called HAMCs. With the use of stir casting technique, a defect free casting is achieved with better mechanical and metallurgical properties.

Surface finish of a HAMCs used for the aerospace application is a very important aspect as it can affect the product life. The technological shift from macro to micro and nano- levels has further increased the thrust on various finishing processes. In addition, the development in materials has created implicit demand for new advanced finishing processes. Amongst the various advanced finishing processes, magnetic abrasive based finishing processes are gaining importance because of their capability to produce good finish with least surface damage. Another reason that magnetic abrasive based finishing processes are getting attention by the researchers has been that the finishing forces in these processes can be controlled easily during finishing.

In order to achieve the objectives, the whole work was carried out in three stages.

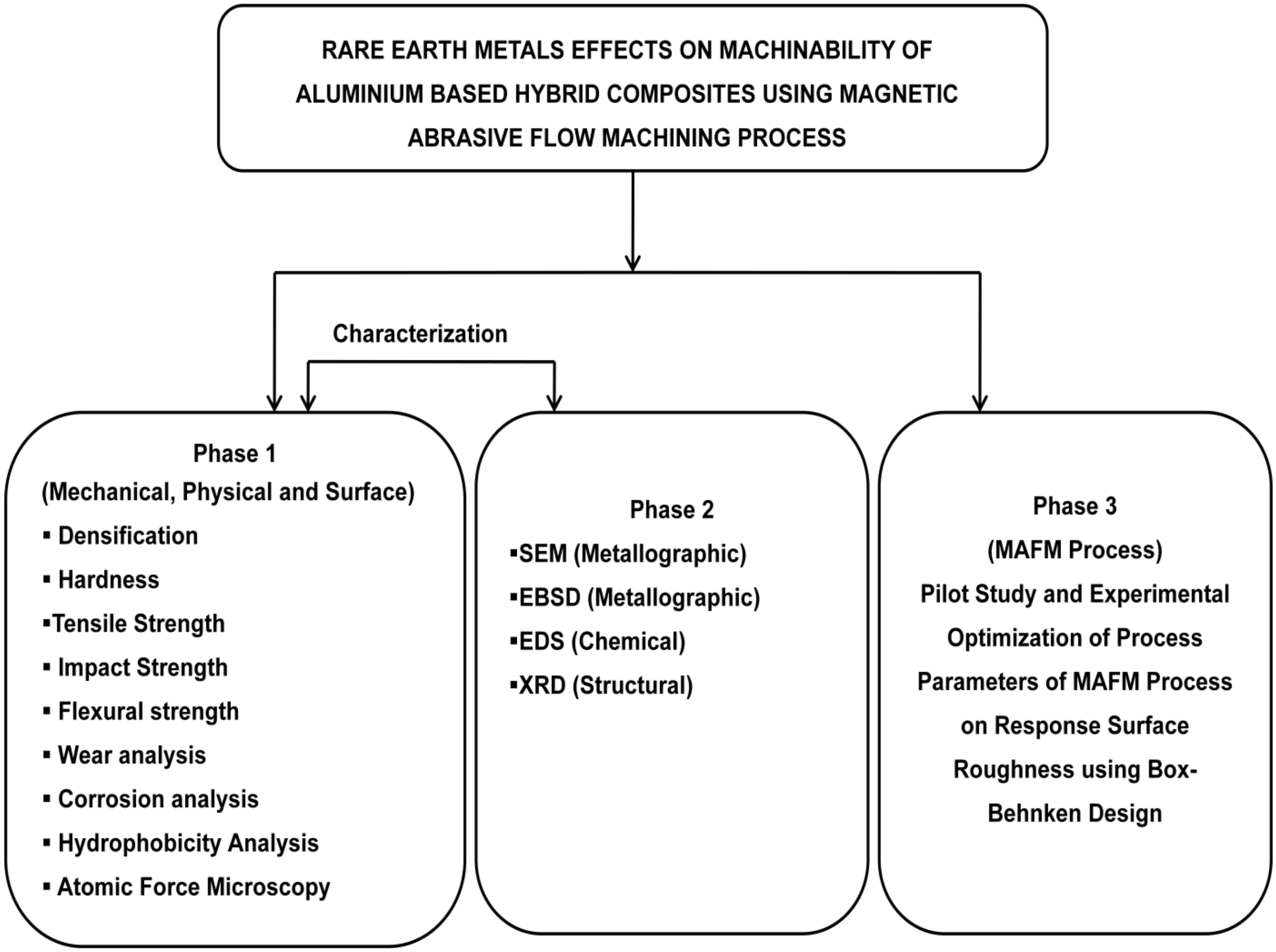

Figure 3.1 Phases of Research Work

Phase 1: Mechanical and Surface Characterization

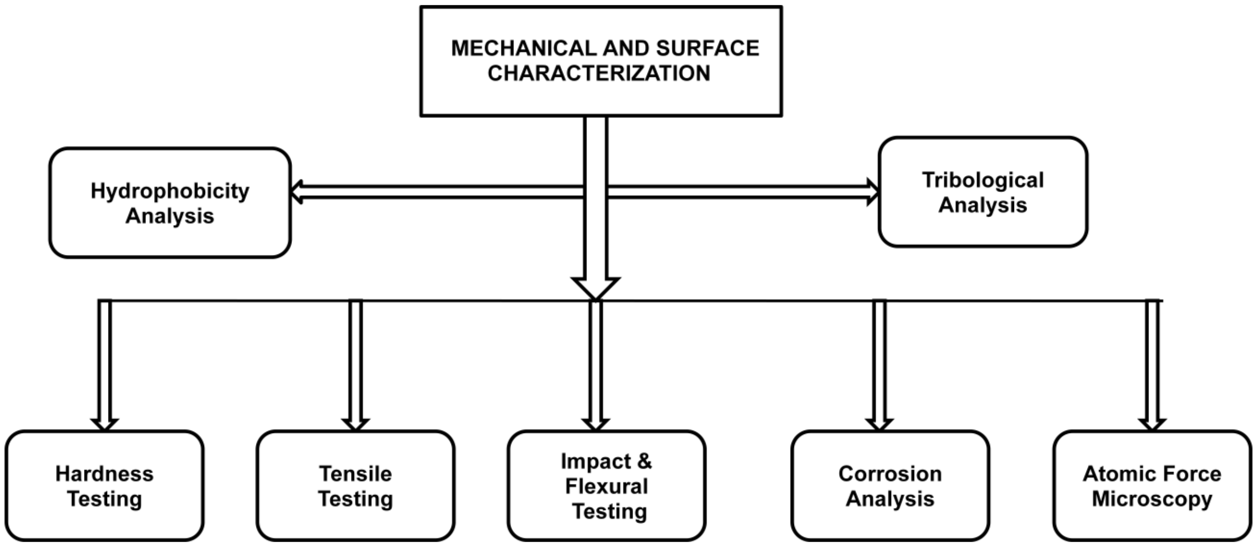

Figure 3.2 Mechanical and Surface Characterization

Phase 3: Metallographic, Chemical and Structural Characterization

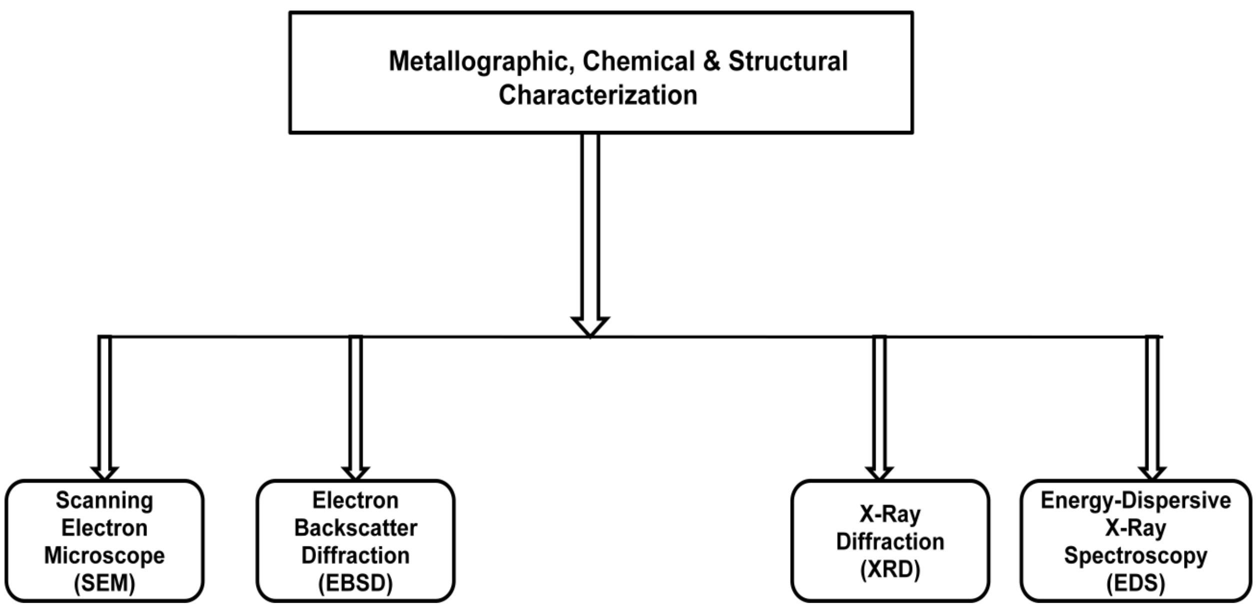

Figure 3.3 Metallographic, Chemical and Structural Characterizations

Phase 3: MAFM Process: Pilot study and experimental Optimization of process parameters of MAFM process on response surface roughness using Box- Behnken Design

CHAPTER 4

EXPERIMENTAL PROCEDURE

4.1 INTRODUCTION

This chapter provides the step wise procedure used to achieve the research objectives. The plan of work was started with the selection of matrix and reinforcement materials through literature review. Fabrication of hybrid composites via stir casting route, mechanical and metallurgical characterization of these hybrid composites was done. Afterwards, the finishing of hybrid composites was done using magnetic abrasive finishing process. The optimization of various process parameters like magnetic flux density, number of cycles and extrusion pressure on performance characteristics using RSM was performed.

4.2 MATERIALS

4.2.1 Selection of Matrix Material

In the literature review, a complete overview for different matrix alloys and reinforcements combinations is reported. Selection of the matrix material is done on the basis of targeted application. In present work the aluminium alloy based composite was developed for an aerospace application. The material used for the study should be stable in the given working temperature and non-reactive too. On the basis of these objectives, aluminum Al-6061 alloy was considered as base matrix alloy and the chemical composition of the matrix material are shown in table 4.1. The chemical composition of the Al-6061 alloy was determined using Wavelength Dispersive X-ray Fluorescence model S8 tiger made in Germany available in Sophisticated Analytical Instrumentation Facility lab of Punjab University, Chandigarh India.

Table 4.1 Chemical Composition of Al-6061-T6 Alloy (wt %)

ELEMENT	Mg	Si	Cu	Zn	Ti	Mn	Cr	Al
Weight (%)	0.84	0.69	0.22	0.07	0.05	0.30	0.08	Balance

4.2.2 Selection of Reinforcement Materials-Alumina, Silicon Carbide and Cerium Oxide

Proper selection of particulate reinforcement material is the backbone of every composite material for enhancing the mechanical and tribological characteristics. Generally ceramic particulate reinforcement are used in the composite material because the hybrid composite based on synthetic ceramic developed for performance optimization are a cost effective. Out of various synthetic particulates, silicon carbide (SiC) and alumina (Al_2O_3) are most commonly used particulates. SiC was used because of its excellent workability, good machinability, low cost, high hardness, capability to hold up at higher temperature, ability to conduct heat, to defy the radiation effect and higher mechanical strength [Young et al., 2007]. The motivation behind adding Al_2O_3 was to additionally improve the properties of Al-6061 based hybrid composite such as mechanical strength, insulation resistance, high hardness, abrasion resistance, corrosion and high temperature resistance [Chonghai et al., 1999]. The various researchers have documented that strength, toughness and ductility of some structural ceramics can be improved by addition of rare earth particulate because of their ability to act as a stabilizer, sintering aids to reduce sintering temperature and production costs [Chonghai et al., 2001]. For this reason cerium oxide (CeO_2) as rare earth particulate was used. Addition of rare earth powder oxides to the Al_2O_3 and SiC as additive can play a major role in the preparation of low cost and high performance hybrid composites [Chonghai et al., 2001]. The particles size of as received reinforcements of Al_2O_3, SiC and CeO_2 are shown by scanning electron microscopy images in figures 4.1 (a-c). These reinforcements were purchased from Alpha Chemika, Mumbai, India. The other details of the reinforcements used in present work are tabulated in table 4.2. The obtained image were processed using a Java- based image analysis software (Make: LUCI; Model: Image J 1.34 S; USA). The reinforcement particles average length, its width and aspect ratio were measured using Image J.

Table 4.2 Details of SiC, Al_2O_3 and CeO_2 Particles

Reinforcements	Average particle size (μm)	Density (g/cm^3)	Purity (%)	Melting point (°C)
SiC	40	3.95	99.9	2072
Al_2O_3	220	3.20	99.9	2700
CeO_2	5	7.22	99.9	2400

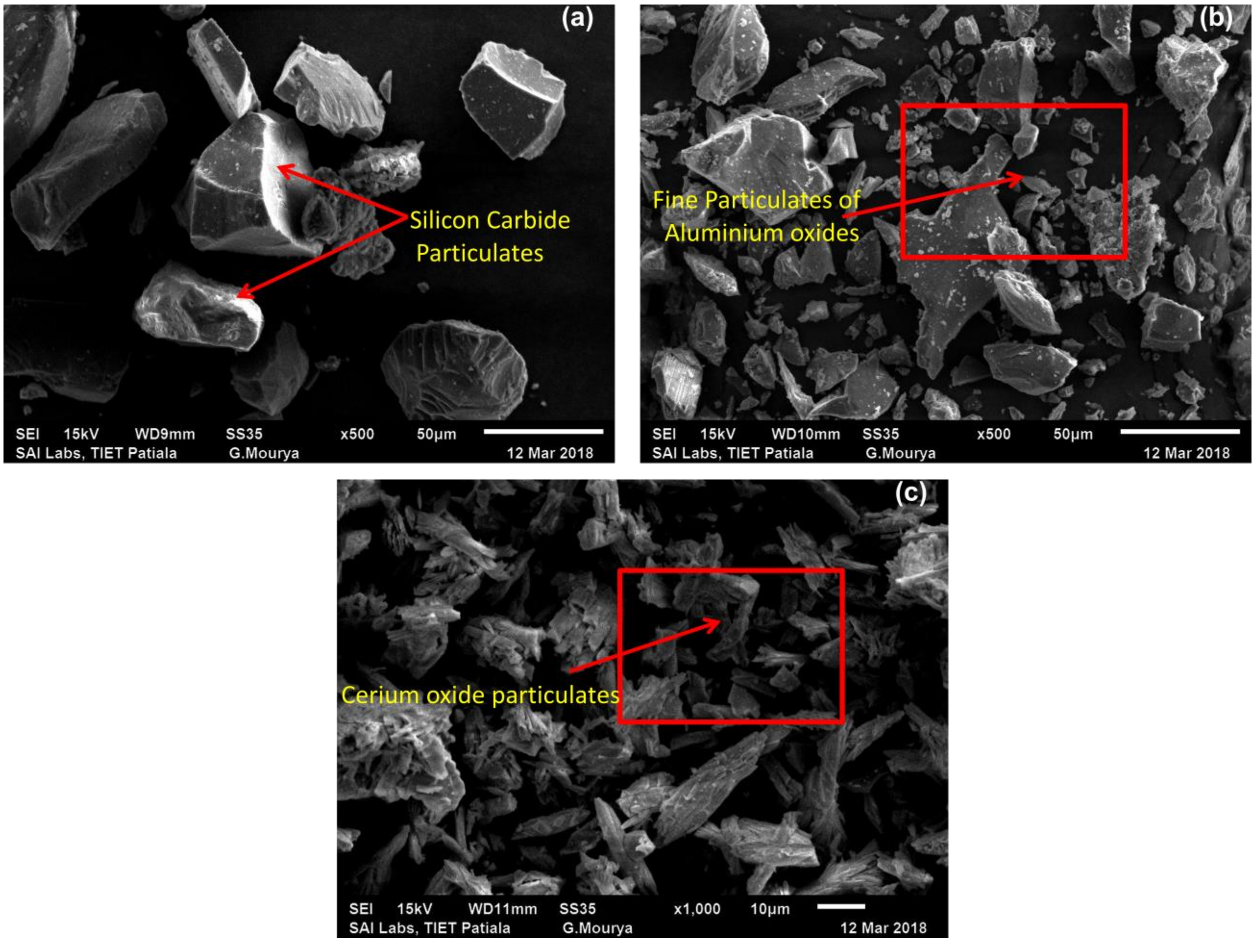

Figure 4.1 SEM Micrograph of Powder Reinforcement used in Composites (a) Silicon Carbide Powder (b) Alumina Powder (c) Cerium Oxide Powder (Courtesy: SAI Labs, Thapar Institute of Engineering and Technology, Patiala)

4.3 BOTTOM POURING STIR CASTING

Al-6061 based hybrid composites were prepared by stir casting method with different weight percent of SiC and Al_2O_3 as reinforcements and traces of CeO_2. The total weight of Al-6061 alloy/Al_2O_3/SiC/CeO_2 composite was kept as 900 gm. Each sample contains different composition of reinforcements as shown in table 4.3. Mould is designed so that in each pass, multiple castings were produced with different sizes of samples for performing various tests. The schematic of the set-up used in present work is shown in figure 4.2. Aluminium alloy was placed inside the graphite crucible and heated to a maximum temperature of 850 °C to convert it into the molten form. The particulates of SiC and Al_2O_3 were mixed thoroughly for uniform distribution of particles and the packets of 5, 10 and 15 wt% of mixture were prepared which were then preheated in an oven for 1 to 2 hour to get their surface oxidized. Similar process was followed to prepare a mixture of (Al_2O_3+SiC+CeO_2). The preheated powder was then fed at uniform rate into the molten metal with the help of a conical hopper. Then mixture was continuously stirred for about 8-10 min at a speed of 350 rpm with the help of a graphite stirrer to get a homogeneous mixture of molten metal with the powder. It also helps to avoid defects like clustering, agglomeration and segregation. The motorized lift type stirrer speed can be varied from 100 rpm to 1500 rpm with a 3 phase AC motor having twin fin blade. The speed of the stirrer was controlled by the variable frequency drive. The molten metal mixture was then poured into a mold having three dies with different size of cavities as 10x15x150 mm^3 (rectangular), 25x220 mm^2 (cylindrical) and 20x220 mm^2 (cylindrical) respectively. After pouring the molten metal, it was allowed to solidify at room temperature. After solidification, the fabricated parts were removed from the mold.

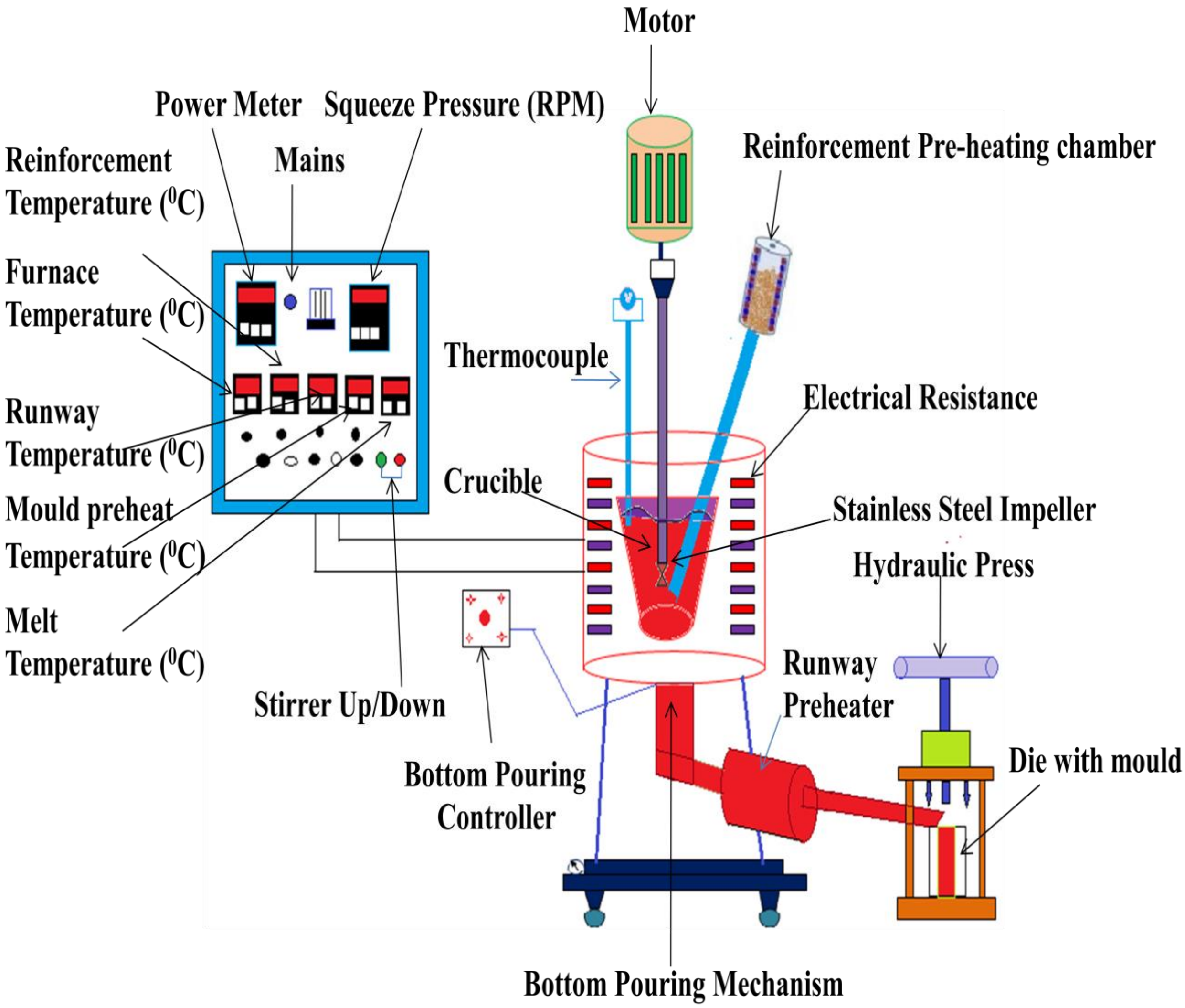

Figure 4.2 Stir Casting Setup (Courtesy: Foundry Shop, PEC, Chandigarh)

Table 4.3 Composition of Powder Reinforcements in Hybrid Composites

Nomenclature of Sample	**Reinforcement Addition in (wt %)**			**Reinforcement Addition in (gms)**		
	Al_2O_3	**SiC**	**CeO_2**	**Al_2O_3**	**SiC**	**CeO_2**
Al-6061/2.5 wt% (Al_2O_3+SiC)	2.5	2.5	0	7.5	7.5	0
Al-6061/5 wt% (Al_2O_3+ SiC)	5	5	0	15	15	0
Al-6061/7.5 wt% (Al_2O_3+ SiC)	7.5	7.5	0	22.5	22.5	0
Al-6061/2.5 wt% (Al_2O_3+SiC)+ 0.5 wt% (CeO_2)	2.5	2.5	0.5	7.5	7.5	1.5
Al-6061/5 wt% (Al_2O_3+ SiC)+ 1.5 wt% (CeO_2)	5	5	1.5	15	15	4.5
Al-6061/7.5wt% (Al_2O_3+ SiC) +2.5 wt% (CeO_2)	7.5	7.5	2.5	22.5	22.5	7.5

The step wise process for fabrication of hybrid composites samples with mixture of (Al_2O_3+SiC+CeO_2) is depicted in figure 4.3.

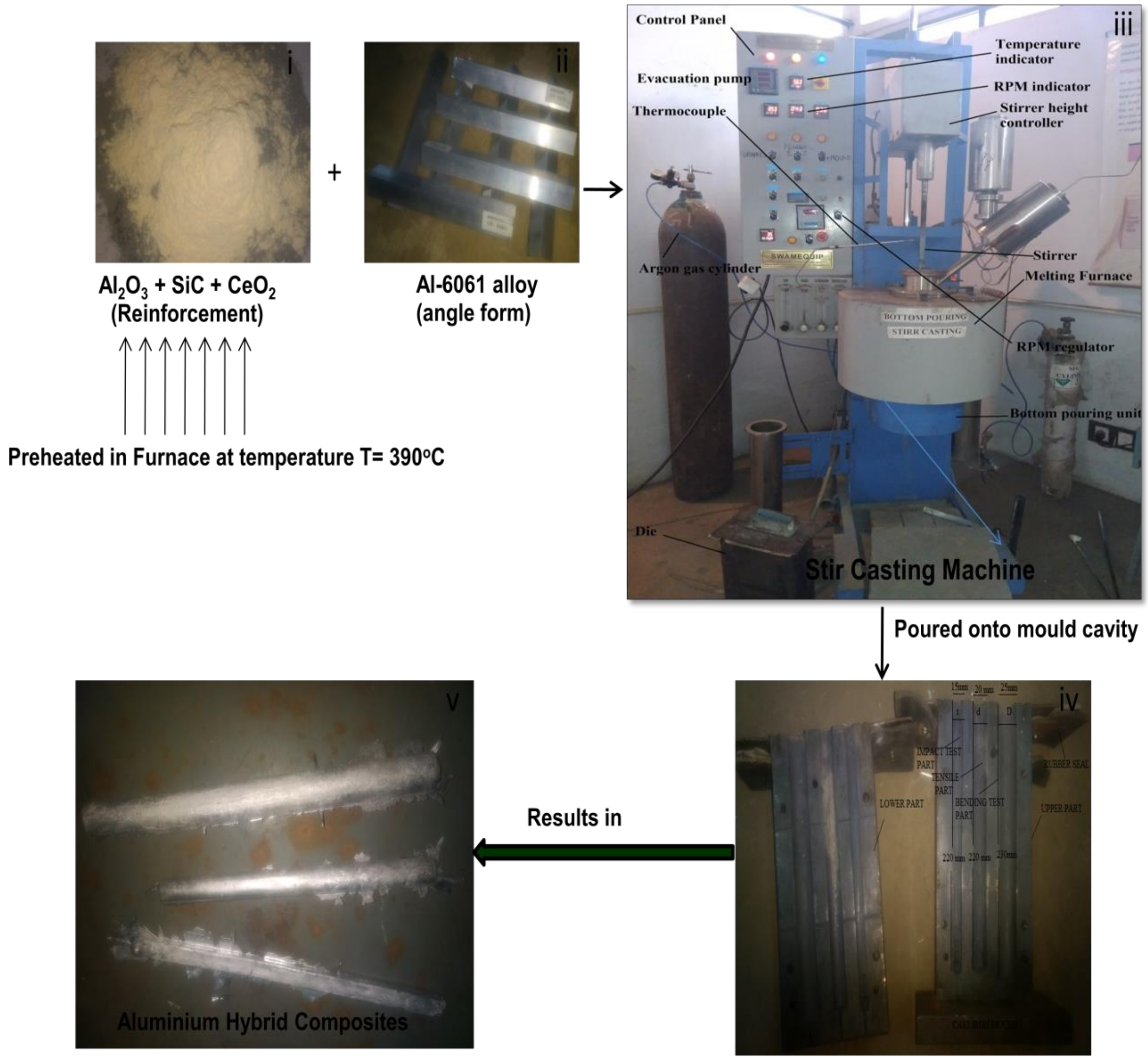

Figure 4.3 Fabrication of Aluminium Hybrid Composite Via Stir Casting

4.4 CHARACTERIZATION OF THE HYBRID COMPOSITES

The characterization of the hybrid composites has been done in four ways viz. physical characterization, metallographic characterization, mechanical characterization and surface characterization.

4.4.1 Physical Characterization

To determine the density and void fraction of prepared composites with different weight percentage of $SiC/Al_2O_3/CeO_2$, all the samples were put under physical characterization testing. Both theoretical and experimental density is measured by the technique [Megahed et al., 2017] and Archimedes's principle for experimental density [Kumar et al., 2017]. The theoretical density of the alloy composites is calculated using rule-of-mixture via equation (4.1), while experimental density is evaluated using water immersion technique based on Archimedes' principle. Thereafter, void content is computed as per equations (4.2) to (4.3).

$$\rho_{th} = \frac{1}{\frac{w_m}{\rho_m}+\frac{w_{ce}}{\rho_{ce}}+\frac{w_{SiC}}{\rho_{SiC}}+\frac{w_{Al2O3}}{\rho_{Al2O3}}} \quad \ldots\ldots\ldots \textbf{Eq. (4.1)}$$

W_m is the wt% of matrix metal; W_{Ce} is the wt% of cerium oxide; W_{SiC} is the wt% of silicon carbide, W_{Al2O3} is the wt% of alumina, ρ_m is the density of matrix alloy, ρ_{Ce} is the density of cerium oxide particles, ρ_{SiC} is the density of the silicon oxide particles and ρ_{Al2O3} is the density of the alumina particles.

$$\textbf{Void Content} = \frac{Theoretical\ Density(\rho_{th}) - Experimental\ Density(\rho_{Ex})}{Theoretical\ Density_{(\rho_{th})}} \quad \ldots\ldots\ldots \textbf{Eq. (4.2)}$$

$$\textbf{Or, } V_p = \frac{(M_m+M_r)}{\rho_c} - \left[\frac{M_m}{\rho_m} + \frac{M_r}{\rho_r}\right] \quad \ldots\ldots\ldots \textbf{Eq. (4.3)}$$

The accurate value of density measured experimentally of different composites samples was calculated by dividing the estimated value of measured weight of a composite sample by its measured volume using a digital weight balance machine having tolerance of ± 0.0001 mg. To achieve the consistency in results, each composite sample having same composition tested thrice.

4.4.2 Metallographic, Chemical and Structural Characterization

The metallographic characterization of the prepared hybrid composite samples was done using scanning electron microscopy (SEM) (Make: JEOL; JSM-6510LV; Japan). Electron back scattered diffraction (EBSD) technique was used to analyse the microstructure of the prepared samples. The chemical characterization or elemental analysis was done using as analytical technique called Energy dispersive spectroscopy (EDS). For structural characterization of the hybrid composite samples, X-ray diffraction (XRD) technique has been used. The steps involved in sample preparation and all experimental details for particular analysis are described in further sections.

4.4.2.1 SEM and EDS Analysis of Hybrid Composites Samples

The samples were prepared using SiC emery paper up to a mesh size of 1500. After a standard procedure of polishing, the composite samples were then etched with a solution of 5 Vol% of concentrated hydrofluoric acid in 95 Vol% H_2O for the microstructure examination. These samples were also deeply etched with a solution of 15 Vol% hydrochloric acid to show the three dimensional morphology of Si phase. The SEM and EDS characterization of specimens were examined directly by SEM with EDS attachment (JEOL; JSM- 6510LV; Japan) as shown in figure 4.4. SEM was used to observe the sample surfaces and proper dispersion of reinforcement particulates in composite material. In SEM microscopy, a particular area of the sample surface was selected to produce a two-dimensional image. This revealed information about the sample including external morphology (texture) and chemical composition.

Figure 4.4 Scanning Electron Microscopy (Make: JEOL; Model: JSM- 6510LV; Japan) (Courtesy: SAI Labs, Thapar Institute of Engineering and Technology, Patiala)

4.4.2.2 Characterization Using EBSD Analysis

The micro structural evolution and the mechanism of stir casted hybrid composites samples were investigated using Electron Back Scattered Diffraction (Make: JEOL; Model: JSM- 7600F; Japan). The accelerating voltage used for the analysis of samples was kept between 0.1 to 30 kv with higher magnification of 100X to 1,000,000X. Samples with maximum hardness values were chosen for EBSD analysis with rectangular shape having dimensions 12 mm x 4 mm. For this purpose hybrid composite samples containing 7.5 wt% of (SiC + Al_2O_3) in alloy as well as 7.5 wt% of (SiC + Al_2O_3) with 2.5 wt% of CeO_2 in alloy were prepared. EBSD analysis showed the grain size values for selected area fraction with their distribution and orientation with average grain size and standard deviation. EBSD analysis of the samples was performed at Metallurgical and Materials Engineering Department, IIT Bombay, (India) as shown in figure 4.5. Grinding of all the samples was done with the help of different emery papers having grades varies from 80 to 1200 grit followed by polishing with 1 μm diamond paste solution. The grounded and polished samples were further electro polished using 20% perchloric acid and 80% ethanol solution on a very fine cloth of velvet for nearly 10 minutes. After that the samples were further processed using ion-beam polishing machine (Precision etching coating system, Make: Gattan; Model: 682). Ion beam polishing was done at 65° rock angle for nearly 5 minutes.

Figure 4.5 3D Electron Back Scattered Diffraction by Field Emission Gun (Make: JEOL; Model: JSM- 7600F; Japan) (Courtesy: National Facility Orientation Imaging Microscopy & X-Ray Bulk Texture, IIT Bombay)

4.4.2.3 Phase determination using XRD analysis

X-Ray diffraction measurements of all the samples of composites were carried out by a Panalytical X'Pert Pro^{TM} diffractometer, Netherland by using CuK radiation and nickel filter at 40 mA under a voltage of 45 kV as shown in figure 4.6. All the specimens were scanned in 2θ range varies from 20^{o} to 110^{o}. The diffractometer being interfaced with X'Pert data collector software provides 'd' values directly on the diffraction pattern. These 'd' values were then used for identification of various phases using ASTM X-Ray diffraction data cards. To confirm the presence of the minor precipitate phases as detected by the diffraction pattern, the'd' values for different phases were obtained using ICSD (International Centre for Diffraction Data) cards available with the software and were manually compared with the diffraction pattern of all the samples.

Fig 4.6 X-Ray Diffractometer (Make: PANalytical; Model: X'Pert Pro; Netherland) (Courtesy: SAI Labs, Thapar Institute of Engineering and Technology, Patiala)

4.4.3 Mechanical and Surface Characterization

4.4.3.1 Hardness

The hardness of the specimen was measured using Vicker’s micro hardness tester and Rockwell hardness tester as shown in figure 4.7 (a-b). Vicker’s micro hardness test specimens were manufactured using grinding operation along with polishing process. In Vicker’s micro hardness test (Make: Wilson; Model: 401/402 MVD; USA), a diamond shape indenter creates the indentation on specimens by varying the quantity of applied loads. A vernier scale attached to the tester was used to calculate the size of indentation marks that is calibrated in terms of the hardness value. The dwell time of indenter was 15 seconds. In the current research, the value of load applied was 5 kg for a dwell time of duration of 10 seconds and value of load and dwell was kept constant for all the samples. For getting the more repeatability in the results, the Vicker’s micro hardness tests were performed thrice for each sample. The Rockwell hardness was measured using the Rockwell hardness tester with a load of 100 kgf for the duration of 10 seconds. The indenter used in this test was a spherical shaped indenter. Once the indentation was completed, the hardness value was indicated on the circular scale attached to the tester.

(a) (b)

Figure 4.7 (a) Vickers Hardness Tester (b) Rockwell Hardness Tester (Courtesy: Solid Mechanics Lab, Thapar Institute of Engineering & Technology, Patiala)

4.4.3.2 Tensile Testing

To evaluate the tensile behavior of the samples a Universal Testing Machine (Make: FIE; Model: UTE-100; India) with capacity 100 KN as shown in figure 4.8 was used. In tensile test yield point, ultimate point and breaking point was observed. All the tests on the specimen were performed at room temperature of 25±3 ^{o}C with relative humidity of 40 to 60%. The tensile test samples were prepared on a CNC machine as per the ASTME-8 standards with a round 'dumbbell' shape as shown in figure 4.9. The gauge length of all the tensile specimens was maintained approximately four times of the diameter as per the standards of ASTME-8 [Verma and Vettivel, 2018]. The hybrid composite samples were pulled with a strain rate of $10^{-4}s^{-1}$ until the failure takes place. The tensile tests were performed five times to get repeatability in results. The ultimate tensile strength, yield strength and % elongation were calculated for the tensile specimen.

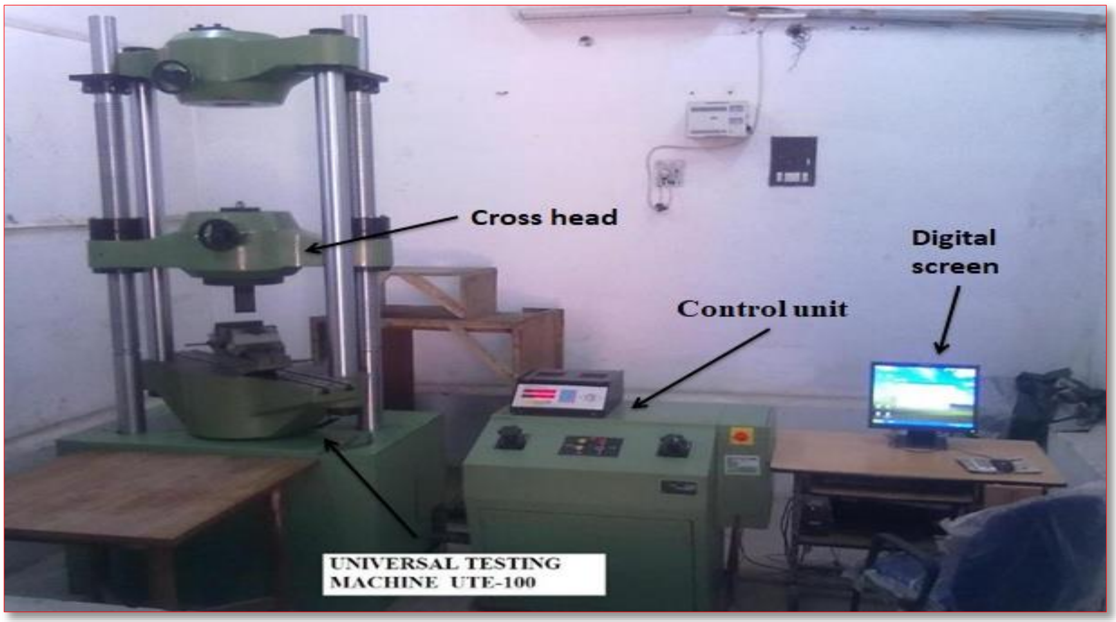

Figure 4.8 Universal Testing Machine (Make: FIE; Model: UTE-100; India) (Courtesy: CITCO-IDFC Testing Laboratory, Chandigarh)

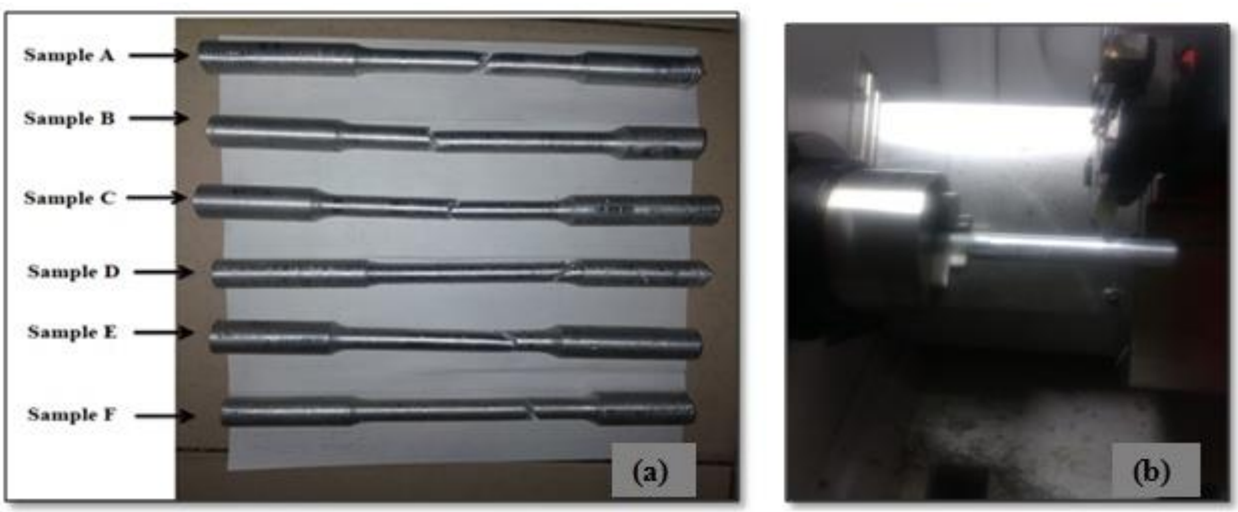

Figure 4.9 Details of Tensile Test (a) Samples after Tensile Testing (b) Tensile Testing on UTM Machine

4.4.3.3 Impact Testing

The charpy impact tests were carried out on impact testing machine as shown in figure 4.10. The dimensions of specimen for impact test was kept as 56x10x10 mm with notch depth and tip radius as 2 and 0.25 mm respectively at an angle of 45^0. Impact tests were performed thrice for each condition to ensure repeatibility and average values were taken for the impact strength. The standards used for the various testing while preparations of specimen are shown in table 4.4.

Table 4.4 Various Standards Used for the Various Mechanical Testing

Standards of Mechanical Testing		
Test Name	**International standard Follow**	**Specifications of sample prepared**
Tensile Testing	ASTM-8	Gauge Length=30mm Diameter of specimen=5mm Strain Rate=$10^{-4}S^{-1}$
Vickers Micro-hardness Test	IS 1501-2002	Load=5 Kg Dwell time=10 Sec Scale used=C-Scale
Impact Testing	ASTM E-23	Dimensions of Specimen= 56x10x10mm Notch Depth= 2 mm Notch tip radius=0.25 mm Angle of notch= of 45^0

Figure 4.10 Impact Testing Machine (Courtesy: Solid Mechanics lab, Thapar Institute of Engineering & Technology, Patiala)

4.4.3.4 Flexural Test

The Flexural testing specimens of fabricated hybrid composites were machined according to ASTM standards. The composite were tested for Flexural strength by using universal testing machine (Make: FIE; Model: UTE-100; India) at room temperature. Three point bending test was used for flexural strength.

4.4.3.5 Dry Sliding Wear Tests

Dry sliding wear tests have been conducted on universal pin-on-disc testing machine. In this setup a cylindrical pin specimens of diameter 10mm and length 12mm was held against the rotating disc of counter face material and sliding motion results in the wear of the pin specimens. Dry sliding wear testing of the samples using pin-on-disc configuration was accomplished on tribometer (Make: Ducom; Model: TR-201E-M2; India) as shown in figure 4.11. A disc of low carbon steel EN-31 having hardness 68 HRC was used as a counter face material. Before starting the wear test all the composite samples were ground with emery paper of different grades, polishing with 0.05μm diamond paste followed by cleaning with acetone. For carrying wear test of the samples, sliding speeds of 0.5, 1 and 2 m/sec under three normal loads values as 10, 20 and 30 N were chosen. All the tests were performed uptil the sliding distance of 2000 m. The parameters used in wear tests are tabulated in table 4.5.

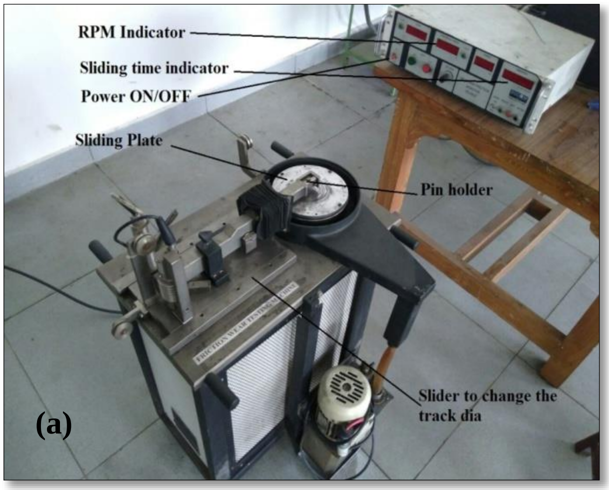

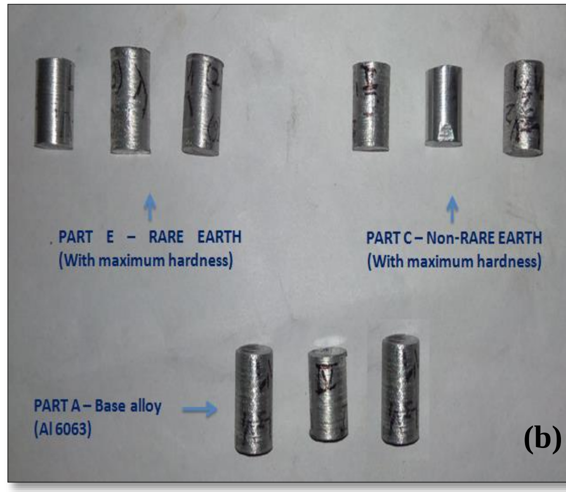

Figure 4.11 Wear Test Set- Up (a) Pin-On-Disc Tribometer (Make: Ducom; Model:TR-201E-M2; India) (b) Pin Shape Hybrid AMCs

Table 4.5 Details of Parameters Used in Sliding Wear Test

Parameters	**Description**
Testing specimens and samples	Pin-on-disc (a) Al-6061 alloy + SiC + Al_2O_3 (b) Al-6061 alloy + SiC + Al_2O_3+ CeO_2
Counter disc	Material of disc = EN 31 Steel Hardness of disc = 68 HRC Diameter of disc = 160 mm
Sliding distance (m)	500, 1000, 1500, 2000
Sliding Velocity (m/sec)	0.5, 1, 2
Normal loads (N)	10, 20,30
Lubrication Condition	Dry condition
Temperature (°C)	Atmospheric temperature

4.4.3.6 Hydrophobicity Analysis

In order to check the hydrophobic behavior of the hybrid composites surface, the samples with different weight percent of reinforcements were prepared. The majority of researchers used contact angle approach for calculating the interaction energy within a liquid and solid due to its simplicity and high accuracy. The sessile drop shape analyzer (Make: Kruss; Model: DSA 100; Germany) is generally suited to calculate the contact angles of hybrid composites with resolution of 0.01 degree. The contact angle measured using DSA 100 lies between 0 to 180 degrees with surface tension range of 0.01 to 2000 mN/m. In sessile drop analyzer, contact angle measurement is done by dispensing a small drop of liquid from probe onto the surface of measurement and taking its images. Afterward, captured images are analyzed with image processing software for measuring value of contact angle. Set-up used for this measurement is shown in figure 4.12. For wettabillity analysis six samples with different compositions of Al_2O_3, SiC and CeO_2 have been prepared in size of 2cm x 2cm.

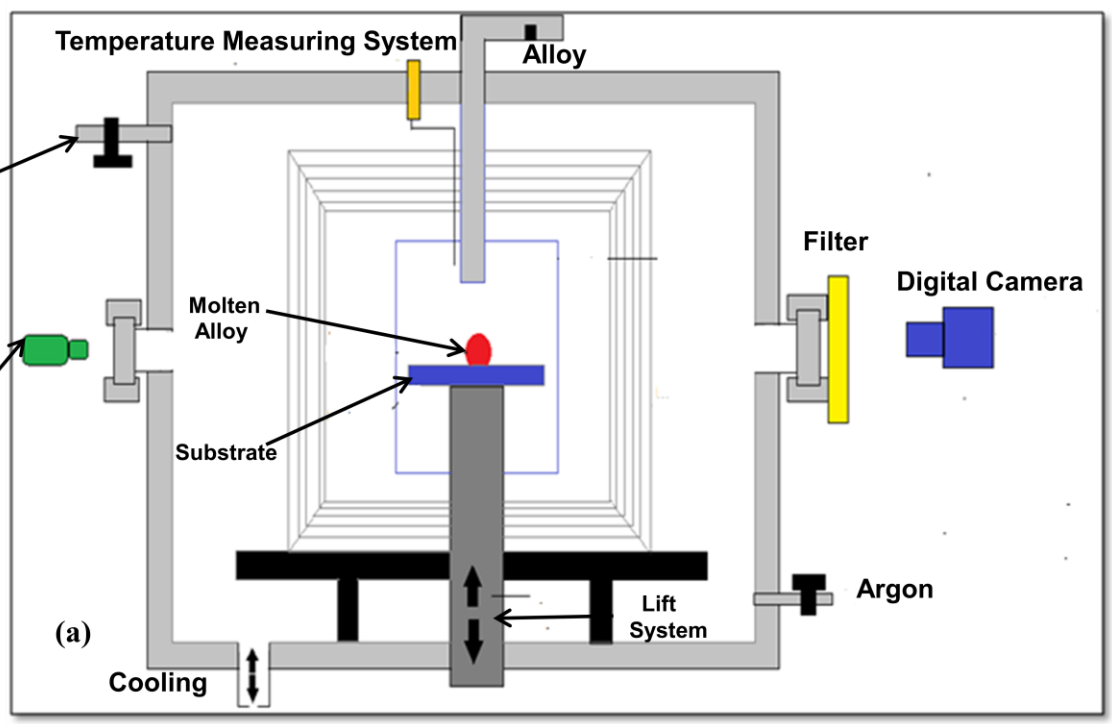

Figure 4.12 Experimental Set-Up of Sessile Drop Analyzer for Measurement of Contact Angle (Make: Kruss; Model: DSA 100; Germany)

Generally, the wettability is described in terms of angle of contact. The concept of wettability between the solid-liquid interfaces was described by various researchers using their own mathematical models with different important characteristics like surface energy and contact angle [Laurent et al., 1987]. After exhaustive literature study for evaluation of interaction energy, Thomas Young model was found to be an accurate mathematical model for it. In this model, Thomas Young used some Laplace equation to find the relation of contact angle with surface energy in order to define the wettability. Following are the equations used to determine the shape of the droplet and the role of contact angle in various boundary conditions as indicated in figure 4.13. Before defining the expression of interaction energy within liquid and solid, assumption is made that solid surface is smooth, inflexible and homogenous [Hashim et al., 2001].

At equilibrium condition, the contact angle (θ) is defined by the Young-Dupre equation as indicated in equation (4.4):

$\gamma_{sv} = \gamma_{sl} + \gamma_{lv}\cos\theta$ ……………………………………………………………………**Eq. (4.4)**

In equation (4.4), the terms γ_{sv} , γ_{sl} and γ_{lv} are specific energies of solid-vapour, solid-liquid and liquid-vapour interface respectively. Here, each specific energy or surface tension force can be taken as tension force per unit area. As demonstrated in figure 4.13(a), fall of fine liquid drop on sample surface replaces a bit of interface formed between solid-vapour by a liquid-vapour and liquid-solid interface. As per the equilibrium condition stated above, decrease in free energy of the system will lead to the phenomenon of liquid spreading [Kalantarian et al., 2009]. The bonding force between the liquidus and solidus i.e. the adhesion force (F_a) is defined as

$F_a = \gamma_{lv} + \gamma_{sv} - \gamma_{sl}$ …………………………………………………………………………**Eq. (4.5)**

After combining both equation (4.5) and (4.6), we get

$F_a = \gamma_{lv}(1 + \cos\theta)$ ……………………………………………………………………...**Eq. (4.6)**

It is clearly evident from the above equations that surface tension of the liquid (γ_{lv}) and contact angle can be used to express bonding force between the liquid and solid phase. This thing can also see in figure 4.14(b-e). It is clearly seen from the figure 4.13(b) that for absolute wetting, the angle of contact $\theta = 0$ and $\gamma_{sv} = \gamma_{lv} + \gamma_{sl}$. Likewise, for good wetting, the contact angle θ should be between 0 and 90 degrees. As indicated by figure 4.13(c), with increase in trend of contact angle, surface tension relation becomes $\gamma_{sv} > \gamma_{sl}$. From figure 4.13(d) it is observed that the contact angle lies between 90 and 180 degrees and as of a very large contact angle (θ), $\gamma_{sv} < \gamma_{sl}$. The increase in the value of surface energy at solid vapour interface as compared to solid-liquid interface is an indication of bad wetting [Kalantarian et al., 2009]. For non-wetting conditions, the contact angle (θ), should be 180 degrees and $\gamma_{sv} = \gamma_{lv} - \gamma_{sl}$ as seen from figure 4.13(e). Hence, surface energy and contact angle measurement are the two factors used as a basis for defining degree of wettability of the surface.

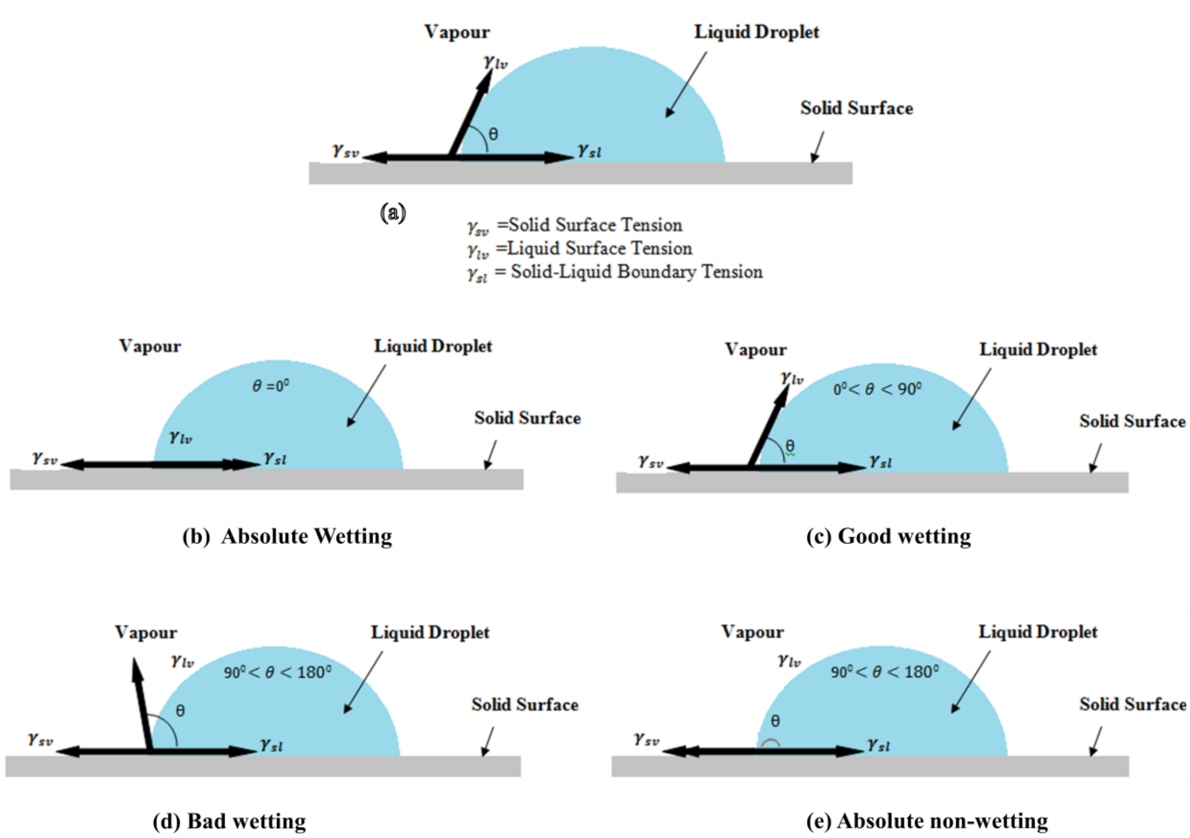

Figure 4.13 (a-e) Dependence of the Surface Wettability on Surface Energy and Contact Angle (θ *in degrees*) [Kalantarian et al., 2009].

Based on the above discussion, the sessile drop analyser method was employed in order to check the wettability of the hybrid composites. The probe liquid usually employs water using the principle as stated by the Thomas Young for determining the contact angle. The comparative analysis of wettability of hybrid composites has been done on the basis of contact angle. Surface of the hybrid composites can become hydrophobic by addition of elements instead of surface modification. These type of composites can become a good choice for making outer body parts of aircraft components including wings, structural components and other accessories which directly comes in contact with water. On the basis of interaction between water and solids in particular the surfaces can be classified as hydrophilic or hydrophobic as shown in figure 4.14. These words are derived from the Greek philosophy which means water-loving and water-fearing respectively. Materials which have very strong affinity towards water are recognized as hydrophilic materials, and cause water to spread whole over its surface and finally maximizing its contact. Most of the materials tend to be found hydrophilic in nature; it means usually water spread upon it during contact. Materials having tendency to keep away water are recognized as hydrophobic materials. Hydrophobic materials generally suited for the wide range of applications because of the low surface energy. Hydrophobic surfaces in particular, have attracted many researchers over the few years because of their wide industrial and technological prospective. Considering this fact, wettability of fabricated hybrid composites has been studied in the current work.

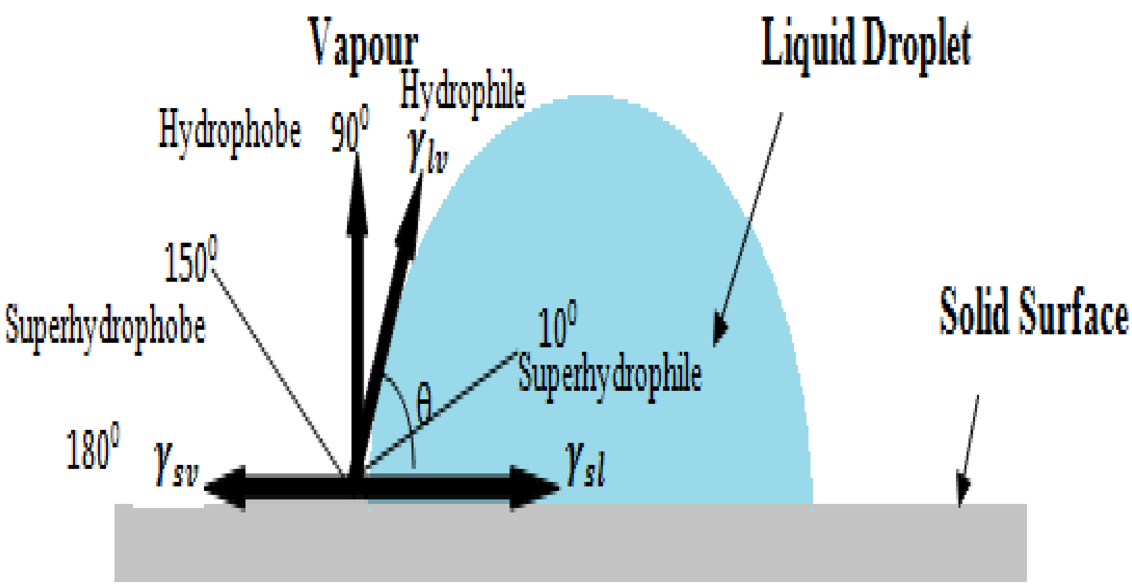

Figure 4.14 Quantification of wetting properties in terms of contact angle (θ) [Kalantarian et al., 2009]

4.4.3.7 Corrosion Analysis

Corrosion behaviour of the hybrid composite samples was analyzed using 3.5% NaCl solution and temperature of 30^0C by potentio dynamic polarization electrochemical method. The hybrid composite samples were made in specification of 20 mm x 30 mm x 1 mm for corrosion test. Before testing, all the samples surfaces were smoothened and polished using silicon carbide emery papers from 220 to 600 grades in accordance with ASTM standard. After preparing smooth surfaces, all the samples were washed with deionized water followed up by drying. The corrosion test rig consists of three electrodes. Area of specimen's exposed surface served as working electrode, second one used as reference electrode was made of saturated silver/silver chloride and last one used as counter electrode of platinum. All the specimens were tested for 24 hours using open-circuit corrosion potential (OCP) test with amplitude of 10 mV, frequency range from 0.01 Hz to 0.10 MHz and potential range varies from -200 mV to +1500 mV. After careful examination and washing in acetone solution of each sample, their surfaces were dried using compressed air for weighting of specimens.

4.4.4 Finishing of Hybrid Composites using Magnetic Abrasive Flow Machining Process

A hydraulically powered experimental set up for MAFM process has been used. In MAFM process, magnetic abrasive medium carrying abrasive particles is extruded through the work piece passage to be finished. The shearing of the magnetic abrasive medium near the work piece surface contributes to material removal and surface finish. Extrusion of the magnetic medium through the passage formed in the work piece fixture is accomplished by driving two opposite pistons containing cylinders using hydraulic actuators. These actuators are moved in desired manner using designed hydraulic circuit. The workpiece fixture designed along the motion of the working fluid is shown in the figures 4.15 (a-b). The MAFM set up with different components such as: double acting hydraulic cylinder (EN-8 steel capable of withstanding up to 10 MPa pressure) with piston arrangements, workpiece holding tooling arrangement, circular fixture of aluminium with appropriate design, two coil type magnets for generating magnetic effect (0-2 Tesla), abrasive media and hydraulic fluid control unit comprises of extrusion pressure gauge, pressure variation system with hydraulic power pack (2 HP motor, with two directional control valve and two pressure gauges with 20.68 MPa) and flange support structure is shown in figure 4.16.

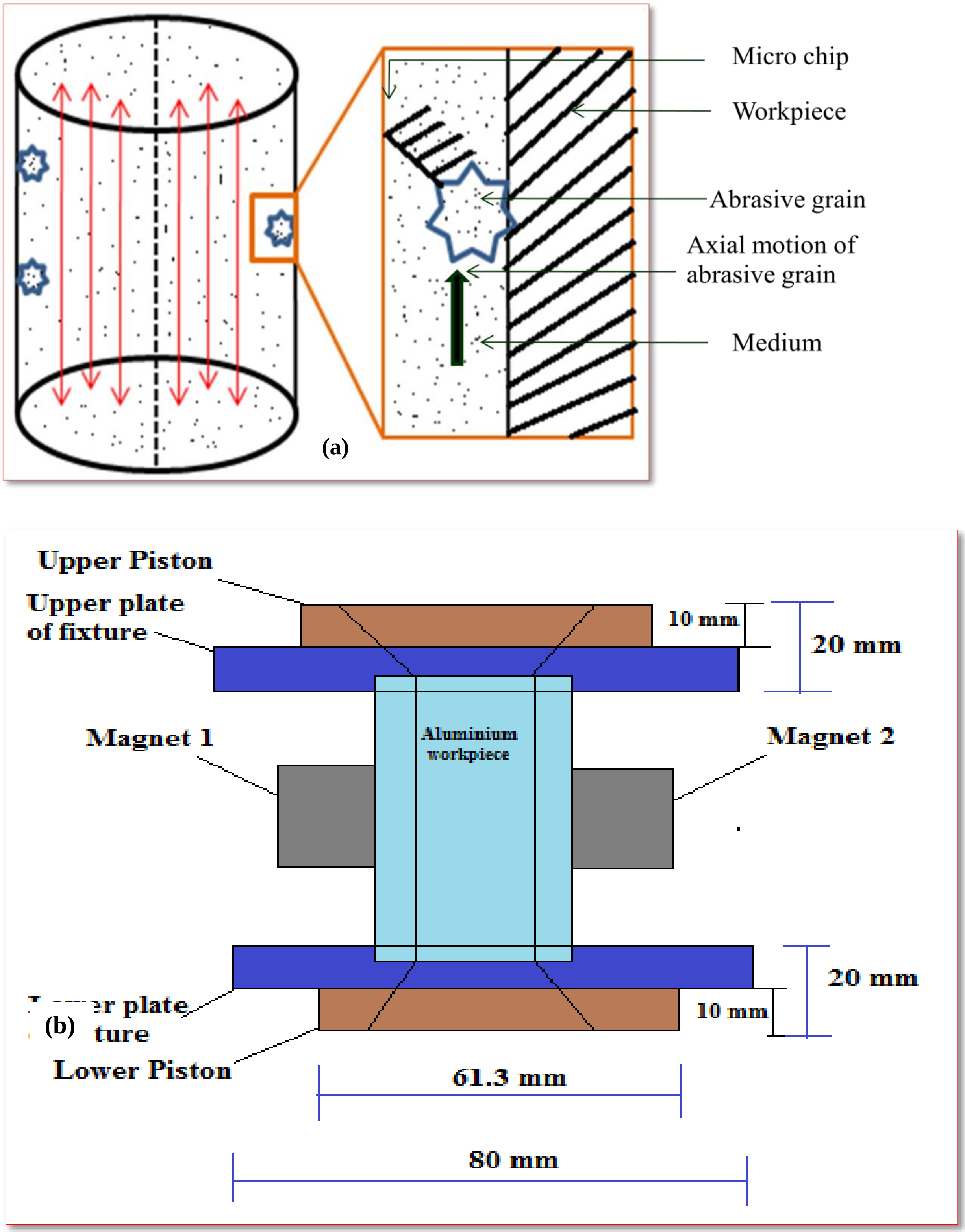

Figure 4.15 (a) Workpiece Fixture Design (b) Motion of working Medium in Workpiece

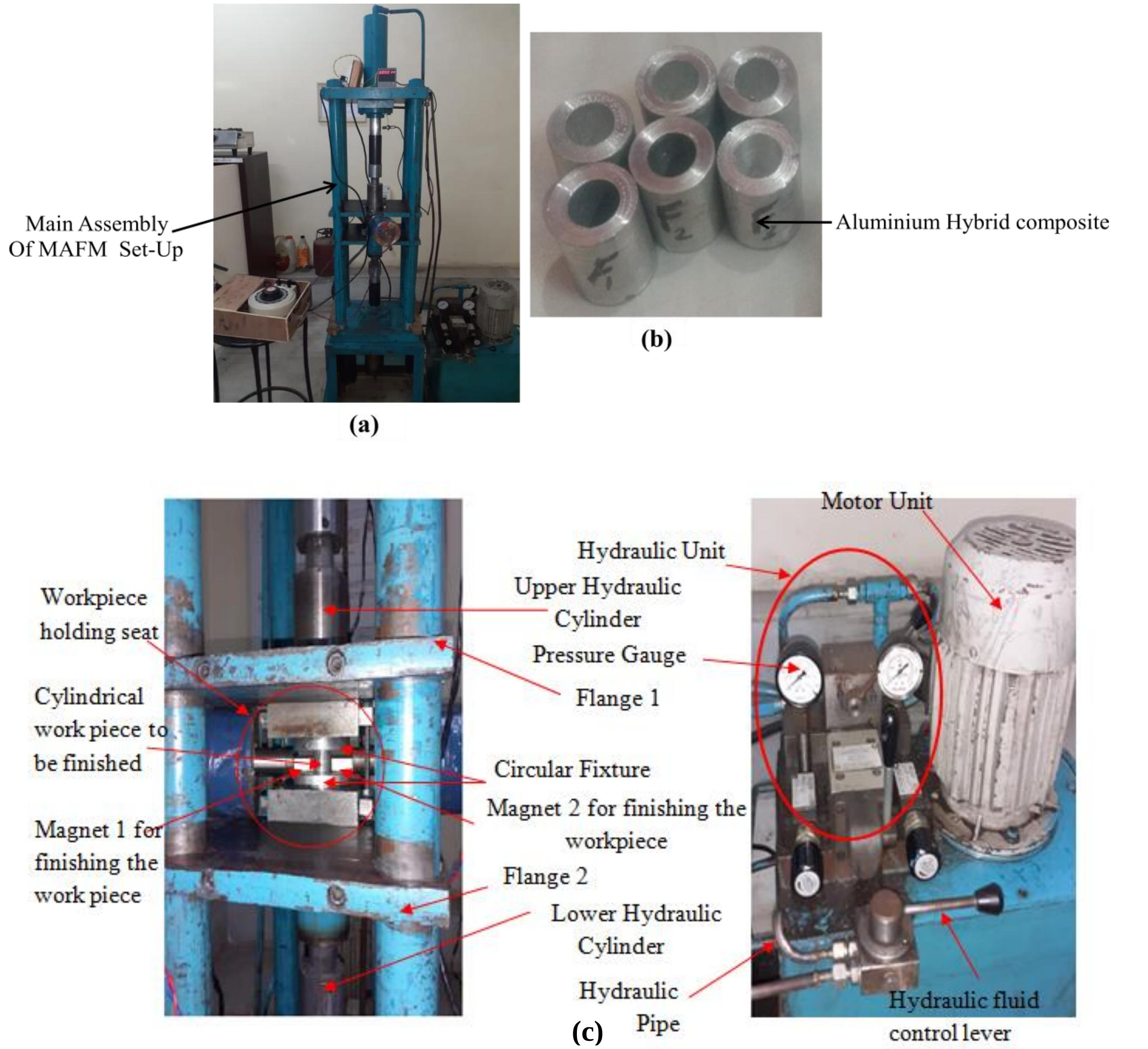

Figure 4.16 (a) Magnetic Abrasive Finishing Process Set-Up (b) Aluminium Hybrid Composites (c) Sectional Parts of MAFM Set-Up

4.4.4.1 Parametric Study of MAFM Parameters using Box-Behnken Design

MAFM is a stochastic procedure and an enormous number of control factors impact its procedure. Any adjustment even in a process parameter may deliver unfortunate results prompting loss of efficiency, decay in surface quality or both. In test contemplates, input factors called as control factors are changed and their effects on outcome performance measures (response) are watched. Each control factor can take a few qualities over the span of experimentation. Such qualities of control factors are called levels or treatments. An examination (likewise called preliminary or run) is a mix of parameters at various levels whose impact on the output is of essential concern.

In order to carry out the experiments, a logical methodology with scientific approach is important to design the tests by assigning equivalent significance to all control factors. An appropriately arranged and executed arrangement of investigations is of prime significance for inferring clear and precise conclusion from the test observations. The one factor in a time (OFTA) approach is a technique used to design and analyzed by changing each factor in turn keeping every single other factor at fixed levels. This strategy is successful just when emphasis is just to estimate main effects of the factors on responses and trial error isn't excessively huge when contrasted with factor impacts, for example, screening tests where it is desirable to isolate inconsequential factors [Montgomery, 2002; Kant and Sangwan,2014].

This strategy experiences genuine downsides that are given underneath:

(i) OFTA approaches require progressively number of runs to appraise impact of variables for the same exactness as got in statistically designed investigations.

(ii) OFTA neglects to address interactions existing between the parameters accepting that each factor carries on independently.

(iii) OFTA considers the impact of just a single parameter at once. In genuine machining process, combined impacts of various control factors yield the output. In this manner, genuine ideal settings can't be obtained when OFTA approach is followed for plan of analyses.

Keeping in view previously mentioned confinements, Sir Ronald A. Fisher conceived factorial experiments design, which center around concurrent change in various factors one after another [Montgomery, 2002; Davim,2003]. A valuable technique named as design of experiments was built up. Design of experiments (DOE) is characterized as, “A collection of mathematical and statistical procedure that are helpful for modelling and investigation of problems in which a response of interest is affected by a few factors and goal is to optimize the response” [Montgomery, 2002; Barbosa et al., 2017].

4.4.4.2 Response Surface Methodology

RSM approach is utilized to do the mathematical modeling of the given problem with simultaneous application of statistical techniques where a large number of independent variables influence the output response. This technique was invented by the Box and Wilson in 1951. Because of its ability to provide the overall result summary of the experiment with parametric study of factors affecting the response, it is widely accepted in many areas like in biotechnology field it is used in reactions and titrations and in production field it has been carried used in machining process, welding process, grinding process, abrasive flow machining [Manna and Bhattacharyya, 2004] and magnetic abrasive flow machining process etc. [Gunaraj and Murugan, 1999] proposed the detailed methodology of the RSM approach:

(i) First to design the series of experimental plan for the satisfactory and consistent measurement of the concerned response.
(ii) Afterwards development of suitable mathematical models for analyzing the affect of second order response with best fittings.
(ii) Next is to find out the optimal combination of the parameters that affects the output response mostly.
(iv) Finally the affect of interaction among various parameters have been analyzed using surface and three dimensional plots.

Keeping in mind the above advantages associated with the RSM approach, a Box-Behnken Design have been applied in the optimization of MAFM process parameters that affects the surface roughness of the hybrid composites.

4.4.4.3 Box-Behnken Design

Box-Behnken design are special types of three-level fractionate factorial designs, which allows modeling of 1st and 2nd order response surfaces. These designs are cost-effective than three-level full factorial designs, particularly for large number of input factors [Bezerra et al., 2008; Candioti et al., 2014; Politis et al., 2017]. We can see that all points used in Box-Behnken designs (figure 4.17 (b)) were selected from the 33 full factorial designs as shown in figure 4.17(a) [Souza et al., 2005]. The special arrangement of the BBD levels allows the number of design points to increase at the same rate as the number of polynomial coefficients. For example, for three factors, the design can be constructed as three blocks of four experiments consisting of a full two-factor factorial design with the level of the third factor set at zero [Souza et al., 2005].

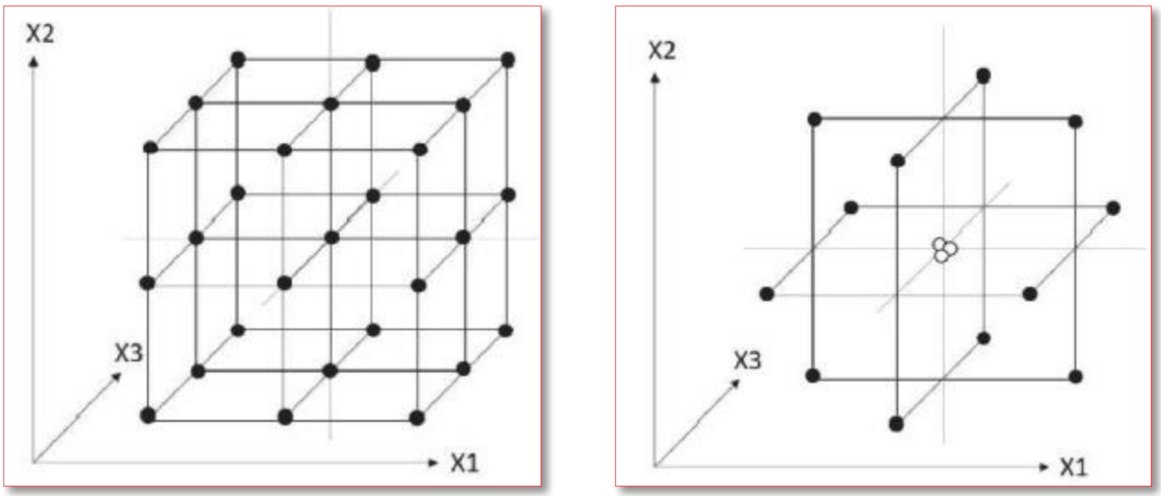

Figure 4.17 (a) Illustration of Three-Level Full Factorial Design Matrix (b) Box- Behnken Design Matrix for Three Input Factors. [Souza et al., 2005]

Outcome of pilot experiments were used as a basis for selection of process parameters with various levels for the plan of main experiments in MAFM process. One-factor-at-a-time approach was used to conduct pilot experiments. The design of experimental run was done using Box- Behnken design. Seventeen experiments were performed on the basis of BBD design taking three control factors at three levels as shown in Table 4.6 with design matrix is shown in Table 4.7. As first-order models often give lack-of fit, a second order regression model was developed. The optimization procedure for RSM is mainly categorized into three stages. A second-order regression model was developed for getting the relationship between the various response factors for BBD as indicated below:

$$Y = \beta_0 + \sum_{i=1}^{k} \beta_i x_i + \sum_{i=1}^{k} \beta_{ii} x_i^2 + \sum_{i<j} \beta_{ij} x_i x_j$$ **……………………….Eq. (4.7)**

Y = response, x_i = (1, 2,…..., k) are the independent process variables. Coefficient β_O = constant and β_i, β_{ii} and β_{ij} are the coefficients of linear, quadratic and interaction terms, respectively.

Table 4.6 Process Parameters and Their Levels

S. No	Process parameters	Notations	Units	Levels		
				1	**2**	**3**
1	Magnetic Flux Density (MFD)	A	Tesla	0.25	0.5	0.75
2	Number of cycles	B	Stroke	80	160	240
3	Extrusion pressure	C	MPa	1.4	2.8	4.2
MAP Grit Size : 200 microns Working gap : 1.00 mm						

Table 4.7 Design Matrix and Output Response

Run	Magnetic Flux density (Tesla)	Number of cycles (stroke)	Extrusion Pressure (MPa)	Initial Surface Roughness (R_1) (μm)	Final Surface Roughness (R_2) (μm)	Change in Surface Roughness ΔR_a (μm)	% improvement
1	0.5	160	2.8	1.38	0.5	0.88	63.70
2	0.5	160	2.8	1.34	0.45	0.89	66.40
3	0.5	240	4.2	1.39	0.45	0.94	67.60
4	0.75	240	2.8	1.43	0.45	0.98	68.53
5	0.5	80	4.2	1.35	0.43	0.92	68.10
6	0.5	240	1.4	1.20	0.36	0.84	70.0
7	0.5	160	2.8	1.21	0.34	0.87	71.90
8	0.25	240	2.8	1.37	0.65	0.72	52.55
9	0.75	160	4.2	1.51	0.48	1.03	68.20
10	0.75	80	2.8	1.41	0.5	0.91	64.50
11	0.5	80	1.4	1.13	0.38	0.75	66.37
12	0.5	160	2.8	1.20	0.35	0.85	70.80
13	0.25	160	1.4	1.26	0.59	0.67	53.17
14	0.25	160	4.2	1.35	0.61	0.74	54.81
15	0.25	80	2.8	1.24	0.56	0.68	54.84
16	0.75	160	1.4	1.21	0.37	0.84	69.40
17	0.5	160	2.8	1.19	0.32	0.87	73.10

Finally, the roughness value of the composites has been calculated by using a contact type stylus based surface roughness tester (Make: Mitutoyo; Model: Surftest SJ-301, Japan) having a least count of 0.001 mm. The cut-off length for the measurement is used as 0.8 mm. For accurate value of the surface roughness, the surface roughness is measured at three different locations [Dhanawade and Kumar, 2016].

CHAPTER 5

RESULTS AND DISCUSSIONS

5.1 INTRODUCTION

In the present work, hybrid composites (Al-6061-Al_2O_3-SiC-CeO_2) and (Al-6061-Al_2O_3-SiC) were prepared by adding 0.5, 1.5, 2.5 wt% of CeO_2 and 5, 10, 15 wt% of (Al_2O_3 + SiC) mixture in equal proportions respectively. One percent by weight of magnesium was also added as a wetting agent. The fabricated composites were machined and tested for various mechanical, surface, metallographic and structural characterizations. This section presents the detailed analysis of results using metallographic, mechanical, structural and surface characterization on fabricated hybrid composites with different compositions of SiC, Al_2O_3 and CeO_2.

5.2 Al-6061/SiC/Al_2O_3/CeO_2 HYBRID COMPOSITES

The casted composite samples are machined in different sizes of 10x15x150 mm^3, 25x220 mm^2 and 20x220 mm^2 as per the ASTM standard.

5.3 METALLOGRAPHIC CHARACTERIZATION

5.3.1 Morphology of SiC, Al_2O_3 and CeO_2 Particulates

The morphology of various reinforcement particles used in the fabrication of composites reveals its shape and size. SEM images of silicon powder at different magnification are shown in figures 5.1(a-b). From SEM micrograph it can be observed that the particles of silicon carbide exhibit faceted morphology with distinct edges and vertices, where particles undergo repeated brittle fracture. The average size of particles was found to be 39 µm, with an aspect ratio of 1.89 as determined from Image J software. The SEM micrograph in figure 5.2 shows alumina particles at two different magnifications, X500 in figure 5.2(a) and X1000 in figure 5.2(b). The average particles size of alumina was found to be 42 µm with an aspect ratio of 1.78. As seen from the micrograph of alumina, its grain appears to be irregular in shape as a result of brittle fracture as shown in figures 5.2(a-b). Figures 5.3(a-b) shows the SEM image of CeO_2 powder particles with cubic crystal structure, confirming the morphology of CeO_2 grains as branched chain non-uniform structures having average particle size of 16 μm with an aspect ratio of 2.99. The morphology details of particles are presented in table 5.1.

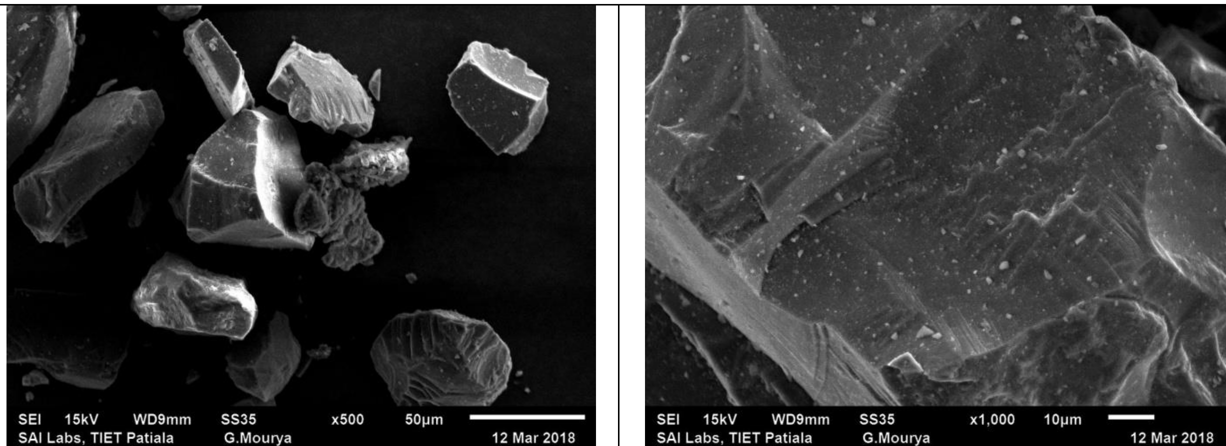

(a) (b)

Figure 5.1 SEM micrograph of silicon carbide particles with different magnifications (a) X500 (b) X1000

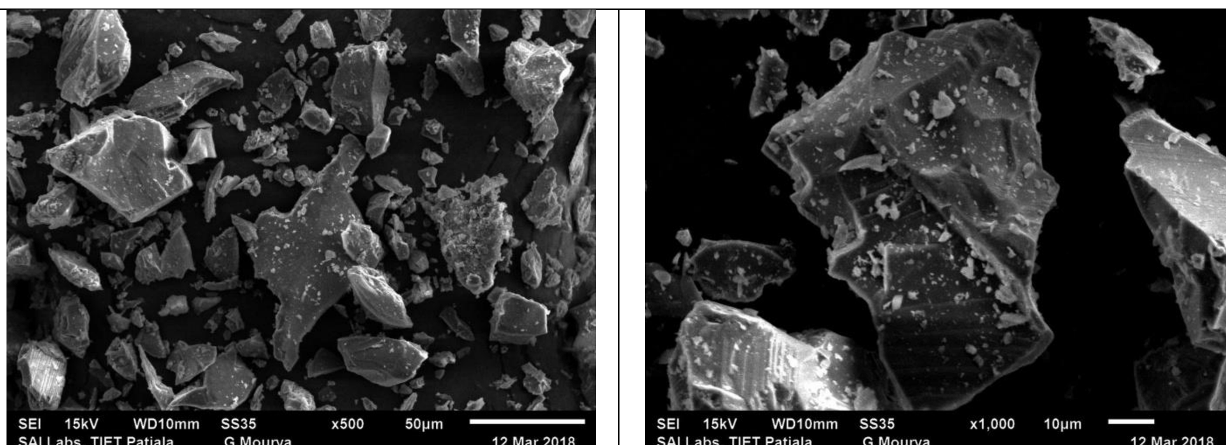

(a) (b)

Figure 5.2 SEM micrograph of alumina particles with different magnification (a) X500 (b) X1000

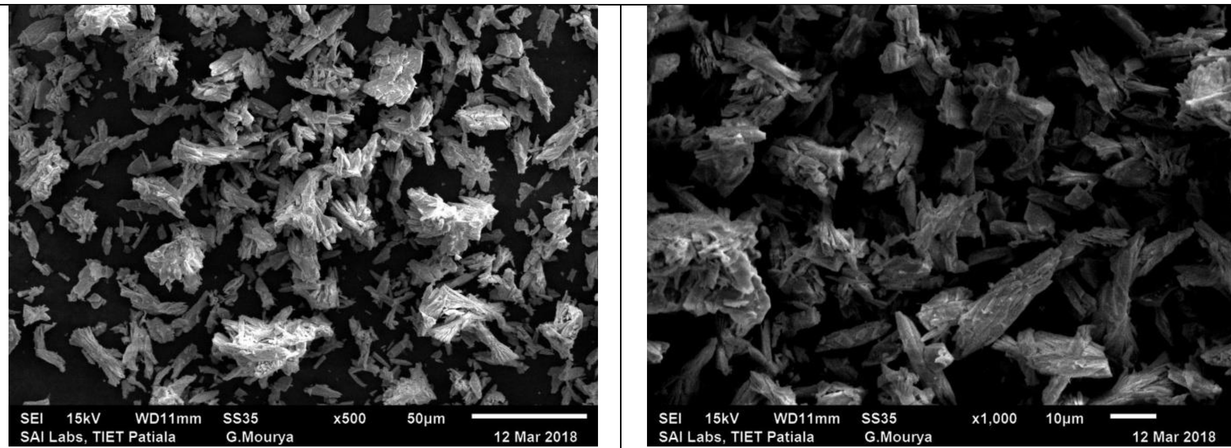

(a) **(b)**

Figure 5.3 SEM micrograph of cerium oxide particles with different magnification (a) X500 (b) X1000

Table 5.1 Morphology of various reinforcement particles

Powders	Average particle length (µm)	Average particle width (µm)	Aspect ratio	Average particle size (µm)
SiC	55.7	29.5	1.89	39
Al_2O_3	50.5	28.3	1.78	42
CeO_2	29.7	9.9	2.99	16

The reinforcement particles used in the composite materials have a very significant role in selecting the required properties for specific applications. Hence the detailed analysis of particle morphology including shape and size is very essential before fabrication of composites. The morphology of reinforcement particles of SiC, Al_2O_3 and CeO_2 has been studied before fabricating the composites. The SiC particles have faceted morphology which improves the stiffness of the aluminium matrix composites. The metal matrix composites with faceted shape of SiC particles showed a higher stiffness due to the phenomenon of strain hardening over the wide area of matrix material [Verma et al., 2001]. As a result of higher stiffness of particles, the composite material becomes best choice for aerospace applications. Moreover, the smaller size of SiC particles (39µm) used in composite material further leads to improvement in the stiffness. The stiffness of the composites material generally depends upon the total surface area of contact between the matrix and reinforcement material. As total surface area increases at the interface of matrix and reinforcement particles, the more amount of load can be transferred to the reinforcement particles which may result in increased stiffness [Wang et al., 2011]. The smaller size of Al_2O_3 particles (42μm) with aspect ratio of 1.78 also resulted in improvement of the composite stiffness and achieving better wear characteristics. Due to incorporation of rare earth oxides (CeO_2) with mean size of 16μm, the properties of composite changed drastically. This may be due to more fine size and acicular (needle) shape of particles. This may be due to reduced size, the cerium oxide particles possess high surface to volume ratios which further helps to enhance the mechanical properties of composites like stiffness, strength and wear resistance. These properties are very critical for particular material to be used for aerospace applications.

5.3.2 Physical Characterization

Density and porosity measurement is a very important step for measuring the performance of composites for specific applications. The theoretical density of composites reinforced with $SiC/CeO_2/Al_2O_3$ in terms of weight fraction was calculated by the formula of rule of mixture given below in equation (5.1).

$$\rho_{tc} = \frac{1}{\frac{W_{Al6061}}{\rho_{Al6061}} + \frac{W_{SiC}}{\rho_{SiC}} + \frac{W_{CeO2}}{\rho_{CeO2}} + \frac{W_{Al2O3}}{\rho_{Al2O3}}} \quad \text{.......... Eq.(5.1)}$$

W_{Al6061} is the wt% of Al6061, W_{SiC} is the wt% of silicon carbide, W_{CeO2} is the wt% of cerium oxide, W_{Al2O3} is the wt% of aluminium oxide, $\rho_{Al\text{-}6061}$ is the density of Al-6061 alloy, ρ_{SiC} is the density of silicon powder, ρ_{CeO2} is the density of cerium oxide powder, ρ_{Al2O3} is the density of aluminium oxide powder.

Table 5.2 represents comparative analysis of experimental and theoretical density. The base alloy Al-6061 theoretically relative density was calculated as 98.88 %.The prepared hybrid composites with 2.5 wt% ($SiC+Al_2O_3$), 5 wt% ($SiC+Al_2O_3$) and 7.5 wt% ($SiC+Al_2O_3$) composition of reinforcement have theoretically relative density was calculated as 99.26 %, 99.63 % and 99.64 %. The theoretically relative density of composites with 0.5 wt% CeO_2, 1.5 wt% CeO_2 and 2.5 wt% CeO_2 was calculated as 99.63 %, 99.64 % and 99.63 % respectively. The above concept of density measurement is applied in preparing the various structural components like antennas, engine static and rotating components, compressors blades used in aerospace industries. These components requires combinations of low density, better stiffness, high strength, high wear resistance and low thermal expansion of aluminium alloy composites [Kainer, 2006].

It is observed from the results that percentage porosity in Al-6061/2.5wt% SiC/2.5wt% Al_2O_3 is 11.1 and whereas with 0.5 wt% of CeO_2 it is 3.62. The percentage porosity in samples with 1.5 and 2.5 wt% of CeO_2 is found to be 3.57 and 3.52 respectively. Similar trends of porosity results were found in the aluminium alloy reinforced with Ni particles. The percentage of void contents was found to be 6.87, 8.57, 3.75, 7.79 and 9.11. The best result of 3.75% void content occurred at 1wt% of nickel particulate [Kumar et al., 2017]. It is evident from the analysis of casted composites that mechanical properties are affected by the porosity. So it is prime consideration to reduce the porosity in the composites before using it for a particular application. Generally the porosity factor can lower the load carrying tendency of the composite by reducing the amount of materials. Moreover, the large scale voids present in the composites acts as stress raisers that ultimately leads to the formation of preferred nucleation sites for crack propagation [Srivatsan et al., 2002]. It can be observed from table 5.2 as the weight percentage of SiC and Al_2O_3 reinforcement increases, the porosity seems to increase. The maximum porosity was found to be 13.6 % for the sample with 7.5 wt% of (SiC+Al_2O_3). This increase in porosity may be due to the formation of particle agglomeration and clustering with increase in the weight percent of the SiC and Al_2O_3. After addition of cerium oxide, the porosity level reduces due to the less formation of air pocket which causes agglomeration and particle clustering. The minimum porosity level was found to be 3.52 after addition of 2.5 wt% of cerium oxide in the composite reinforced with 7.5 wt% of (SiC+Al_2O_3).

Table 5.2 Comparative analysis of experimental and theoretical density

Nomenclature of sample	Theoretical Density ($gmcc^{-3}$)	Experimental Density ($gmcc^{-3}$)	Relative Density (%)	Void Content (%)
Al-6061 alloy	2.70	2.67	98.88	11.1
Al-6061/2.5 wt% (Al_2O_3+SiC)	2.73	2.71	99.26	7.3
Al-6061/5 wt% (Al_2O_3+ SiC)	2.77	2.76	99.63	3.5
Al-6061/7.5 wt% (Al_2O_3+ SiC)	2.81	2.80	99.64	13.6
Al-6061/2.5 wt% (Al_2O_3+SiC)+ 0.5 wt% (CeO_2)	2.76	2.75	99.63	3.62
Al-6061/5 wt% (Al_2O_3+ SiC)+ 1.5 wt% (CeO_2)	2.80	2.79	99.64	3.57
Al-6061/7.5wt% (Al_2O_3+ SiC) +2.5 wt% (CeO_2)	2.84	2.83	99.64	3.52

5.3.3 SEM and EDS Analysis of Hybrid composites

The micro-structural study is conducted on the fabricated composites in order to see the effect of different reinforcements SiC, Al_2O_3 and CeO_2 at the reinforcement-matrix interface using SEM. The microstructures of hybrid composites with different compositions of reinforcement at different magnifications are shown in figures 5.4 (a-f). The microstructure of hybrid composite with 2.5 wt% (SiC+Al_2O_3) mixture showed in figure 5.4 (a) reveals the presence of silicon and alumina particulates in dendrite tree like structure. Generally, these dendrites growth is responsible for the improvement of composite properties and it depends upon the cooling rate of the composite. Improper cooling results in larger dendrites formation while the small dendrites results due to proper cooling of the composite during solidification. Smaller shape of dendrite tree as seen in figure 5.4 (b) may results in higher ductility of the composites after casting. The spherical shape of the SiC particles tends to increase the bonding between the particles that further tends to increase the tensile strength of the material. Also the fine structure of the Al_2O_3 particles provide better strength to the composites and are very difficult to pull-out from the matrix [Young et al., 2007]. It is evident from the figure 5.4 (c) of hybrid composites with 7.5 wt% (SiC+Al_2O_3) that the pattern of Al_2O_3 particles seems to be very fine as compared to the particle pattern of the SiC. As of the flaky shape of the Al_2O_3 particles, it is very difficult to pull out these particles as compared to the SiC particles of spherical shape. This difficulty in pulling of particles may results in the improvement of tensile properties of the hybrid composites. Further improvements in mechanical properties have been observed after addition of rare earth oxides with composition varies from 0.5 to 2.5 wt%. It can be seen from the SEM image shown in figure 5.4 (d) that the degree of agglomeration reduced after addition of CeO_2 particles. This reduced agglomeration results in formation of smooth surface in the composites. In similar way trends of grain refinement was seen by [Chonghia et al., 2001] with addition of europium (Eu) as rare earth in the aluminium alloy A356. The refinement efficiency enhanced with the addition of the Eu content in the alloy [Chonghia et al., 1999]. Very smooth and fine surface of the A-356 aluminium alloy was seen after addition of 0.5 wt% of Yttrium [Zheng and Yongmei, 2008]. The large dendritic structures as seen in figure 5.4(a) on the surface of (Al_2O_3 + SiC) composite structures that occurred during solidification of the composites and sometimes tend to reduce the strength of the material disappear continuously after the addition of rare earth oxide as shown in figures 5.4 (e-f). Various other defects like micro cuts on the surface and pores formation can also be seen on the surface of (Al_2O_3 + SiC) composite which are negligible after addition of rare earth oxide as shown in figures 5.4 (e-f). The CeO_2 particles react with the aluminium oxide particles to form a uniformly dispersed phase. Cerium oxide particulate helps in matrix grain refinement as seen from the microstructural figure 5.4 (f) of the composites. The similar phenomenon of grain refinement of matrix was observed in the aluminium alloy reinforced with europium as rare earth metal [Chonghia et al., 1999]. It was further observed that 0.5 wt% of europium can significantly refine the primary Si crystals in the aluminium alloy which results in the transfer of coarse star like grain into fine blocky shape [George et al., 2005]. It is evident from the microstructure figure 5.4 (f) that stronger the matrix-fibre interface, stronger will be the capability of the fibre to resist various forces acting on it. Addition of rare element helps to improve the tensile properties and enhance the ductility of the components which makes them suitable for the aerospace and defence application. It was reported that due to the refinement and modification of primary Si crystals, the tensile strength and elongations are improved significantly with increasing the concentration of 0.5 wt% of europium as rare earth metal [George et al., 2005]. Present results are in agreement with these trends. The eutectic silicon was modified with the addition of yttrium, which resulted in improving the fluidity of the alloy and improvement in mechanical properties of the alloy [Chonghia et al., 1999].

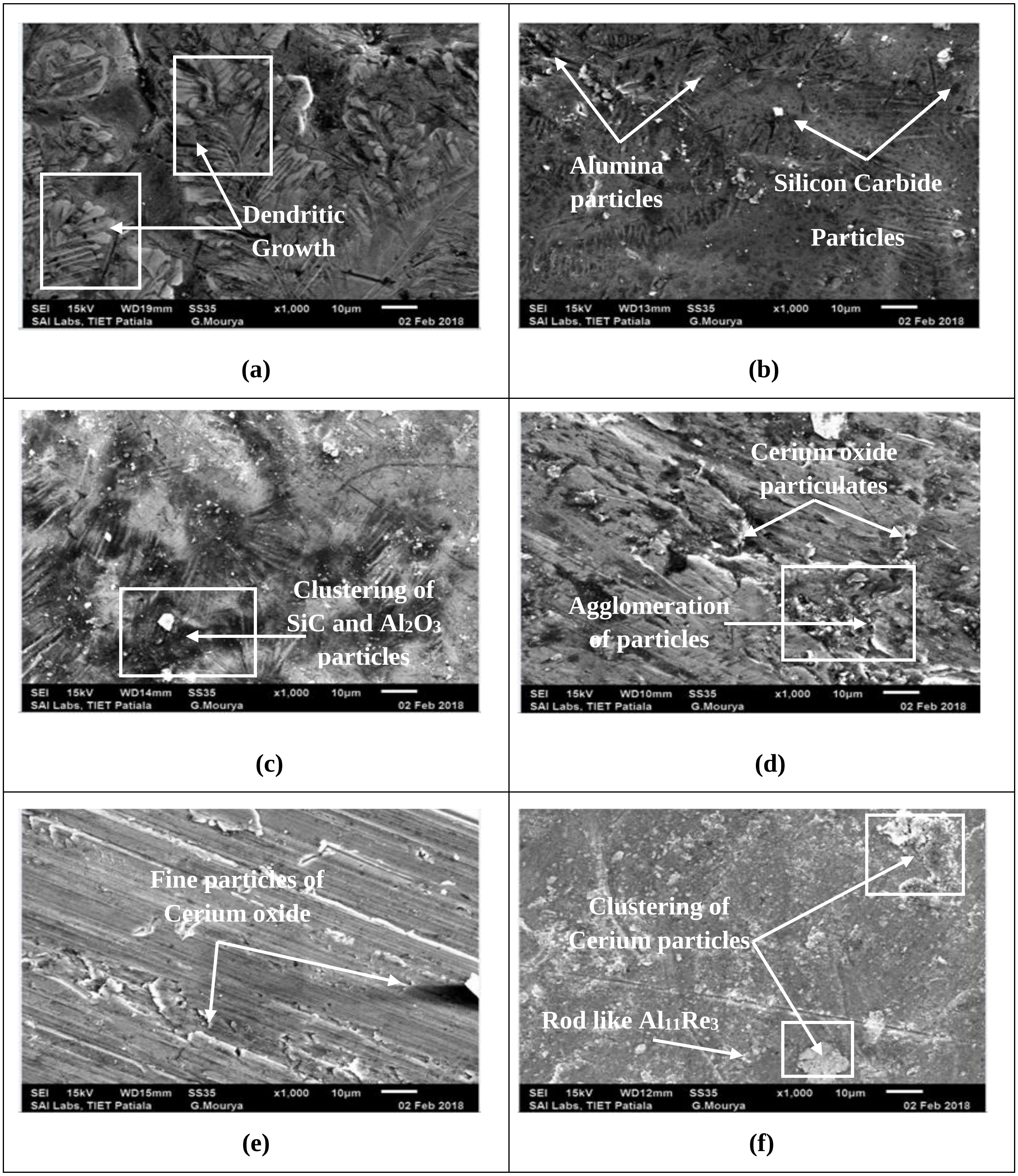

Figure 5.4 SEM images of Hybrid Composites (a) 2.5 wt% (Al_2O_3 + SiC) (b) 5 wt% (Al_2O_3 + SiC) (c) 7.5 wt% (Al_2O_3 + SiC) (d) 2. 5 wt% (Al_2O_3 + SiC) + 0.5 wt% CeO_2 (e) 5 wt% (Al_2O_3 + SiC) + 1.5 wt% CeO_2 (f) 7. 5 wt% (Al_2O_3 + SiC) + 2.5 wt% CeO_2 [Sharma et al., 2019]

EDS analysis of the composites are shown in figures 5.5 (a-f). EDS analysis showed the presence of elements like C, O, Mg, Al and Si as observed from the peaks in hybrid composites reinforced with SiC and Al_2O_3 as shown in figure 5.5 (a). An oxygen and carbon content is also visible in the spectrum. Various spectrums were selected for analyzing the composites where a good metallurgical bonding could be observed. The smooth surface of the composites samples showed proper grain refinement and no harmful reactions are observed on the surface. Aluminium carbide (Al_4C_3) was also found in the spectrum. Aluminium carbide may be formed due to reaction between aluminium and carbide molecules. The aluminium carbide is hazardous for Al-SiC interface and its growth is retarded by proper selection of working temperature and stirring time. Very small peaks of magnesium (Mg) were also observed in the spectrum that showed magnesium as a wetting agent helps in binding the reinforcement particles together. Figure 5.5(b) presents the elemental analysis of Al-6061/5 wt% (SiC + Al_2O_3) hybrid composite. It confirms the presence of main constituents like C, O, Mg, Al and Si. Figure 5.5(c) shows the element analysis of Al-6061/7.5 wt% (SiC + Al_2O_3) hybrid composite. It again confirms the presence of main constituents like C, O, Mg, Al, Si and Fe with atomic percent of 21.45 %, 24.70 %, 0.38 %, 51.57 %, 1.14 % and 0.76 %. Some amount of iron has also found in the composition due to the impurities present in the aluminium alloy.

EDS analysis of Al-6061/2.5wt% (SiC + Al_2O_3)/0.5 wt% CeO_2 hybrid composite with elemental compositions of C, O, Al, Si, Mg, Fe and Ce indicated by figure 5.5(d). The atomic percent of various elements was observed as 55.70 %, 21.61 %, 21.47 %, 0.38 %, 0.33 %, 0.43 % and 0.10 %. Therefore, these results of SEM-EDS analysis indicate the incorporation of reinforcement particles of Al_2O_3/SiC/CeO_2 in Al-matrix composites produced by the stir casting process. Similarly, EDS figure 5.5(e) of Al-6061/5wt% (SiC + Al_2O_3)/1.5 wt% CeO_2 suggest the main constituent elements like C, O, Mg, Al, Si and Ce with different atomic percentage. The elemental compositions with different atomic percent of elements like C, O, Al, Si, Mg and Ce were observed as 34.90 %, 9.08 %, 54.24 %, 0.86 %, 0.62 % and 0.29 % respectively as shown in figure 5.5(e). EDS figure 5.5(f) of Al-6061/7.5wt% (SiC + Al_2O_3)/2.5 wt% CeO_2 hybrid composite depicts the presence of silicon and oxygen which confirms the dispersion of silica in cerium oxide elements. The elemental compositions with different atomic percent of elements like C, O, Al, Si and Ce were observed as 18.54 %, 58.74 %, 2.58 %, 0.10 % and 20.04 %.

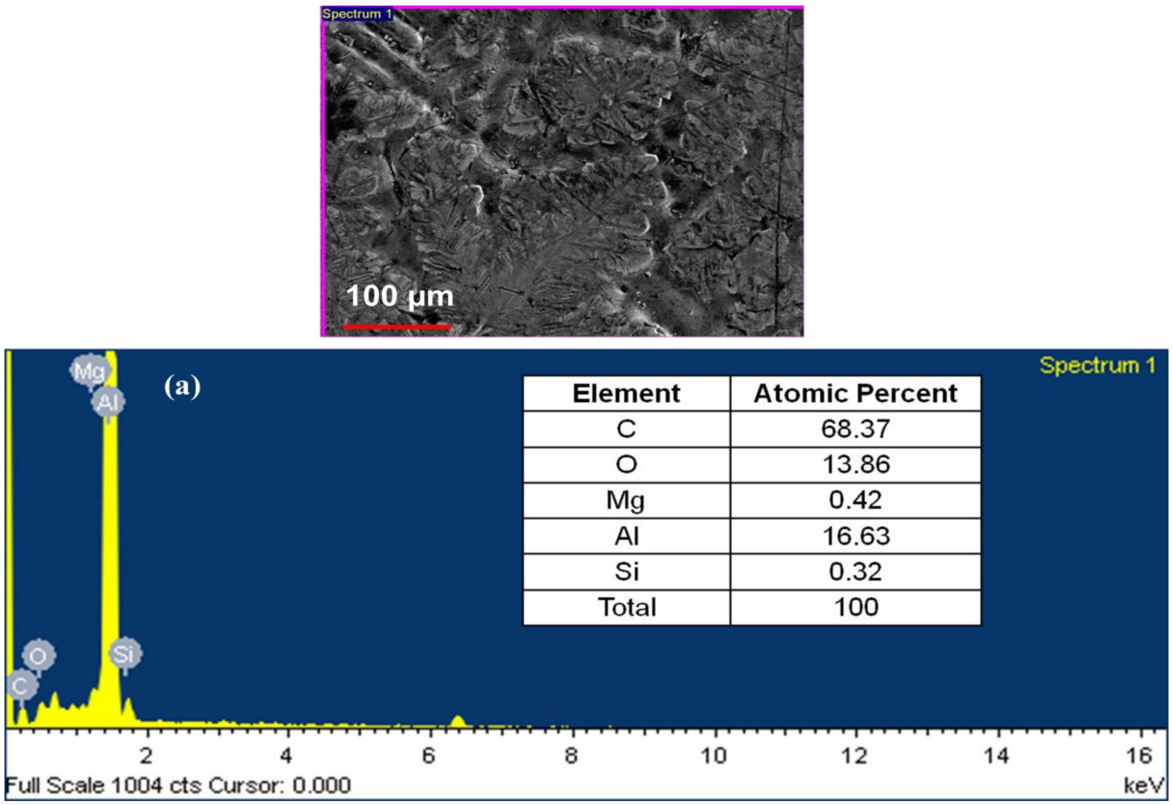
Spectrum 1
100 µm
(a)
Spectrum 1
Element | Atomic Percent
C | 68.37
O | 13.86
Mg | 0.42
Al | 16.63
Si | 0.32
Total | 100
Mg
Al
O
C
Si
2 4 6 8 10 12 14 16
Full Scale 1004 cts Cursor: 0.000
keV

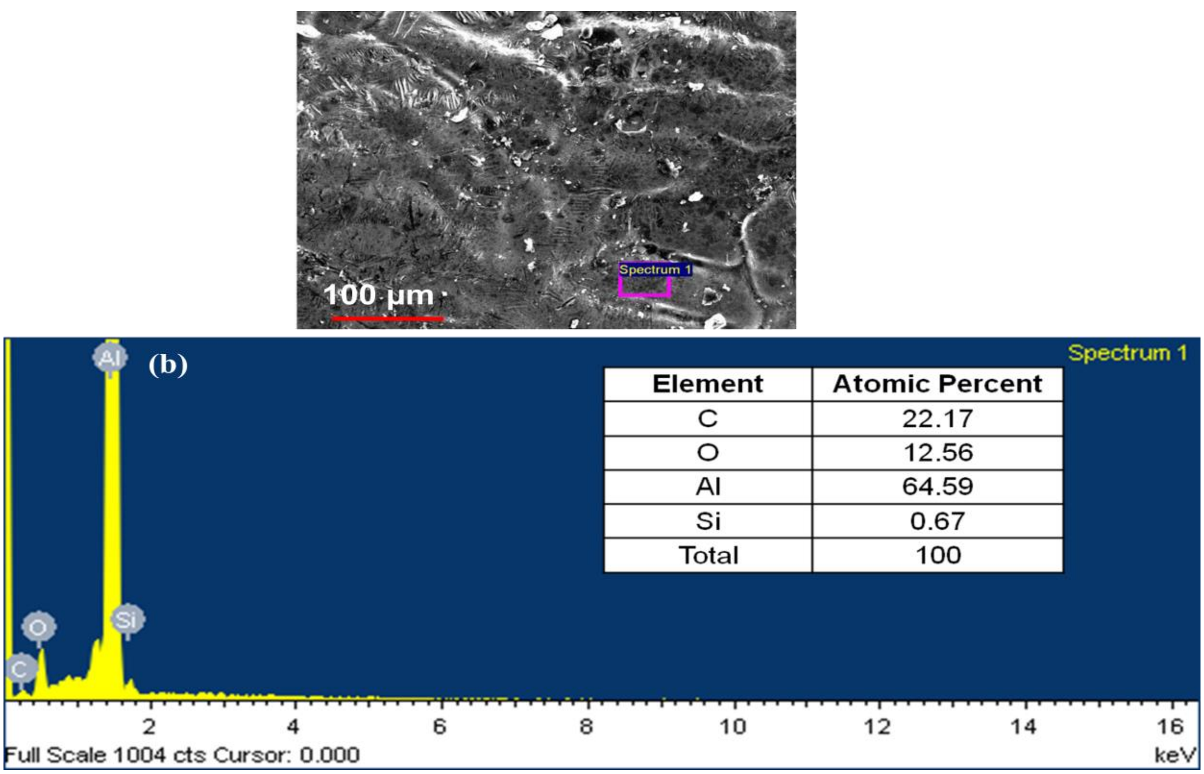
Spectrum 1
100 µm
(b)
Spectrum 1
Element | Atomic Percent
C | 22.17
O | 12.56
Al | 64.59
Si | 0.67
Total | 100
Al
O
C
Si
2 4 6 8 10 12 14 16
Full Scale 1004 cts Cursor: 0.000
keV

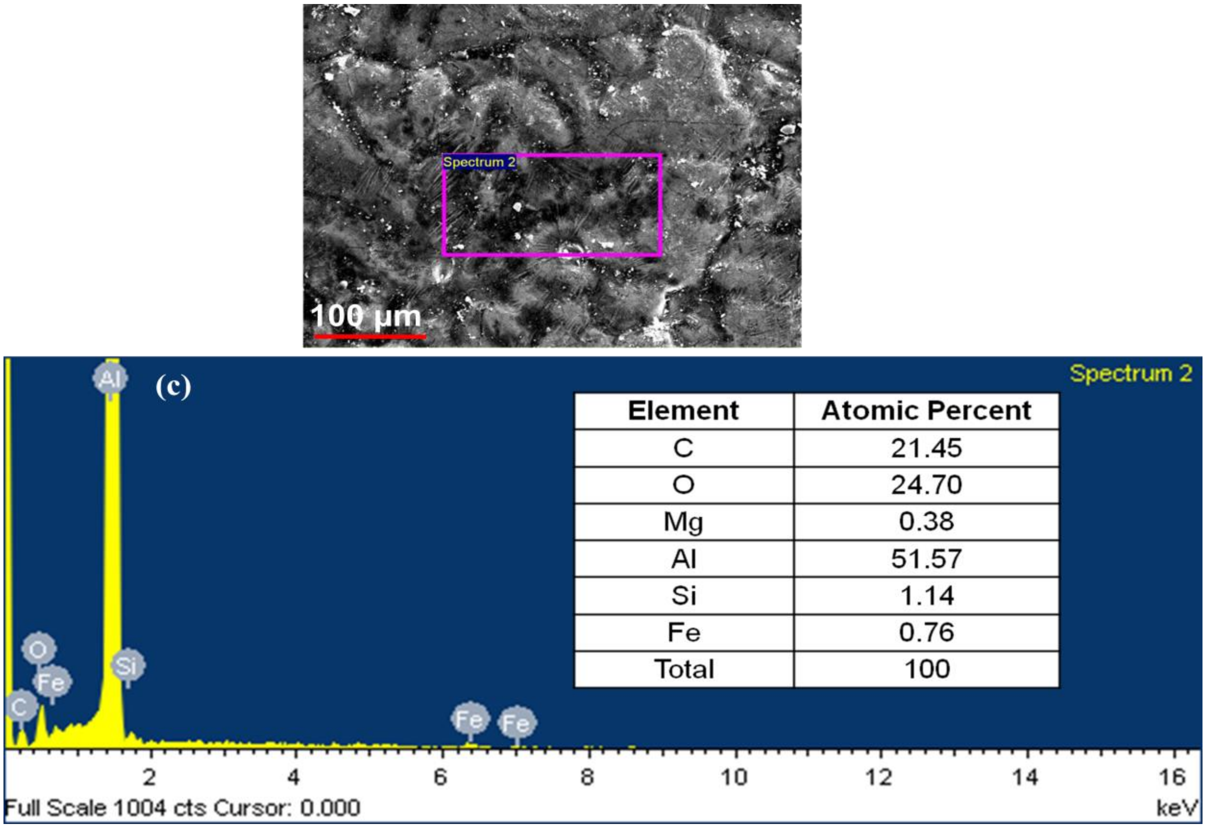

Element	Atomic Percent
C	21.45
O	24.70
Mg	0.38
Al	51.57
Si	1.14
Fe	0.76
Total	100

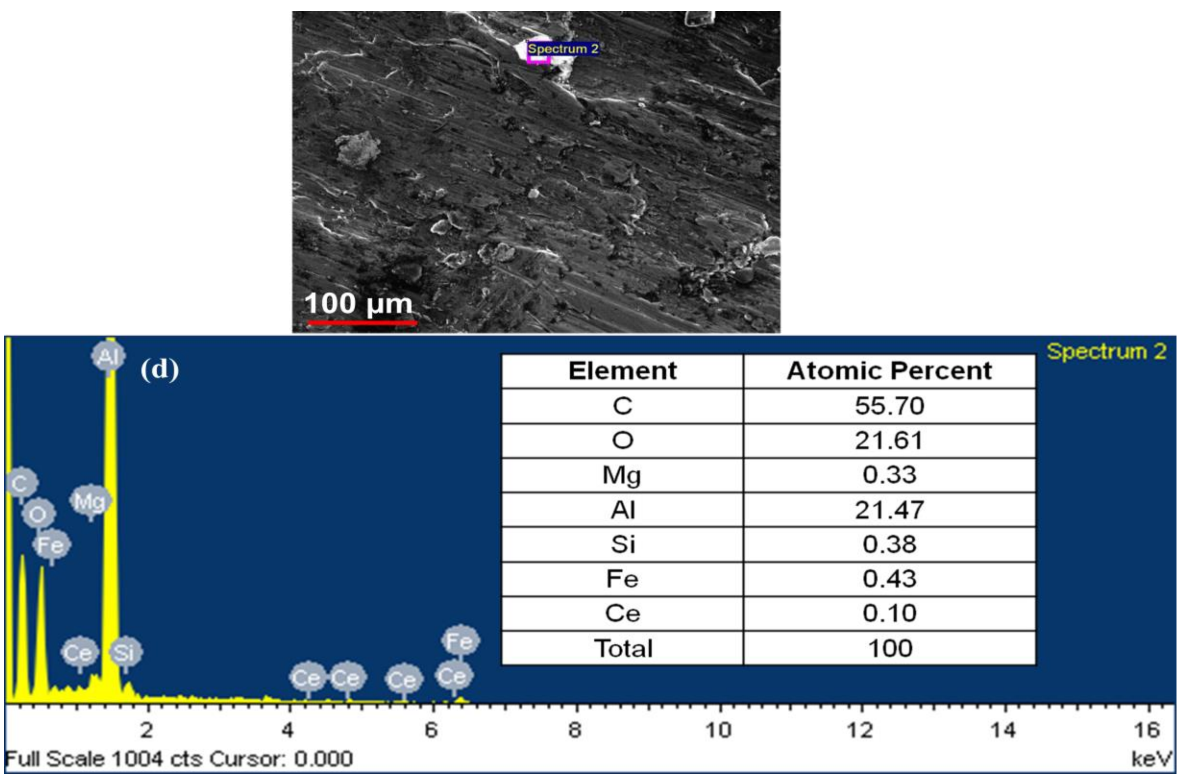

Element	Atomic Percent
C	55.70
O	21.61
Mg	0.33
Al	21.47
Si	0.38
Fe	0.43
Ce	0.10
Total	100

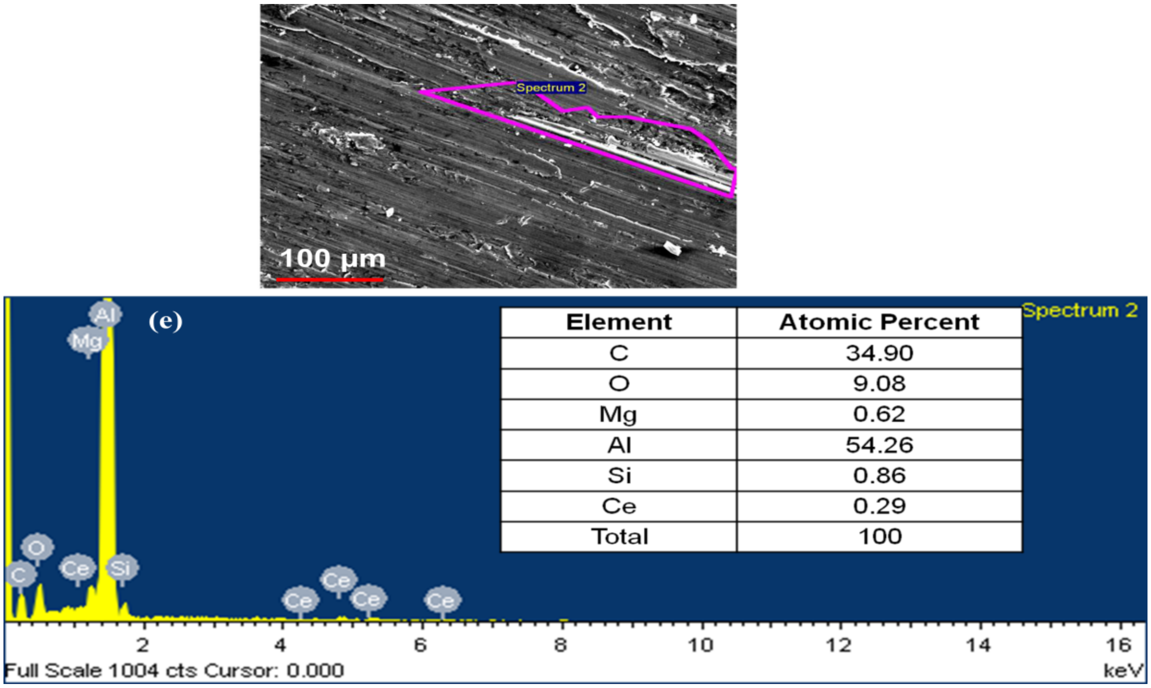

Element	Atomic Percent
C	34.90
O	9.08
Mg	0.62
Al	54.26
Si	0.86
Ce	0.29
Total	100

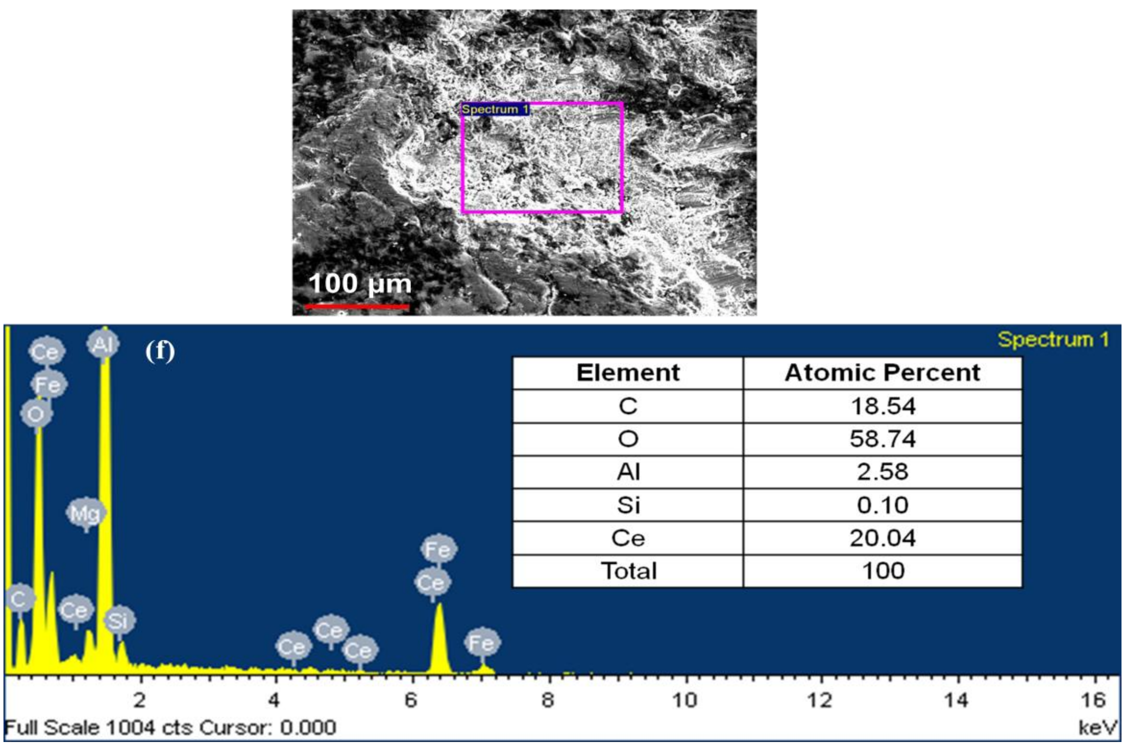

Element	Atomic Percent
C	18.54
O	58.74
Al	2.58
Si	0.10
Ce	20.04
Total	100

Figure 5.5 EDS images of Hybrid Composites (a) 2.5 wt% (Al_2O_3 + SiC) (b) 5 wt% (Al_2O_3 + SiC) (c) 7.5 wt% (Al_2O_3 + SiC) (d) 2. 5 wt% (Al_2O_3 + SiC) + 0.5 wt% CeO_2 (e) 5 wt% (Al_2O_3 + SiC) + 1.5 wt% CeO_2 (f) 7. 5 wt% (Al_2O_3 + SiC) + 2.5 wt% CeO_2 [Sharma et al., 2019]

5.3.4 EBSD analysis of Hybrid Composites

The microstructural evaluation of aluminium hybrid composites with 7.5 wt% (SiC + Al_2O_3) and 7.5 wt% (SiC + Al_2O_3) with 2.5 wt% CeO_2 were observed using EBSD analysis. Results of the EBSD analysis are shown in figures (5.6-5.10). The various colors and crystallographic orientation has been observed in the stereographic triangles as shown in figure 5.6.

An EBSD image of Al-6061/7.5 wt% (SiC + Al_2O_3) hybrid composite and Al-6061/7.5 wt% (SiC + Al_2O_3)/2.5 wt% CeO_2 hybrid composite is depicted by figures 5.6(a-b). EBSD micrographs suggest that grain boundaries formed in composites are in uniform pattern. It can be understood from the EBSD figure 5.7(b) that addition of rare earth oxides resulted in grain refinement in the matrix of aluminium. As a result, more new grains nucleate and migrate their boundaries with the addition of the SiC and Al_2O_3 particles as indicated in figure 5.6(a). Fig 5.6(b) confirms the grain refinement of the hybrid composite due to the uniform distribution of rare earth oxides into the aluminium matrix. It can be observed from figure 5.7 (a) that the grain size of the composite reinforced with SiC and Al_2O_3 varied from 20 μm to 120 μm. But after addition of RE particles, the most of the grain lies in the range of 60 μm as shown in figure 5.7 (b). The reduction in grain size occurs due to the behavior of RE particles acted as grain nucleating agents. The grain refinement originates from several ways. RE particles oppose the growth of aluminium grains. The location of RE particles becomes nucleating sites for grains and the aluminium grains tend to grow on them. The temperature in the region around rare earth particles drop down resulting in an under cooling effect. This resulted in various number of nucleation sites wherever RE particles are present in the casting. The resistance for aluminium grain growth increases with increased nucleation sites. The net result is refinement of grains in the composites. The tendency of formation of refined grain increases with increased content of rare earth particles.

The detailed EBSD analysis on hybrid composites was determined in rolling direction (RD) and transverse direction (TD) as shown by the inverse pole figure 5.8. The crystallographic orientations parallel to the normal direction have been shown by different colors in inverse pole figure. The grain orientations with maximum intensities was observed as 4.959 in case of hybrid composites reinforced with 7.5 wt% (SiC + Al_2O_3) as shown in figure 5.8 (a). After incorporation of 2.5 wt% cerium oxide in hybrid composite, the maximum intensity of grain orientation was observed as 2.561 as shown in figure 5.8 (b). Image quality (IQ) maps (figure 5.9) are associated with the quality of the EBSD patterns of the grains existing in the composites reinforced with Al_2O_3, SiC and CeO_2. Lighter areas signify higher pattern quality as shown in figure 5.9 (a-b) indicative of finer grain size with the addition of cerium oxide. The grain boundaries are characterized by a weak EBSD pattern due to the overlapping of diffraction patterns from neighbouring grains.

The hybrid composites with the addition of 7.5 wt% (SiC + Al_2O_3) reinforcement showing high angle grain boundaries (HAGB) with most of the misorientation angle are within the range of 30^o to 50^o as shown in figure 5.10 (a). But after incorporation of 2.5 wt% cerium oxide in the aluminium hybrid composite, the misorientation angles are less than 10^o showing low angle grain boundaries (LAGB). Although, the composites reinforced with cerium oxide generally consisted of large number of finer grains, which is evidence of high strength exhibited by these composites.

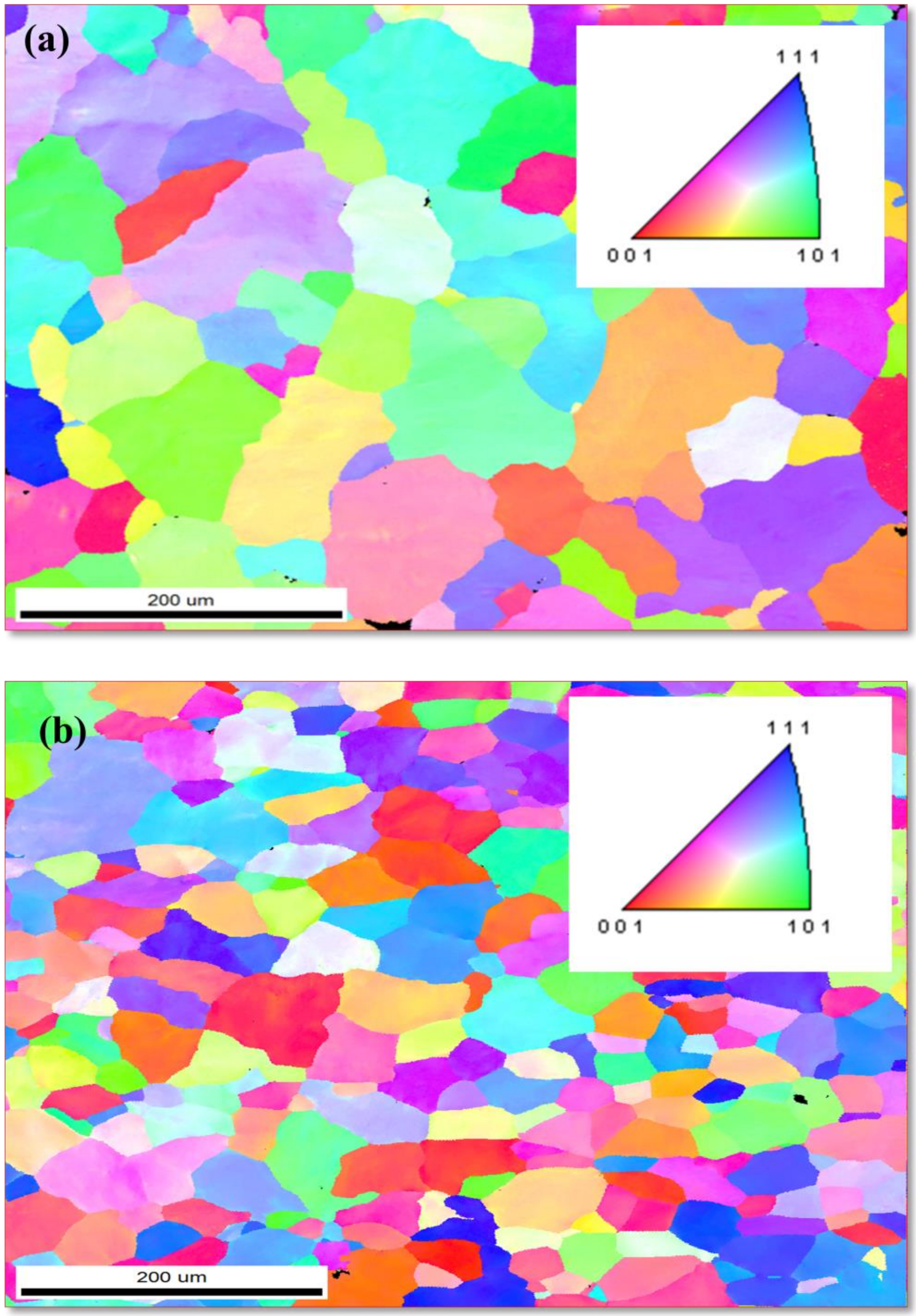

Figure 5.6 Ordinary EBSD Microstructural Pictures with Grain Boundary) for Various Composites (a) Al6061-5wt% (SiC+ Al_2O_3) (b) Al6061-5wt% (SiC+ Al_2O_3)-2.5wt% CeO_2

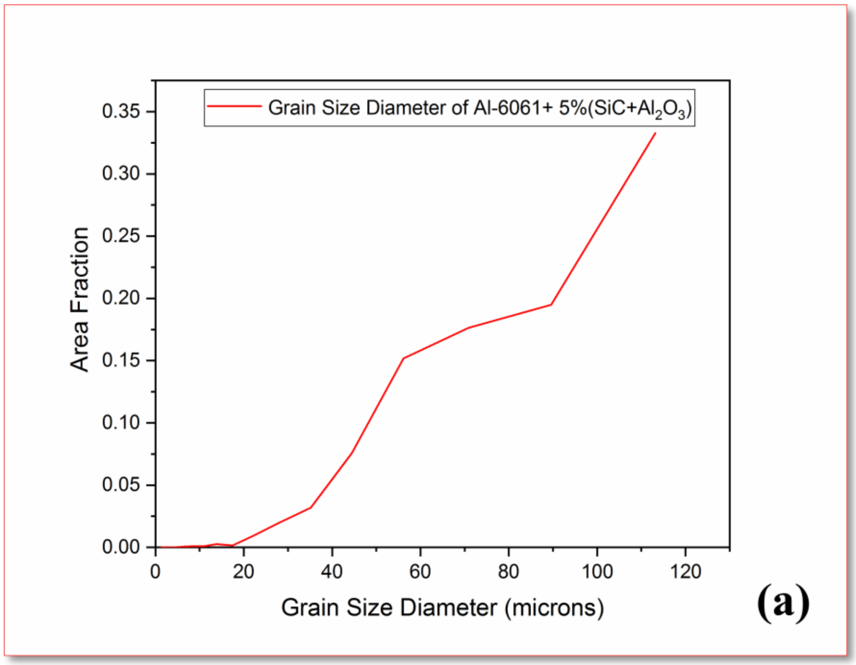

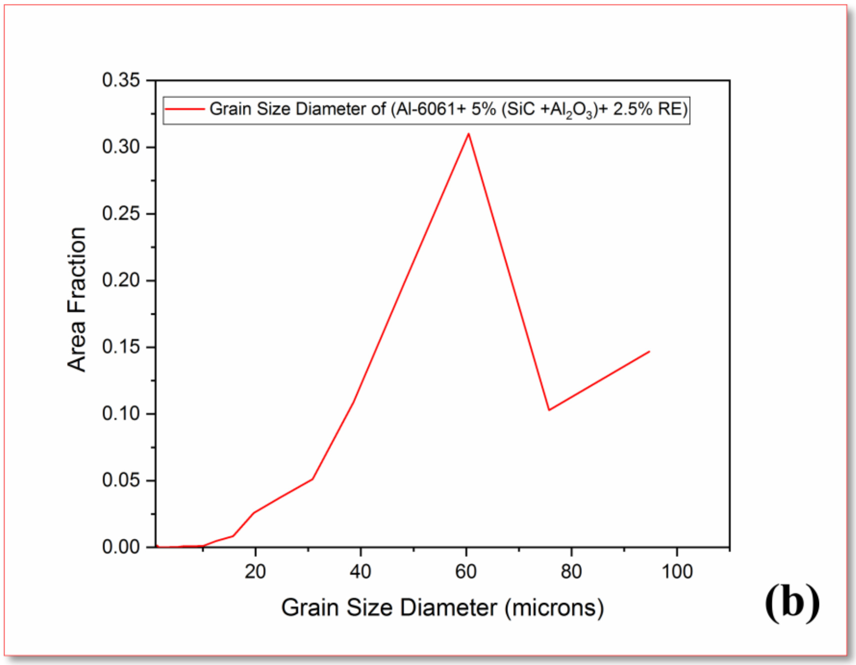

Figure 5.7 Grain Size Distribution as a Function of Area Fraction for Various Composites (a) Al6061-5wt% (SiC+ Al_2O_3) (b) Al6061-5wt% (SiC+ Al_2O_3)-2.5wt% CeO_2

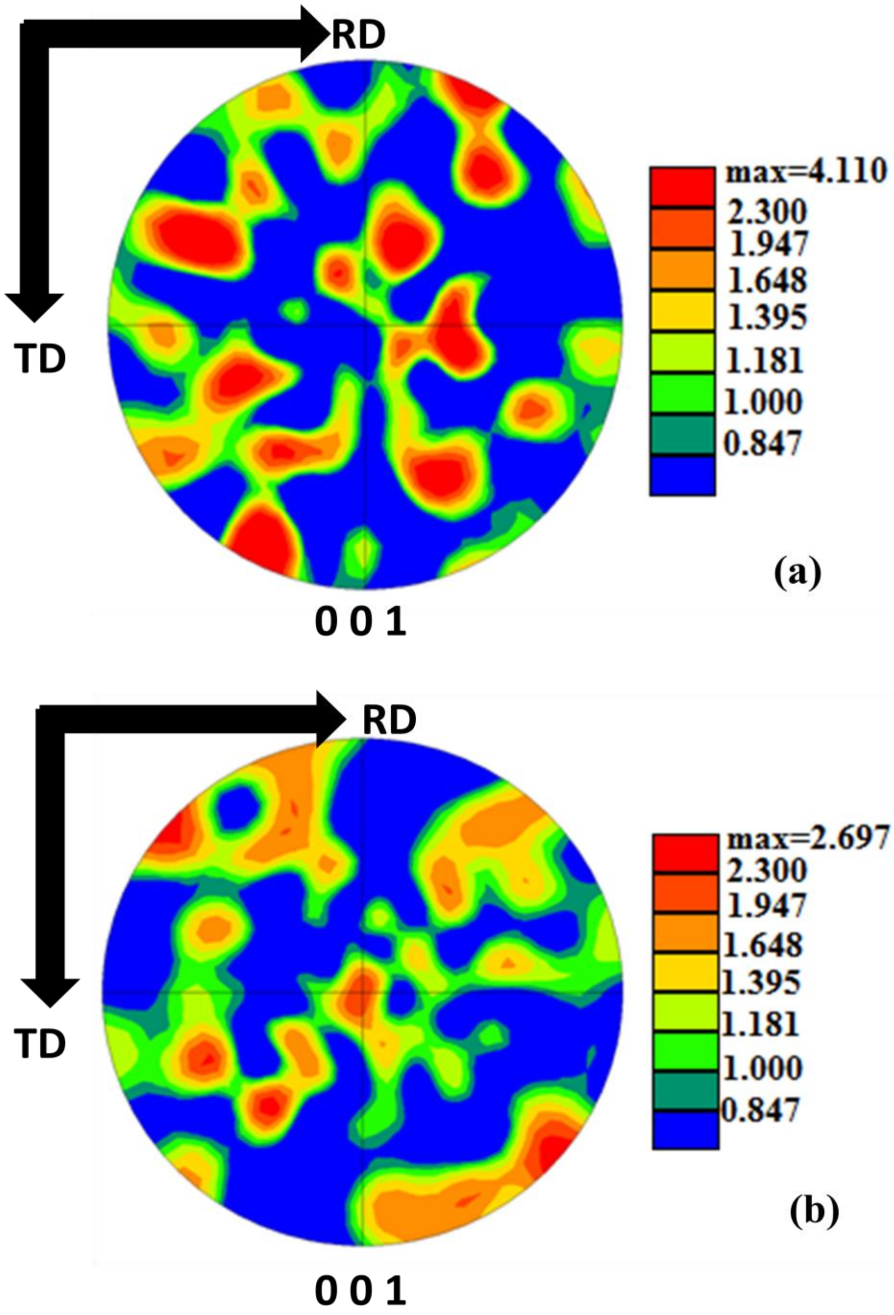

Figure 5.8 Inverse Pole Figure (IPF) for Various Composites (a) Al6061-5wt% (SiC+ Al_2O_3) (b) Al6061-5wt% (SiC+ Al_2O_3)-2.5wt% CeO_2

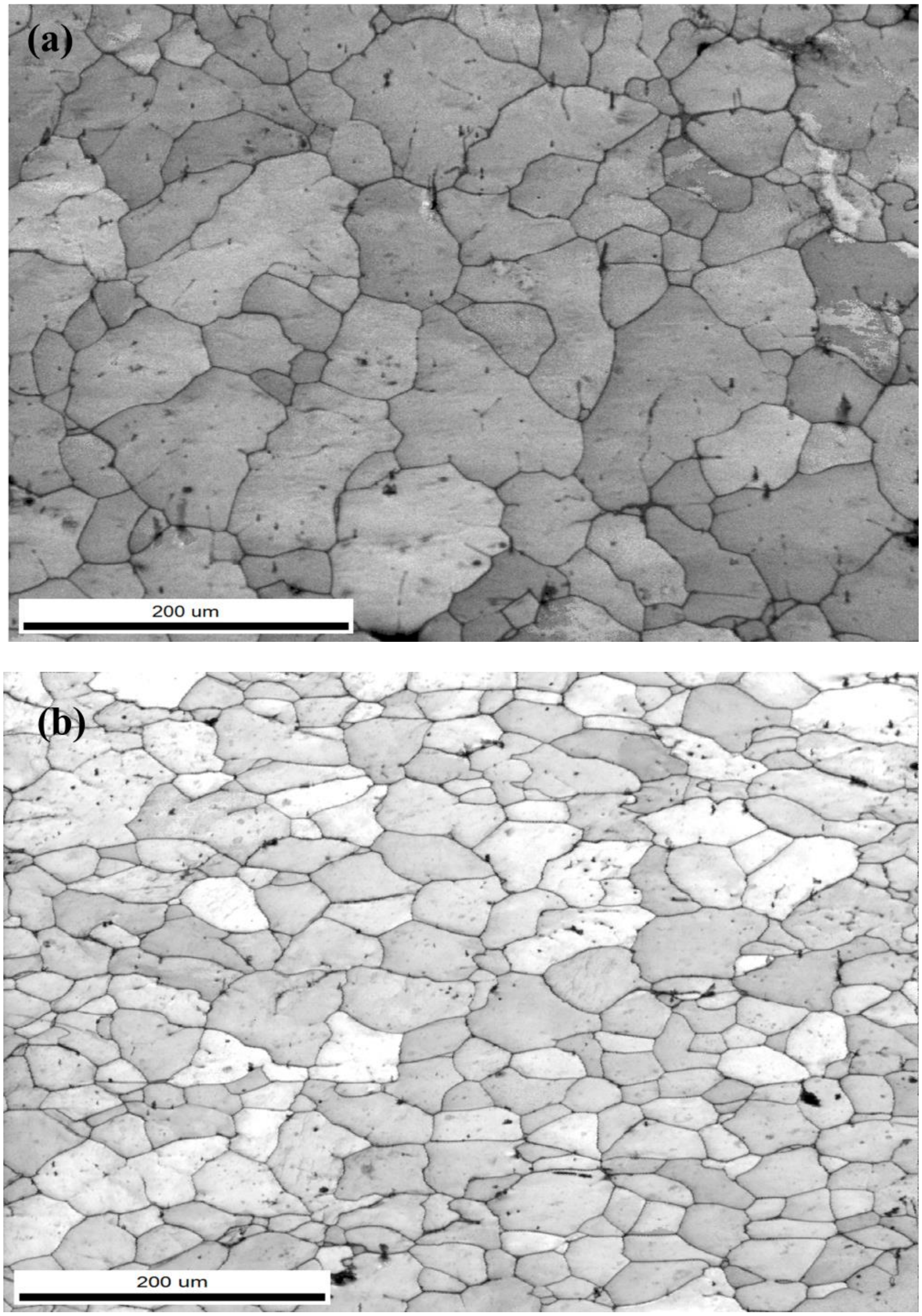

Figure 5.9 Grain Boundary with Image Quality Map (IQM) for Various Composites: (a) Al6061-5wt% (SiC+ Al_2O_3) (b) Al6061-5wt% (SiC+ Al_2O_3)-2.5wt% CeO_2

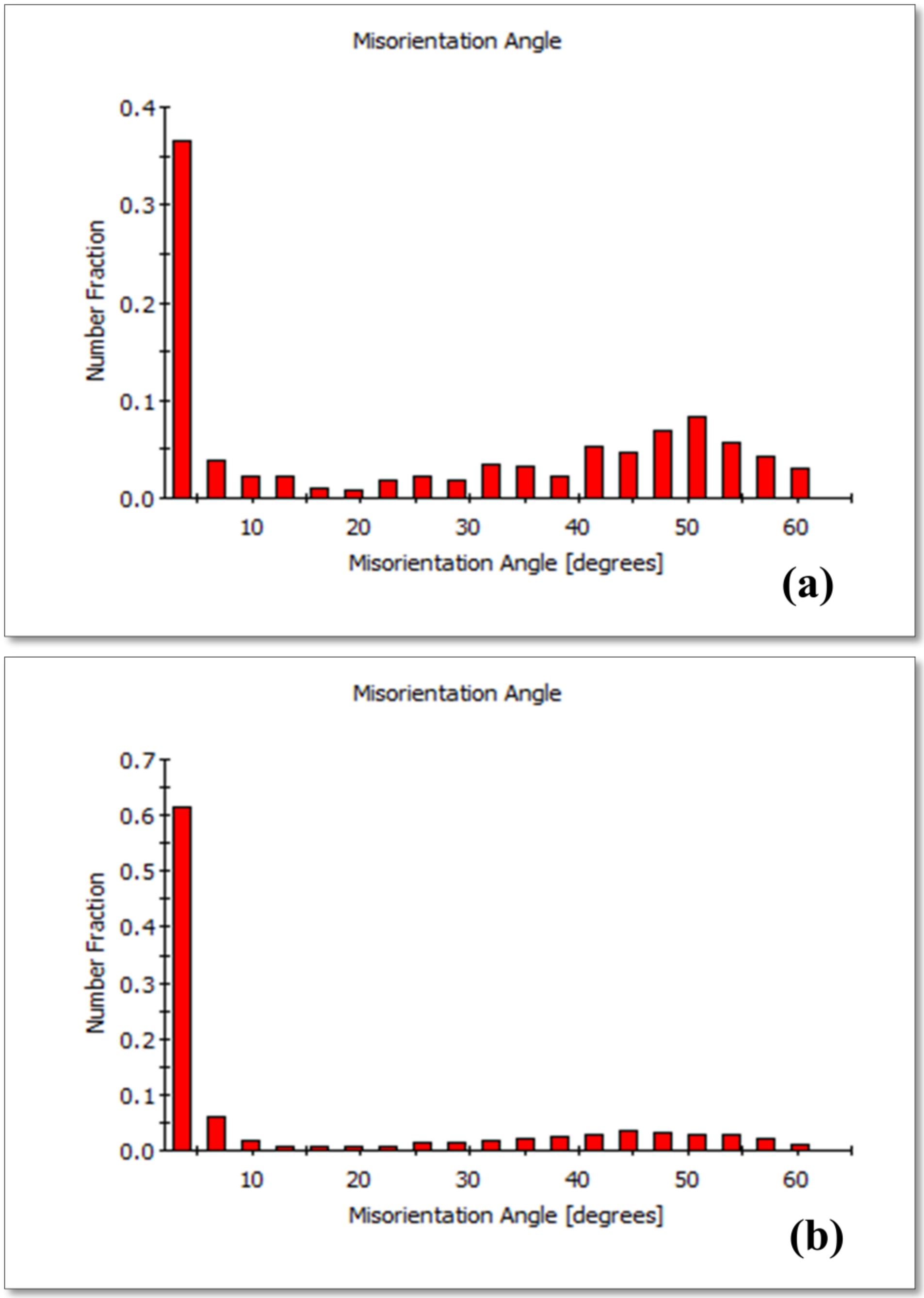

Figure 5.10 Misorientation Angle Histogram for Various Composites (a) Al6061-5wt% (SiC+ Al_2O_3) (b) Al6061-5wt% (SiC+ Al_2O_3)-2.5wt% CeO_2

5.3.4 Phase Determination using XRD Analysis

X-ray diffraction is an important technique to understand the properties of hybrid composites based on various powder mix elements like CeO_2, Al_2O_3 and SiC. Each plot of XRD pattern indicates the phases formed in samples consisting various percentage composition of reinforcing elements. In most of the cases, the highest peak was observed on 2θ scale. The various patterns for different composition of Al_2O_3 and SiC powder based hybrid composites are shown in figure 5.11. As the parent material mainly consists of aluminium in matrix form, the large peak corresponds to the parent metal. XRD analysis also revealed that the smaller peak corresponds to the presence of various phases like SiO_2, Mg (CO_3), $FeAl_2Si$ in hybrid composites. The various patterns for different composition of CeO_2, Al_2O_3 and SiC powder based hybrid composites are shown in figure 5.12. Phase analysis of the hybrid sample with CeO_2 modified aluminium alloy illustrated that occurrence of α-Al, $Al_{11}Ce_3$, Al_4Ce, Al_3Ce and Al_8Mg_5 phases. The existence of different oxides of cerium in material is a sign of successful addition of the cerium oxide as a rare earth oxide in the composite.

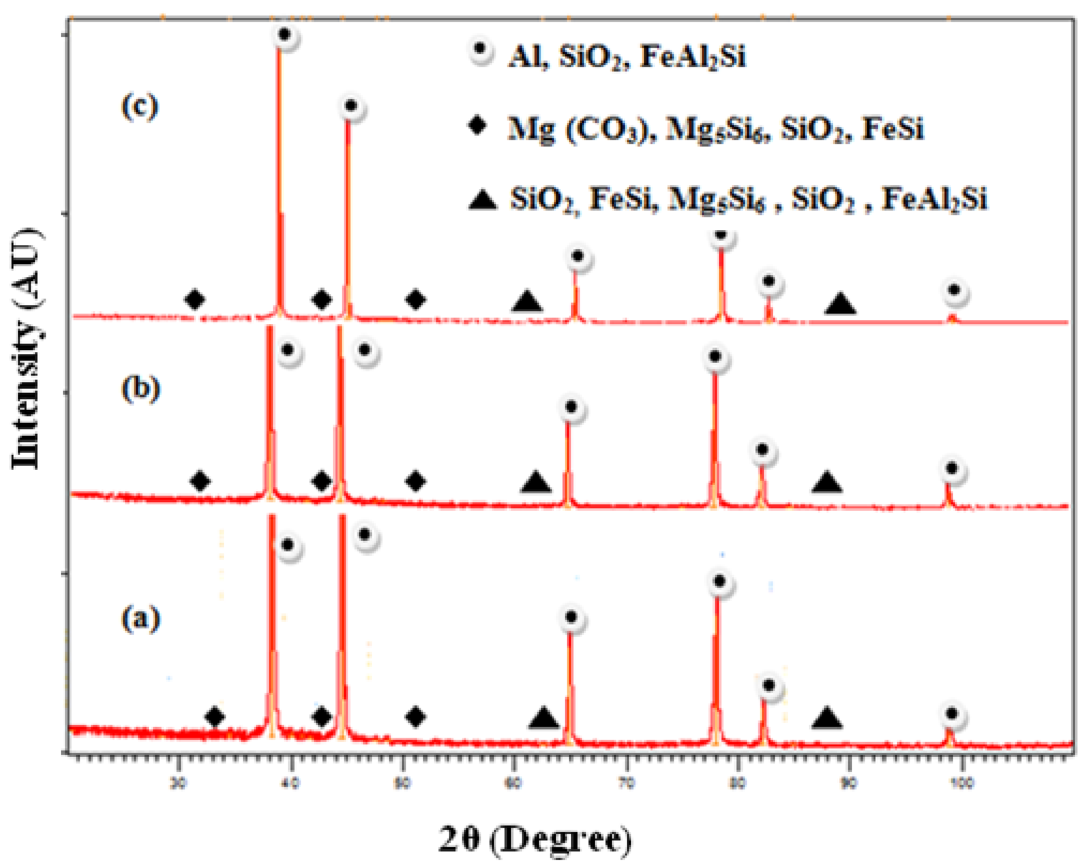

Figure 5.11 XRD Pattern without Rare Earth (a) 2.5 wt% (Al_2O_3 + SiC) (b) 5 wt% (Al_2O_3 + SiC) (c) 7.5 wt% (Al_2O_3 + SiC)

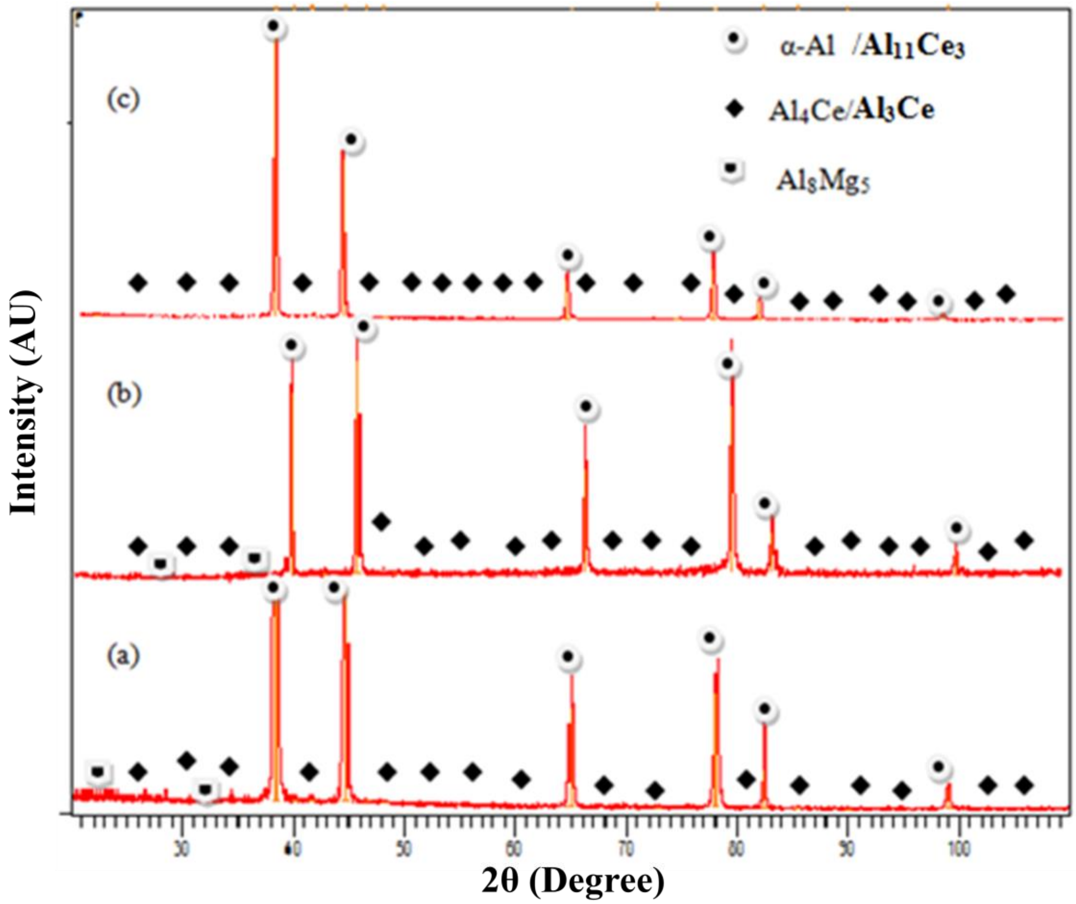

Figure 5.12 XRD Pattern with Rare Earth (a) 2.5 wt% (Al_2O_3 + SiC) + 0.5 wt% CeO_2 (b) 5 wt% (Al_2O_3 + SiC) + 1.5 wt% CeO_2 (c) 7.5 wt% (Al_2O_3 + SiC) + 2.5 wt% CeO_2

5.4 MECHANICAL AND SURFACE CHARACTERIZATION

5.4.1 Ultimate Tensile Strength (UTS) and Percentage Elongation

The results of tensile test performed on hybrid composite samples are specified as stress-strain diagram in figures 5.13(a-f). Figure 5.13(a) shows the effect of 2.5 wt% ($SiC+Al_2O_3$) addition in composites on UTS. It shows that UTS of the aluminium alloy increases with increase in wt% of reinforcement composition. The tests reveals that UTS rose from 26 MPa for base alloy to 28 MPa at 2.5 wt% addition of ($SiC+Al_2O_3$). This enhancement in UTS is 7.69 % corresponding to maximum force of 4.35 KN. With further increase of reinforcement of ($SiC+Al_2O_3$) up to 5 wt%, UTS of hybrid composite rose up to 54 MPa with percentage improvement of 107.6% as compared to base alloy Al-6061 as indicated by figure 5.13(b). This improvement in UTS may be resulted from the significant increase in the dislocation density throughout the composite as of large difference in the coefficient of thermal expansion between the Al-6061 matrix and $SiC+Al_2O_3$ particle [Bodunrin et al., 2015]. Figure 5.13(c) revealed that the UTS rose up to 73 MPa with the addition of 7.5 wt% of ($SiC+Al_2O_3$) in hybrid composites as compared to 54 MPa for sample with 5 wt% of ($SiC+Al_2O_3$) corresponding to maximum force of 12.75 KN. The percentage elongation is found only 2.1 % with the addition of 5 wt% of ($SiC+Al_2O_3$) and it again rises up to 6.8 % after addition of 7.5 wt% of ($SiC+Al_2O_3$).

The addition of cerium oxide as rare earth oxides have much more significant effect in improving the UTS and percentage elongation of composite as compared to composite with only SiC and Al_2O_3 reinforcements. The tensile tests on hybrid composite reveals that with the addition of 0.5 wt% of CeO_2, UTS of hybrid composite with 5 wt% of ($SiC+Al_2O_3$) rose from 30 MPa to 89 MPa as shown in figure 5.13(d) correspond to a maximum force of 14.85 KN. As observed from the stress-strain figures shown in 5.13(e-f) on addition of 1.5 wt% of CeO_2 and 2.5 wt% of $CeO_{2,}$ UTS of hybrid composite with 5 wt% and 7.5wt% of ($SiC+Al_2O_3$) rose from 54 MPa to 102 MPa and 73 MPa to 123 MPa respectively corresponds to maximum force of 16.40 KN and 20.45 KN. The percentage elongation rose from 10% to 11.5 %. It is observed that the hybrid composite with 2.5 wt% of CeO_2 gives superior UTS as compared to the counterpart with 0.5 wt% and 1.5 wt% of CeO_2. This increase in UTS was due to the formation of $Al_{11}RE_3$ phase that reduced the quantity of eutectic β- particles in the matrix. Addition of RE mixture resulted in increasing the dispersion of reinforcement in the molten metal. As, there was a sudden decrease in the value of UTS and percentage elongation on addition of 3.5 wt% cerium oxide. Clustering of RE particulates at high concentration may have affected ability of the sample to resist tensile force and the material break easily. The current results are comparable with the tensile results of composites with Nb as rare earth particulates. The optimum quantity for the better ductility and strength was found to be 5 wt% [Shanti et al., 2012]. From the research findings on scandium reinforced aluminium composites, it has been reported that there exists an 0.15 wt% optimum percentage of scandium for which the yield strength and UTS are maximum increased [Shi et al., 2017].

The dispersion of ($SiC+Al_2O_3$) is improved significantly with the addition of CeO_2 particulates. Moreover, the composite having CeO_2 additive had a smaller grain matrix as compared to the composite without CeO_2 additive as indicated by the SEM micrographs. The resistance to dislocation movements, dislocation density and their interaction with the reinforcing particles resulted in the improvement of tensile strength and strain hardening. Increase in the tensile elongation may be attributed to the reduced matrix grain size and the improvement of the ($SiC+Al_2O_3$) particle dispersion. The tensile strength of the aluminium alloy showed increasing trend when infiltration of Al_2O_3 and SiC preform was mixed into them. The honeycomb structure of the preform due to the growth of alumina grains help in enhancement of tensile properties [Altinkok et al., 2004].

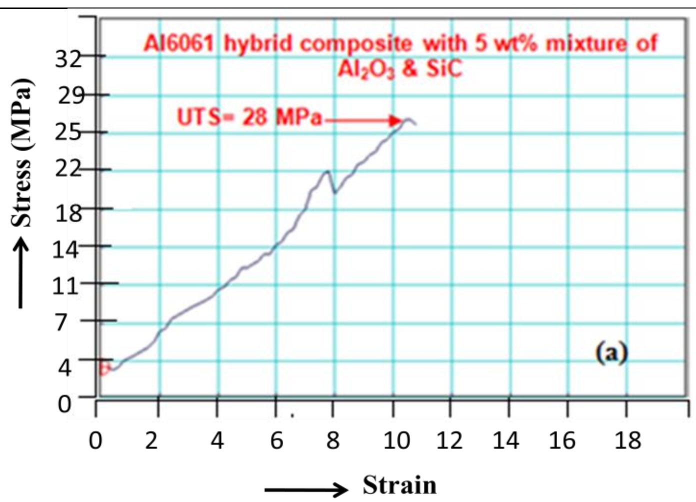

Results Corresponds to Graph 5.13(a)	
Maximum Force	4.350KN
Displacement at Maximum Force	5.200mm
Maximum Displacement	5.400mm
Cross-sectional area	164.059mm^2
Elongation	2.00%

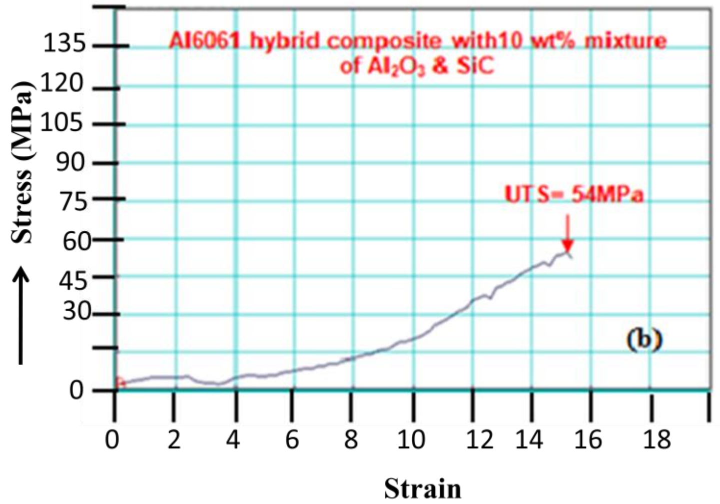

Results Corresponds to Graph 5.13(b)	
Maximum Force	9.900KN
Displacement at Maximum Force	7.600mm
Maximum Displacement	7.700mm
Cross-sectional area	181.770mm^2
Elongation	2.1%

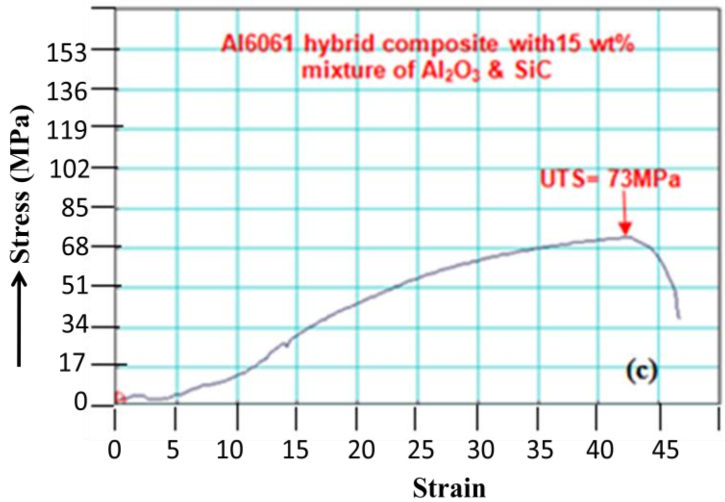

Results Corresponds to Graph 5.13(c)	
Maximum Force	12.750KN
Displacement at Maximum Force	21.00mm
Maximum Displacement	23.400mm
Cross-sectional area	175.609mm^2
Elongation	6.8%

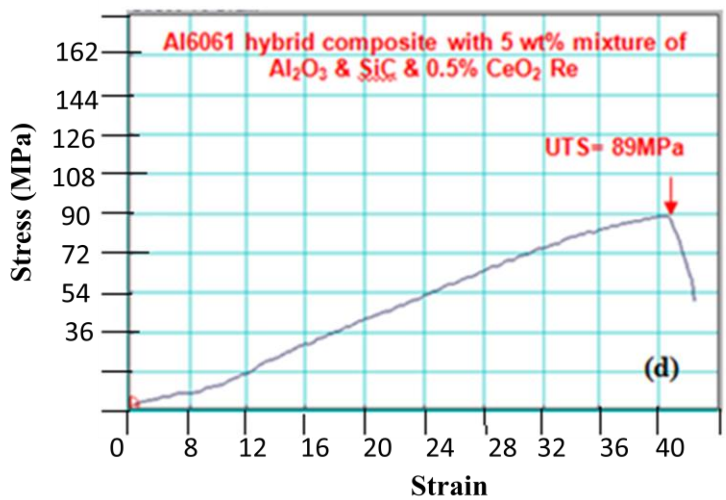

Results Corresponds to Graph 5.13(d)	
Maximum Force	14.850KN
Displacement at Maximum Force	18.00mm
Maximum Displacement	19.200mm
Cross-sectional area	167.024mm^2
Elongation	7.2%

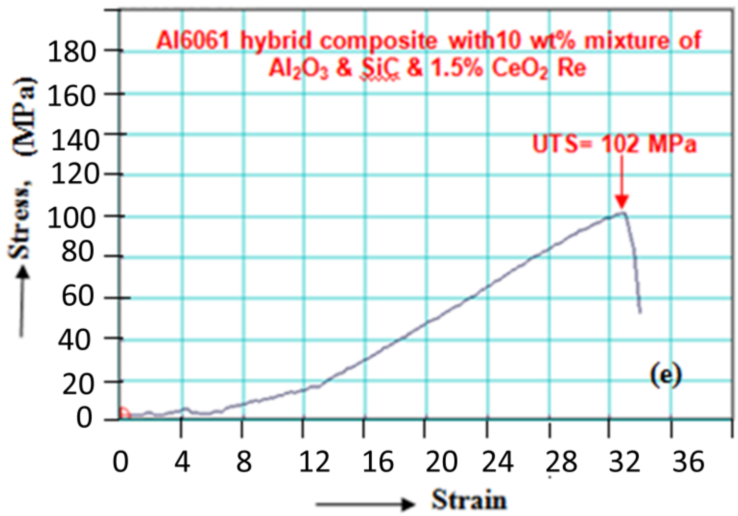

Results Corresponds to Graph 5.13(e)	
Maximum Force	16.400KN
Displacement at Maximum Force	16.400mm
Maximum Displacement	17.000mm
Cross-sectional area	161.346mm^2
Elongation	10.0%

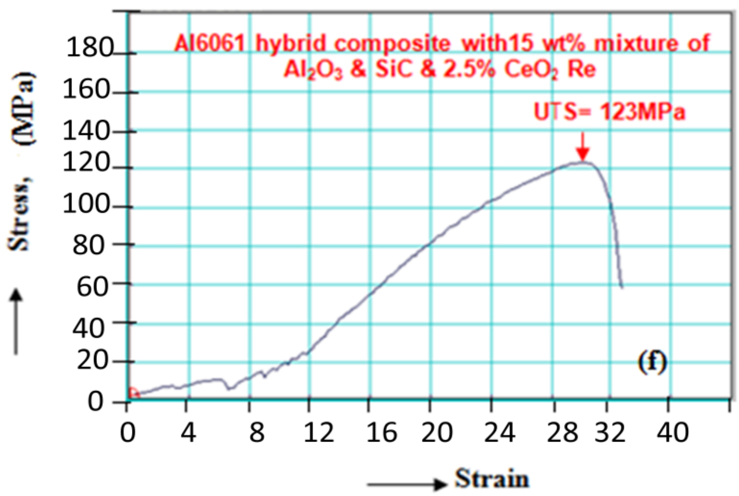

Results Corresponds to Graph 5.13(f)	
Maximum Force	20.450KN
Displacement at Maximum Force	15.000mm
Maximum Displacement	16.400mm
Cross-sectional area	166.338mm^2
Elongation	11.5%

Figure 5.13 Tensile Test Results of Composite Samples Showing Stress vs Strain Relationship

It can be seen from the table 5.3 that with increase in wt% of reinforcements, the value of tensile strength as well as percentage elongation increases. It shows that both the strength and ductility of the material increases with increase in wt% of reinforcement composition. Better homogeneity of the mixture as observed from the microstructure analysis of composites may have led to the enhancement in their properties. After addition of cerium in A356 aluminium alloy, cracks no longer easily grow along the interface of eutectic silicon and aluminum matrix. The elongation enhanced when the level of cerium added in the A356 is more than 0.6 wt% [Torre et al., 2013]. Present results are in agreement with these trends.

Table 5.3 Tensile Properties of Composites

Nomenclature of sample	Ultimate tensile strength (MPa)	Tensile Yield strength (MPa)	Elongation (%)	Impact Strength (J)
Al-6061/2.5wt% (Al_2O_3+SiC)	28	27	2.0	22
Al-6061/5wt% (Al_2O_3+ SiC)	54	52	2.1	30
Al-6061/7.5wt% (Al_2O_3+ SiC)	73	41	6.8	34
Al-6061/2.5wt% (Al_2O_3+SiC)+ 0.5wt%(CeO_2)	89	51	7.2	50
Al-6061/5wt% (Al_2O_3+ SiC)+ 1.5wt%(CeO_2)	102	54	10.0	56
Al-6061/7.5wt% (Al_2O_3+ SiC) +2.5wt%(CeO_2)	123	60	11.5	46

The graphical representations of the tensile test results showing combined effects of wt% reinforcement addition on the ultimate tensile strength (UTS) and percentage elongation of all the samples are shown in figure 5.14.

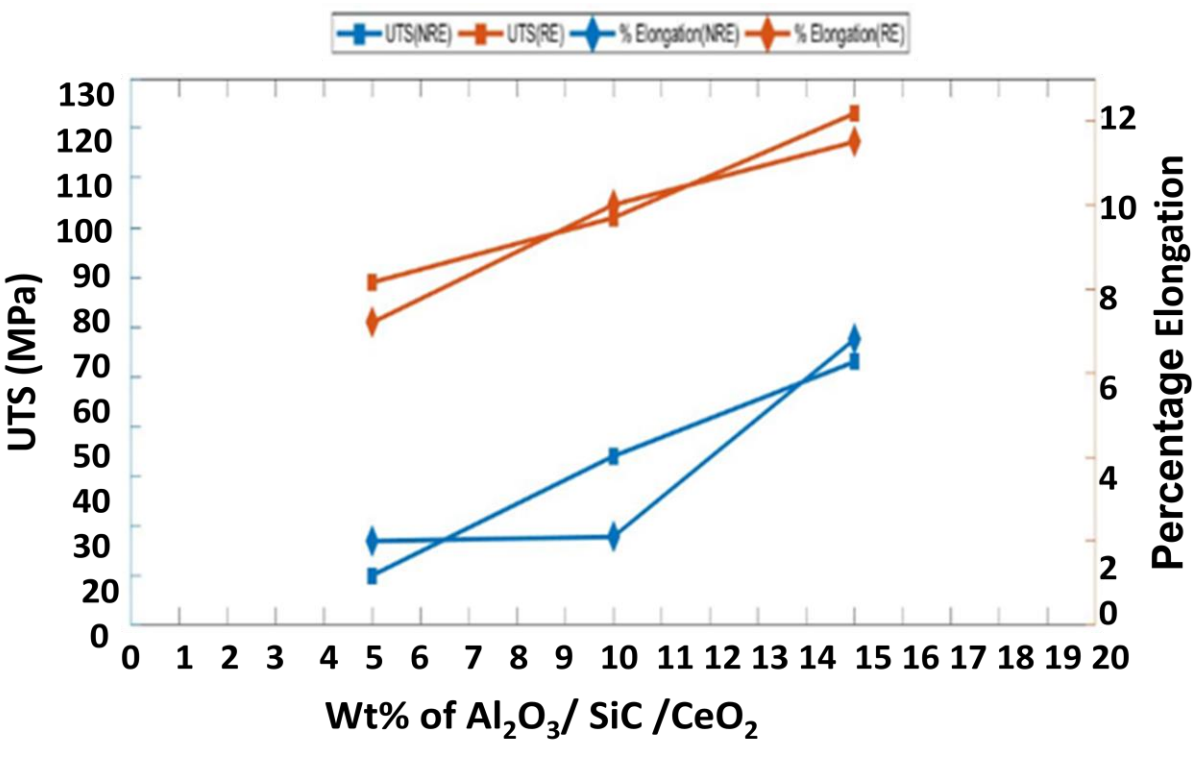

Figure 5.14 Combined Effect of Weight Percentage of Reinforcement Added on UTS and Percent Elongation of the Composites

5.4.2 Measurement of Hardness

Vickers hardness of the base alloy Al-6061 and all other hybrid composite samples with different compositions of SiC, Al_2O_3 and CeO_2 are tabulated in table 5.4. Initially Vickers hardness of Al-6061 is found to be 77 HV. After addition of 2.5 wt% ($SiC+Al_2O_3$), Vickers hardness of composite rose to 81 HV. The percentage increase in hardness of Al-6061 is found to be 5.19%. With further increase in weight percent of ($SiC+Al_2O_3$) to 5 wt%, the hardness of Al-6061 rose from 77 HV to 84 HV with a percentage improvement of 9.09%. The value of hardness increases further up to 88 HV after addition of 7.5 wt% of ($SiC+Al_2O_3$) with percent improvement of 14.28%.

It can be seen from the table 5.4 that Vickers hardness of the composites with content of rare earth oxides shows better results. The hardness of the as received Al-6061 alloy is 77 HV. It is evident that the hardness of the Al-6061 alloy composites is enhanced by 10.38 % from 77 HV to 85 HV after addition of 2.5 wt% ($SiC+Al_2O_3$) and 0.5 wt% of cerium oxide. After addition of 1.5 wt% of cerium oxide in composites with 5 wt% of ($SiC+Al_2O_3$), the hardness increased by 15.58 % from 77 HV to 89 HV as compared to base alloy Al-6061. In composites with 7.5wt% of ($SiC+Al_2O_3$), the hardness is enhanced by 22.07 % from 77 HV to 94 HV after addition of 2.5 wt% of cerium oxide. The Rockwell hardness of the base alloy Al-6061 increased from 61.73 HRB to 82.6 HRB with a percentage increase of 33.80% with the addition of 2.5wt% of cerium oxide. Whereas in case of 7.5 wt% of ($SiC+Al_2O_3$), the hardness value increased from 61.73 HRB to 71.8 HRB with a percentage increase of only 16.32%.

Result of hardness testing reveals that the hardness of the composite samples reinforced with cerium oxide as an additive is higher in comparison to the composites without rare earth oxide. It can also be observed from the results that with 0.5 wt% of rare earth oxide, hardness value was little bit higher and at 1.5 wt% there was a slight more increase in its hardness value but when the composition reached 2.5 wt% there was a sudden increase in the hardness value as compared to the base alloy and non rare earth composites. This may be due to the strong and hard reinforcement particles that help in the direct strengthening of matrix by providing hindrance to dislocation movement [George et al., 2005]. Similar trends of increase in hardness were observed in Gr/Al composites reinforced with neodymium particles of 0.2 wt%, 0.5 wt% and 2.0 wt% [Wang et al., 2011]. In addition, the effect might be more prominent since a few reinforcements are in sub micron size range and get well distributed by stir casting. It is observed that fine and smooth grain size of composite samples may have improved the hardness as per the Hall-Petch effect. The similar agreement in the results of increased hardness of Mg alloy with decrease in its grain size was observed [Arora et al., 2013]. It is also believed that homogeneous dispersion of reinforcement may have helped in pinning of dislocations and retardation of grain growth [Zohoor et al., 2012; Hossieni et al., 2015]. Similar trend of pinning effect was also seen in the aluminium composites reinforced with SiC and Gr [Bodunrin et al., 2015]. Moreover it can also be seen that with increase in reinforcement in the cases (Al_2O_3+SiC +CeO_2) as well as (Al_2O_3+SiC) composites there is an increase in the hardness values. Increase in density with the increase in amount of reinforcement may be the reason for same. Particle reinforcement addition to the 2218 Al-alloy resulted in increase of density [Tirth, 2017].

Table 5.4 Vickers hardness of composites

Nomenclature of sample	HV 1	HV 2	HV 3	HV 4	HV 5	HV (average)
Al alloy	77.20	78.00	77.40	77.50	76.90	77
Al-6061/2.5wt% (Al_2O_3+SiC)	80.60	81.20	80.70	81.30	80.90	81
Al-6061/5wt% (Al_2O_3+ SiC)	83.70	83.80	83.30	83.90	83.00	84
Al-6061/7.5wt% (Al_2O_3+ SiC)	87.90	87.80	88.30	88.40	88.60	88
Al-6061/2.5wt% (Al_2O_3+SiC)+ 0.5wt%(CeO_2)	84.30	84.60	84.70	84.80	84.60	85
Al-6061/5wt% (Al_2O_3+ SiC)+ 1.5wt%(CeO_2)	88.80	8.60	88.70	88.40	88.70	89
Al-6061/7.5wt% (Al_2O_3+ SiC) +2.5wt%(CeO_2)	93.60	93.70	93.20	93.60	93.40	94

5.4.3 Impact Strength

Figure 5.15 shows the effect of rare earth oxide content on the impact strength of Al-6061 alloy composites. The graph indicates that the impact energy increases with increase in rare earth oxide from 50 J at 0.5 wt% of CeO_2 to 56 J at 1.5 wt% of CeO_2 in the unfilled matrix. The impact strength of the base alloy and samples of hybrid composites are represented in table 5.3. The impact strength of base alloy increases from 18 J to 22 J with percentage improvement of 18 % after addition of 2.5 wt% (SiC+Al_2O_3). With further increase in weight percent of (SiC+Al_2O_3) up to 5 wt% and 7.5 wt%, the impact strength measurement showed a value of 30 J and 34 J. From figure 5.15, it is clearly visible that the value of impact strength continues to increase with increase in the percentage of SiC, Al_2O_3 and rare earth elements but after addition of 2.5wt% of rare earth oxide, the impact strength value of the composite decreases. After addition of 0.5 wt% of cerium oxide, the impact strength of base alloy rises from 18 J to 50 J. On further addition of cerium oxide up to 1.5 wt%, impact strength rises from 18 J to 56 J with. But after further addition of rare earth up to 2.5 wt%, a sharp decline in the impact strength has been seen with value of 46 J. The decrease in value of impact strength as of increase in the amount of rare earth oxides may be due to change in property of composite from ductile to brittle. Further, the ability of a material to absorb shock decreases and it break with less force as compared to other prepared composites. Failure of reinforcement particles by cracking and decohesion due to presence of intrinsic defects in the composite microstructure can also be the cause for reduction in impact strength of composites [Alaneme et al., 2019]

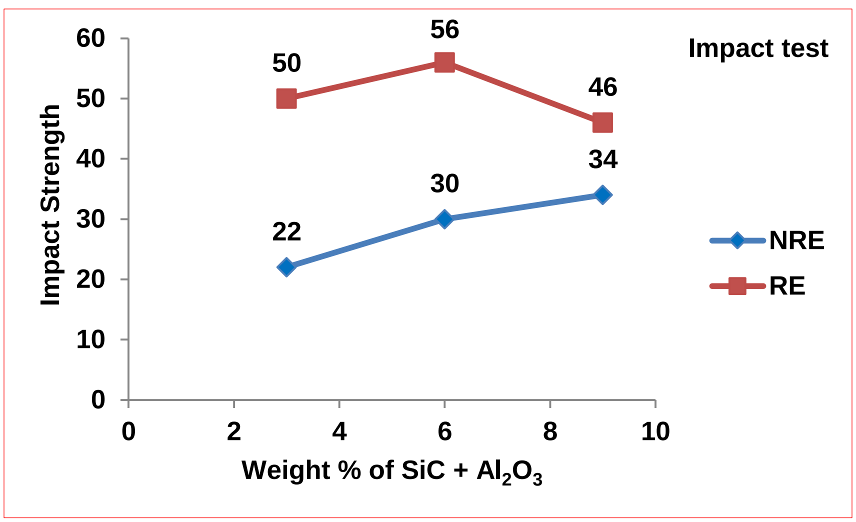

Figure 5.15 Impact Strength Distributions for Non-Rare Earth and Rare Earth Composites

5.4.4 Flexural Strength

In three-point bending test, the maximum bending load is evaluated for different samples with varying compositions of reinforcements. Then finally; the load values of different hybrid composites are converted into flexural strength (MPa) value. The flexural testing specimens of fabricated hybrid composites are machined according to ASTM standards. The flexural strength results of the samples are shown in figure 5.16.

These results reveals that addition of particulate reinforcements content lead to decrease in interspatial distance between various reinforcements and matrix grain that reduces the number of dislocations at the grain boundaries in the microstructure. Hence, the enhancement in the flexural strength is observed in composite samples in comparison to Al-6061 alloy. The enhancement of the flexural strength is also possible due to strong bonding between the reinforcement and matrix. Initially the flexural strength of the base alloy is measured as 340 MPa as indicated in figure 5.16. After addition of 2.5 wt% ($SiC+Al_2O_3$) reinforcement, the flexural strength of alloy rises from 340 MPa to 390 MPa with a percentage improvement of 14.7 %. With addition of 5 wt% of ($SiC+Al_2O_3$), the percentage improvement in flexural strength is observed to be 23.52 % with a value of flexural strength as 420 MPa. On further addition of weight percentage of ($SiC+Al_2O_3$) up to 7.5 wt%, the flexural strength rises from 340 MPa to 450 MPa. The flexural strength of the composites with SiC and Al_2O_3 further increases after addition of cerium oxide with weight percent of 0.5 wt% to 2.5 wt%. The flexural strength was found to be 515 MPa, 580.75 MPa and 615.6 MPa with different content of cerium oxide. The structure and properties of the reinforcements controls the mechanical properties of the composites that may attributes in strong interface for transfers and distribution of the load from the matrix to the reinforcements [Wang et al., 1992]. In other research, addition of graphite to aluminium alloy decrease the flexural strength and it can be overcome by the addition of Al_2O_3 particulates in the hybrid composites. The flexural strength of composite was increased by 23% than that of Al-7075 base alloy after addition of alumina particles [Kumar et al., 2017]. Similar results of flexural strength were found in the AlTiC master alloy with traces of mixed rare earth elements (Nd, Ce, La and Pr). The optimum value of flexural strength was found to be 617.6 MPa in composite sample with 0.5 wt% of rare earth elements [Xihua et al., 2008].

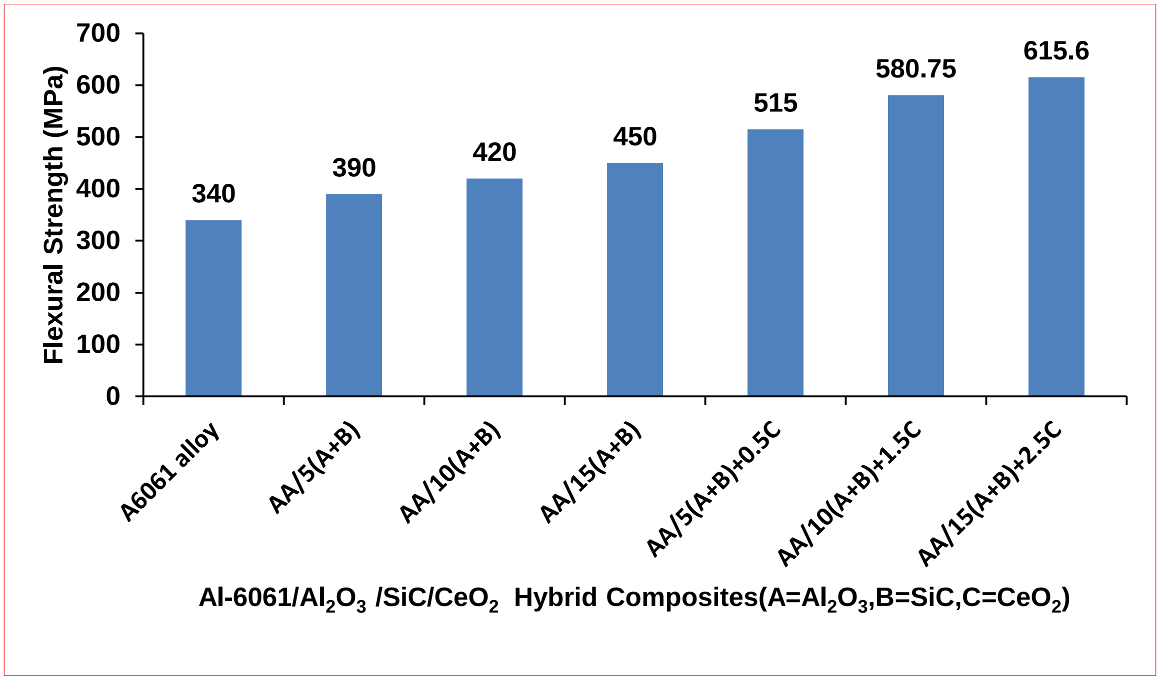

Figure 5.16 Effect of Weight Percentage of Reinforcement Addition on Flexural Strength of the Hybrid Composites

5.5 WEAR ANALYSIS

For wear analysis, two composite samples one from with RE and one from without RE having maximum hardness values are selected. Figure 5.17 shows the wear rate plots for stir casted hybrid composites under different loading and sliding velocity conditions. Figures 5.17 (a-c) shows the wear rates obtained for the hybrid composites at sliding velocities of 0.5 m/s, 1 m/s and 2 m/s respectively at different loads ranging from 10 N to 30 N. It is evident from the curves that stir casted hybrid composites with cerium oxide as RE compounds has consistently shown better wear resistant throughout the range of parameters investigated. Similar results of improving the wear behaviour have also been seen in double synthetic ceramics used in the making of aluminium composites [Bodunrin et al., 2015]. However, the both types of hybrid composites have demonstrated uniform wear rate over a large part of sliding distance corresponding to all loads and sliding velocities. It is apparent from the figure 5.17 (a) that the hybrid composites with cerium oxide examined at 0.5 m/s sliding velocity and normal load 10 N exhibited the least wear rate. It can be further observed from the figures that maximum mass loss per sliding distance occurred at lower value of the velocity and it decreased with the further increase in sliding velocity for both the type of composites. A significant improvement of 87.28 % in wear rate is found by introducing 2.5 wt % of CeO_2 in hybrid composites reinforced with 7.5 wt % of both SiC and Al_2O_3 as compared to base metal at velocity of 0.5 m/s and normal load of 10 N. Whereas at same investigated conditions, in case of hybrid composite with only 7.5 wt % of both SiC and Al_2O_3 addition, only 38 % improvement in wear rate in comparison to base metal is found. At velocity of 0.5 m/s and normal load of 20 N, the REs based composites demonstrated a 77.5% improvement in wear performance as compared to the base alloy, whereas the hybrid composites with 7.5 wt % of both SiC and Al_2O_3 only showed 32% improvement. Corresponding to velocity of 0.5 m/s and normal load of 30 N, the REs based composites exhibited a 68.83% improvement in wear rate while only 22% improvement in wear rate is observed for the sample of composite with 7.5 wt % of SiC and Al_2O_3. Figure 5.17 (b) depict the comparative analysis of wear rates for hybrid composites with and without RE addition and the base alloy. It can be analyzed from the figure that maximum mass loss per sliding distance occurred at the value of maximum load i.e. at 30 N and it decreased linearly with decrease in the normal load values. From the wear rate curve shown in figure 5.17(c), the percentage improvement of 44.93 % and 34.95 % in wear rate is found by addition of 2.5 wt %

of CeO_2 in hybrid composites as compared to base metal at velocity of 2 m/s and normal load of 20 N and 30 N respectively. The decrease in the wear rates with change in the sliding speed from 1 m/s to 2 m/s were found to be higher in comparison to change in sliding velocity from 0.5 m/s to 1 m/s. It may be an indication of different wear mechanisms that occurs at different sliding speeds and normal load values. Consolidated impact of normal loads and sliding velocities on wear rate depicted with the help of a wear rate map is represented in figure 5.18(a). Contour map shown in figure 5.18 (a) indicate the occurrence of highest wear rates at maximum load and lowest velocities. The 3D shape plot of figure 5.18 (b) demonstrates the variation in abrasive wear under all investigated conditions of loads and velocities. It can be observed that during wear test at low value of normal load and sliding velocity, wear loss occurs due to the abrasion. The extent of abrasion wear found to decrease with increase in normal load and sliding velocity. Similar trends of wear rate of composites increases with increases load linearly also observed in Al-2218 (wrought aluminium-copper) composites reinforced with Al_2O_3 and TiO_2 fabricated by stir casting [Tirth, 2017].

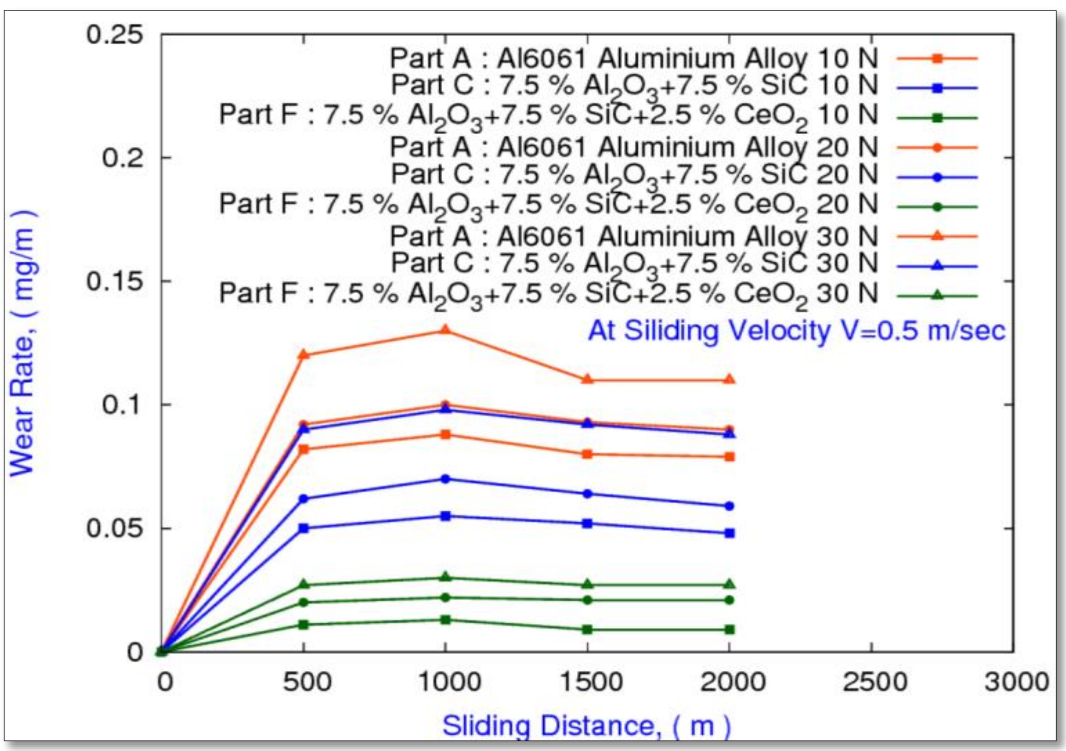

(a)

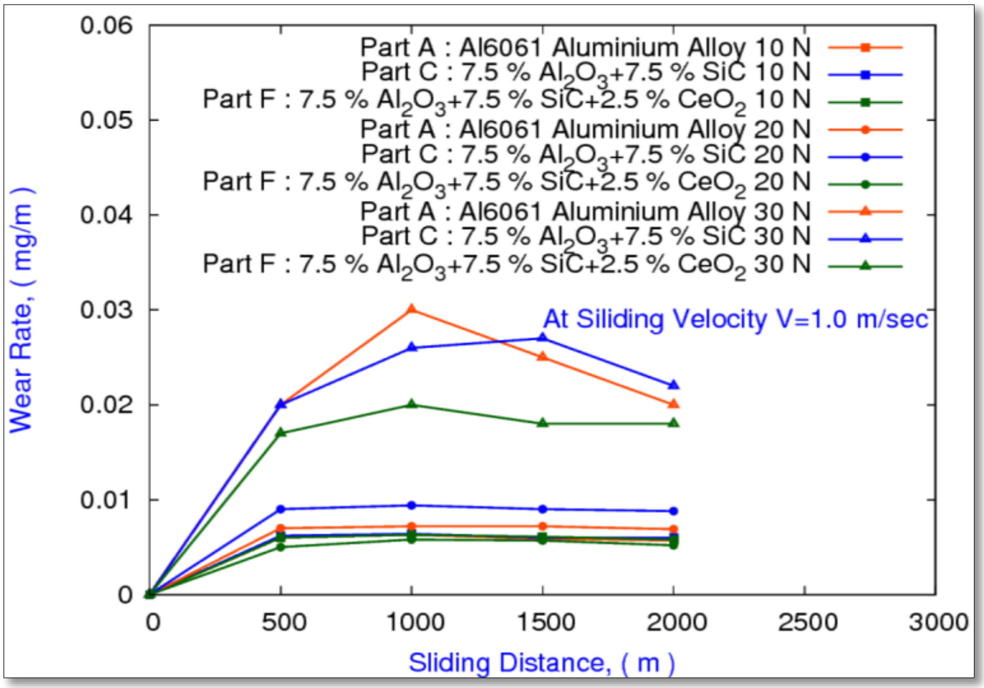

(b)

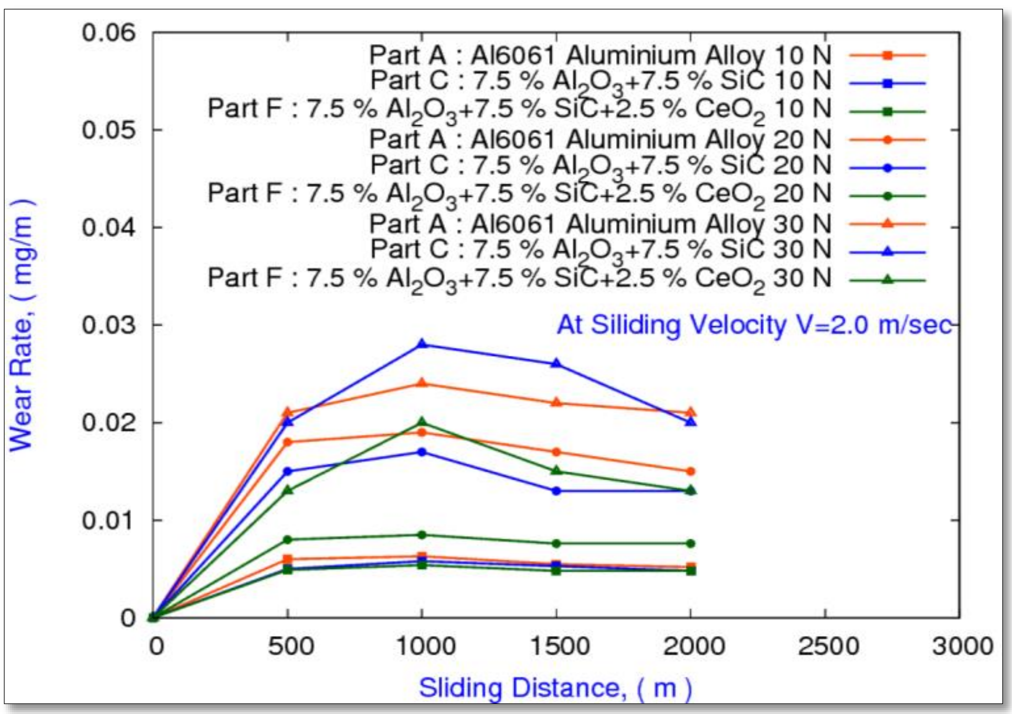

(c)

Figure 5.17 Progressive Wear Rate Plots for Al-6061 alloy, Al-6061 Alloy with $SiC+Al_2O_3+CeO_2$ and Al-6061 alloy with $SiC+Al_2O_3$ at Sliding Velocity of (a) 0.5 m/s (b) 1 m/s (c) 2.0 m/s [Sharma et al., 2019]

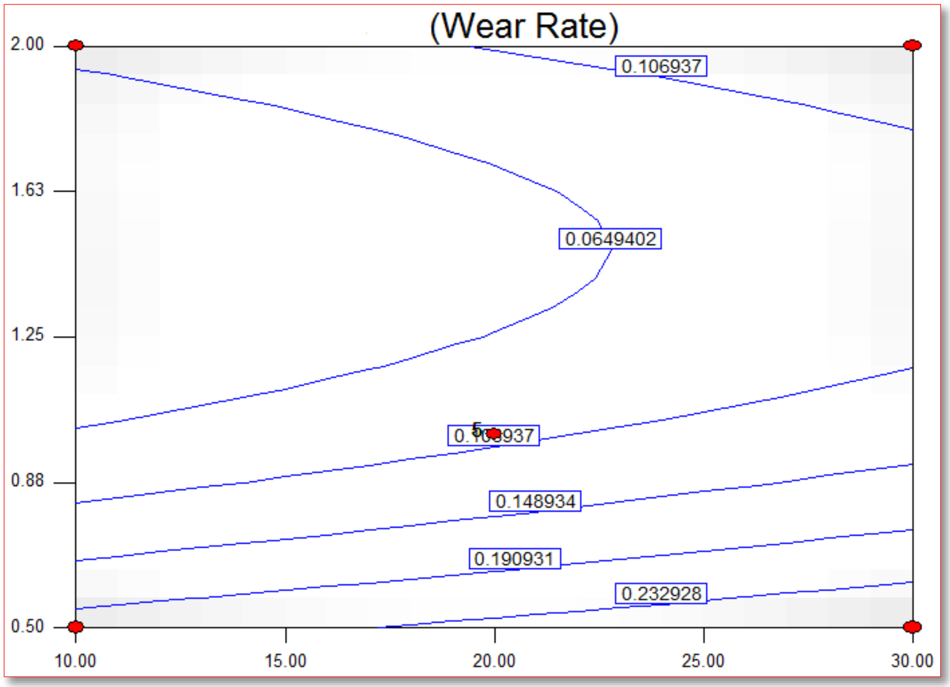

(a)

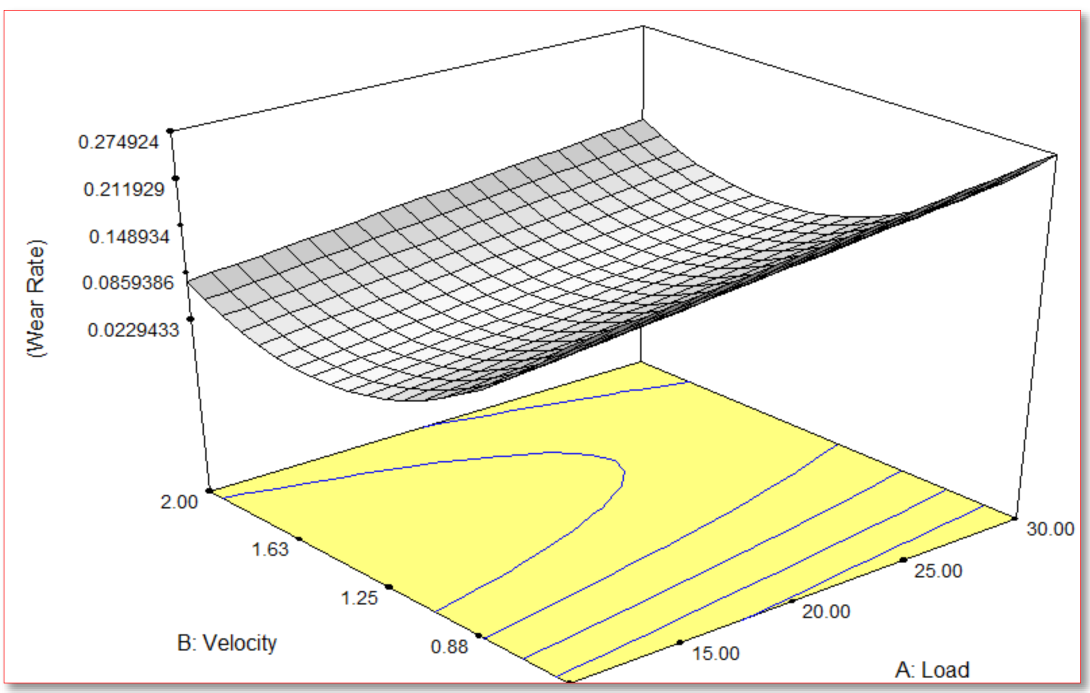

(b)

Figure 5.18 Contour Plot Representing (a) Wear Rate for Al-6061 RE Hybrid Composites Reinforced with SiC+Al_2O_3 at all Examined Conditions (b) Variation of Abrasion Wear with Sliding Velocity and Normal Load

5.5.1 Wear Mechanism Analysis of Worn Surfaces of Alloy and Hybrid Composites

SEM examinations of base metal alloy and hybrid composites reinforced with SiC, Al_2O_3 and CeO_2 disclosed five different operating wear mechanisms. From these five mechanisms plastic deformation, abrasion and delamination demonstrated the dominating effect while adhesion and oxidation have shown less abundant effect. It was further observed from the investigation, that the wear rate of the base alloy and composite samples showed nearly similar wear mechanisms. From the prominent wear mechanisms a few differences are observed at different conditions, which have been specified below.

5.5.1.1 Wear Analysis at Sliding Velocities 0.5 m/s,1 m/s and 2 m/s with Normal load of 10 N

SEM images of worn surface of hybrid composites subjected to 10 N load during wear investigation are shown in figure 5.19. Different types of wear mechanisms are studied from the SEM pictures shown in figure 5.19 depending upon the type and nature of the particulate reinforcement. Figure 5.19(a) shows the worn surface of the composite sample comprises of SiC+Al_2O_3 reinforcment at load of 10 N and velocity of 0.5 m/s. It can be observed from the image that at 10 N normal load and veocity of 0.5 m/sec that the marks of abrasive wear, ploughing and plastic deformation are evident on the surface of hybrid composites reinforced with SiC+Al_2O_3. The fractured surface looks like as broken particles as seen from the worn surfaces of hybrid composites. Finally, the results from EDS analysis of the worn surface of SiC+Al_2O_3 reinforced hybrid composites reveals the presence of significant amount of oxygen at surface. It was concluded that surface oxidation results in the oxidation wear of the surface. These results are in similar to the results of earlier research findings related to wear analysis of aluminium alloy composite reinforced with rare earth elements (cerium, lanthanum and neodymium) at varying weight percent of 1 wt% , 2 wt% and 3 wt% [Asl et al.,2010].

It is observed from the figure 5.19(c) that abrasion, ploughing and delamination are the most dominating wear mechanisms to cause wear on the surface of the CeO_2 additive based hybrid composites. From these factor abrasion is found to cause more severe effect on the wear properties. Scanning electron microscopy also investigated that the abrasion, delamination and plastic deformation were found to be most abundant wear mechanism in composites based on aluminium alloy reinforced with traces amount of rare earth mixtures elements [Asl et al., 2010].

Weight loss and friction coefficient get reduced with the addition of CeO_2 additive to the $SiC+Al_2O_3$ hybrid composites. The probability of abrasion wear in the Al-6061-($SiC+Al_2O_3+CeO_2$) hybrid composites is low and hence delamination is the predominant factor for the wear to be occurred. It can be obviously observed from the figure 5.19(c) that the for the composite sample with content of cerium oxide particulate as 2.5 wt %, delamination increases, which ultimately leads to increase in brittle fracture. Decreased fracture toughness with higher CeO_2 additive cause more brittle fracture on the surface of hybrid composites. It is clearly indicated from the figure 5.19(d) of Al-6061 alloy that wear mechanism is dominated by the formation of the pit and the microcracks on the worn surface. The microcracks which are extended continuously on the worn surfaces. Surface oxidation can also be seen in the form of oxide layer. At velocity of 0.5 m/s and load 10 N, a very large pit may be observed on surface of worn out sample. This pit may results in the increase of wear volume and ultimately increases rate of wear of the Al-6061 alloy. It may be observed from the figure 5.19(e) and figure 5.19(f) for the hybrid composite samples at velocities of 1 m/s and 2 m/s that strong interfacial adhesion with addition of cerium oxide in the composite makes SiC and Al_2O_3 not easy to detach from the Al-6061 matrix surface and prevents the rubbing off of Al-6061. This prevention of matrix may resulted in improvement of the wear properties of $SiC+Al_2O_3$ hybrid composites after treatment with RE compounds. Further presence of intermetallic phase of $Al_{11}RE_3$ in shape of rod was observed in the microstructure. Presence of intermetallic phases may be the reason for enhanced mechanical properties at elevated temperatures which further improves the load bearing capacity of Al-6061 hybrid composites reinforced with $SiC+Al_2O_3$.

From SEM investigation, gross plastic deformation, delamination and abrasion wear are found to be the most dominant mechanism for wear while oxidation and adhesion are found to be less dominant in all the samples. Traces of parallel grooves can be noticed on most of the sample surfaces. These scratches may be formed due to hard asperities of counterface or detached particles that removed from disk or pin and comes in surface contact. Same type of wear mechanism was observed by a researcher worked on aluminium alloy composite. Figure 5.19(c) illustrates typical feature of such mechanisms. Abrasion is the prevailing wear mechanism at lower loads of 10 N at a speed of 0.5 m/s. There is no detectable distinction between the extent of abrasion on pure Al-6061 alloy and Al-6061-RE composite. However on the surfaces of samples with RE content, tiny fragments of aluminium alloy are discovered (figure 5.19e). This may be due to the presence of brittle $Al_{11}Ce_3$ intermetallic phase that may be arranged in sliding direction and provides three body abrasion wear [Asl et al., 2010].

With progression of wear these grooves become wider and deeper in a way that their facet changes to some extent but still abrasion is the dominant wear mechanism. Abrasive wear facilitates the wear process where hard reinforcing materials exist and become load bearing constituent part. Slightly better wear resistance of pure Al-6061 alloy at inferior loads may be related to more ductility of this material [Asl et al., 2010].

Plastic deformation is more considerable for pure Al-6061 alloy, while in the case of Al-6061-RE composite, less aspects of plastic deformation are evident. This fact may be related to existence of $Al_{11}Ce_3$ phase that prohibits severe deformation and subsequently diminishes wear rates values. Therefore Rare Earth contents comprise constructive effect on wear behaviour of Al-6061 alloy chiefly at rigorous conditions.

Finally, it seems that formation of $Al_{11}Ce_3$ intermetallic phase that helps in achieving suitable mechanical properties at elevated temperatures with enhanced load bearing capacity of Al-6061 alloy. This may be the reason that at more severe conditions of highest normal load and sliding speed, specimens containing RE particles showed superior wear resistance particularly to plastic deformation.

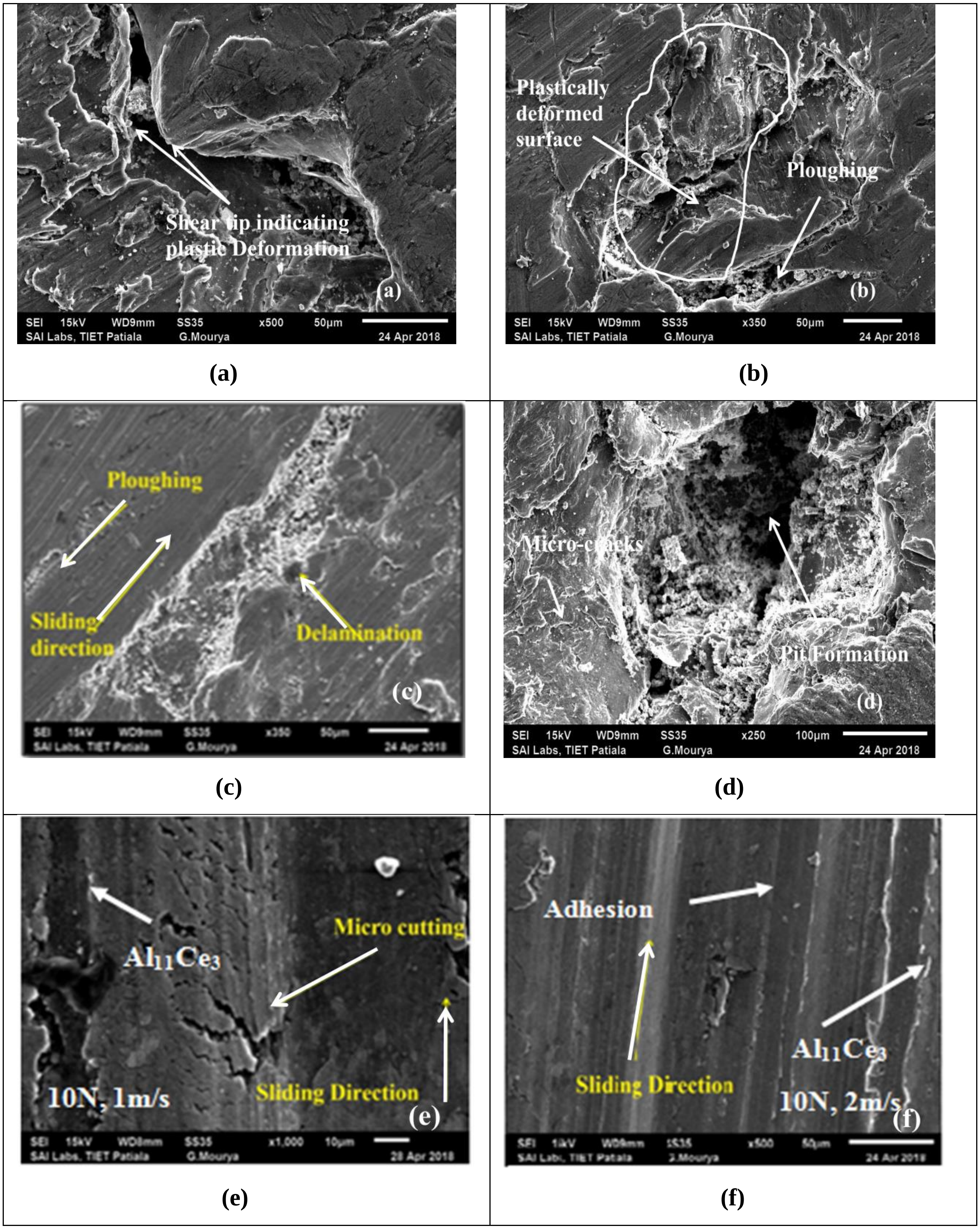

Figure 5.19 SEM Images of the Wear Specimens at load 10 N (a)-(b) Composite with Al_2O_3+SiC Mixture (c) RE Hybrid Composite with Al_2O_3+SiC + CeO_2 Mixture (d) Al-6061 Base Alloy (e) RE Hybrid Composite with Al_2O_3+SiC+CeO_2 Mixture (f) RE Hybrid Composite with Al_2O_3+SiC + CeO_2 Mixture

5.5.1.2 Wear Analysis at sliding velocities 0.5 m/s, 1 m/s and 2 m/s with normal load of 20 N

The SEM images of the hybrid composites and base alloy subjected to wear test at sliding velocity 0.5 m/s and normal load 20 N are shown in figures 5.20(a-e). The abrasive wear including surface cracks, microcutting and plastic deformation on the worn surface are observable. These are more intense at the value of 20 N normal load as compared with the 10 N load. The SEM images of worn surface revealed that fractured surface looks like as broken particles because of the high shear force. High value of normal load may be the reason for this fracture. The worn surface of the SiC+Al_2O_3 hybrid composites also shows the presence of plastic deformation. The sub surface cracks, extended upto the surface, are also seen on the worn surface. Oxidation of surface in the form of oxide layer formation is also observed. It can be observed from the figure 5.20(c) and figure 5.20(d) that microcutting, ploughing and delamination are the most dominating factors to cause wear on the surface of the CeO_2 additive based hybrid. At a load of 20 N and sliding velocity of 0.5 m/s, the large cracks are observed on the surface of Al-6061 base alloy. These cracks may have increased the wear volume and ultimately increased the rate of wear as observed from the figure 5.20(e). The formation of huge cracks on the worn surface are due to the abrasion wear that are revealed from the presence of abrasion grooves, fractured particles and oxidation in sample tested at 20 N normal load and 0.5 m/s sliding velocity. These results are similar to the observation in friction stir processed Mg alloy [Arora et al., 2013]. Ploughing action of the hard surface contact uasually results in the formation of grooves on the surface of aluminium composites reinforced with steel and graphite fabricated by the stir casting process [Alaneme et al., 2019]. Deeper and large cracks have been seen in the aluminium alloy reinforced with rare earth elements corresponding to the value of normal load of 20N at particular velocity of 0.25 m/s and 0.5 m/s [Asl et al., 2010]. It was concluded from the figure 5.20(f) that the surface appearance of the CeO_2 particulate based hybrid composites is very clean and shiny as compared to the SiC+Al_2O_3 reinforced hybrid composites without much traces of abrasion. It illustrates the reduction in wear rate because of the presence of rod like $Al_{11}RE_3$ intermetallic phases.

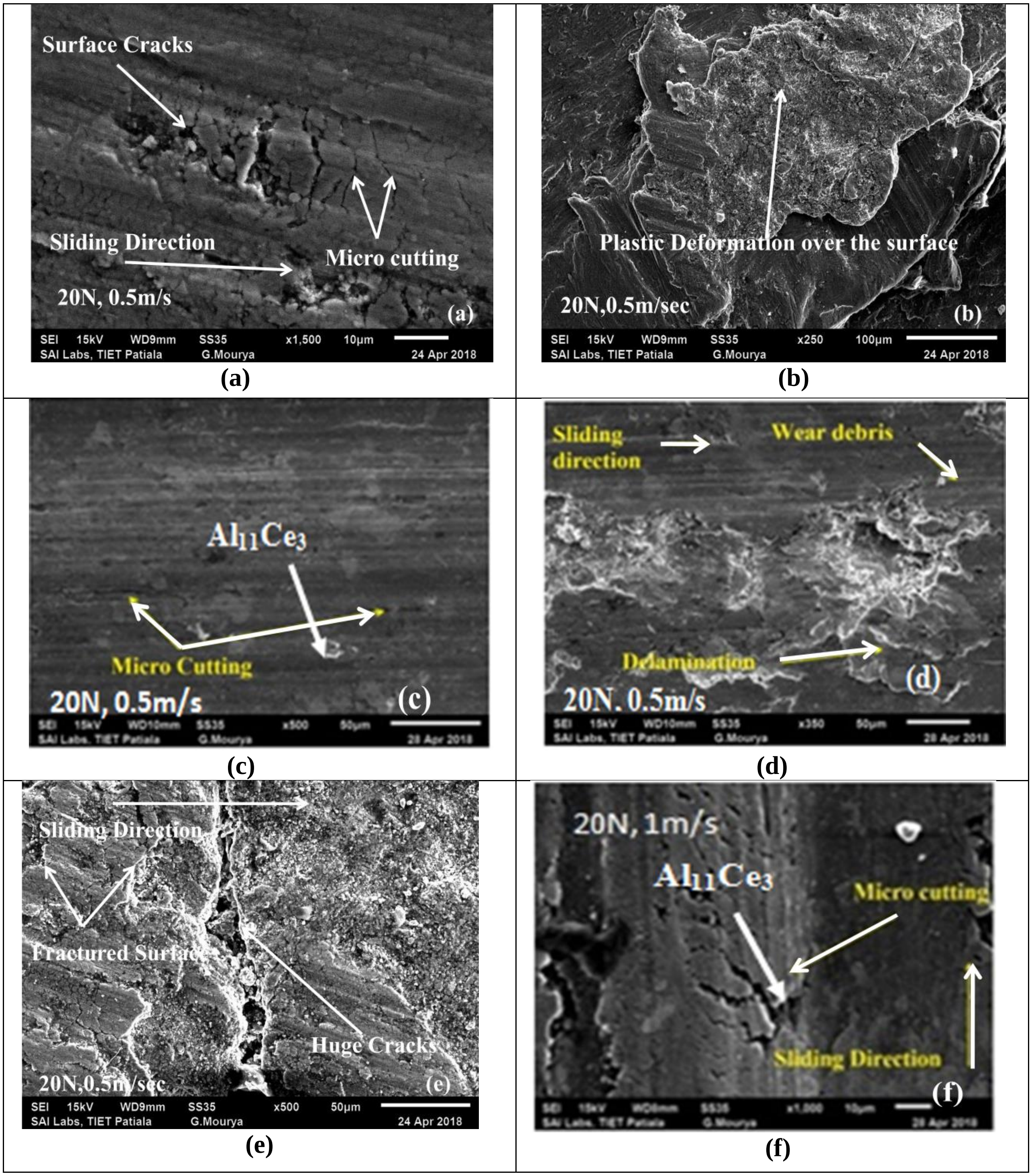

Figure 5.20 SEM Images of the Wear Specimens at load 20 N (a)-(b) Composite with Al_2O_3+SiC mixture, (c)-(d) RE Hybrid Composite with Al_2O_3+SiC+ CeO_2 Mixture (e) Al-6061 Base Alloy (f) RE Hybrid Composite with Al_2O_3+SiC+CeO_2 Mixture [Sharma et al., 2019]

5.5.1.3 Wear Analysis at sliding velocities 0.5 m/s, 1 m/s and 2 m/s with normal load of 30 N

Figure 5.21 demonstrates the SEM images of the base alloy and hybrid composites subjected to wear testing at a load of 30 N and distinctive sliding velocities. Different types of wear mechanisms are visible on the surface of worn samples of the hybrid composite reinforced with (Al_2O_3+SiC) as indicated by the SEM image shown in figure 5.21(a). It was observed from the figure 5.21 (a) that subsurface cracks, surface cracks and ploughing effect are visible on the surface of the composites. Other than these indications of abrasion in the form of ploughing, sub surface cracks and partially broken oxide layer is also observable in the figure 5.21(a). EDS investigation also supported the surface oxidation of the worn surface under the condition of 30 N load and sliding velocity 0.5 m/sec. The results are in agreement with steel and graphite reinforced aluminium composite that shows the ploughing action on the hard surface causes wear to be occurred [Alaneme et al., 2019].

In case of hybrid composites with the reinforcement of cerium oxide, the mechanism of wear is dominated by the ploughing as indicated by the figure 5.21(b). As compared to (SiC+Al_2O_3) hybrid composites, the wear rate is found to be less as only one type of wear mechanism is found to be dominant. This dominance of only one type of mechanism can be due to very fine size of the cerium particles. The effects observed to be more effective at 30 N normal load as compared to the 20 N and 10 N load. It is observed from the figure 5.21(c) of Al-6061 alloy that wear is dominated by ploughing and the cracks on its surface. The surface cracks are extended continuously on the worn surfaces. Surface oxidation can also be seen in the form of oxide layer. At velocity of 0.5 m/s and load 30 N, a large broken surface of oxide layer can be seen. This large broken surface may have resulted in the increase of wear volume and ultimately increased the rate of wear for the composite sample. It is obvious from the SEM pictures that the surface appearance of the worn surface of the Al-6061 alloy shows large amount of abrasion as compared to the SiC+Al_2O_3+CeO_2 reinforced hybrid composites indicated in figure 5.21(d) and figure 5.21(e). However, the specimen surface is subjected to severe plastic deformation and subcracks during test as observed by the micrograph. At higher load, the formation of intermetallic phase $Al_{11}Ce_3$ further enhances the load bearing capacity of RE based hybrid composites. The effect of Rare Earth compounds on the wear rate is found significant at higher loads. The hybrid composites containing RE in traces amount when tested at velocity of 2 m/s and load 30 N displayed superior wear resistance in comparison to pure Al-6061 alloy. Among the Rare Earth enriched hybrid composites, sample having 2.5 wt% CeO_2 RE particulate showed better performance to wear.

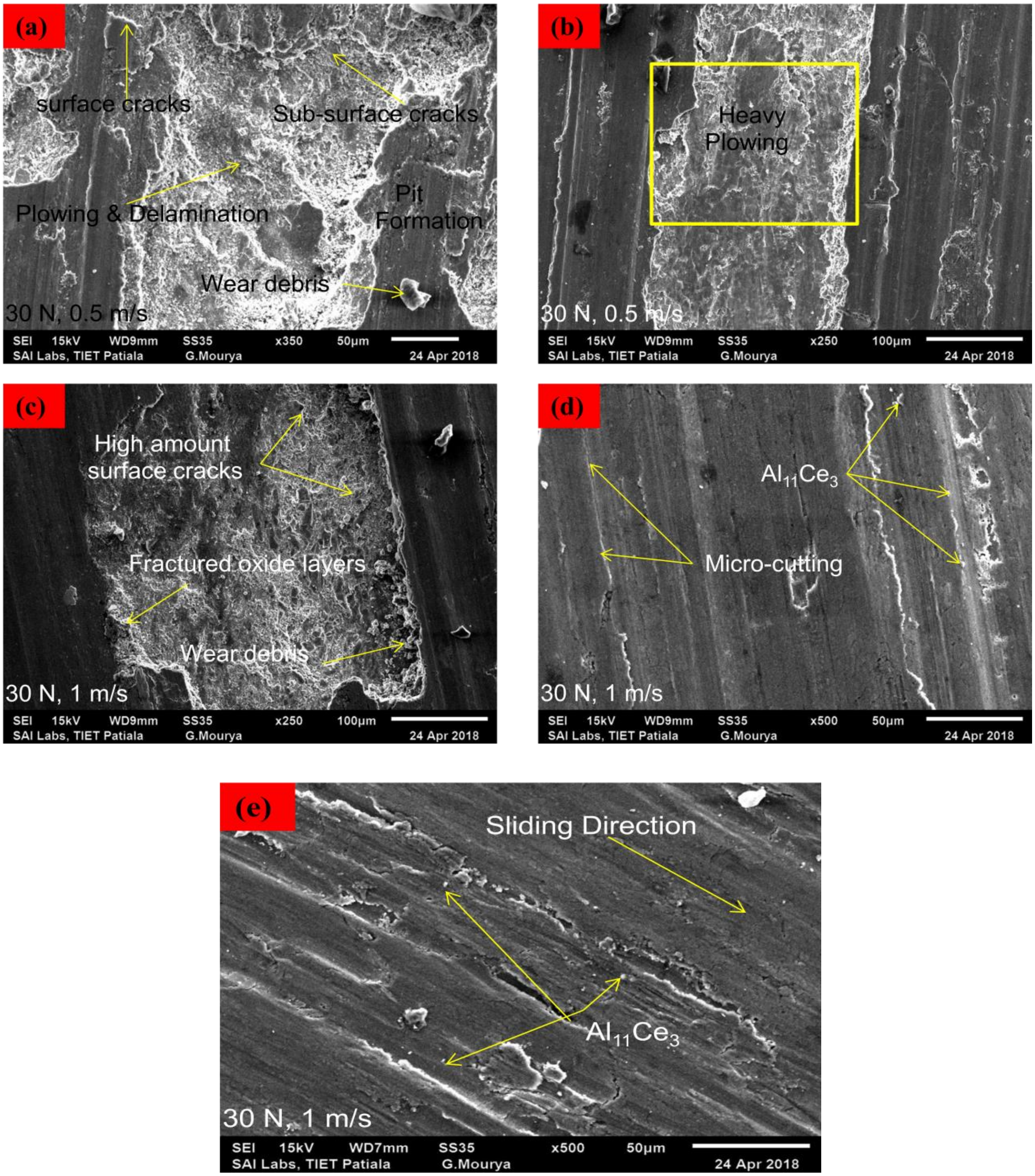

Figure 5.21 SEM Images of the Wear Specimens at load 30 N (a) Composite with Al_2O_3+SiC Mixture (b) Composite with Al_2O_3+SiC + CeO_2 Mixture (c) Al-6061 Base Alloy (d) RE Hybrid Composite with Al_2O_3+SiC + CeO_2 Mixture (e) RE Hybrid Composite with Al_2O_3+ SiC + CeO_2 Mixture [Sharma et al., 2019]

5.5.1.4 Subsurface Analysis of Hybrid Composites

The subsurface analysis of worn surface of hybrid composites through SEM images as shown in figure 5.22 revealed their sub structural characteristics. The SEM image shown in figure 5.22(a) is of the base metal alloy of Al-6061 at sliding velocity of 0.5 m/s and normal load of 20 N. The SEM showed in figure 5.22(b) is of Al-6061 hybrid composites reinforced with Al_2O_3 and SiC while the figure 5.22(c) corresponds to the Al-6061 hybrid composites reinforced with Al_2O_3, SiC and traces amount of rare earth elements tested under the same operating conditions.

The SEM micrograph of Al-6061 base alloy shows that needle shaped elongated trenches are present inside the microstructure because of splintering of β-phase precipitates during the examination of wear testing. Some broken precipitates are also seen at the fractured surface of the alloy. SEM as shown in figure 5.22(b) represents the subsurface material deformation details of the Al-6061 hybrid composites reinforced with Al_2O_3 and SiC. These subsurface material deformations on the surface of the specimen look like in the form of flow field. It is observed that such type of flow field supports in the formation of the plastic deformation over the surface and the softened material get extruded in the sliding direction during the wear testing. The subsurface cracks initiated at that place where the material showed some non-homogeneity or imperfections [Altinkok, 2004; Asl et al., 2010]. Plastic deformation is more considerable in the Al-6061 hybrid composites reinforced with Al_2O_3 and SiC while in case of Al-6061 hybrid composites reinforced with Al_2O_3, SiC and traces of rare earth elements, less parts of plastic deformation are obvious from the SEM picture in figure 5.22(c). This is due to the fact that the existences of $Al_{11}Ce_3$ phase that prohibits plastic deformation and subsequently diminishes wear rate values [Asl et al., 2010; Li and Cheng, 2006]. RE addition greatly improved the high temperature properties of the Al-6061 hybrid composites due to the formation of rod like intermetallic phase $Al_{11}Ce_3$. These intermetallics ultimately reduced the amount of β-phase particles in the matrix and finally led in the development of high thermal stability.

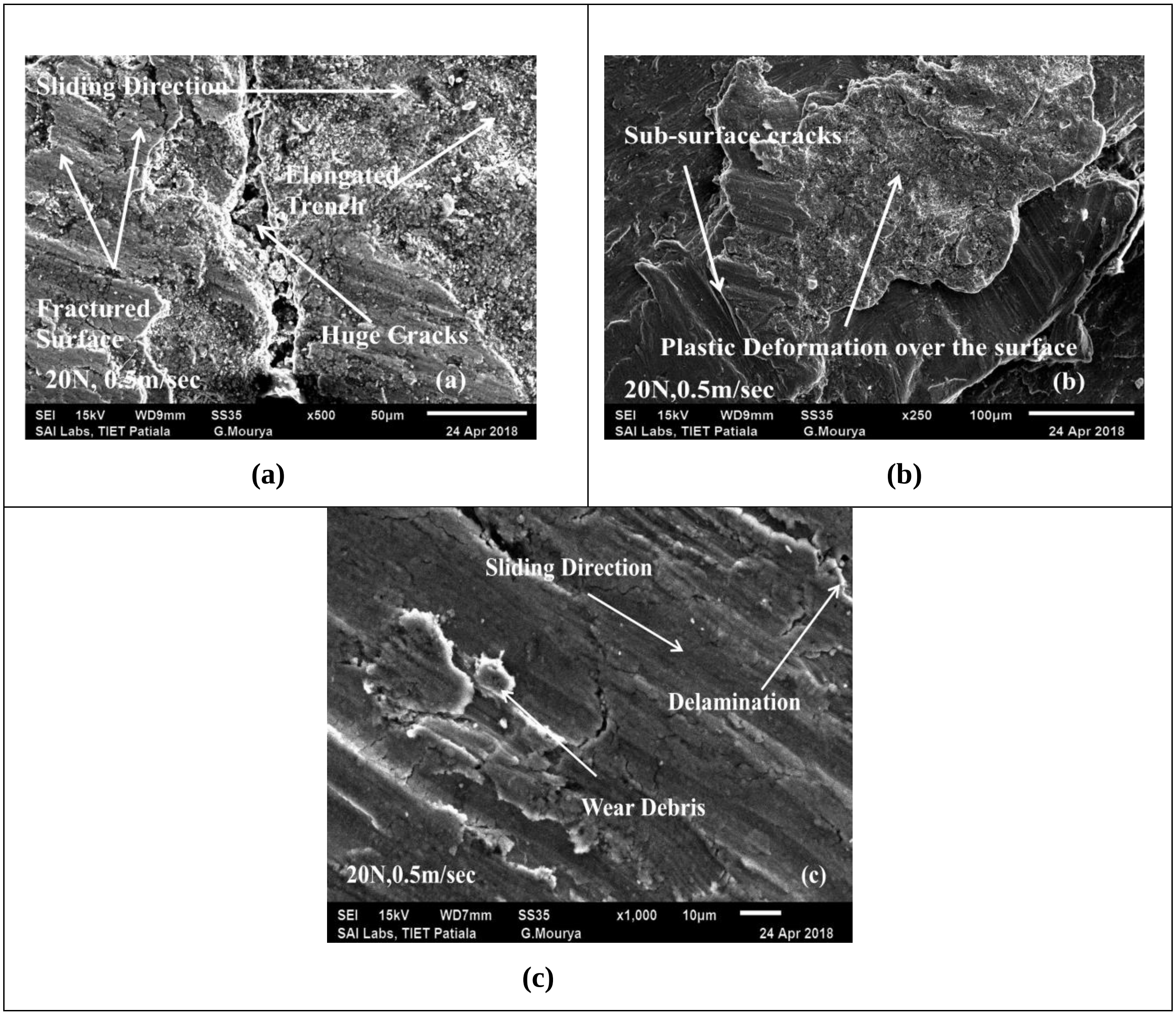

Figure 5.22 SEM Micrograph Showing Subsurface Microstructure of Worn Samples at 20 m/s Sliding Velocity Corresponding to Normal Load of 20 N

5.5.2 Specific Wear Rate Analysis

Specific wear rate plots of hybrid composites with and without REOs are shown in figures 5.23(a-c). All the specific wear plot are plotted by taken normal load as abscissa and specific wear rate as ordinate at three different velocities 0.5 m/s, 1 m/s and 2 m/s. Results of improved specific wear rate achieved after addition of REOs in composites reinforced with the mixture of silicon carbide and alumina. Specific wear rate shows an increasing trend after rise in the value of normal load. The rate of specific wear for Al-6061 alloy goes on increasing as compared to other composites reinforced with $SiC/Al_2O_3/CeO_2$ as per wear rate equation(5.2) given below :

$$S = K\frac{PL}{3H} \quad \text{Eq. (5.2)}$$

S= Specific wear rate, H=Hardness (HV), P=Normal load (N), L=Sliding distance (m) and K= Dimensionless quantity depend upon wear constant. As it is already stated that the composites with REOs have greater microhardness as compared to the composites without REOs. The composites with greater microhardness have a tendency to worn out less rapidly as compared to lesser microhardness counterparts. Hence the composites with REOs shows better wear resistance characteristics as indicated from figures 5.23(a-c). The maximum value of wear rate is found to be at high value of normal load and decreases with diminishing in normal load.

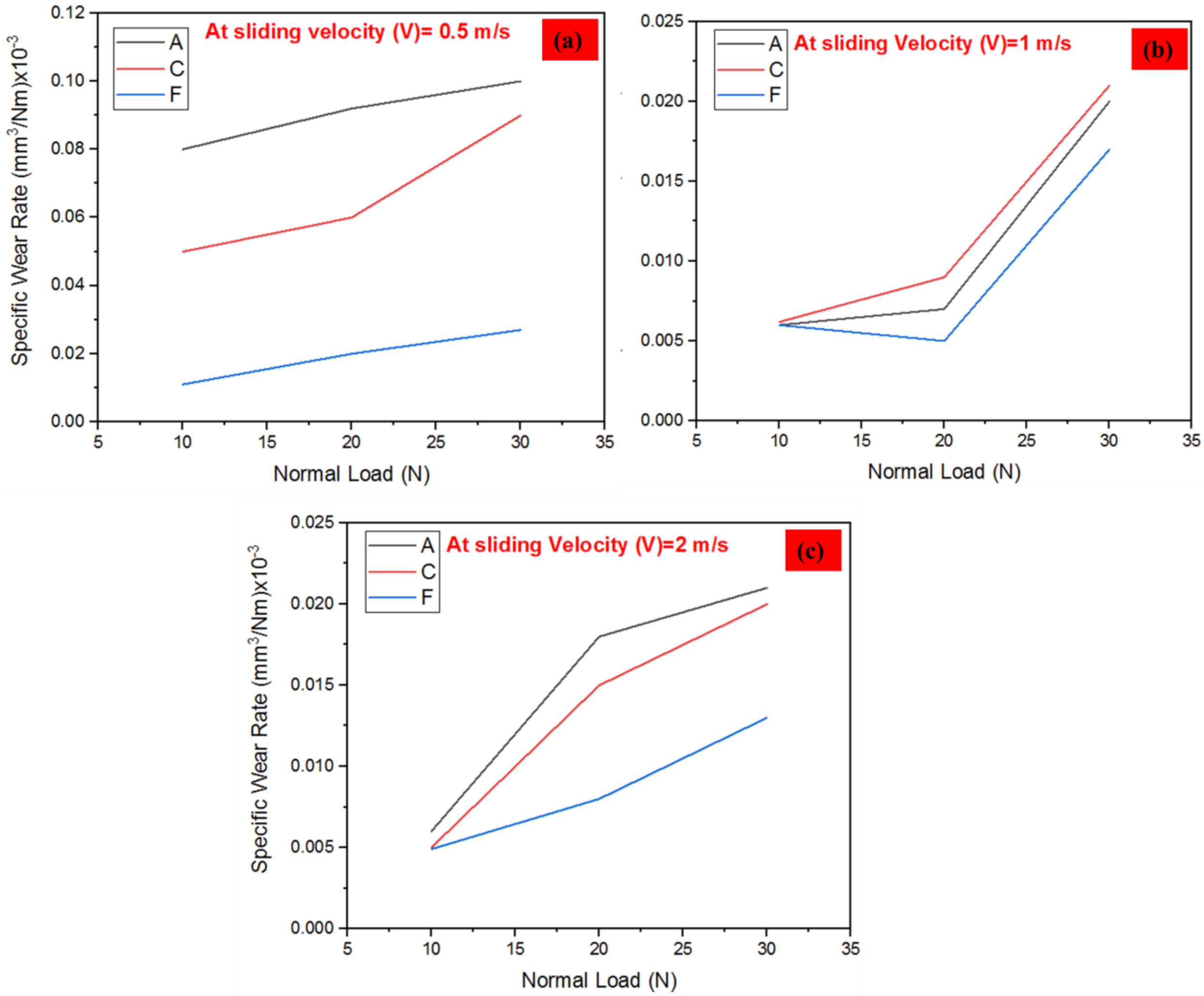

Figure 5.23 Graphical Representation of Cumulative Weight Loss at (a) 0.5 m/sec (b) 1 m/sec (c) 2 m/sec Sliding Velocities

5.6 EVALUATION OF WETTABILITY

Figures 5.24 (a-a1) shows the sessile drop image on the surface of Al-6061 matrix hybrid aluminum composites having only 2.5 wt% (Al_2O_3 + SiC). The average values of contact angle on the hybrid composite using water is found to be 87.94^0 with standard deviation of 1.58. The figure 5.25(a) depicts the various values of contact angles during 20 repetitive tests using sessile drop experiment. The value of contact angle of 87.94^0 suggests that the surface of the hybrid composite behave like a hydrophilic after incorporation of 2.5 wt% (Al_2O_3+ SiC). It has been observed that in some ceramics like aluminium oxide, the scarcity of a shielding effect permits the metal atom to bond with hydrogen with interfacial water molecules [Giovambattista et al., 2007; Granick and Bae, 2008]. In current situation, water molecules are able to keep their hydrogen-bonding network on alumina, resulting in hydrophilicity. After addition of 5 wt% (Al_2O_3+ SiC) in aluminium alloy as indicated in figures 5.24 (b-b1), the average contact angle rises up to 96.72^0 resulted in hydrophobic nature of the composite. The standard deviation is found to be 0.50. The figure 5.25(b) depicts the various values of contact angles during 20 repetitive tests using sessile drop experiment. After incorporation of 5 wt% (SiC+ Al_2O_3) contact angle improved significantly due to surface energy. Similar kinds of results were observed when SiC particles alone were mixed in molten aluminium alloy [Hashim et al., 2001]. The results obtained in present investigation are in line with the published research findings. It is observed from figures 5.24(c-c1) that on addition of 7.5 wt% (SiC+Al_2O_3), the contact angle increases up to 98.52^0 with standard deviation of 0.70. It means that the composite surface shows better wetting properties on addition of more amounts of silicon carbide and alumina. The figure 5.25(c) depicts the values of contact angles during 20 repetitive tests using sessile drop experiment and the surface of hybrid composites shows hydrophobicity.

Figures 5.26 (a-a1) shows the sessile drop image on Al-6061 matrix hybrid aluminum composites with 2.5 wt% (Al_2O_3+ SiC) and 0.5 wt% CeO_2. The average values of contact angle on the hybrid composite using water is increases significantly up to 99.07^0 as compared to composites with 2.5 wt% (Al_2O_3+SiC) as 87.94^0. Due to incorporation of rare earth oxide, the surface of composites moves toward hydrophobic nature with standard deviation of 2.20 respectively. The unfilled electron shells in the 4f orbitals in rare earth oxide materials are shielded by filled electrons in their outer shells, which are believed to result in a lower tendency to bond with nearby water molecules resulting in hydrophobicity [Azimi et al., 2013]. The figure 5.27(a) depicts the various values of contact angles during 20 repetitive tests using sessile drop experiment. After addition of 1.5 wt% of CeO_2 in 5 wt% (Al_2O_3+SiC) reinforced composites as seen in figures 5.26(b-b1), the average contact angle rises up to 99.39^0 resulted in hydrophobic nature of the composite. The standard deviation is found to be 1.14. The figure 5.27(b) depicts the various values of contact angles during 20 repetitive tests using sessile drop experiment. This is due to the fact that as the wt% of rare earth oxides increases the polarity of the surface material decreases which ultimately leads to decrease in surface energy and increased hydrophobicity [Hass et al., 1998; Cohen et al., 2019]. The exceptional electronic arrangement of atoms in REOs helps to diminish polar interactions, inhibit hydrogen bonding with contacting surface, and turn them into intrinsically hydrophobic. The better phenomenon of hydrophobicity was observed in composites with 2.5 wt% of CeO_2. After incorporation of CeO_2 with an amount of 2.5 wt% in composites reinforced 7.5 wt% (Al_2O_3+SiC) as indicated in figures 5.26(c-c1), the better results of increase in contact angle have been achieved. The contact angle rises up to 100.78^0 with standard deviation of 0.75 respectively improved. The figure 5.27(c) depicts the contact angle values after repetition of 20 tests. Similar kinds of results were found when lanthanum is mixed into aluminium along with the alumina [Shao et al., 2004]. Present results are in close agreement with these research findings.

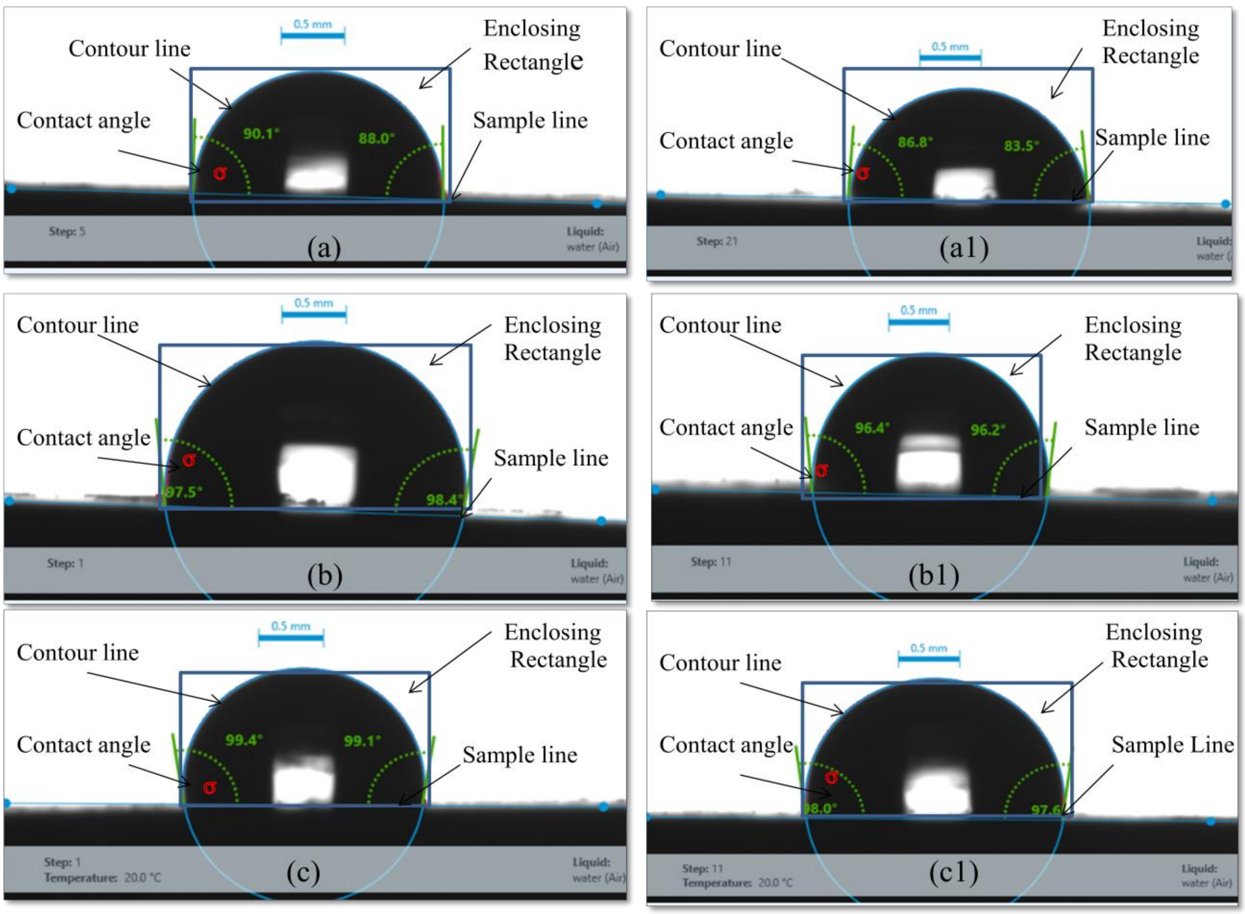

Figure 5.24 Presentation of Sessile Drop for the Hybrid Composites (a-a1) with 2.5wt% (Al_2O_3+SiC) (b-b1) with 5wt% (Al_2O_3+SiC) (c-c1) with 7.5wt% (Al_2O_3+SiC) at 20^0C

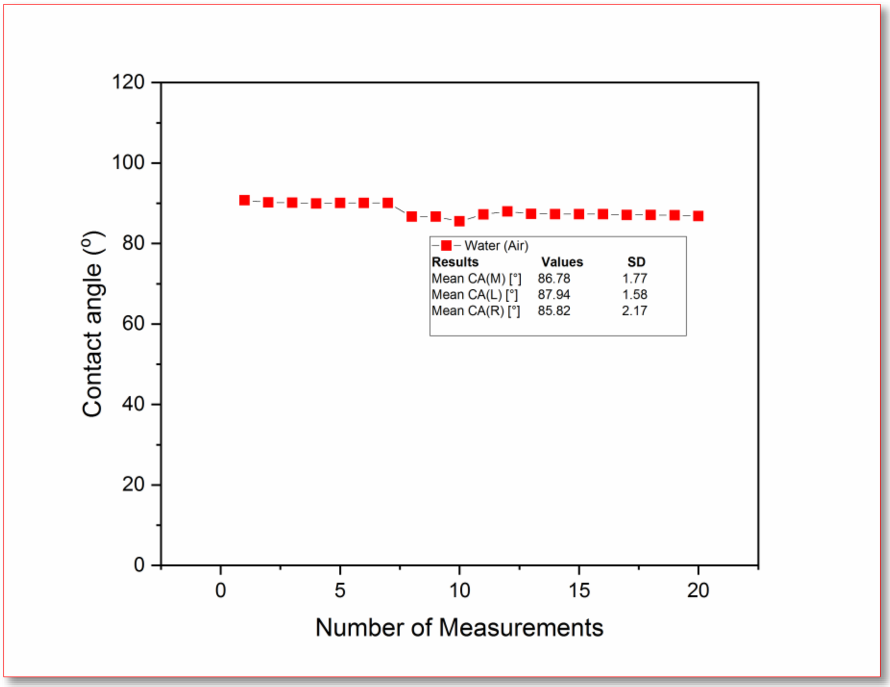
Contact angle (°)
Number of Measurements
Water (Air)
Results Values SD
Mean CA(M) [°] 86.78 1.77
Mean CA(L) [°] 87.94 1.58
Mean CA(R) [°] 85.82 2.17

(a)

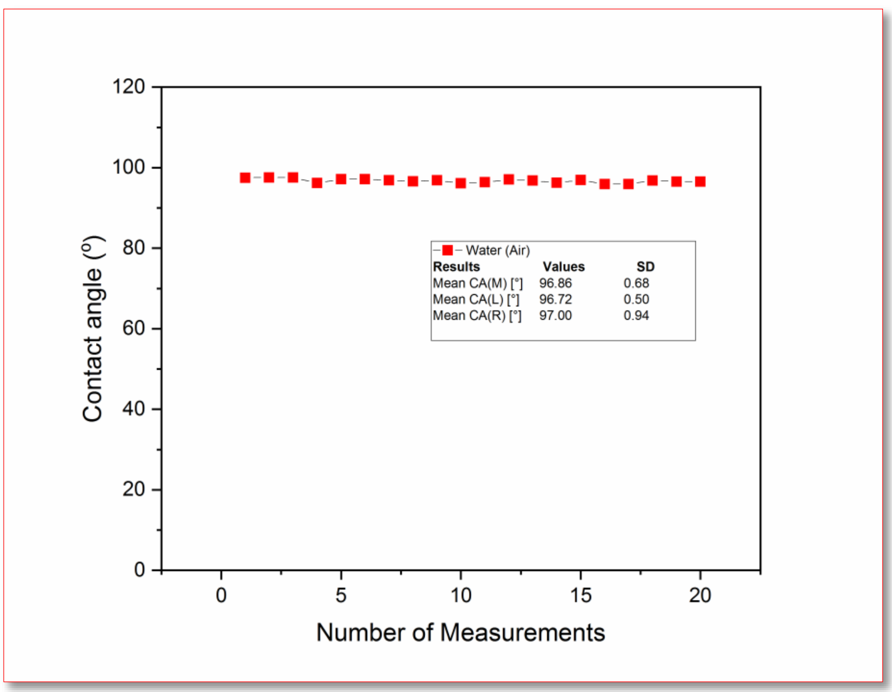
Contact angle (°)
Number of Measurements
Water (Air)
Results Values SD
Mean CA(M) [°] 96.86 0.68
Mean CA(L) [°] 96.72 0.50
Mean CA(R) [°] 97.00 0.94

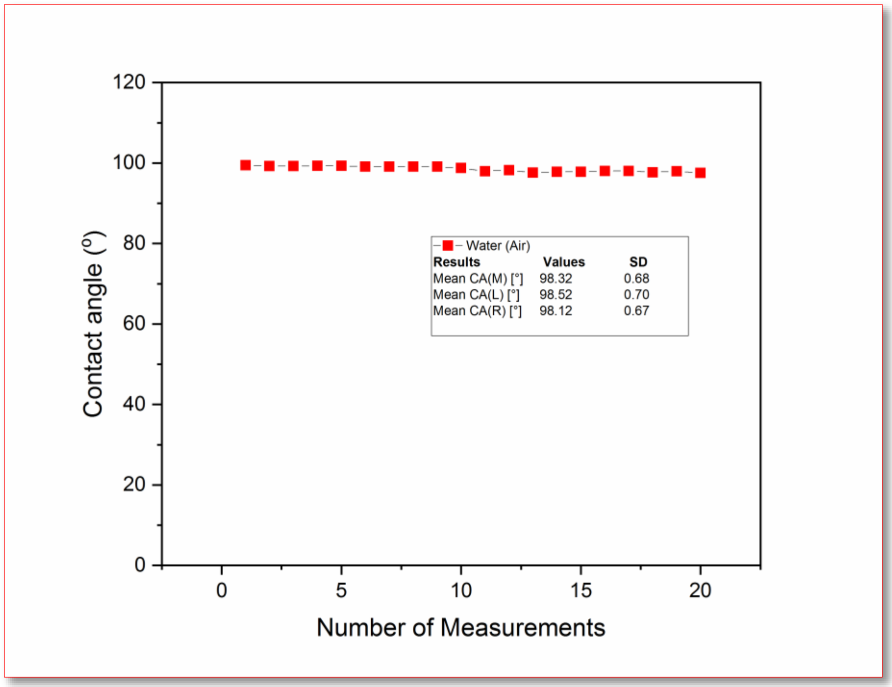

(c)

Figure 5.25 Contact Angle Measurements on Hybrid Composite Samples Using Sessile Drop Analyzer with (a) 2.5wt% (Al_2O_3+SiC) (b) 5wt% (Al_2O_3+SiC) (c) 7.5wt% (Al_2O_3+SiC)

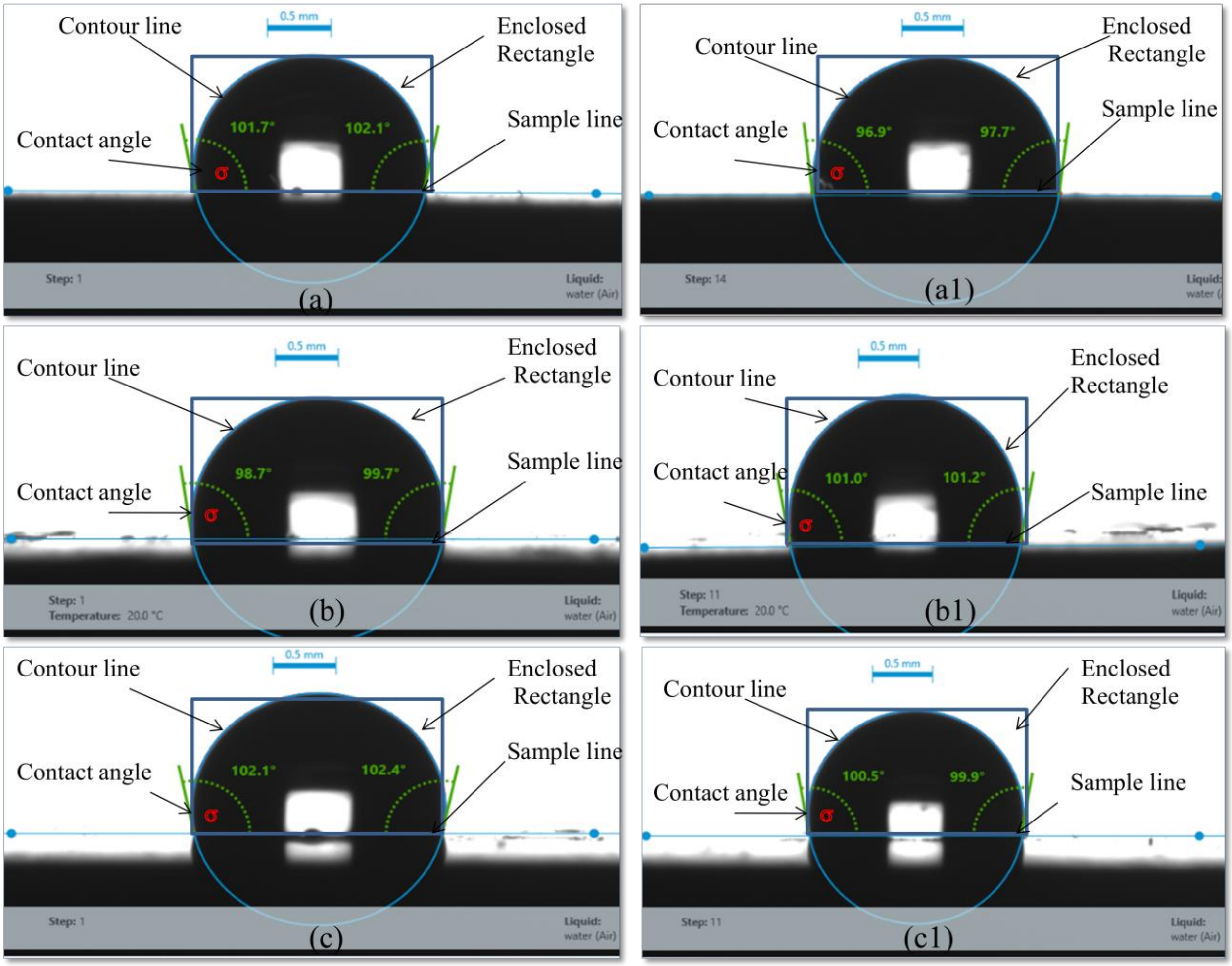

Figure 5.26 Presentation of Sessile Drop for the Hybrid Composites with Rare Earth Oxides, (a, a1) with 2.5wt% (Al_2O_3+SiC)+ 0.5wt% REO (b,b1) with 5wt% (Al_2O_3+SiC)+ 1.5wt% REO (c,c1) with 7.5wt%(Al_2O_3+SiC)+ 2.5wt% REO at 20^0C

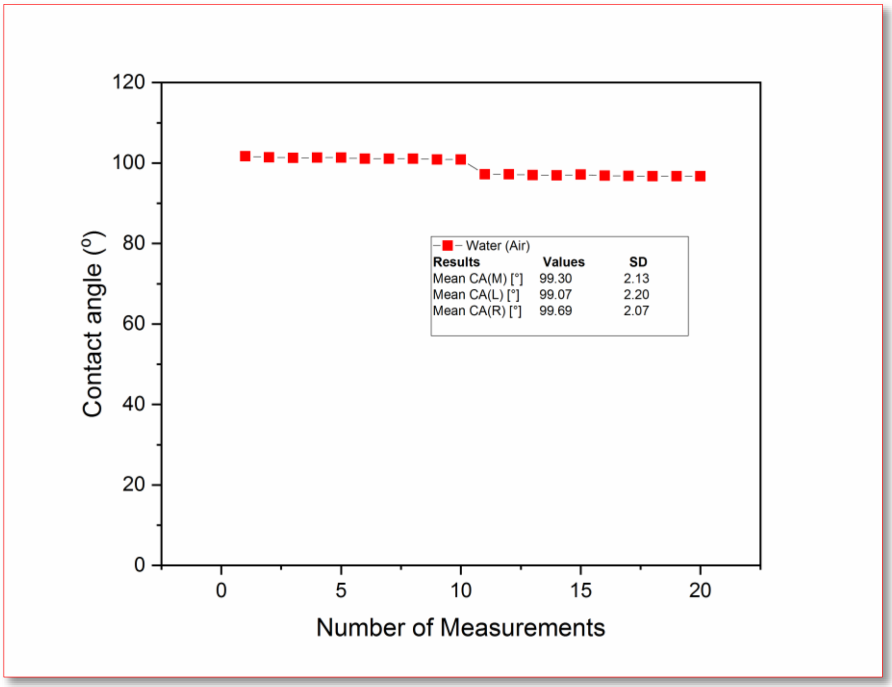
Contact angle (°)
120
100
80
60
40
20
0
0
5
10
15
20
Number of Measurements
Water (Air)
Results Values SD
Mean CA(M) [°] 99.30 2.13
Mean CA(L) [°] 99.07 2.20
Mean CA(R) [°] 99.69 2.07

(a)

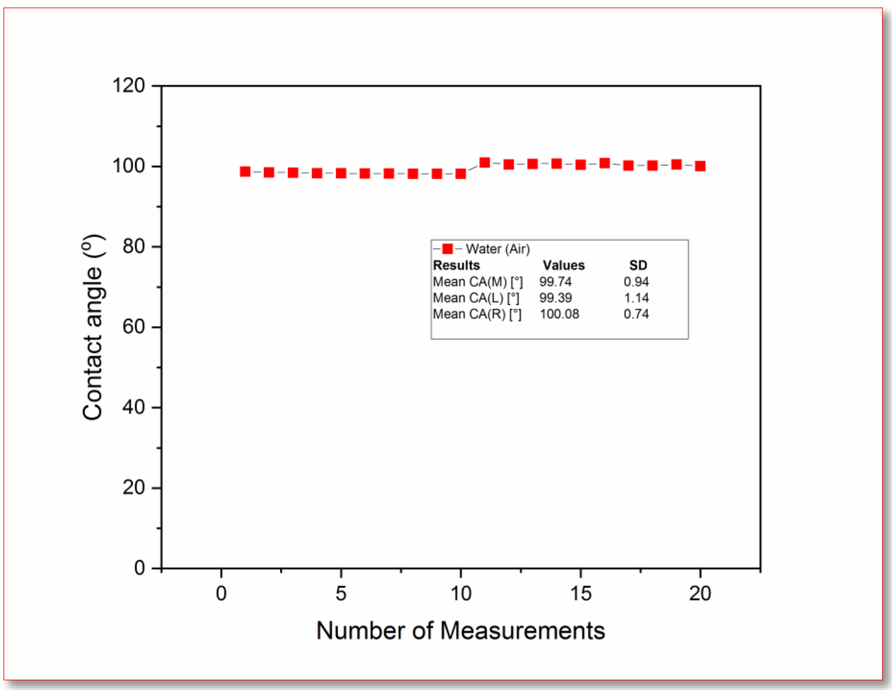
Contact angle (°)
120
100
80
60
40
20
0
0
5
10
15
20
Number of Measurements
Water (Air)
Results Values SD
Mean CA(M) [°] 99.74 0.94
Mean CA(L) [°] 99.39 1.14
Mean CA(R) [°] 100.08 0.74

(b)

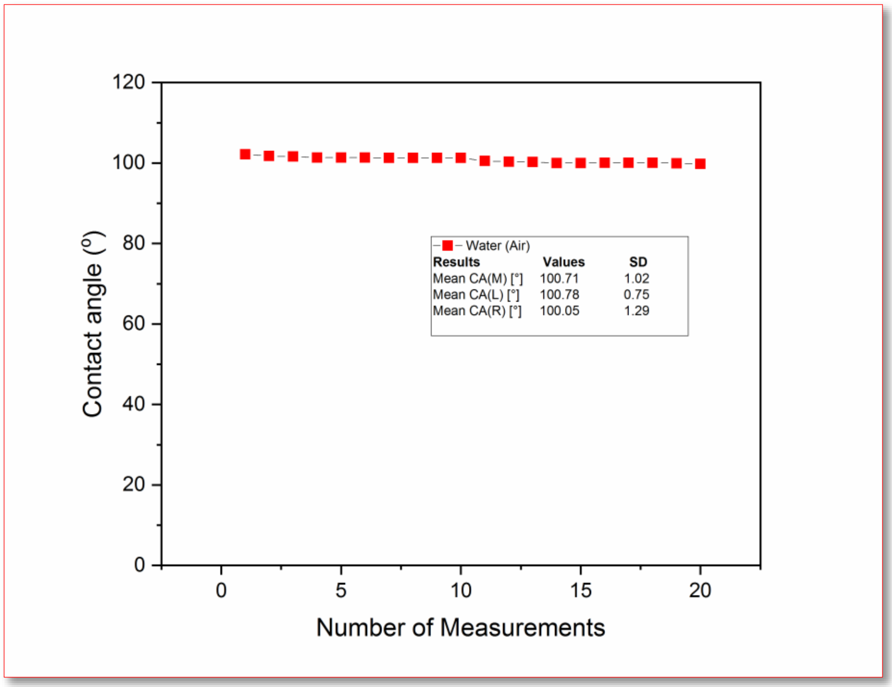

(c)

Figure 5.27 Contact Angle Measurements on Hybrid Composite Samples Using Sessile Drop Analyzer (a) with 2.5wt% (Al_2O_3+SiC)+ 0.5wt% REO (b) 5wt% (Al_2O_3+SiC)+1.5 wt% REO (c) 7.5wt%(Al_2O_3+SiC)+ 2.5 wt% REO

5.7 ASSESSMENT OF CORROSION RESISTANCE PERFORMANCE OF HYBRID COMPOSITES WITH REOs

The corrosion tests are performed on various samples of hybrid composites with different weight percent of REOs at the temperature of 35^{0}C in 3.5 weight percent of sodium chloride solution. Table 5.5 indicates the value of corrosion current density, various potential, and slopes achieved at cathodic and anodic reaction, and rate of corrosion achieved during the immersion test under NaCl solution. Under the test condition, initially the starting potential have a value of -1.5 V for all the hybrid composite samples and E_{corr} values were fixed in between - (0.920 to 1.0)V which is high as compared to base alloy. It is observed that as the weight percent of cerium oxide as REOs in the composite increases, the corrosion current density (I_{corr}) shows a trend of decreasing nature. Due to the addition of hard particles in the form of oxides in the matrix of base alloy Al-6061 helps in the improvement of corrosion resistance because of physical property and hydrophobocity nature of REOs. The exceptional electronic arrangement of atoms in REOs, nonexistence of polar interactions, and their hydrophobic characteristics, it is believed that REOs ceramic based composites can be efficacious for inhibiting electrochemical reactions and make them unique composites which will be used for inhibiting the fauling and corrosion related applications [Azimi et al., 2013]. It is also stated that uniform dispersion of the REOs into the matrix of Al-6061 alloy leads to improvement in the corrosion resistance property of hybrid composites as shown in figure 5.28. Corrosion resistance improves significantly of the hybrid composites after incorporation of REOs with increased weight percent. The similar trends of corrosion resistance behavior were found when Al-Mg matrix alloy reinforced with SiC [Candon, 2009]. [Shimizu et al., 1995] have observed that with the addition of SiC into the Al-7075 matrix alloy, the corrosion resistance improves significantly by resisting the stress that causes corrosion while immersing into the 3.5% NaCl solution.

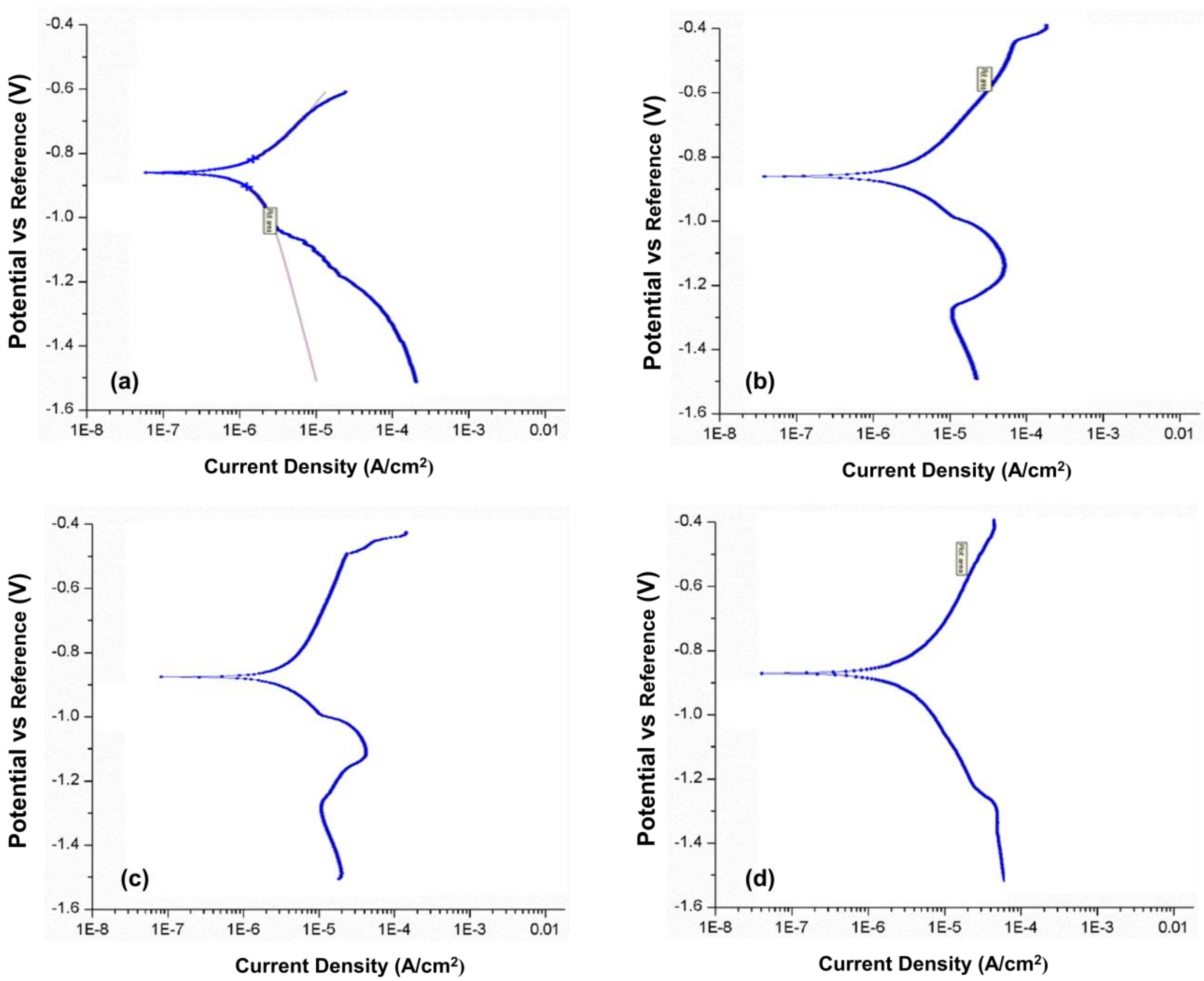

Figure 5.28 Potentiodynamic Polarization Curves of Hybrid Composites with (a) pure Al-6061 alloys, (b) 0.5 wt% of REOs (c) 1.5 wt% of REOs (d) 2.5 wt% of REOs

Table 5.5 Calculations of Corrosion Resistance for Al-6061 Composites with REOs at 3.5% NaCl Solution

S.No	Composition	Anodic Tafel Constant, β_A(mV/dec)	Cathodic Tafel Constant, β_C(mV/dec)	Corrosion Current Density, I_{corr} ($\mu A/cm^2$)	Corrosion Potential, E_{corr} (mV)	Corrosion Rate (mpy)
1.	Al-6061	134.5	545.6	9.490	-945.0	3.512
2.	Al-6061/2.5wt%($SiC+Al_2O_3$)/0.5wt%REO	38.20	577.5	4.980	-699.0	0.98
3.	Al-6061/5wt%($SiC+Al_2O_3$)/ 1.5wt%REO	48.10	482.8	2.510	-712.0	0.27
4.	Al-6061/7.5wt%($SiC+Al_2O_3$)/2.5wt%REO	82.50	274.5	0.799	-794.5	0.16

It was observed from the SEM as shown in figure 5.29 that the rate of corrosion in Al-6061 alloy composites decreases as the value of REOs varies from the 0.5 wt% to 2.5 wt% in corrosive medium of 3.5 wt% NaCl. It can be observed from the figures 5.29 (a-c) that the effect of corrosion is more at rough places as compared to smooth surfaces. The corrosion resistance of Al-6061 alloy improved with addition of REOs and this improvement could attribute to depression of the micro-galvanic couples. It can be observed from the results that uniform dispersion of REOs into the matrix of Al-6061 alloy may be another factor in improvement of corrosion resistance of hybrid composites as shown in figure 5.29. Corrosion resistance improved significantly of the hybrid composites after increased weight percent addition of REOs.

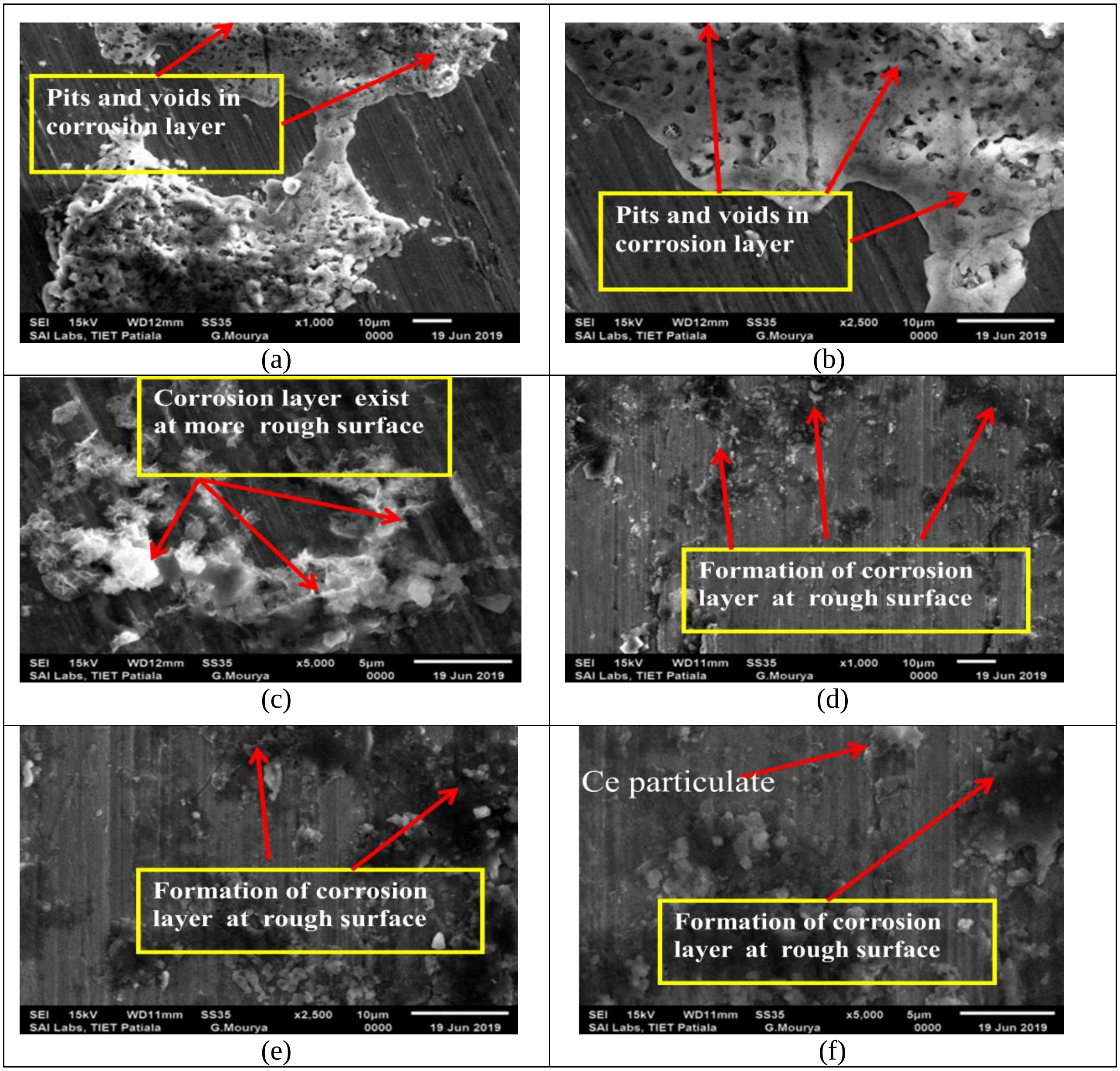

Figure 5.29 SEM Micrograph of Corroded Samples (a) 0.5wt% of REOs (b) 1.5wt% of REOs (c) 2.5wt% of REOs (d) 0.5wt% of REOs (e) 1.5wt% of REOs (f) 2.5wt% of REOs at 3.5% NaCl Solution

5.8 RESULTS OF MAFM PROCESS DURING INTERNAL FINISHING OF HYBRID COMPOSITES

The material and methods chapter focused on carrying out preliminary investigations on various process parameters that significantly affects output response. Pilot experiments were carried out to identify the range of various process parameters to achieve best surface finish. The results obtained from the pilot experiments were used in planning the main experimentation. Details of different experimental runs at different level of parameters and value of output responses are shown in table 4.6. This section also focuses on the results of main experimentation to see the effects of individual parameters and their interactions on output response (surface roughness). Design Expert 6.0.7® software has been used to check the adequacy of the fitted model using regression analysis. The percentage contribution of individual factor is determined using ANOVA. The desirability approach is used for response optimization. The validation of the model is assured by percentage error that represents percentage difference between experimental and predicted value. The predictions from this model were validated by conducting validation experiments. Figure 5.30 shows the flow chart of the various steps involved in the analysis of results and optimization. These steps are discussed in the following sections and sub sections.

5.8.1 Assessment of the Adequacy of Model Testing

Three dissimilar tests namely sequential model sum of squares, lack of fit and statistical summary of model have been performed to assess the adequacy of model for surface roughness during finishing of composites using MAFM process. Increase in the complexity of the model due to individual parameters is shown by sequential sum of squares test. This test selects the highest order polynomial. For model adequacy, a term with highest value of F and lower value of p is selected [Montgomery, 2002]. The lack of fit test is a measure of the failure of the model to represent data points in the experimental domain that are not included in the regression analysis. Finally, the variations are observed in the model that cannot be accounted by random error [Montgomery, 2002]. For the model to be fit, this test should indicate insignificant lack of fit. A p-value, greater than 0.05 nullifies the lack of fit of the model to the response data and the model can be utilized for prediction of response parameter at 95% of confidence level. Statistical summary of model describe the value of standard deviation, R^2, predicted R^2 and prediction error sum of squares (PRESS) of the model.

Generally, a model with lesser standard deviation, R^2 closer to 1 and smaller value of PRESS is selected [Montgomery, 2002]. Tables 5.6 shows the data related to sequential model sum of squares, lack of fit test and model summary statistics for surface roughness. Quadratic models are recommended for surface roughness by the Design Expert® software after performing above mentioned three tests.

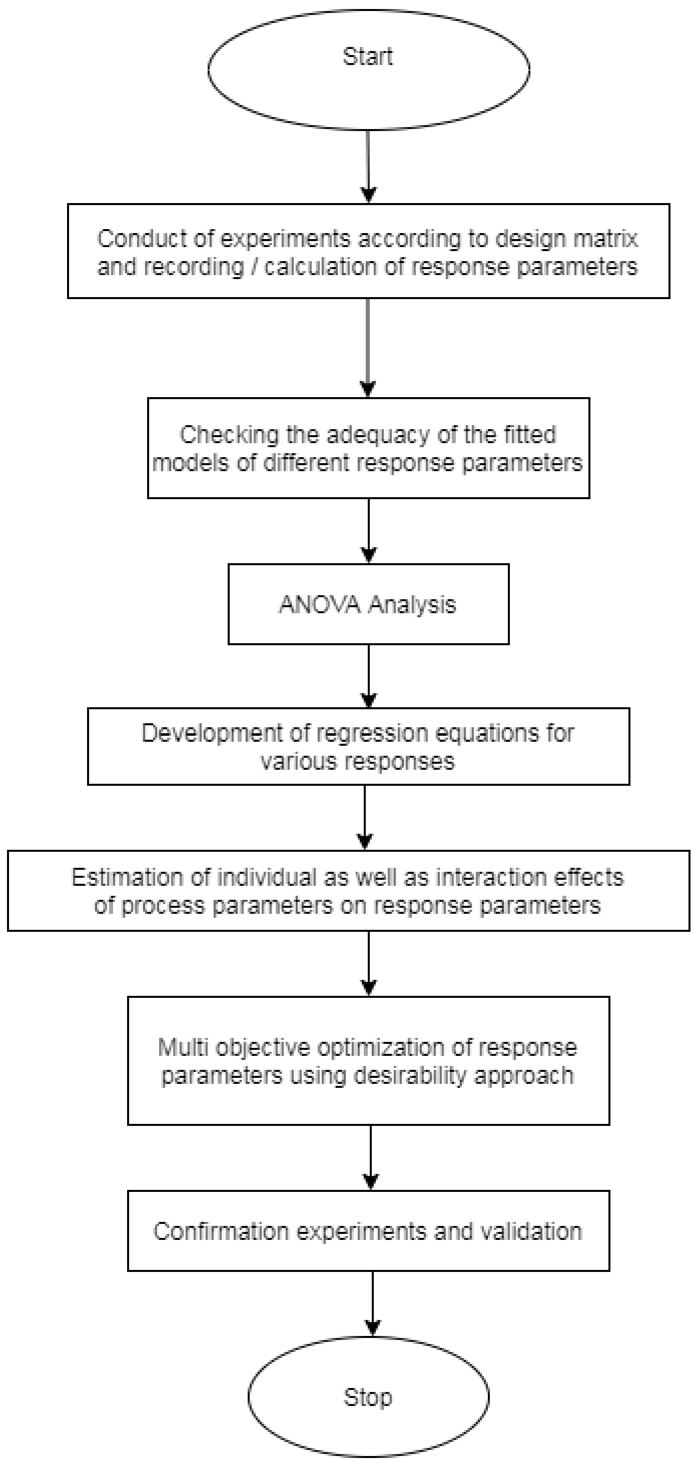

Figure 5.30 Steps Involved in Analysis of Results and Optimization of Responses

5.8.2 Analysis of Variance (ANOVA) and Mathematical Models of Response Characteristics

Analysis of variance is used to analyze the results statistically. ANOVA checks the value of R^2 as it explains the ratio of variability explained by the model to the total variability inherent in the observed data of experiments. It also shows adequate precision that measures signal to noise ratios. A ratio greater than 4 indicates the model to be fit. Process variables having p-value less than 0.05 are considered significant terms for the given response parameters. The backward elimination method eliminates the insignificant terms to adjust the fitted quadratic models. The hierarchy of different models is preserved to develop the mathematical models as it is observed that only hierarchical models are invariant under linear transformations [Piexto, 1987]. The results and analysis for output response i.e. surface roughness from ANOVA are discussed in following sections. The adequacy of the model for the output response (surface roughness) is depicted in table 5.6.

Table 5.6 Adequacy checking of model of surface roughness

Sequential Model Sum of Squares						
Source	**Sum of Squares**	**Degrees of Freedom**	**Mean Square**	**F-Value**	**Prob.> F (p-value)**	**Remarks**
Mean	12.20	1	12.20			
Linear	0.15	3	0.050	45.49	< 0.0001	
2FI	0.00485	3	0.00162	1.71	0.2286	
Quadratic	0.00852	3	0.00284	20.82	0.0007	Suggested
Cubic	0.000075	3	0.0000250	0.11	0.9476	
residual	0.000880	4	0.000220			
Total	12.36	17	0.73			
Lack of Fit Tests						
Source	**Sum of Squares**	**Degrees of Freedom**	**Mean Square**	**F-Value**	**Prob.> F (p-value)**	**Remarks**
Linear	0.013	9	0.00149	6.79	0.0404	
2FI	0.00859	6	0.00143	6.51	0.0455	
Quadratic	0.0000750	3	0.0000250	0.11	0.9476	Suggested
Cubic	0.000	0				
Pure error	0.000880	4	0.000220			
Model Summary Statistics						
Source	**Standard Deviation**	**R-Squared**	**Adjusted R-Squared**	**Predicted R-Squared**	**Press**	**Remarks**
Linear	0.033	0.9130	0.8930	0.8413	0.026	
2FI	0.031	0.9425	0.9080	0.8015	0.033	
Quadratic	0.012	0.9942	0.9868	0.9844	0.002575	Suggested
Cubic	0.015	0.9947	0.9786			

5.8.2.1 Analysis of Variance and Mathematical Model for Surface Roughness

As discussed in section 5.8, quadratic model using backward elimination approach for surface roughness is recommended by Design expert 6.0.7® software. The backward elimination method eliminates the insignificant terms to adjust the fitted quadratic models and in the present work backward elimination process is used to eliminate the insignificant terms. In addition to this normal plot of residuals and residual versus predicted plots has been shown in figures 5.31(a-b). The data of surface roughness is normally distributed. Most of residuals are falling on the straight line, implying that errors are normally distributed. The results of surface roughness measurement after ANOVA test for composite samples finished by MAFM process are discussed in following sections. Adequacy of the model is checked using ANOVA at 95 % confidence level as discussed in above section and presented in table 5.7. Table shows that F-value of the model is 210.69 and corresponding p-value is 0.0001. Thus, quadratic model is significant at 95% confidence level. The p-value of lack of fit is greater than 0.05. Thus, lack of fit is insignificant. Further, lack of fit value of 0.90 implies that it is not significant relative to pure error. Moreover, R^2 value is 0.98. This confirms that accuracy and general ability of polynomial model is good and it suggests that quadratic model can be used to navigate in the design space.

The regression equations for change in surface roughness in coded and actual form are shown as equations (5.3) and (5.4).

Final equation in terms of coded factors

$\Delta(R)_a$ = + 0.87+ 0.12 x A + 0.030 x B + 0.066 x C-0.044 x A^2 + 0.030 x A x C -0.018 x B x C ……………………………………………………………………………………**Eq.(5.3)**

Final equation in terms of actual factors

$\Delta(R)_a$ = + 0.31667 + 0.92944 x Magnetic Flux Density + 8.12500 x 10^{-4} x Number of cycles + 0.029464 x Extrusion Pressure - 0.70444 x Magnetic Flux Density^2 + 0.085714 x Magnetic Flux Density x Extrusion Pressure - 1.56250 x 10^{-4} x Number of cycles x Extrusion Pressure ……………………………………………………………………………………**Eq.(5.4)**

Table 5.7 Results of ANOVA for effect of parameters (main and interaction) on Surface Roughness

Source	Sum of Squares	DOF	Mean Square	F- Value	Prob> F	Remarks	Contribution (%)
Model	0.16	6	0.027	210.69	<0.0001	Significant	
A	0.11	1	0.11	836.10	<0.0001	Significant	68.75
B	0.00720	1	0.00720	55.68	<0.0001	Significant	4.5
C	0.035	1	0.035	271.55	<0.0001	Significant	21.87
A^2	0.008210	1	0.00821	63.49	<0.0001	Significant	5.13
AC	0.00360	1	0.00360	27.84	0.0004	Significant	2.25
BC	0.00123	1	0.00123	9.47	0.0117	Significant	0.769
Residual	0.00129	10	0.00129				
Lack of Fit	0.000413	6	0.0000688	0.31	0.9009	Not significant	
Cor Total	0.16	16					

Standard Deviation	0.011	R^2	0.9922
Mean	0.85	Adjusted R^2	0.9874
Coefficient of Variation	1.34	Predicted R^2	0.9821
PRESS	0.00296	Adequate Precision	50.022

Legend: A- Magnetic Flux Density, B- Number Of Cycles, C- Extrusion Pressure

Table 5.7 clearly shows the percentage contribution of process parameters on the percentage improvement in surface roughness (PISF) as observed from the ANOVA results. It is observed that the percent contribution of magnetic flux density with a value 68.75 % suggested to be the most influencing factors on PISF. After that the extrusion pressure with percent contribution of 21.87 % is second influencing parameters for PISF. Finally, the number of cycle is observed to be the least influencing parameters with percent contribution of 4.5 %.

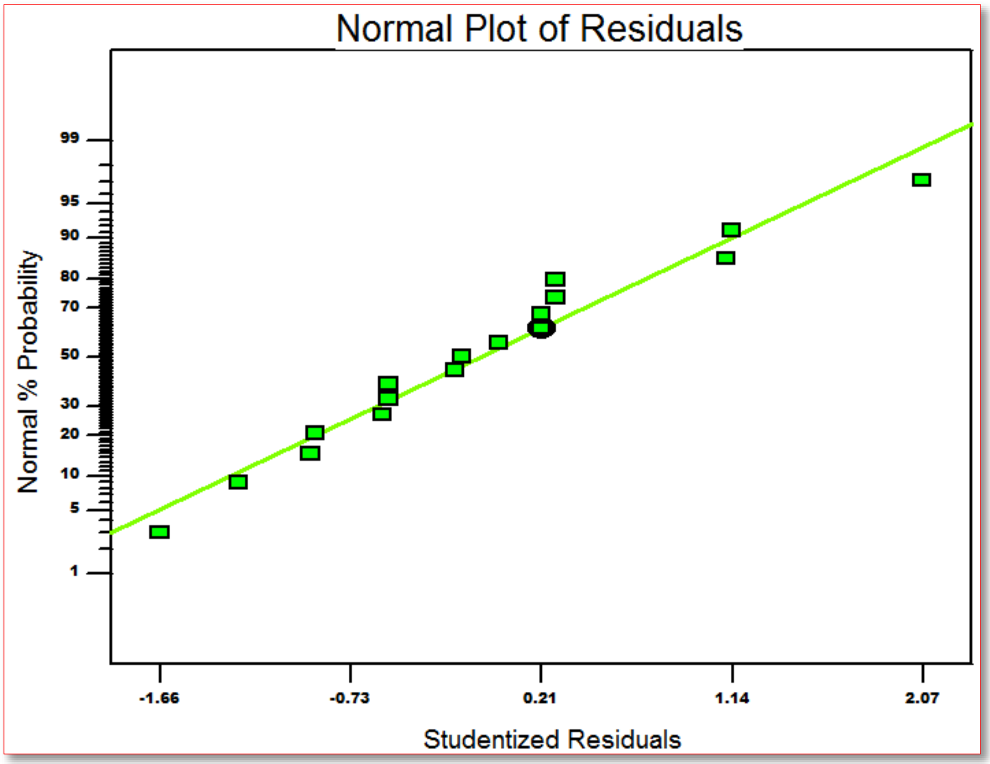

(a)

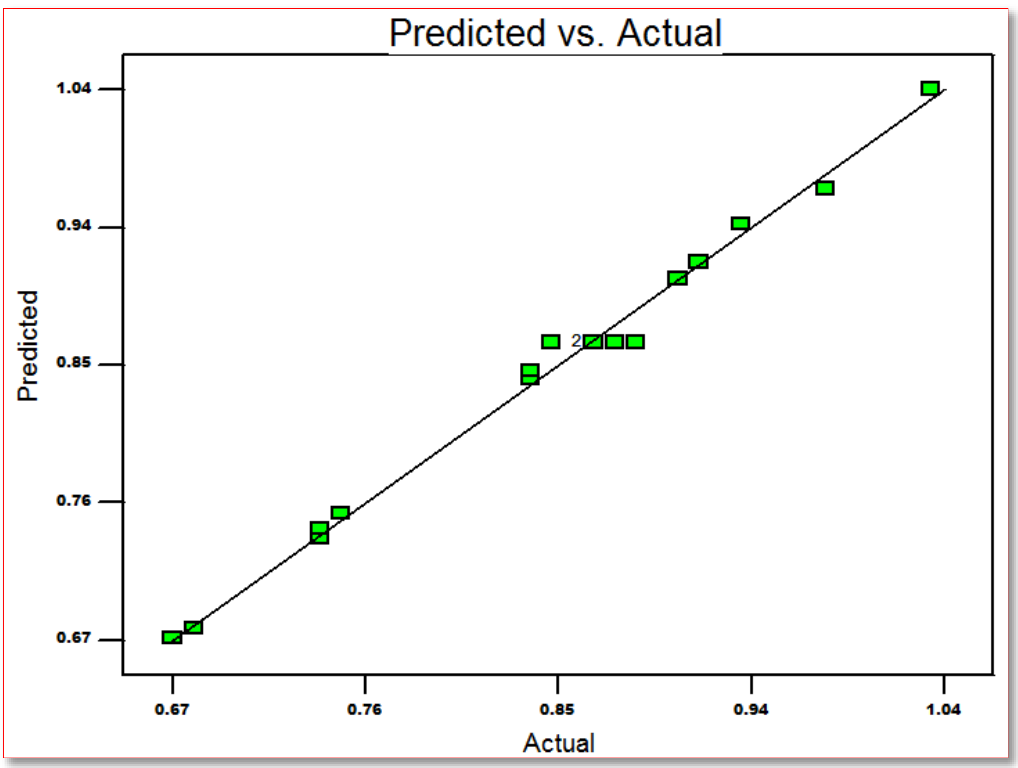

(b)

Figure 5.31 (a) Normal Probability Plots of Residuals for Surface Roughness (b) Plot of Actual Versus Predicted of Surface Roughness

5.8.2.2 Effect of Magnetic Flux Density (MFD), Number of Cycles and Extrusion Pressure on Change in Surface Roughness (ΔR_a)

The response (ΔR_a) has been calculated using the regression equation (5.1) in order to determine the effect of magnetic flux density (A), number of cycles (B) and extrusion pressure (C) on internal finishing of aluminium composites reinforced with SiC, Al_2O_3 and CeO_2. The initial surface roughness before MAFM process has been maintained within a small range. Although, if it varies over a wide range, then the change in surface roughness (ΔR_a) will also be different for a similar input process conditions. The high and low surface roughness value depends upon the amplitude of the peaks formed on the surface. High amplitude value of peaks on surface results in high surface roughness and low amplitude value of peaks on the surface results in low value of surface roughness. It has been reported by some researchers that the surface comprises of high amplitude peaks can be easily finished in comparison to low amplitude peaks results in higher value of (ΔR_a) [Sankar et al., 2009]. The higher rate of material removal as well as finishing occurs in the surface with high value of R_a. Therefore it is very essential to select the initial surface conditions before doing the MAFM process as it significantly affect the material removal rate and surface finish.

The change in surface roughness values (ΔR_a) w.r.t the magnetic flux density is depicted in figure 5.32(a). The magnetic flux density varied from 0.25 Tesla to 0.75 Tesla for finishing of internal cavities in composite samples. Initially the larger peaks are found in the composites and these peaks are lowered down after application of a magnetic flux density around the internal cavity of work piece. The change in surface roughness values (ΔR_a) increases non-linearly with the increase in magnetic flux density from 0.25 to 0.50 Tesla. The percentage rise in change in surface roughness value (ΔR_a) is found to be more in the region where MFD varies from 0.25 to 0.5 Tesla as compared to the region having intensity varies from 0.50 to 0.75 Tesla. This may be due to the fact that at low value of magnetic flux density, the surface finish is found to be good due to the less MRR from the composite surface. In addition, the magnetic force exerted by the magnets results in a normal force that acts on the internal surface of the aluminium composite. This normal force between the magnet and work component may have resulted in rise of material removal rate [Zhang et al., 2018]. [Yamaguchi and Shinmura, 2004] also suggested that at 0.37 Tesla, better surface characteristics of alumina ceramic components were achieved and our results are in good agreement with their results. The improvement in the surface roughness was also observed at low value of magnetic flux density (0.50 Tesla) during the finishing of aluminium by vibration assisted magnetic abrasive finishing process [Judal et al., 2013].

During the initial set of experimental condition, the numbers of cycles are varied as per the design of experiments from 80 to 240 while finishing of the internal surface of hybrid composites. Figure 5.32 (b) depicts the effect of number of cycles on (ΔR_a) during finishing of hybrid composites. It is observed that as the number of cycles increases from 80 to 240, the (ΔR_a) varies linearly as shown in figure 5.32(b). The possible reason of increase in the (ΔR_a) could be the increase in continuous interaction of abrasive particles with increase in number of cycle. The maximum value of change in surface roughness (ΔR_a) occurs at 240 cycles. With increase in the number of cycles, there is a slight decrease in change in surface roughness (ΔR_a). At higher value of cycles, the abrasive particles will try to create abrasion on the hybrid composite surface which creates some indented marks on the surface. As a result of indentation, the reinforcements SiC, Al_2O_3 and CeO_2 pullouts from the surface of aluminium hybrid composites. These results of change in surface roughness with number of cycles are in agreement with the results observed on the surface of STS 304 pipes during finishing by magnetic abrasive machining process [Yamaguchi and Shinmura, 2004]. During finishing of aluminium alloy using vibration assisted magnetic abrasive finishing process, it has been reported that the surface roughness results are of similar trend with the increase of processing time as the number of cycle increases [Judal et al., 2013].

The change in roughness value also shows an increasing trend with the change in value of extrusion pressure from 1.4 to 4.2 MPa as depicted by figure 5.32(c). It is observed that as the extrusion pressure increases from 1.4 to 4.2, the (ΔR_a) varies linearly. As the extrusion pressure increases, shear force helps in removing surface undulation or large peaks from the internal cavity of composite. On further increase in extrusion pressure beyond 2.8 MPa, the radial force increases on the abrasive grains which may further increases the projected area of penetration. Due to deep scratches and pullout of the reinforcements from the work surface may have resulted in decreased value of change in surface roughness [Sankar et al., 2009].

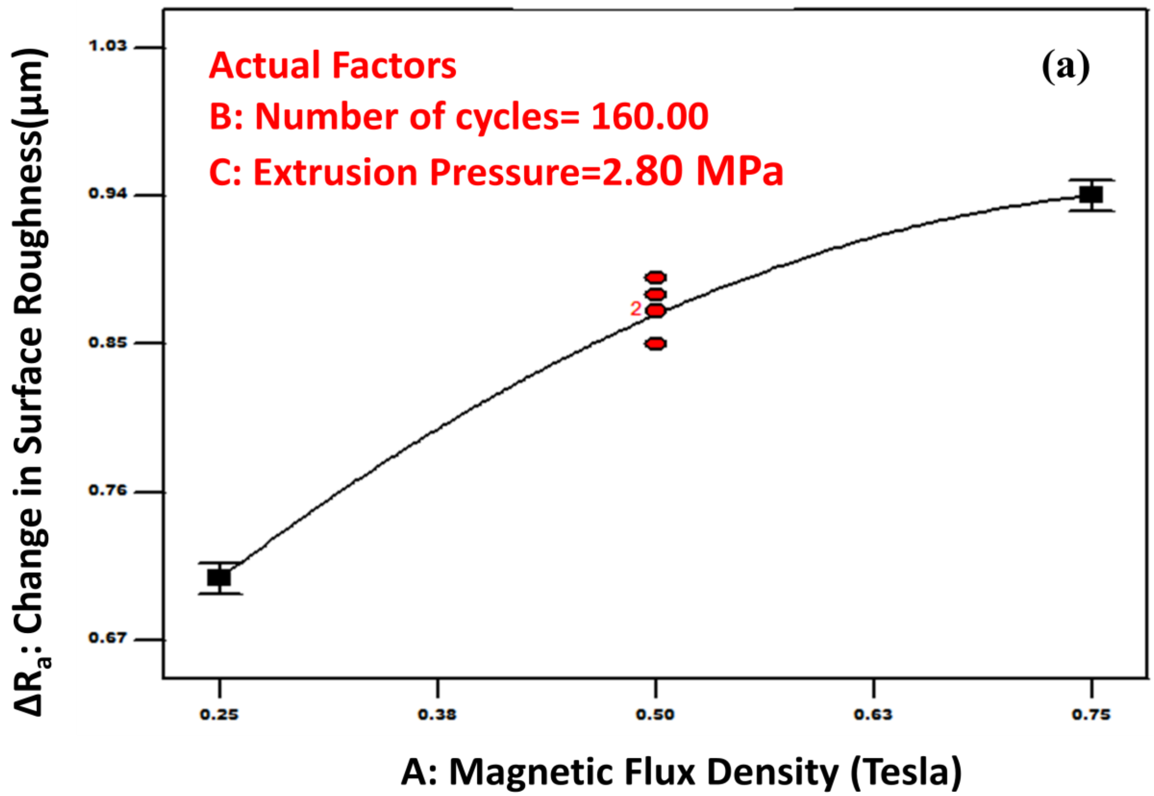

Actual Factors
B: Number of cycles= 160.00
C: Extrusion Pressure=2.80 MPa
(a)
ΔRa : Change in Surface Roughness(μm)
1.03
0.94
0.85
0.76
0.67
2
0.25
0.38
0.50
0.63
0.75
A: Magnetic Flux Density (Tesla)

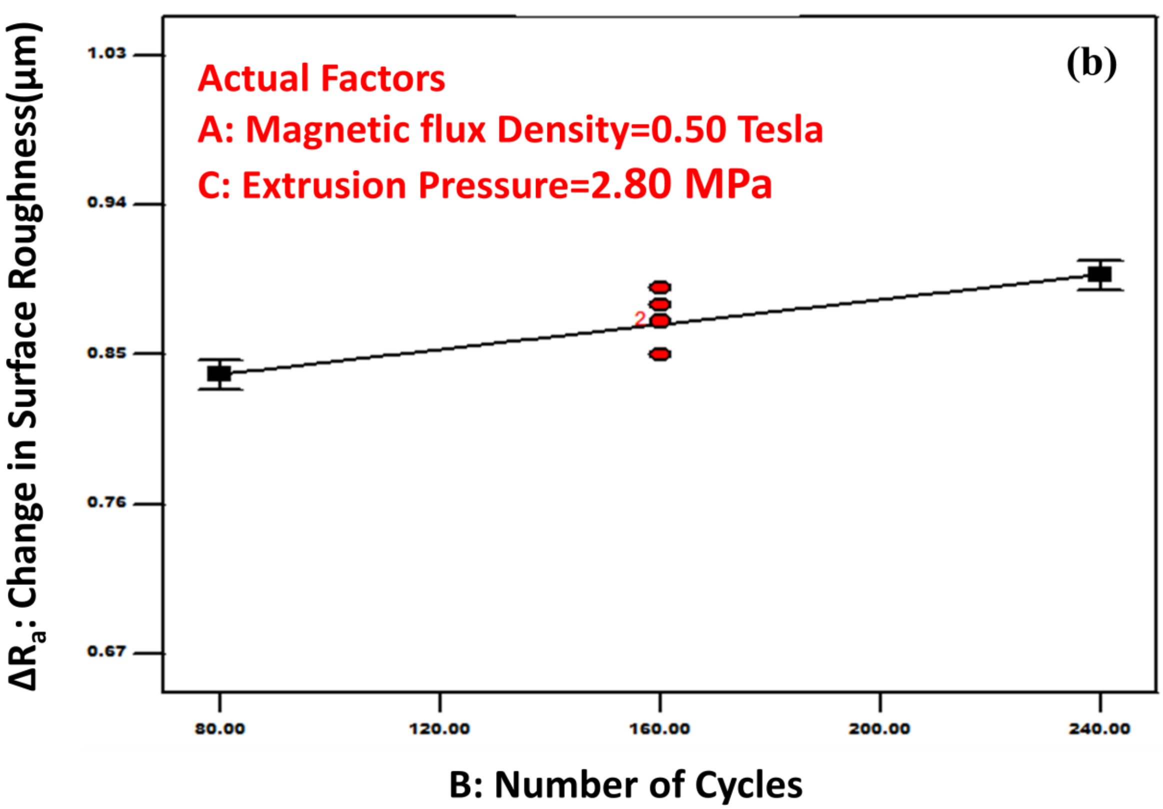

Actual Factors
A: Magnetic flux Density=0.50 Tesla
C: Extrusion Pressure=2.80 MPa
(b)
ΔRa : Change in Surface Roughness(μm)
1.03
0.94
0.85
0.76
0.67
2
80.00
120.00
160.00
200.00
240.00
B: Number of Cycles

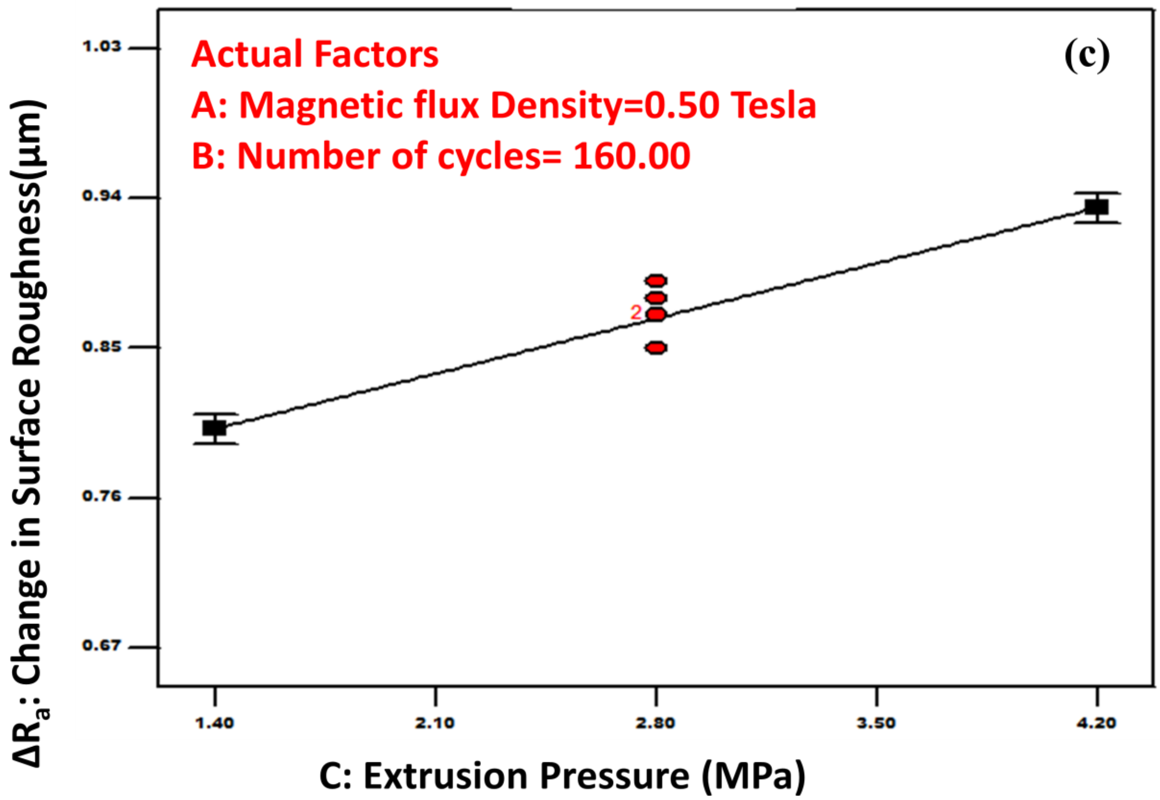

Figure 5.32 One Factor Plot to Analyze the Effect of Machining Parameters on the Change in Surface Roughness

5.8.2.3 Effect of Parameters Interactions on Change in Surface Roughness (ΔR_a)

The interaction effect generally occurs in a situation where more than one parameter involved with both the parameters affect the response in different way. For finishing of aluminium composites, the interaction effect between magnetic flux density and extrusion pressure is observed and depicted by figure 5.33 (a). From the figure it can be observed that at lower value of magnetic flux density of 0.25 Tesla corresponding to low value of extrusion pressure (1.4 MPa), the percentage change in surface roughness is low. While at moderately higher value of magnetic flux density (0.50 Tesla) and increased extrusion pressure to 2.8 MPa, the percentage change in surface roughness is significantly high. This is due to the fact that at moderate value of magnetic flux density, the carbonyl iron particles (CIPs) holds the abrasives particles more firmly. This results in the rise of cutting force on abrasive particles and thus creating more finishing action. Extrusion pressure with moderate value affects the final forces acting on the abrasive grains that causes abrasion resulted in reduction of peaks on the surface of composites.

In case of fast moving medium with high value of extrusion pressure and high value of magnetic field, the abrasive particles pass from the middle portion of the composites before able to strike the surface. This happens due to magnetic abrasive particles stick the walls near to the electromagnetic poles. At the center of the workpiece, it seems that abrasive medium passes through with no abrasion on the internal surface [Singh et al., 2020]. The abrasive medium does not show significant results of material removal at high value of extrusion pressure and magnetic flux density. This resulted in a less percentage improvement in change in roughness.

The other significant interaction effects shown in figure 5.33(b) are observed between number of cycles and extrusion pressure while finishing aluminium hybrid composite samples. From the figure 5.33 (b), it can be observed that at low value of number of cycles and extrusion pressure, the percentage change in surface roughness is found to below. Whereas with simultaneous increase in number of cycles and extrusion pressure, the resulted percentage change in surface roughness value is significant. The improvement in change in surface roughness could be due to the increase in time of contact of abrasive with the workpiece as the number of cycle increases. Further with the increase in extrusion pressure the shearing of peaks starts to increase and that may results in increase in (ΔR_a). With further rise in number of cycles with increase in extrusion pressure, the percentage improvement of change in surface roughness decreases. Due to further increase in number of cycles, the abrasive particle starts abrading the same surface again and again. This abrasion may results in fall of (ΔR_a). At high value of extrusion pressure, the surface of composites gets damaged due to increase in penetration and as a result of penetration the surface have full of deep scratches. The deep scratches cause the reinforcement to pull out from the composite surface and hence (ΔR_a) decreases. The surface plot as shown in figure 5.34 (a) depicts the change in surface roughness with the change of magnetic flux density and extrusion pressure simultaneously. The figure 5.34 (b) shows the variation in change in surface roughness with change in number of cycles and extrusion pressure.

The 3-D interaction plots shown in figure 5.35 (a) depicts the change in surface roughness due to change and magnetic flux density and extrusion pressure simultaneously. The figure 5.35 (b) shows the variation in change in surface roughness with interaction effect of both change in number of cycles and extrusion pressure. The roughness profile shown in figures 5.36(a)-(b) indicates the decrease in surface roughness from 1.51 μm to 0.48 μm with optimized parameters of 0.75 Tesla of magnetic flux density, 160 numbers of cycles and 4.2 MPa extrusion pressure. It is observed from the 3-D image as shown in figure 5.36(d) that in the composite samples with different weight percentage of REOs the surface roughness improved significantly as compared to figure 5.36(c). The more irregularities are seen on the composite before MAFM process due to large formation of peaks.

Figure 5.37 shows the topography of finished hybrid composites before MAFM process and after MAFM process. It can be seen from the two dimensional AFM image shown in figure 5.37(a) that the surface generated consists of deep scratches having grooves due to interaction of abrasive cutting points during surface grinding process.This may be due to grooves and scratches resulting in rough surface. The surface consists of very large amount of peaks and valleys and the (R_a) values as seen in the figure 5.37(c). After finishing with the MAFM process, the surface of the composites looks fine with small width and heights of peaks and valleys as shown in figure 5.37(b) and figure 5.37(d).

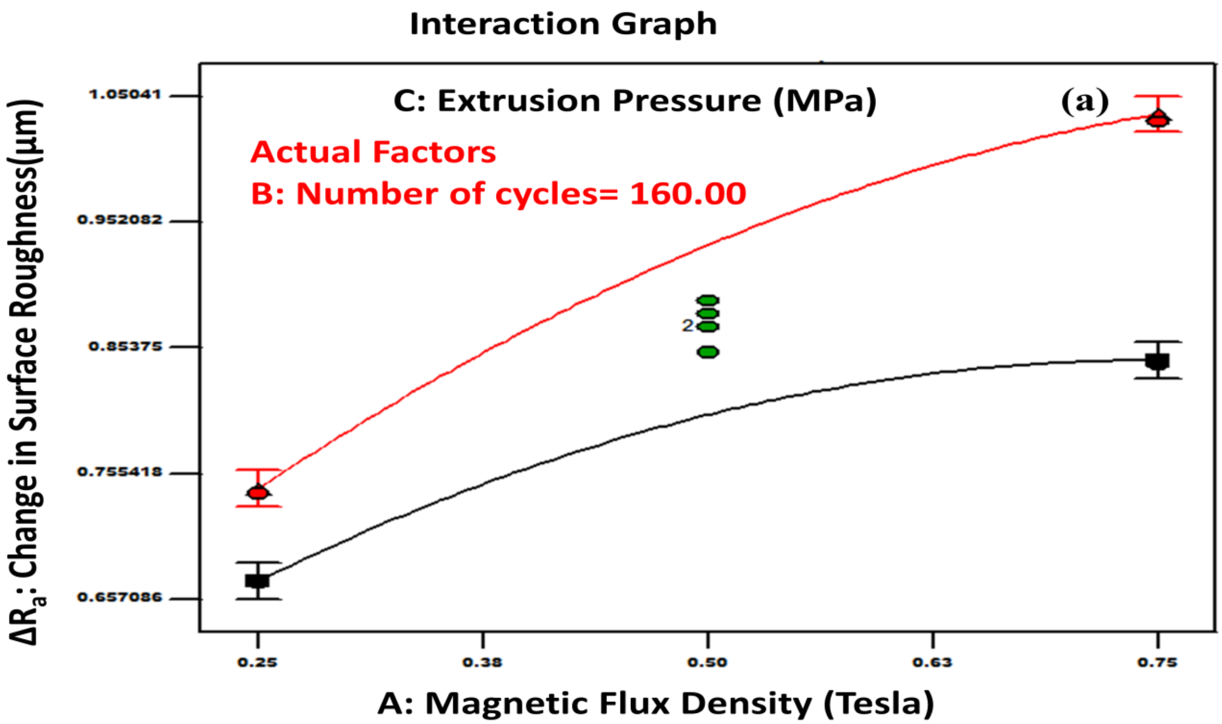

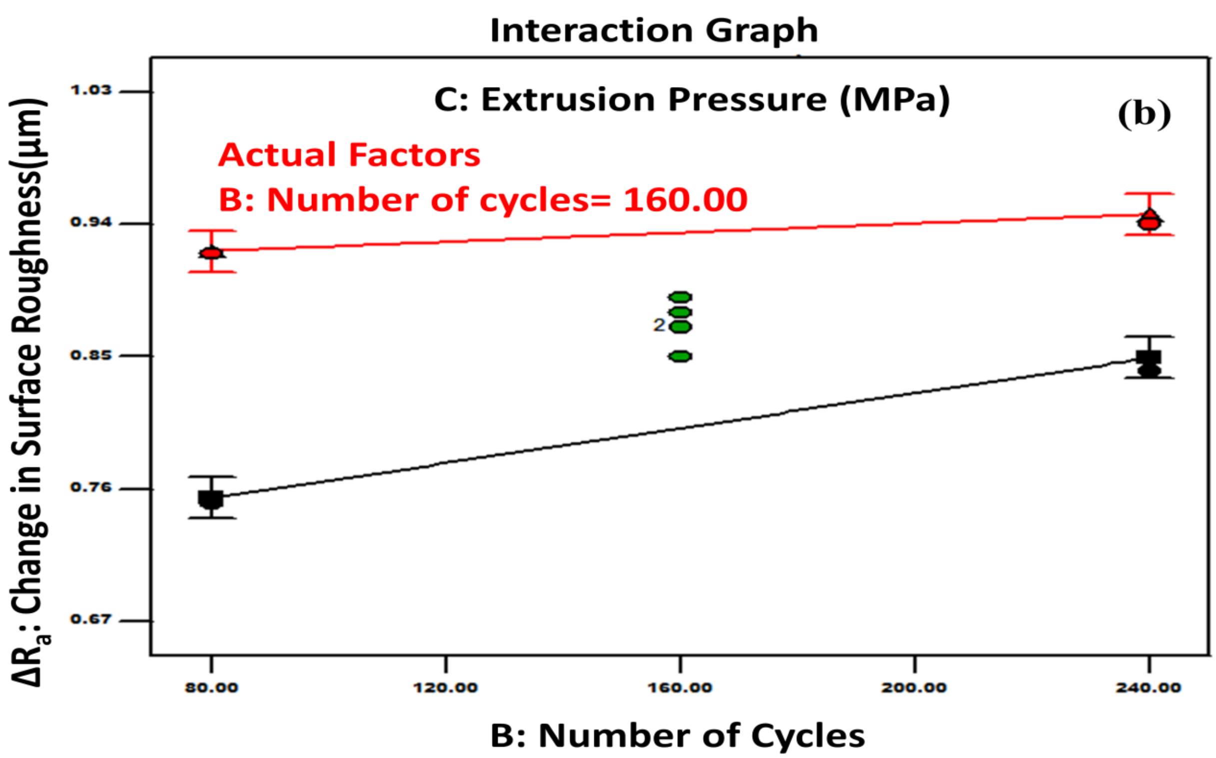

Figure 5.33 Interaction Plot to Analyze the Effect of Machining Parameters on the Change in Surface Roughness

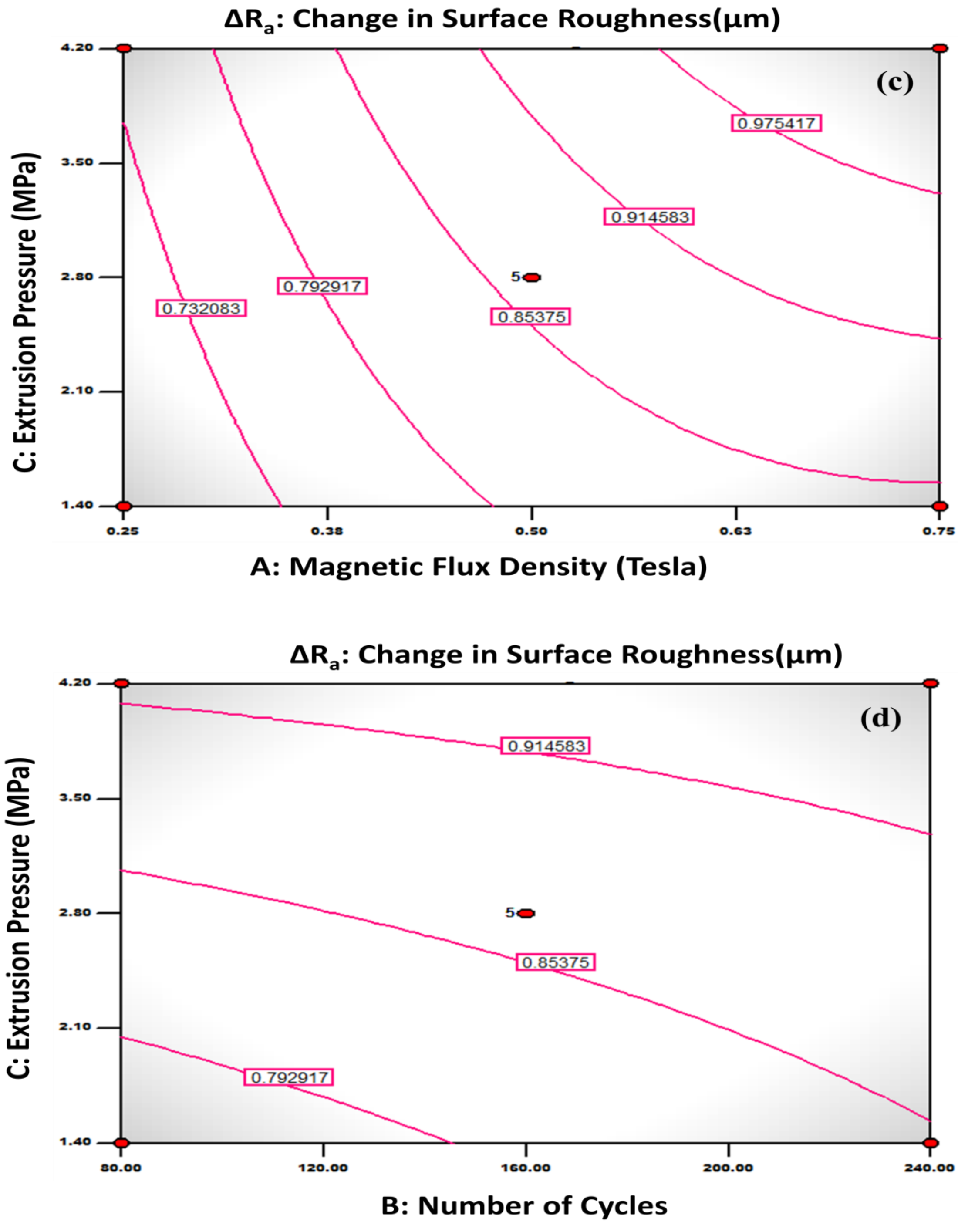

Figure 5.34 Contour Plots to Analyze the Effect of Machining Parameters on the Change in Surface Roughness

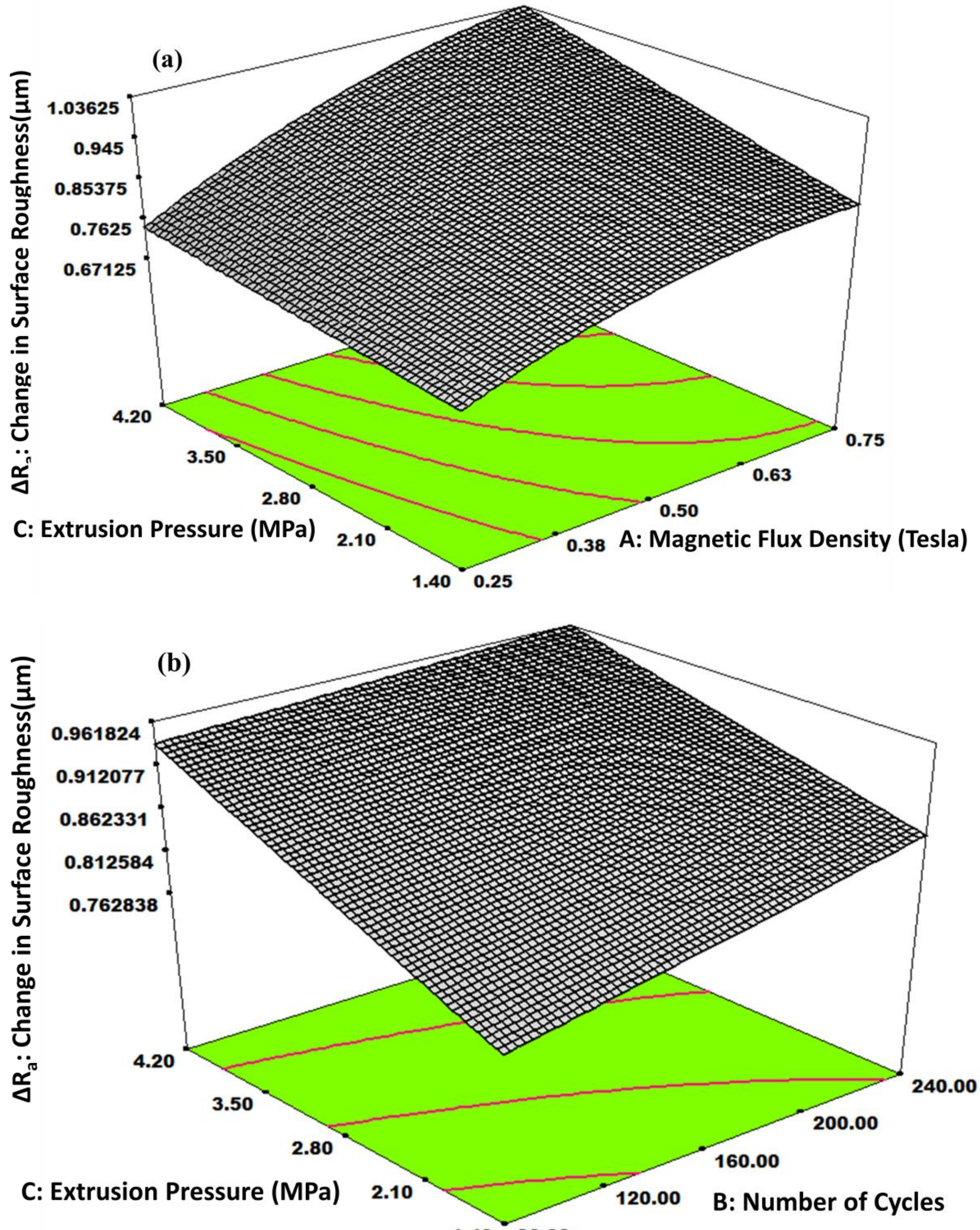

Figure 5.35 3-D Surface to Analyze the Effect of Machining Parameters on the Change in Surface Roughness

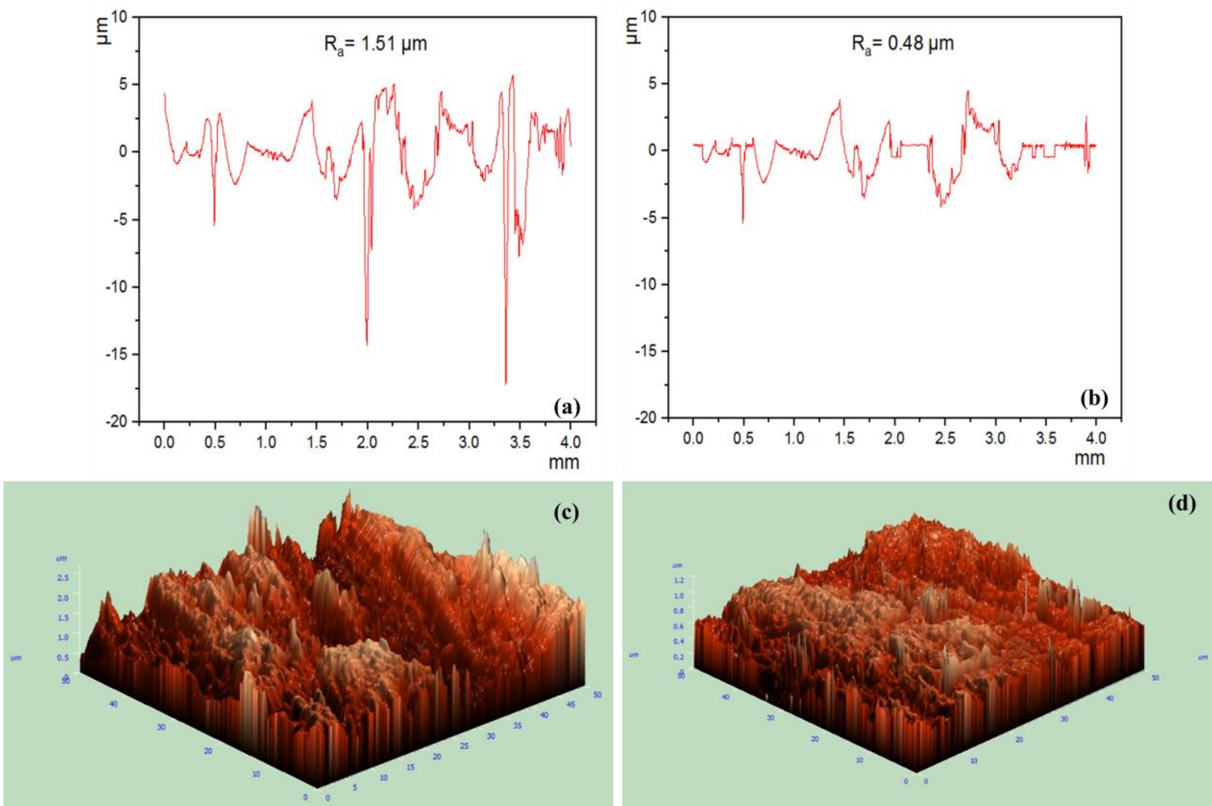

Figure 5.36 (a) Surface roughness profile before MAFM (b) Surface roughness profile after MAFM (c) AFM plot before MAFM (d) AFM plot after MAFM process at 0.75 Tesla, 160 number of cycles and 4.2 extrusion pressure during internal finishing of aluminium composite

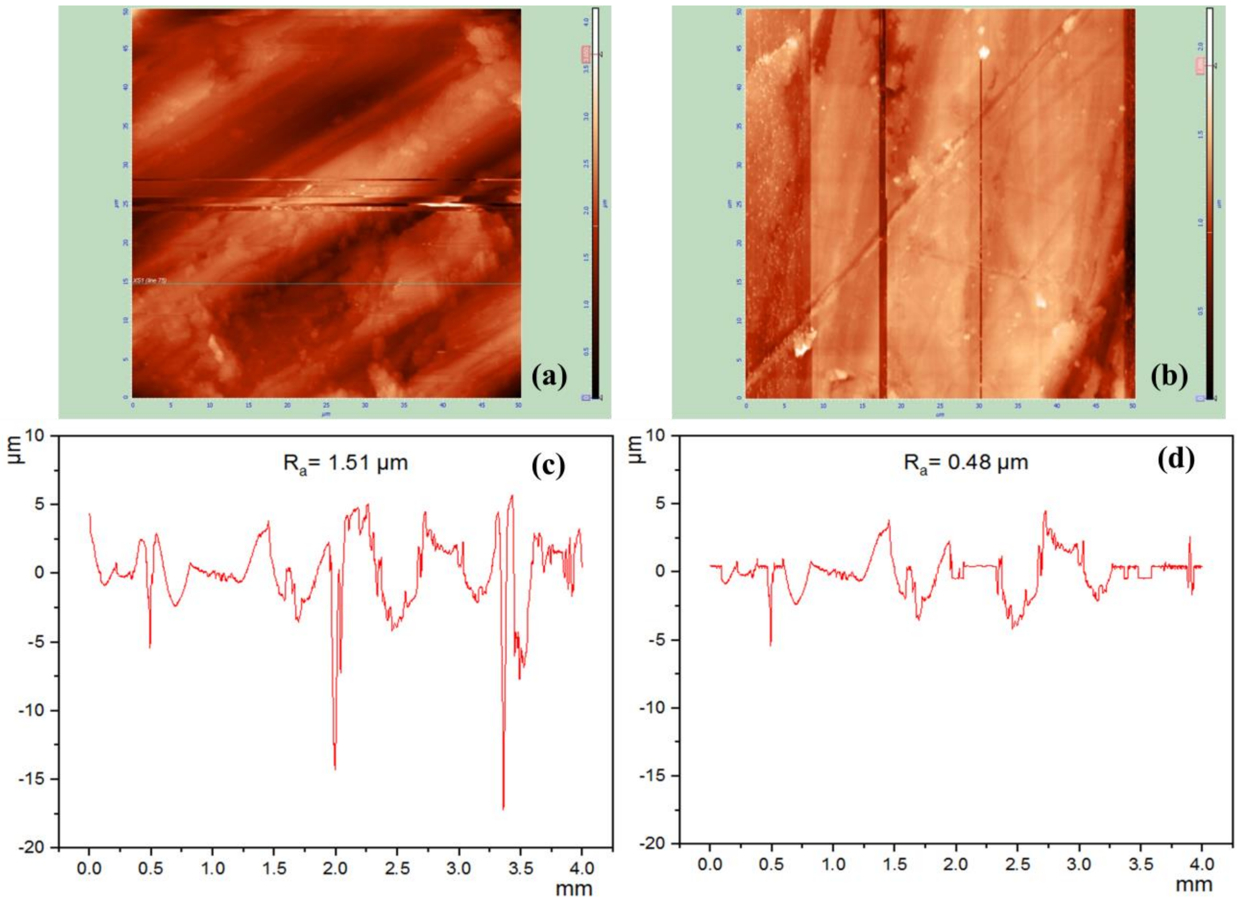

Figure 5.37 AFM image of the cross-section (a) Before MAFM (b) After MAFM (c) Surface Profile before MAFM (d) Surface profile after MAFM

5.8.2.4 Optimization of Surface Roughness using Desirability Approach

Now days, as competition increases single response optimization will not serve the purpose of industries because all responses have different nature and they contradict with each other [Rajesh et al., 2013; Karnik et al., 2008]. To overcome this problem, optimization techniques have emerged as one of the most successful tool which provides optimum result by optimization of responses using developed models. The desirability function approach has been used for multi-response optimization but sometimes it is also beneficial in single response. Multiple responses combined and converted into single response is called as desirability function (d_i). The value of desirability function (d_i) ranges from 0 to 1. A zero represents that the one or more responses fall outside their acceptance limit and one represents the ideal case [Pradhan, 2013; Azam et al., 2015]. As the value of d_i increases, a model becomes more desirable. Table 5.8 shows the upper and lower limit of input parameters and responses and also shows the goal, weights and importance assigned to each parameters. The desirability ramp plots and bar plots used to identify the optimized parameters is shown in figures 5.38 (a-c).

Figure 5.38(a) depicts that optimized values of magnetic flux density as 0.75 Tesla, number of cycles as 172 and extrusion pressure as 4.13 MPa for output response as surface roughness. Figure 5.38 (b) depicts the 3D surface plot of desirability which is formed by superimposing the contour plots of individual responses in which the bottom green portion shows the optimum region for the response surface roughness. It is evident from the desirability plot figure 5.38 (c) that desirability for input variables i.e. magnetic flux density, number of cycles and extrusion pressure is 1.00. The desirability of output response surface roughness is also 0.97.The combined desirability for both input and output parameters are 0.97.

Table 5.8 Maximal and minimal limits of input parameters and output response and its importance

Parameters	Goal	Lower Limit	Upper Limit	Lower Weight	Upper Weight	Importance
A: Magnetic Flux Density (Tesla	is in range	0.25	0.75	1	1	3
B: Number of cycles	is in range	80	240	1	1	3
C: Extrusion Pressure (MPa)	is in range	1.4	4.2	1	1	3
Change in Surface Roughness	maximize	0.67	1.03	1	1	3

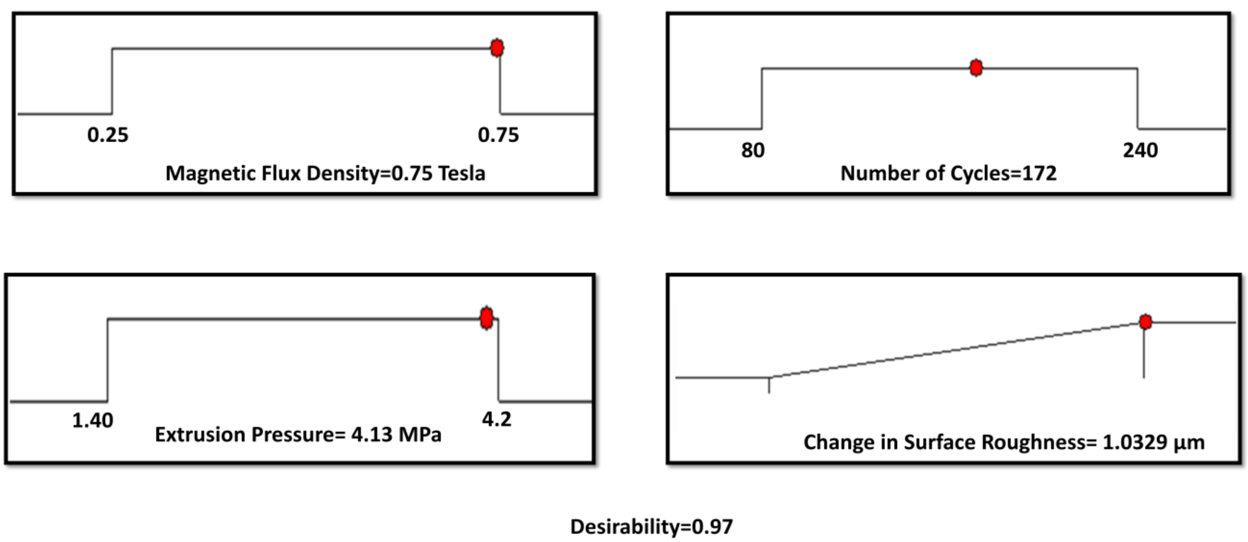

(a)

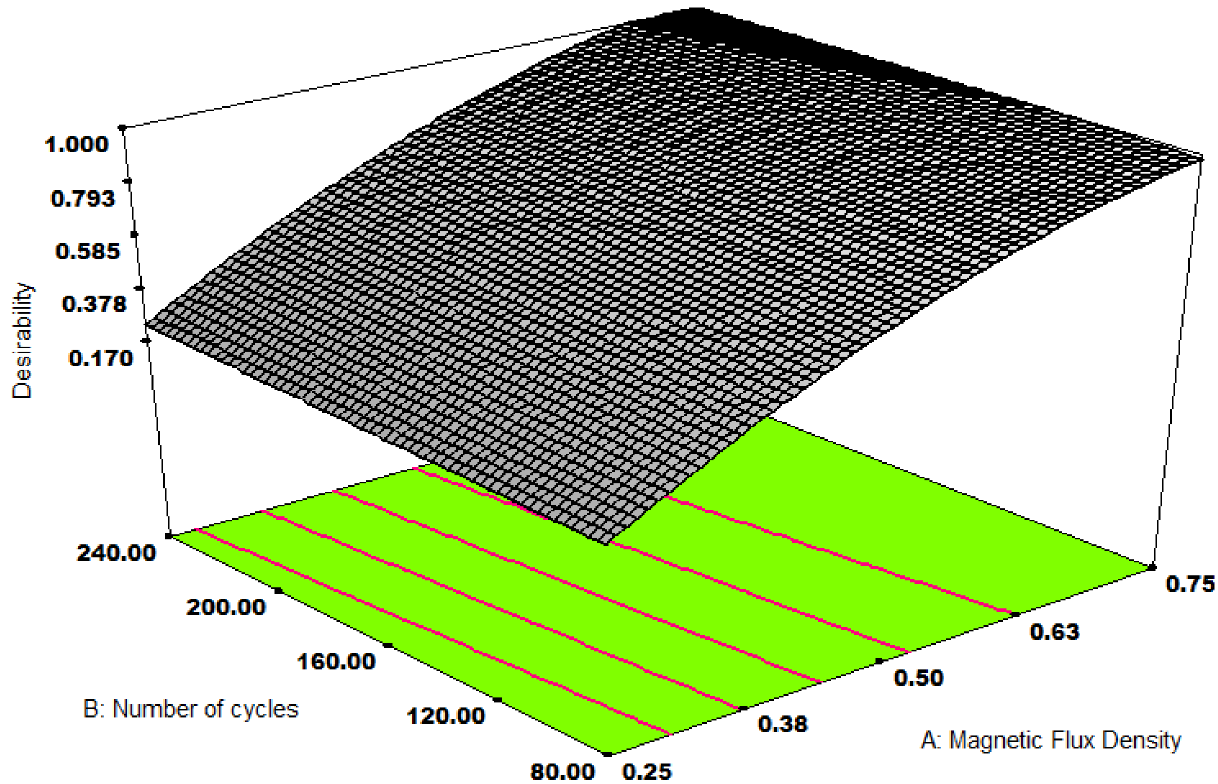

(b)

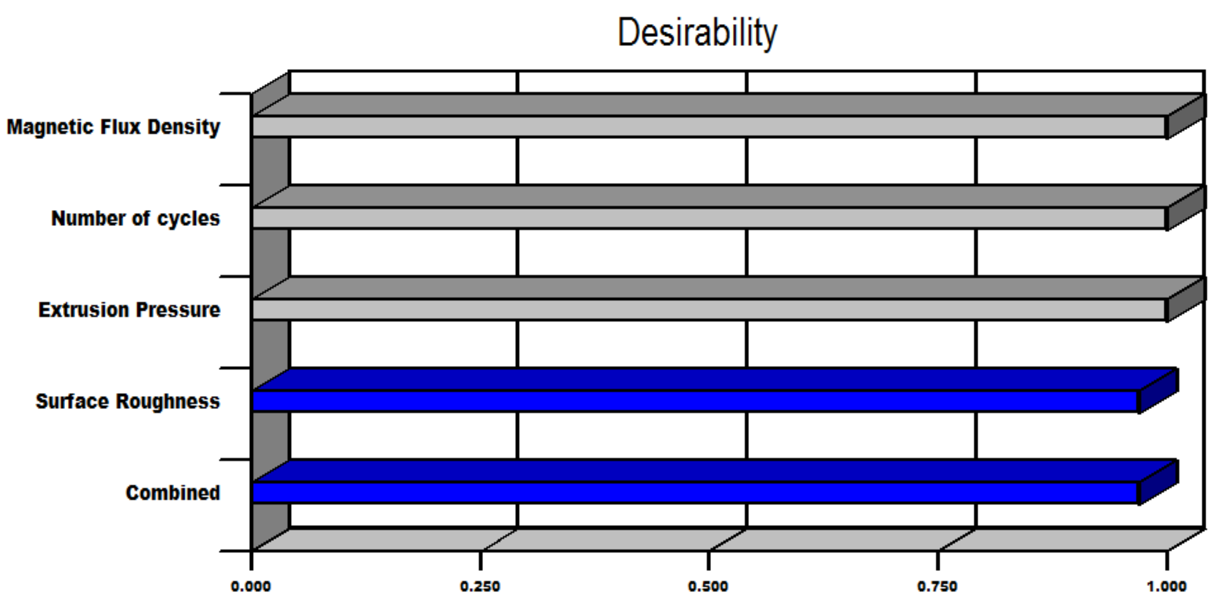

(c)

Figure 5.38 (a) Response Optimization using Desirability plot (b) 3-D Surface desirability plot (c) Desirability analysis for hybrid composites using Bar graph

5.8.2.5 Confirmatory Experiments

Confirmation experiment was conducted to verify the improvement in performance characteristics. The confirmatory experiment was conducted to check the percentage of model prediction error between experimental result and predicted result. The error is lies within ± 5% that confirms the excellent repeatability of the results. The error was calculated using the formula as shown in equation (5.5).

$$\% \,\mathbf{Prediction\ error} = \frac{Experimental\ result - Predicted\ result}{Experimental\ result} \times 100 \ldots\ldots\ldots\ldots\ldots\ldots\ldots\ldots \textbf{Eq. (5.5)}$$

Table 5.9 Comparison of Experimental Results with Predicted Results to Validate Model

Response	**Predicted (µm)**	**Experimental (µm)**	**Error (%)**	**Desirability**
Change in Surface Roughness (ΔR_a)	1.08	1.032	4.65	0.97

CHAPTER 6

CONCLUSIONS AND SCOPE FOR FUTURE WORK

6.1 CONCLUSIONS

In the previous chapters, fabrication of aluminium (Al-6061) based hybrid composites via stir casting using different reinforcements SiC, Al_2O_3 and CeO_2 has been explored. The mechanical, surface and metallographic characterization of the composites has been done. Afterwards, MAFM process parameters analysis and optimization for finishing of hybrid composites has been discussed. The major conclusion of the current research work along with the future scope is list down in this chapter.

6.1.1 Conclusions Drawn from Mechanical Characterization

1) Al-6061 hybrid composites mixed with (SiC+Al_2O_3) were successfully stir casted with addition of 0.5, 1.5 and 2.5 weight percent of cerium oxide.
2) Al-6061 hybrid composite mixed with (SiC+Al_2O_3) showed better mechanical properties with addition of cerium oxide. The tensile strength increased from 28 MPa to 123 MPa with addition of 2.5 weight percent of cerium oxide and 7.5 weight percent of each (SiC + Al_2O_3). Percentage elongation was increased from 2.0% to 11.5% with the increase in amount of CeO_2, SiC and Al_2O_3 reinforcement. This increase may be due to the formation of $Al_{11}RE_3$ particulates that reduced the quantity of eutectic β- particles in the matrix. Addition of RE mixture resulted in increasing the dispersion of reinforcement in the molten metal.
3) Micro-hardness of the Al-6061 hybrid composite was increased from 77 HV to 94 HV with addition of 2.5 weight percent of cerium oxide and 7.5 weight percent of each (SiC + Al_2O_3). Whereas it showed an increase from 77 HV to 88 HV with addition of 7.5 weight percent of each (SiC + Al_2O_3).
4) Rockwell hardness of the Al-6061 hybrid composite was increased from 61.73 HRB to 82.6 HRB with addition of 2.5 weight percent of cerium oxide and 7.5 weight percent of (SiC + Al_2O_3). Whereas it showed an increase from 61.73 HRB to 71.8 HRB with addition of 7.5 weight percent of each (SiC + Al_2O_3). This increase in hardness may be due to the strong and hard reinforcement particles that cause the strengthening of matrix by providing

hindrance to dislocation movement. It was further observed that fine grain size in composite samples with REOs may have improved their hardness according to the Hall- Petch effect.

5) The impact strength of Al-6061 hybrid composites was found to be increased from 18 J to 56 J after addition of cerium oxide up to 1.5 weight percent. But after further addition of 2.5 weight percent cerium oxide, decrease in the impact strength has been observed to 46 J. The decrease in value of impact strength may be due to change in ductile to brittle behaviour.

6) The flexural strength of the Al-6061 hybrid composites increased up to 615.6 MPa with addition of 2.5 weight percent of cerium oxide and 7.5 weight percent of (SiC + Al_2O_3). Whereas it showed an increase from 340 MPa to 450 MPa with addition of 7.5 weight percent of (SiC + Al_2O_3).

6.1.2 Conclusions Drawn from Wear Analysis

1. It was found that wear rate improved significantly by addition of 2.5 weight percent of CeO_2 in Al-6061 alloy reinforced with 7.5 weight percent of both SiC and Al_2O_3 as compared to base alloy tested at normal load of 10 N and sliding velocity 0.5 m/s. It was further observed that wear rate increased by 38 % with addition of 7.5 weight percent of both SiC and Al_2O_3.

2. At velocity of 0.5m/s and normal load of 20N, Al-6061 hybrid composites showed a 77.5% improvement in wear rate with addition of 2.5 weight percent of CeO_2 and 7.5 weight percent of SiC and Al_2O_3. Whereas it showed 32 % improvement in wear rate with addition of 7.5 weight percent of SiC and Al_2O_3.

3. At velocity of 0.5m/s and normal load of 30N, Al-6061 hybrid composites showed a 68.83% improvement in wear rate with addition 2.5 weight percent of CeO_2 and 7.5 weight percent of SiC and Al_2O_3.Whereas it showed 22 % improvement in wear rate with addition of 7.5 weight percent of SiC and Al_2O_3.

4. Gross plastic deformation, delamination and abrasion were observed to be most dominant wear causing mechanisms in Al-6061 hybrid composites. Abrasive wear activated mostly at the low value of sliding velocities and normal loads.

5. Al-6061 hybrid composites with cerium oxide showed better resistance to plastic deformation occurring at more severe operating conditions as due to presence of intermetallic phase $Al_{11}Ce_3$. This phase helps in acquiring excellent mechanical properties even at elevated temperatures.

6.1.3 Conclusions Drawn from Metallographic, Structural and Chemical Characterization

1. The microstructure of Al-6061 hybrid composites with ($SiC+Al_2O_3$) mixture showed the presence of silicon and alumina particulates in dendrite tree like structure after solidification of molten metal. It was also observed from SEM analysis that the degree of agglomeration reduced after addition of CeO_2 particles. This reduced agglomeration results in formation of smooth surface.

2. XRD analysis showed the presence of various phases like SiO_2,$Mg(CO_3)$ and $FeAl_2Si$ in hybrid composites reinforced with SiC and Al_2O_3. XRD study of Al-6061 hybrid composites showed the presence of α-Al ,SiO_2, Mg_5Si_6, MgO, Al_4Ce, Al_3Ce and $Al_{11}Ce_3$ phases with addition of 0.5 to 2.5 cerium oxide by weight percent. The presence of Al_4Ce, Al_3Ce and $Al_{11}Ce_3$ phases confirmed the addition of the cerium oxide in the Al-6061 hybrid composites.

3. Presence of elements namely C, O, Mg, Al and Si was confirmed by EDS analysis as observed from the peaks in hybrid composites reinforced with SiC and Al_2O_3. Aluminium carbide (Al_4C_3) was also found in the spectrum. Aluminium carbide may be formed due to reaction between aluminium and carbide molecules. EDS analysis of Al-6061 hybrid composites showed the elemental composition of C, O, Al, Si, Mg, Fe and Ce with addition of 0.5 to 2.5 cerium oxide by weight percent.

4. EBSD analysis of Al-6061 hybrid composites revealed the fine grains size with addition of 2.5 weight percent of cerium oxide reinforced with 7.5 weight percent of SiC and Al_2O_3. Formation of uniform grain boundaries was observed from EBSD analysis.

6.1.4 Conclusions Drawn From Hydrophobicity and Corrosion Analysis

1. Hydrophobicity of the Al-6061 hybrid composites surface reinforced with SiC/Al_2O_3 was improved with addition of 0.5 to 2.5 cerium oxide by weight percent. The texture formed on the surface of aluminium hybrid composites showed a water contact angle of 100.78^0 with addition

of 2.5 cerium oxide by weight percent. Improvement in hydrophobicity of composites makes them more durable under critically environment conditions.

2. Al-6061 hybrid composites surface showed hydrophobicity for pH range of water droplets from 1.09 to 13.79. There was no variation in water contact angles on the resulting surface when the pH is varied from 1.07 to 13.79.

3. The hydrophobicity of Al-6061 hybrid composites was improved with the addition of rare earth oxides because of the intrinsic hydrophobic nature of rare earth oxides.

4. The addition of cerium oxide resulted in significant improvement in corrosion resistance of the Al-6061 hybrid composites.

6.1.5 Conclusions Drawn from Parametric Analysis of MAFM Process using Box-Behnken Design

1. Magnetic flux density and extrusion pressure have most significant effect on surface roughness during the internal finishing of the Al-6061 hybrid composites as compared to the number of cycles.

2. The optimum value of change in surface roughness of Al-6061 hybrid composites was observed to be 1.03 µm with percentage improvement in surface finish of 68.2 % using desirability approach. This percentage improvement was observed at magnetic flux density of 0.75 Tesla, numbers of cycles 172 and extrusion pressure 4.13 MPa.

3. The addition of magnetic abrasive particles resulted in increase of material removal rate and good surface finish of Al-6061 hybrid composites was obtained.

4. At magnetic flux density of 0.75 Tesla (optimal value), the chain of carbonyl iron particles held the abrasives particles more firmly that resulted in the increase of cutting force on abrasive particles. This increase of cutting force resulted in improvement in surface finish.

5. At extrusion pressure of 4.13 MPa (optimal value), the cutting force acting on the abrasive grains increased the abrasion and may be resulted in reduction of peak height on the surface of Al-6061 hybrid composites.

6. At number of cycle's of 172 (optimal value), the percentage improvement in surface finish of 68.2 % was obtained. This may be due to increase in time of contact of abrasive particles on the surface of Al-6061 hybrid composites.

7. Good agreement in results with error of only 4.65 percent was found between the experimental and predicted values obtained using developed model.

6.2 SUGGESTIONS FOR FUTURE WORK

1. In the future work, the mixed amount of rare earth oxides like CeO_2 and La_2O_3 can be explored in the preparation of aluminium hybrid composites for their mechanical and metallurgical characterization.

2. Evaluation of fatigue failure may be done for the samples of aluminium hybrid composites with mixed amount of rare earth oxides.

3. Evaluation of coefficient of heat transfer at matrix/reinforcement interface of the composite with suitable boundary conditions using simulation tool such as computational fluid dynamic.

4. Applications of other optimization technique like Levenberg-Marquardt Algorithm (LMA) neural networks, genetic algorithm and central composite design technique for analysis of the results can be explored.

LIST OF RESEARCH PUBLICATIONS

The following is the list of research papers published in Journals/Conferences as a part of present research work is given below:

PAPERS PUBLISHED IN INTERNATIONAL JOURNALS (SCI-Indexed)

1. V.K. Sharma, V. Kumar, R.S Joshi. Effect of addition on wear behaviour of an Al-6061 based hybrid composite. **Wear**, 2019, 426-427, 961-974. **(SCI; IF- 4.108)**.
2. V.K. Sharma, V. Kumar, R.S Joshi. Investigation of rare earth particulate on tribological and mechanical properties of Al-6061alloy composites for aerospace application. **Journal of Material Research & Technology**, 2019, 8(4), 3504-3516. **(SCI; IF- 5.289)**.
3. V.K. Sharma, V. Kumar, R.S Joshi. Experimental investigation on effect of RE oxides addition on tribological and mechanical properties of Al-6063 based hybrid composites, **Material Research Express**, 2019, 6(8), 1-38. **(SCI; IF -1.929)**.
4. V.K. Sharma, V. Kumar, R.S Joshi, D. Sharma. Experimental analysis and characterization of SiC and RE oxides reinforced Al-6063 alloy based hybrid composites, **The International Journal of Advanced Manufacturing Technology**, 2020,108, 1173-1187. **(SCI; IF -2.633)**.
5. V.K. Sharma, V. Kumar, R.S Joshi. Parametric study of Aluminum-Rare Earth based composites with improved hydrophobicity using Response Surface Method, **Journal of Material Research & Technology**, 2020, 9(3), 4919-4932. **(SCI; IF -5.289)**.
6. V.K. Sharma, V. Kumar, R.S Joshi. Investigation on Surface Roughness during Finishing of Al-6061 Hybrid Composites tube With Traces of Rare Earth Metals Using Magnetic Abrasive Flow Machining, 2019, **Advances in Unconventional Machining and Composites,** ISBN 978-981-329-471-4. **(Springer Procedia Non SCI)**.

PAPER PRESENTED IN INTERNATIONAL CONFERENCES

1. V.K. Sharma, V. Kumar, R.S Joshi, D. Sharma. Experimental analysis and characterization of SiC and RE oxides reinforced Al-6063 alloy based hybrid composites, 2020, 108, 1173-1187. 40th International **MATADOR** Conference on Advanced Manufacturing Hangzhou, China on 8-10 July 2019. **(SCI; IF -2.633)**.

2. V.K. Sharma, V. Kumar, R.S Joshi. Effect of addition on wear behaviour of an Al-6061 based hybrid composite. Wear (22nd International Conference on **Wear of Materials**, Miami Florida USA, 14-18 April, 2019), 2019, 426-427/961-974. **(SCI; IF- 4.108)**.

REFERENCES

1. Tjong, S.C., 2014, "Processing and deformation characteristics of metals reinforced with ceramic nanoparticles", *Nanocrystalline materials*, pp. 269-304.

2. Rino, J.J., Chandramohan, D., Sucitharan, K.S., 2012, "An overview on development of aluminium metal matrix composites with hybrid reinforcement", *International Journal of Science and Research*, Vol.1, No.3, pp.196-203.

3. Alaneme, K.K., Bodunrin, M.O., 2011, "Corrosion behavior of alumina reinforced aluminium (6063) metal matrix composites", *Journal of Minerals & Materials Characterization & Engineering*, Vol.10, No.12, pp.1153-1165.

4. Das, D.K., Mishra, P.C., Singh, S., Pattanaik, S., 2014, "Fabrication and heat treatment of ceramic-reinforced aluminium matrix composites- a review", *International Journal of Mechanical and Materials Engineering*, Vol. 9, No.6, pp.1-15.

5. Oghenevweta, J.E., Aigbodion, V.S., Nyior, G.B., Asuke, F., 2014, "Mechanical properties and microstructural analysis of Al-Si-Mg/carbonized maize stalk waste particulate composites", *Journal of King Saud University - Engineering Sciences*, Vol. 28, pp. 222-229.

6. Shivaraja, H.B., Kumar, B.P., 2014, "Experimental determination and analysis of fracture toughness of MMC", *International Journal of Science and Research*, Vol.3, No.7, pp.887-892.

7. Alaneme, K.K., Aluko, A.O., 2012, "Fracture toughness (K1C) and tensile properties of as-cast and age-hardened aluminium (6063)-silicon carbide particulate composites", *Scientia Iranica*, Vol. 19, No.4, pp. 992-996.

8. Li, H. R., Lin, J., Zhang, H.J., Fu, L.S., Meng, Q. G., and Wang, S.B., 2002, "Preparation and Luminescence properties of Hybrid materials containing europium (III) complexes covalently bonded to a silica matrix", *Chemistry of Materials*, Vol. 14, No.9, pp.3651-3655.

9. Guo, X., Wang, L., Wang, M., Qin, J., Zhang, D., and Lu, W., 2012, "Effects of degree of deformation on the microstructure, mechanical properties & texture of hybrid-reinforced titanium matrix composites", *Acta Materialia*, Vol. 60, No. (6-7), pp.2656-2667.

10. Wang, X., Chen, G., Yang, W., Hussain, M., Wang, C., Wu, G., and Jiang, D., 2011, "Effect of Nd content on microstructure and mechanical properties of Gr_f/Al composite", *Material Science and Engineering: A*, Vol.528, No. 28, pp.8212-8217.

11. Xihua, Z., Changxia, L., Musen, L., Hua, Z.J.,2008, "Research on toughening mechanisms of alumina matrix ceramic composite material improved by rare earth additive", *Journal of Rare Earths*, Vol.26, No.3, pp.367-370.

12. Torre, A.A., Bustamante, R.P., Cisneros, J.C., Esparza, C.D., Prieto, H.M., Sanchez, R.M., 2013, "Mechanical properties of the A356 aluminium alloy modified with La/Ce", *Journal of Rare Earths*, Vol.31, No.8, pp.811-816.

13. Chai, T.L., Easton, M.A., Zhu, S.M., Gibson, M.A., Birbilis, N., and Nie, J.F., 2009, "The effect of alloy composition on the microstructure and tensile properties of binary Mg-rare earth alloys", *Intermetallics*, Vol.17, No.7,pp.481-490.

14. Kenton, T., 2009, "The future of mechanical surface finishing", *Metal Finishing*, Vol.107, No.5, pp.22-24.

15. Jain, V.K., 2009, "Magnetic field assisted abrasive based micro-nano-finishing", *Journal of Materials Processing Technology*, Vol. 209, No.20, pp.6022-6038

16. Yamaguchi, H., Shinmura, T., Ikeda, R., 2007, "Study of internal finishing of austenitic stainless steel capillary tubes by magnetic abrasive finishing", *Journal of Manufacturing Science and Engineering*, Vol.129, No.5, pp. 885-892.

17. Surappa, M.K., Rohatgi, P.K., 1981, "Preparation and Properties of aluminum alloy ceramic particle composites", *Journal of Material Science*, Vol. 16, pp.983-993.

18. Mao, F., Yan, G., Xuan, Z., Cao, Z., Wang, T., 2015, "Effect of Eu addition on the microstructures and mechanical properties of A356 aluminium alloys", *Journal of Alloys and Compounds*, Vol. 650, No.25, pp.896-906.

19. Yang, Y., Lan, J., Li, X., 2004, "Study on bulk aluminium matrix nano-composite fabricated by ultrasonic dispersion of nano-sized SiC particles in molten aluminium alloy", *Material Science and Engineering: A*, Vol. 380, No.1-2, pp. 378-383.

20. Kandpal, B.C., Kumar, J., Singh, H., 2018, "Manufacturing and technological challenges in Stir casting of metal matrix composites-A Review", *Materials Today: Proceedings*, Vol.5, pp.5-10.

21. Lloyd, D.J., 1994, "Particle reinforced Al-Mg metal matrix composites", *International Materials Review*, Vol. 39, No.1, pp. 1-23.

22. Samuel, A.M., Liu, H., Samuel, F.H., 1993, "On the castability of Al-Si/SiC particle-reinforced metal-matrix composites: Factors affecting fluidity and soundness", *Composite Science and Technology*, Vol. 49, No.1, pp.1-12.

23. Clyne , T., 2000, "An introductory overview of MMC systems, types, and developments. In A. K. and C. Zweben (Ed.), Comprehensive composite materials, Elsevier B.V., 821-842.

24. Properties of Metal Matrix Composites. ASTM Handbook on composites Vol.21, pp.845.

25. Alaneme, K.K., Fajemisin, A.V., Maledi, N.B., 2019, "Development of aluminium- based composites reinforced with steel and graphite particles: structural, mechanical and wear characterization", *Journal of Material Research and Technology*, Vol.8, No.1, pp. 670-682.

26. Rana, R.S., Purohit, R., Sharma, A.K., Rana, S., 2014, "Optimization of wear performance of Aa 5083/10 wt% SiC composites using Taguchi method", *Procedia Materials Science*, Vol. 6, pp. 503-511.

27. Kumar, N.G.S., Ravindranath, V.M., Shankar, G.S.S., 2014, "Mechanical and wear behavior of aluminum metal matrix hybrid composites", *Procedia Materials Science*, Vol.5, pp.908-917.

28. James, J.S., Venkatesan, K., Kuppan, P., Ramanujam, R., 2014, "Hybrid aluminum metal matrix composites reinforced with SiC and TiB_2", *Procedia Engineering*, Vol. 97, pp.1018-1026.

29. Singh, G., Goyal, S., 2016, "Microstructure and mechanical behavior of AA6082-T6/SiC/B_4C based aluminum hybrid composites", *Particulate Science and Technology*, Vol.36, No.2, pp.154-161.

30. Selvam, D.R., Robinson, J., Dinaharan, D.S., 2013, “Syntheses and characterization of Al6061- fly ash- SiC composites by stir casting and compocasting methods”, *Energy Procedia*, Vol.34, pp. 637-646.

31. Madheswaran, K., Sugumar, S., Elamvazhudi, B., 2015, “Mechanical characterization of aluminum- boron carbide composites with influence of calcium carbide particles”, *International Journal of Emerging Technology and Advanced Engineering*, Vol. 5, pp. 492-496.

32. Prabhakar, S.N., Radhika, N., Raghu, R., 2014, “Analysis of tribological behavior of aluminum/B_4C composites under dry sliding motion”, *Procedia Engineering*, Vol.97, pp.994-1003.

33. Pal, M.K., Sandhu, S.S., Kalia, R., Ghosh, A., 2015, “Identification of optimum composition and mechanical properties of Al-Ni metal matrix composites”, *Journal of Mineral and Materials Characterization and Engineering*, Vol.3, pp.326-334.

34. Prakash, K.S., Balasundar, P., Nagaraja, S., Gopal, P.M., Kavimani, V., 2016, “Mechanical and wear behavior of Mg-SiC-Gr hybrid composites”, Journal of Magnesium and Alloys, Vol.4, pp. 197-206.

35. Kaushik, N.C., Rao, R.N., 2016, “Effect of grit size on two body abrasive wear of Al6082 hybrid composites produced by stir casting method”, *Tribology International*, Vol. 102,pp.52-60.

36. Liu, Y., Li, W., Xu, B., Cai, X., Li, C.Q., 2004, “The behavior and effect of rare earth CeO_2 on In-situ TiC/Al composite”, *Metallurgical and Materials Transactions A*, Vol.35, No.8, pp.2511-2515.

37. Singh, V.K., Chauhan, S., Gope, P.C., Chaudhary, A.K., 2015, “Enhancement of Wettability of Aluminum Based Silicon Carbide Reinforced Particulate Metal Matrix Composite”, *High Temperature Materials and Processes*, Vol. 34, No.2, pp. 163-170.

38. Poovazhagan, L., Rajkumar, K., Saravanamuthukumar, P., Ibrahim, S.J.I., Santosh, S., 2015, “Effect of Magnesium Addition on Processing the Al-0.8 Mg-0.7 Si/SiCp Metal Matrix Composites”, *Applied Mechanics and Materials,* Vol. 787, pp. 553-557.

39. Kozhukharov, S., Kozhukharov, V., Schem, M., Aslan, M., Wittmar, M., Wittmar, A., Veith, M., 2012, "Protective ability of hybrid nano-composite coatings with cerium sulphate as inhibitor against corrosion of AA2024 aluminium alloy", *Progress in Organic Coatings*, Vol.73, pp. 95-103.

40. Devaraju, A., Kumar, A., Kotiveerachari, B., 2013, "Influence of addition of Grp/Al_2O_{3p} with SiCp on wear properties of aluminum alloy 6061-T6 hybrid composites via friction stir processing", *Transactions of Nonferrous Metals Society of China*, Vol. 23, No.5, pp.1275–1280.

41. Kumaran, S.T., Uthayakumar, M., Slota, A., Aravindan, S., Zajac, J., 2015, "Machining behavior of AA6351-SiC-B_4C hybrid composites fabricated by stir casting method", *Journal of particulate Science and Technology*, Vol. 34, No.5, pp.586-592.

42. Ravindran, P., Manisekar, K., Vinoth, K.S., Rathika, P., 2013, "Investigation of microstructure and mechanical properties of aluminum hybrid nano-composites with the additions of solid lubricant", *Materials & Design*, Vol. 51, pp.448-456.

43. Radhika, N., Subramanian, R., 2013,"Effect of reinforcement on wear behavior of aluminium hybrid composites", *Tribology-Materials, Surfaces & Interfaces*, Vol.7, No.1, pp.36-41.

44. Tan, A., Teng, J., Zeng, X., Fu, D., Zhang, H., 2017, "Fabrication of aluminium matrix hybrid composites reinforced with SiC microparticles and TiB_2 nanoparticles", *Powder Metallurgy*, Vol.60, No.1, pp.66-72.

45. Rajeswari, B., Amirthagadeswaran, K.S., Anbarasu, K.G.,2015, "Investigation on mechanical properties of aluminium 7075-silicon carbide-alumina hybrid composite using Taguchi method", *Australian Journal of Mechanical Engineering*, Vol. 13, No. 2, pp. 127-135.

46. Kumar, H.G.P., Xavior, M.A., 2016, "Encapsulation and Microwave Hybrid Processing of Al 6061-Graphene-SiC Composites", *Materials and Manufacturing processes*, Vol.33, No.1, pp. 19-25.

47. Jackson, M.J., Machado, A.R., Silva, M.B.D. Machining of Titanium and Nickel Alloys for Aerospace Applications, Springer; 1st ed. 2020 edition (Aug. 11 .2020).

48. Quanming, Q., Xikum, L., Tai, Q., Haitao, Z., Honghao, Y, Ruiting, M., 2007, “Application of Rare Earths in Advanced Ceramic Materials”, *Journal of Rare Earths*, Vol.25, No.2, pp.281-286

49. Tsai, Y., Lee, S., Lin, C.K., 2011, “Effect of trace Ce addition on the microstructures and mechanical properties of A356 (AL–7SI–0.35 Mg) aluminum alloys”, *Journal of the Chinese Institute of Engineers*, Vol. 34, No.5, pp.609-616.

50. Bai, G., Liu, Z., Lin, J., Yu, Z., Hu, Y., Wen, C., 2016, “Effects of the addition of lanthanum and ultrasonic stirring on the microstructure and mechanical properties of the situ Mg_2Si/Al composites”, *Materials & Design*, Vol. 90, pp.424-432.

51. Baldacim, S. A., Santos, C., Silva, O.M.M., Silva, C.R.M., 2004, “Ceramics composites Si_3N_4-$SiC_{(w)}$ containing rare earth concentrate (CRE) as sintering aids”, *Materials Science and Engineering:A*, Vol. 367 No.1-2, pp. 312-316.

52. Inoue, M., Otsu, H., Kominami, H., Inui, T., 1995, “Glycothermal synthesis rare earth aluminium garnets”, *Journal of Alloys and Compounds*, Vol. 226, No.1-2, pp. 146-151.

53. Terao, R., Tatami, J., Meguro, T., Komeya, K., 2002, “Fracture behavior of A1N ceramics with rare earth oxides”, *Journal of the European Ceramic Society*, Vol. 22, No.7, pp. 1051-1059.

54. Xu, C., Ai, X., 2001, “Particle dispersed ceramic composite reinforced with rare earth additions”, *International Journal of Refractory Metals and Hard Materials*, Vol.19, No.2, pp.85-88.

55. Kenyon, A. J., 2002, “Recent developments in rare-earth doped materials for optoelectronics”, *Progress in Quantum Electronics*, Vol.26, pp.225-284.

56. Young, W. K., Yong, S. C., Toshiyuki, N., Mamoru, M., Lee, Y.H., 2007, “High-temperature strength of silicon carbide ceramics sintered with rare-earth oxide and aluminum nitride”, *Acta Materialia*, Vol. 55, pp.727-736.

57. Jain, V.K., Singh, D.K., Raghuram, V., 2008, “Analysis of performance of pulsating flexible magnetic abrasive brush (P-Fmab)”, *Machining Science and Technology*, Vol. 12, No.1, pp.53-76.

58. Yin, S., Shinmura, T., 2004, “A comparative study: polishing characteristics and its mechanisms of three vibration modes in vibration-assisted magnetic abrasive polishing”, *International Journal of Machine Tools and Manufacture*, Vol. 44, No.4, pp.383-390.

59. Mulik, R.S., Pandey, P.M., 2011, “Ultrasonic assisted magnetic abrasive finishing of hardened AISI 52100 steel using unbonded SiC abrasives”, *International Journal of Refractory Metals and Hard Materials*, Vol. 29, No.1, pp.68-77.

60. Mulik, R.S., Pandey, P.M., 2012, “Experimental investigations and modeling of finishing force and torque in ultrasonic assisted magnetic abrasive finishing”, *Journal of Manufacturing Science and Engineering*, Vol. 134, No.5, pp.1-12.

61. Singh, S., Shan, H.S., Kumar, P., 2002, “Wear behavior of materials in magnetically assisted abrasive flow machining”, *Journal of Materials Processing Technology*, Vol. 128, pp.155-161.

62. Kala, P., Pandey, P., 2015,“Comparison of finishing characteristics of two paramagnetic materials using double disc magnetic abrasive finishing” , *Journal of Manufacturing Processes*, Vol. 17, pp. 63-77.

63. Ko, S.L., Baron, Y.U., Park, J.I., 2007, “Micro Deburring for precision parts using magnetic abrasive finishing method”, *Journal of Materials Processing Technology*, Vol. 187, pp. 19-25.

64. Zou, Y.H., Jiao, A.Y., Aizawa, T., 2010, “Study on plane magnetic abrasive finishing process-experimental and theoretical analysis on polishing trajectory”, *Advanced Material Research*, Vol. 126-128, pp.1023-1028.

65. Kim, T.W., Kwak, J.S., 2010, “A study on deburring of magnesium alloy plate by magnetic abrasive polishing”, *International Journal of Precision Engineering and Manufacturing*, Vol. 11, No.2, pp. 189:194.

66. Yamaguchi, H., Shinmura, T., 2004, “Internal finishing process for alumina ceramic components by a magnetic field assisted finishing process”, *Precision Engineering*, Vol. 28, No.2, pp. 135:142.

67. Givi, M., Tehrani, A.F., Mohammadi, A., 2012, “Polishing of the aluminum sheets with magnetic abrasive finishing method”, *The International Journal of Advanced Manufacturing Technology*, Vol.61, No. (9-12), pp. 989-999.

68. Nguyen, A.T., Reiter, S., Rigo, P., 2014, “A review on simulation-based optimization methods applied to building performance analysis”, *Applied Energy*, Vol.113, pp.1043-1058.

69. Lin, C.T., Yang, L.D., Chow, H.M., 2007, “Study on magnetic abrasive finishing in free-form surface operations using the Taguchi method”, *The International Journal of Advanced Manufacturing Technology*, Vol. 34, pp.122-130.

70. Singh, D.K., Jain, V.K., Raghuram, V., 2004, “Parametric study of magnetic abrasive finishing process”, *Journal of Materials Processing Technology*, Vol.149, No.1-3, pp. 22-29.

71. Barman, A., Das M.,2017, “Design and fabrication of a novel polishing tool for finishing free form surfaces in magnetic field assisted finishing (MFAF) process”, *Precision Engineering*,Vol.49, pp.61-68.

72. Kwak, J.S., 2012, “Mathematical model determination for improvement of surface roughness in magnetic-assisted abrasive polishing of nonferrous AISI316 material”, *Transactions of Nonferrous Metals Society of China*, Vol.12, No.3, pp.s845-s850.

73. Bharath, V., Nagaral, M., Auradi, V., Kori, S.A.,2014, “Preparation of 6061Al-Al2O3 MMC's by Stir Casting and Evaluation of Mechanical and Wear Properties”, *Procedia Materials Science*,Vol.6, pp.1658-1667.

74. Chonghai, X., Xing, A., Chuanzhen, H., Deng, J.X., 1999, “Micro-structural characterization of toughening mechanisms of ceramic tool material with rare earth additive”, *Journal of the Chinese Electron Microscopy Society* (in Chin.), Vol.18, No. (4): 443.

75. Chonghai, X., Xing, A., (2001), “Particle dispersed ceramic composite reinforced with rare earth additions”, *International Journal of Refractory Metals and Hard Materials*, Vol.19: 85.

76. Megahed, M., Attai, M.A., Abdelhameed, M., Shafei, A.G., 2017, “Tribological Characterization of Hybrid Metal Matrix Composites Processed by Powder Metallurgy”, *Acta Metallurgica Sinica*, Vol.30, No.8, pp.781-790.

77. Kumar, A., Patnaik, A., Bhat, I.K., 2017, “Investigation of nickel metal powder on tribological and mechanical properties of Al-7075 alloy composites for gear materials”, *Powder Metallurgy*, Vol.60, No.5, pp.371-383.

78. Singh, S., Pal, K., 2019, “Effect of texture evolution on mechanical and damping properties of SiC/$ZnAl_2O_4$/Al composite through friction stir processing”, *Journal of Materials Research and Technology*, Vol. 8, No. 1,pp.222-232.

79. Verma, N., Vettivel, S.C., 2018, “Characterization and experimental analysis of boron carbide and rice husk ash reinforced AA7075 aluminium alloy hybrid composite”, *Journal of Alloys and Compounds*, Vol.741, pp.981-998.

80. Laurent, V., Chtan, D., Eustathopoulos, N., 1987, “Wettability of SiC by aluminium and Al-Si alloys”, *Journal of Material Science*, Vol. 22, pp.244-250.

81. Hashim, J., Looney, L., Hashmi, M. S. J., 2001, “The wettability of SiC particles by molten aluminium alloy”, *Journal of Materials Processing Technology*, Vol. 119, No.1-3, pp. 324-328.

82. Kalantarian, A., David, R., Neumann, A.W., 2009, “Methodology for high accuracy contact angle measurements”, *Langmuir*, Vol.25, No.24, pp. 14146-14154.

83. Montgomery, D.C., 2002, “Design and Analysis of Experiments”, 4th ed. Wiley New York.

84. Kant, G., Sangwan, K.S., 2014, “Prediction and optimization of machining parameters for minimizing power consumption and surface roughness in machining”, *Journal of Cleaner Production*, Vol. 83, pp.151-164.

85. Davim, J.P., 2003, “Design of optimisation of cutting parameters for turning metal matrix composites based on the orthogonal arrays”, *Journal of Materials Processing Technology*, Vol.132, No.1-3, pp. 340-344.

86. Barbosa, A.Q., Da Silva, L.F.M., Abenojar, J., Figueiredo, M., 2017, “Analysis of the effect of size, amount and surface treatment on the tensile strain of a brittle adhesive reinforced with micro cork particles”, *Applied Adhesion Science*,Vol.5, No.9, pp.1-16.

87. Manna, A., Bhattacharyya, B., 2004, “Investigation for optimal parametric combination for achieving better surface finish during turning of Al/SiC-MMC”, *The International Journal of Advanced Manufacturing Technology*, Vol.23, pp.658-665.

88. Gunaraj, V., Murugan, N., 1999,“Application of response surface methodologies for predicting weld base quality in submerged arc welding of pipes”, *Journal of Materials Processing Technology*, Vol. 88, pp. 266–275.

89. Bezerra, M.A., Santelli, R.E., Oliveira, E.P., Villar, L.S., Escaleira, L.A., 2008, “Response surface methodology (RSM) as a tool for optimization in analytical chemistry”, *Talanta*, Vol.76, No.(5), pp.965-977.

90. Candioti, L.V., De, Z.M.M., Cámara, M.S., Goichoechea, H.C., 2014, “Experimental design and multiple response optimization. Using the desirability function in analytical methods development”, *Talanta*, Vol.124, pp.123-138.

91. Politis, S.N., Colombo, P., Colombo, G., Rekkas, D.M., 2017, “Design of experiments (DoE) in pharmaceutical development”, *Drug Development and industrial Pharmacy*, Vol.43, No.6, pp.89-901.

92. Souza, A.S., Dos S., Walter, N.L., Ferreira, S.L.C., 2005, “Application of Box–Behnken design in the optimization of an on-line pre-concentration system using knotted reactor for cadmium determination by flame atomic absorption spectrometry”. *Spectrochimica Acta Part-B*, Vol. 609, pp. 737-742.

93. Dhanawade, A., Kumar, S., 2016,“ An Experimental Study of Surface Roughness in Abrasive Waterjet Machining of Carbon Fiber Reinforced Polymer using Orthogonal Array with Grey Relational Analysis”, *Journal of Manufacturing Engineering*, Vol.11,No.1,pp.001-006.

94. Verma, V. K., Kamat, S.V., Mahajan, Y.R., Kutumbarao, V.V., 2001,“Effect of reinforcement size on low strain yielding behaviour in Al-Cu-Mg/SiCp composites”, *Materials Science and Engineering: A*, Vol. 318, No.(1-2), pp.57-64.

95. Wang, Z., Song, M., Sun, C., H., 2011, "Effects of particle size and distribution on the mechanical properties of SiC reinforced Al-Cu alloy composites", *Materials Science and Engineering: A*, Vol. 528, No.3, pp.1131-1137.

96. Kainer, K.U., 2006, "Metal Matrix Composites: Custom- made materials for automotive and Aerospace Engineering", Wiley- VCH verlag GmbH & Co., ISBN 3-527-31360-5.

97. Srivatsan, T.S., Hajri, M.A., Petraroli, M., Hotton, B., Lam, P.C.,2002, "Influence of silicon carbide particulate reinforcement on quasistatic and cyclic fatigue fracture behavior of 6061 aluminum alloy composites", *Materials Science and Engineering: A*, Vol. 325, No.(1-2),pp.202-214.

98. Zheng, L., Yongmei, H., 2008, "Effect of yttrium on the microstructure of a semi-solid A356 Al alloy", *Rare Metals*, Vol.27, No.5, pp:536-540.

99. George, R., Kashyap, K.T., Rahul, R., Yamdagni, S., 2005, "Strengthening in carbon nanotube/aluminum (CNT/Al) composites", *Scripta Materialia*, Vol. 53, No.10, pp. 1159-1163.

100. Sharma, V. K., Kumar, V., Joshi, R. S., 2019, "Effect of RE addition on wear behaviour of an Al-6061 based hybrid composite", *Wear*, Vol.426-427, pp.961-974.

101. Bodunrin, M.O., Alaneme, K.K., Chown, L.H., 2015, "Aluminium matrix hybrid composites: a review of reinforcement philosophies; corrosion and tribological characteristics", *Journal of Materials Research and Technology*, Vol. 4, No.4, pp.434-445.

102. Shanti, M., Jayaramanavar, P., Vyas, V., Seenivasan, D.V.S., Gupta, M., 2012, "Effect of niobium particulate addition on the microstructure and mechanical properties of pure magnesium", *Journal of Alloys and Compounds*, Vol.513, pp.202-207.

103. Shi, C., Zhang, L., Wu, G., Zhang, X., Cheng, A., Tao, J., 2017, "Effects of Sc addition on the microstructure and mechanical properties of cast Al-3Li-1.5Cu-0.15Zr alloy", *Materials Science and Engineering: A*, vol.680, pp.232-238.

104. Altinkok, N., 2004, "Microstructure and Tensile Strength Properties of Aluminium Alloys Composites Produced by Pressure-assisted Aluminium Infiltration of Al_2O_3/SiC Preforms", *Journal of Composite Materials*, Vol. 38, pp.1533-1543.

105. Wang, X., Chen, G., Yang, W, Hussain, M., Wang, C., Wu, G., Jiang, D., 2011, "Effect of Nd content on microstructure and mechanical properties of Gr_f /Al composite", *Materials Science and Engineering: A*, Vol.528, No.28, pp. 8212-8217.

106. Arora, H.S., Singh, H., Dhindaw, B.K., 2013, "Wear behaviour of a Mg alloy subjected to friction stir processing", *Wear*, Vol. 303, No. 1-2, pp.65-77.

107. Zohoor, M., Givi, M.K.B., Salami P.,2012 "Effect of processing parameter on fabrication of Al-Mg/Cu composites via friction stir processing", *Materials & Design*, Vol. 39, pp.358-365.

108. Hossieni, S.A., Ranjbar, K., Dehmolaei, R., Amirani, A.R.,2015, "Fabrication of Al5083 surface composites reinforced by CNTs and cerium oxide nano particles via friction stir processing", *Journal of Alloys and Compounds*, Vol. 622, pp.725-733.

109. Tirth, V., 2017, "Dry Sliding Wear Behavior of 2218 Al-Alloy-Al_2O_3 (TiO_2) Hybrid composites", *Journal of Tribology*, Vol.140, pp.1-9.

110. Wang, N., Wang, Z., Weatherly, G.C., 1992, "Formation of magnesium aluminate (spinel) in cast SiC particulate-reinforced Al (A356) metal matrix composites",*Metallurgical Transactions A*, Vol.23, pp.1423-1430.

111. Asl, K.V., Masoudi, A., Khomamizadeh, F., 2010,"The effect of different rare earth elements content on microstructure, mechanical and wear behavior of Mg-Al-Zn alloy", *Materials Science and Engineering: A*, Vol. 527, No.7-8, pp.2027-2035.

112. Giovambattista, N., Debenedetti, P.G., Rossky, P.J., 2007, "Effect of Surface Polarity on Water Contact Angle and Interfacial Hydration Structure", *The Journal of Physical Chemistry*, Vol.111, No.32, 9581-9587.

113. Granick, S., Bae, S.C., 2008, "CHEMISTRY: A Curious Antipathy for Water", *Science*, Vol.322, No.5907, pp. 1477-1478.

114. Hass, K. C., Schneider, W.F., Curioni A, Andreoni, W., 1998, "The Chemistry of Water on Alumina Surfaces: Reaction Dynamics from First Principles", *Science*, Vol.282, No.5387, pp. 265-268.

115. Cohen, N., Dotan, A., Dodiuk, H., Kenig, S., 2019, “Superhydrophobic Coatings and Their Durability”, *Materials and Manufacturing Processes*, Vol. 31, No. 9, pp.1143-1155.

116. Shao, N., Dai, J.W., Li, G.Y., Nakae, H., Hane, T., 2014, “Effect of La on the wettability of Al_2O_3 by molten aluminium”, *Materials Letters*, Vol.58, No.14, pp. 2041-2044.

117. Candan, S., 2009, “An investigation on corrosion behaviour of pressure infiltrated Al-Mg alloy/SiC p composites”, *Corrosion Science*, Vol. 51, No.6, pp.1392-1398.

118. Shimizu, Y., Nishimura, T., Matsushima, I., 1995, “Corrosion resistance of Al-based metal matrix composites”, *Materials Science and Engineering: A*, Vol. 198, No.(1-2), pp.113-118.

119. Piexto, J.L., 1987, “Hierarchical model selection in polynomial regression models”, *The American Statistician*, Vol. 41, No.4, pp. 311-313.

120. Sankar, M.R., Ramkumar, J., Jain, V.K., 2009, “Experimental investigation and mechanism of Material Removal in Nano finishing of MMCs using Abrasive Flow Finishing (AFF) process”, *Wear*, Vol. 266, No. 7, pp.688-698.

121. Zhang, J., Hu, J., Wang, H., Kumar, A.S., Chaudhari, A., 2018, “A novel magnetically driven polishing technique for internal surface finishing”, *Precision Engineering*, Vol 54, pp.222-232.

122. Singh, P., Singh, L., Singh, S., 2020, “Analyzing Process Parameters for Finishing of Small Holes Using Magnetically Assisted Abrasive Flow Machining Process”, *Journal of Bio-and Tribo-Corrosion*, Vol. 6, No.17, pp.1-10.

123. Rajesh, S., Devaraj, D., Pandian, R.S., Rajakarunakaran, S., 2013, “Multiresponse optimization of machining parameters on red mud-based aluminum metal matrix composites in turning process”, *The International Journal of Advanced Manufacturing Technology*, Vo. 67, No.(1-4), pp.811-821.

124. Karnik, S., Gaitonde, V., Davim, J., 2008, “A comparative study of the ANN and RSM modeling approaches for predicting burr size in drilling, *The International Journal of Advanced Manufacturing Technology*, Vol. 38, No.(9-10), pp.868-883.

125. Pradhan, M., 2013, “Estimating the effect of process parameters on MRR, TWR and radial overcut of EDMed AISI D2 tool steel by RSM and GRA coupled with PCA”, *The International Journal of Advanced Manufacturing Technology*, Vol. 68, No.(1- 4), pp.591-605.

126. Azam, M., Jahanzaib, M.,Wasim, A., Hussain, S., 2015, “Surface roughness modeling using RSM for HSLA steel by coated carbide tools”, *The International Journal of Advanced Manufacturing Technology*, Vol.78, No.(5-8), pp.1031-1041.